

Technical Report
APPROACH OF TURBULENT BOUNDARY LAYER
TO SIMILARITY

by

Dusan L. Zoric

U. S. Army Research Grant

DA-AMC-28-043-65-G20

Fluid Dynamics and Diffusion Laboratory

College of Engineering

Colorado State University

Fort Collins, Colorado

September 1968

CER68-69DLZ9



018401 0575031

ABSTRACT

APPROACH OF TURBULENT BOUNDARY LAYER TO SIMILARITY

A large scale turbulent boundary layer with no pressure gradient, developed on a flat plate 95 feet long has been investigated. Theoretical considerations of the existence of local similarity yield the requirements which should be found in the turbulent boundary layers in order that similarity exists. Measurements of the mean motion, the turbulent velocity components and the turbulent shear stress have been made for the free stream velocity range 60 to 100 ft/sec. Reynolds numbers based on the boundary layer thickness were of the order of 10^6 . Turbulence quantities were evaluated from a single rotating hot-wire probe along the entire length of the boundary layer.

For all quantities measured, the uncertainty intervals were calculated in order to provide a measure of the reliability of the results. The large scale turbulent boundary layers are shown to approach closely the theoretical requirements for similarity. Displacement and momentum thickness grow as a linear function of x-coordinate, the form factor is constant. The constant wall shear stress requirement is very closely approached. An asymptotic similarity form is considered and reported. For similarity function of the turbulent shear stress distribution across the boundary layer thickness, an approximate linear function is proposed. The best average universal velocity profile is tabulated.

ACKNOWLEDGMENTS

The author wishes to express his sincere gratitude to his advisor, Professor V. A. Sandborn, for his guidance and valuable advice.

Sincere appreciation is extended to other members of the graduate committee, Dr. J.E. Cermak, Dr. L.V. Baldwin, Dr. B. Bean and Dr. P. Todorovic, for their comments and review of this dissertation.

The author also wishes to express his appreciation for technical assistance in the experimental work to Mr. H. Wang. Special thanks are also given to the shop personnel for cooperation in construction and maintenance of the equipment.

To those who assisted in typing and printing this dissertation the author extends his gratitude.

The project was supported by the Integrated Army Meteorological Wind Tunnel Research Program under Grant DA-AMC-28-043-65-G20.

TABLE OF CONTENTS

<u>Chapter</u>		<u>Page</u>
	LIST OF TABLES	viii
	LIST OF FIGURES	ix
	LIST OF SYMBOLS	xiv
I	INTRODUCTION	1
II	THEORETICAL BACKGROUND	4
	2.1 Turbulent Boundary Layer	4
	2.2 Law of the Wall	6
	2.3 Outer Portion of the Turbulent Boundary Layer	9
	2.3.1 The velocity defect law	10
	2.3.2 The logarithmic region	12
	2.3.3 Contemporary treatments of the outer portion of the turbulent boundary layer	13
	2.4 Conditions for Local Similarity in the Turbulent Boundary Layer	17
	2.5 Distribution and Order of Magnitude of the Individual Terms in the Momentum Equation of the Mean Flow	24
III	INSTRUMENTATION AND EXPERIMENTAL FACILITIES	26
	3.1 Wind Tunnel Facility	26
	3.2 Instruments	28
	3.2.1 Pitot-static tube	28
	3.2.2 Hot-wire probe actuator and carrier	28
	3.2.3 Hot-wire probe	30
	3.2.4 Integrator	31
IV	DATA REDUCTION, CALIBRATION PROCEDURES AND POSSIBLE SOURCES OF ERRORS	33
	4.1 Mean Velocity Measurements	33

TABLE OF CONTENTS - Continued

<u>Chapter</u>		<u>Page</u>
	4.1.1 Calibration of mean velocity measurement instrumentation.	33
	4.1.2 Possible sources of errors in the mean velocity measurements.	34
	4.1.3 Mean velocity calculations.	37
	4.2 Turbulence Measurements.	38
	4.2.1 The hot-wire anemometer	39
	4.2.2 Hot-wire sensitivity to velocity and yaw.	40
	4.2.3 Hot-wire calibrations	45
	4.2.4 Possible sources of error in turbulence measurements.	49
	4.3 Uncertainty Intervals.	52
V	RESULTS AND DISCUSSION.	55
	5.1 The Character of the Measured Turbulent Boundary Layer	55
	5.2 Mean Velocity Measurements and Similarity in Outer Portion of the Turbulent Boundary Layer.	57
	5.3 Turbulence Measurements and Similarity in the Outer Portion of the Turbulent Boundary Layer.	66
VI	CONCLUSIONS	72
	BIBLIOGRAPHY.	75
	APPENDIX A.	79
	APPENDIX B.	83
	APPENDIX C.	91
	TABLES.	102
	FIGURES	123

LIST OF TABLES

<u>Table</u>		<u>Page</u>
I	MEAN VELOCITY DISTRIBUTIONS.	103
II	TURBULENT BOUNDARY LAYER PARAMETERS.	116
III	UNIVERSAL VELOCITY DISTRIBUTION.	118
IV	TURBULENCE QUANTITIES.	119

LIST OF FIGURES

<u>Figure</u>		<u>Page</u>
1	Definition sketch of the boundary layer.	124
2	Wind tunnel.	125
3	The pressure distribution.	126
4	Free stream turbulence intensity at the entrance of the test section.	127
5	Schematic of the hot-wire probe carrier.	128
6	Hot-wire probe carrier, crosswise probe position	129
7	Hot-wire probe carrier, streamwise probe position. . . .	129
8	Probes	130
9	Integrating circuit.	131
10	Operational amplifier of the integrating circuit	132
11	Integrating circuit calibration curve.	133
12	Block diagram of the mean velocity measurement instrumentation.	134
13	Calibration of Trans-Sonics pressure meter against the Merriam micromanometer	135
14	The wall effect expressed as a function of y/D after MacMillan.	136
15	Turbulence effect on mean velocity measurement	137
16	Turbulence effect on Δh shift - nonlinear averaging. . .	138
17	Typical calibration curve of Trans-Sonics pressure meter versus pressure differential	139
18	Hot-wire with respect to the coordinate system	140
19	Typical hot-wire calibration curve	141
20	Velocity sensitivity for $\pm 40^\circ$ angle of yaw.	142
21	Velocity sensitivity for $\pm 45^\circ$ angle of yaw.	143

LIST OF FIGURES - Continued

<u>Figure</u>		<u>Page</u>
22	Angle sensitivity for $\pm 40^{\circ}$ yaw for a "perfect" hot-wire.	144
23	Angle sensitivity for $\pm 40^{\circ}$ yaw for a "real" hot-wire	145
24	Comparison of turbulence measurement with a horizontal and vertical hot-wire near the tunnel floor. Station 46 ft.	146
25	Comparison of turbulence measurement with a horizontal and vertical hot-wire near the tunnel floor. Station 66 ft.	147
26	Mean velocity distributions. $U_{\infty} \approx 60$ ft/sec. Origins: (0+30) ft/sec	148
27	Mean velocity distributions. $U_{\infty} \approx 75$ ft/sec. Origins: (0+40) ft/sec.	149
28	Mean velocity distributions. $U_{\infty} \approx 84$ ft/sec. Origins: (0+50) ft/sec	150
29	Mean velocity distributions. $U_{\infty} \approx 95$ ft/sec. Origins: (0+60) ft/sec	151
30	Mean velocity distributions. $U_{\infty} \approx 61$ ft/sec. Origins: (0+30) ft/sec	152
31	Mean velocity distributions. $U_{\infty} \approx 82$ ft/sec. Origins: (0+40) ft/sec	153
32	Nondimensional velocity profile. $U_{\infty} \approx 95$ ft/sec	154
33	Nondimensional velocity profile. $U_{\infty} \approx 60$ ft/sec	155
34	Comparison of measured mean velocity profile and velocity profile calculated by Mellor's method. $U_{\infty} \approx 81$ ft/sec. $x = 20$ ft.	156
35	Comparison of measured mean velocity profile and velocity profile calculated by Mellor's method. $U_{\infty} \approx 81$ ft/sec. $x = 70$ ft.	157
36	Universal velocity profile A.	158
37	Boundary layer development. $U_{\infty} \approx 60$ ft/sec. $x_1 = 7$ ft 11 in.	159

LIST OF FIGURES - Continued

<u>Figure</u>		<u>Page</u>
38	Boundary layer development. $U_{\infty} \approx 75$ ft/sec. $x_1 = 7$ ft 11 in.	160
39	Boundary layer development. $U_{\infty} \approx 85$ ft/sec. $x_1 = 7$ ft 11 in.	161
40	Boundary layer development. $U_{\infty} \approx 95$ ft/sec. $x_1 = 7$ ft 11 in.	162
41	Boundary layer development. $U_{\infty} \approx 61$ ft/sec	163
42	Boundary layer development. $U_{\infty} \approx 82$ ft/sec	164
43	Displacement thickness comparison	165
44	Momentum thickness comparison	166
45	Effect of skin friction on form factor H.	167
46	Comparison of friction coefficient values	168
47	Universal velocity profile B.	169
48	Turbulent boundary layer velocity distributions at zero pressure gradient on a flat plate.	170
49	Comparison of turbulent shear stress distribution along the boundary layer length. $U_{\infty} \approx 60$ ft/sec.	171
50	Comparison of u-component of turbulence distributions along the boundary layer length	172
51	Comparison of v-component of turbulence distributions along the boundary layer length	173
52	Turbulence intensities, $U_{\infty} \approx 60$ ft/sec. $x = 10$ ft. . . .	174
53	Turbulence intensities, $U_{\infty} \approx 60$ ft/sec. $x = 20$ ft. . . .	175
54	Turbulence intensities, $U_{\infty} \approx 60$ ft/sec. $x = 30$ ft. . . .	176
55	Turbulence intensities, $U_{\infty} \approx 60$ ft/sec. $x = 40$ ft. . . .	177
56	Turbulence intensities, $U_{\infty} \approx 60$ ft/sec. $x = 50$ ft. . . .	178
57	Turbulence intensities, $U_{\infty} \approx 60$ ft/sec. $x = 60$ ft. . . .	179
58	Turbulence intensities, $U_{\infty} \approx 60$ ft/sec. $x = 70$ ft. . . .	180
59	Turbulence intensities, $U_{\infty} \approx 60$ ft/sec. $x = 80$ ft. . . .	181

LIST OF FIGURES - Continued

<u>Figure</u>		<u>Page</u>
60	\overline{uv}/U^2 distribution. $U_\infty \sim 60$ ft/sec. $x = 10$ ft.	182
61	\overline{uv}/U^2 distribution. $U_\infty \sim 60$ ft/sec. $x = 20$ ft.	183
62	\overline{uv}/U^2 distribution. $U_\infty \sim 60$ ft/sec. $x = 30$ ft.	184
63	\overline{uv}/U^2 distribution. $U_\infty \sim 60$ ft/sec. $x = 40$ ft.	185
64	\overline{uv}/U^2 distribution. $U_\infty \sim 60$ ft/sec. $x = 50$ ft.	186
65	\overline{uv}/U^2 distribution. $U_\infty \sim 60$ ft/sec. $x = 60$ ft.	187
66	\overline{uv}/U^2 distribution. $U_\infty \sim 60$ ft/sec. $x = 70$ ft.	188
67	\overline{uv}/U^2 distribution. $U_\infty \sim 60$ ft/sec. $x = 80$ ft.	189
68	Comparison of w-component of turbulence distributions along the boundary layer length.	190
69	Turbulence intensity distributions in the canopy flow field	191
70	Turbulent shear stress distribution. $U_\infty \sim 60$ ft/sec. $x = 10$ ft	192
71	Turbulent shear stress distribution. $U_\infty \sim 60$ ft/sec. $x = 20$ ft	193
72	Turbulent shear stress distribution. $U_\infty \sim 60$ ft/sec. $x = 30$ ft	194
73	Turbulent shear stress distribution. $U_\infty \sim 60$ ft/sec. $x = 40$ ft	195
74	Turbulent shear stress distribution. $U_\infty \sim 60$ ft/sec. $x = 50$ ft	196
75	Turbulent shear stress distribution. $U_\infty \sim 60$ ft/sec. $x = 60$ ft	197
76	Turbulent shear stress distribution. $U_\infty \sim 60$ ft/sec. $x = 70$ ft	198
77	Turbulent shear stress distribution. $U_\infty \sim 60$ ft/sec. $x = 80$ ft	199
78	Behavior of \overline{uv}/U_∞^2 along the boundary layer length . . .	200
79	Behavior of $\sqrt{\overline{u^2}}/U_\infty$ along the boundary layer length . .	201

LIST OF FIGURES - Continued

<u>Figure</u>		<u>Page</u>
80	Behavior of $\sqrt{v^2}/U_\infty$ along the boundary layer length. .	202
81	Behavior of $\sqrt{w^2}/U_\infty$ along the boundary layer length. .	203

LIST OF SYMBOLS

<u>Symbol</u>	<u>Definition</u>	<u>Dimensions</u>
A	Constant of heat-loss equation	
a	Constant	
B, B ₁	Constants of heat-loss equation	
b	Constant	
C	Constant	
C _r	Constant of roughness function	
c _f	Local skin-friction coefficient	
D	External diameter	L
D ₁	Constant	
d	Displacement	L
E	Mean voltage	V
E ₀	Mean voltage at zero velocity	V
e	Voltage fluctuation	V
$\overline{e^2}$	Mean square of voltage fluctuation	V ²
$\sqrt{\overline{e^2}}$	Root mean square of voltage fluctuation	V
F	Velocity function	
φ	Velocity function	
f	Velocity function	
G	Velocity function	
g	Velocity function	
H	Form factor	
h	Velocity function	
I	Electrical current	A
I ₁	Shape parameter	

LIST OF SYMBOLS - Continued

<u>Symbol</u>	<u>Definition</u>	<u>Dimensions</u>
K	Velocity function	
k_r	Roughness scale	L
L	Velocity function	
l	Velocity function	
m	Exponent	
P	Mean static pressure	M/LT ²
P_∞	Static pressure outside boundary layer	M/LT ²
q	Dynamic pressure	M/LT ²
R	Operating resistance of hot wire	Ω
R_a	Resistance of hot wire at room temperature	Ω
Re_θ	Reynolds number based on momentum thickness	
Re_δ	Reynolds number based on boundary layer thickness	
S_U	Sensitivity of voltage w.r.t. velocity	VT/L
S_V	Sensitivity of voltage w.r.t. angle	VT/L
S_w	Sensitivity of voltage w.r.t. angle	VT/L
U	Local mean velocity in x direction	L/T
U_a	Actual mean velocity in x direction	L/T
U_{eff}	Effective mean velocity	L/T
U_{TOT}	Total velocity	L/T
U_τ	Shear velocity	L/T
U_∞	Free stream velocity	L/T
u,v,w	Velocity fluctuations in x, y, z direction	L/T
$\sqrt{u^2}, \sqrt{v^2}$	Root mean square of velocity fluctuations	L/T
$\sqrt{w^2}$		

LIST OF SYMBOLS - Continued

<u>Symbol</u>	<u>Definition</u>	<u>Dimensions</u>
\overline{uv}	Time mean value of product u and v	L^2/T^2
\overline{uw}	Time mean value of product u and w	L^2/T^2
V	Local mean velocity in y direction	L/T
x	Distance along the wind tunnel center line downstream from the sawtooth fence	L
y	Distance normal to test section floor measured from the floor up	L
z	Distance normal to x-y plane measured from the wind tunnel center plane	L
β	Constant	
Δ	Length scale	L
Δh	Pressure difference	M/LT ²
δ	Boundary layer thickness	L
δ^*	Displacement thickness	L
ϵ_τ	Eddy viscosity	L^2/T
ζ	Angle of attack	
η	Nondimensional distance from wall	
θ	Momentum thickness	L
μ	Absolute viscosity	M/LT
ν	Kinematic viscosity	L^2/T
\square	Velocity function	
ρ	Mass density	M/L ³
τ	Shear stress	M/LT ²
τ_o, τ_w	Wall shear stress	M/LT ²
ϕ	Mean angle of hot wire with x coordinate in x-y plane	
ψ_1	Velocity function	

LIST OF SYMBOLS - Continued

<u>Symbols</u>	<u>Definition</u>	<u>Dimensions</u>
ψ_2	Velocity function	
ψ_{12}	Velocity function	
ψ	Mean angle of hot wire with x coordinate in x-z plane	
ω	Velocity parameter	

Chapter I

INTRODUCTION

Despite efforts of investigations over several generations, an adequate model for turbulence is not yet available. The statistical theory of turbulence which provides the basis for the study of turbulence, though successful, has been confined to homogeneous and isotropic turbulence. The lack of a satisfactory theory for turbulent shear flow description points to a semiempirical and phenomenological approach. The available mathematical methods are not sufficient to obtain a general solution of the Navier-Stokes equations. From the viewpoint of engineering application, one must believe that experimental results should be relied on whenever possible to acquire an insight and information for the basis of a theoretical approach.

This investigation deals with the thick boundary layer along a 90 foot long flat plate, with zero pressure gradient. The velocity profiles of the laminar boundary layer on a flat plate are similar at all stations along the plate. Since both laminar and turbulent boundary layers are subject to the same basic boundary layer concept, one can suspect that the similarity may be found in the turbulent boundary layer under certain conditions. The classical theoretical treatments by von Kármán (22) and Prandtl (38) and the experimental work of Elias (10) have assumed such a similarity. These treatments, however, covered only a narrow range of Reynolds numbers. Since then, quantitative measurements of the turbulent boundary layer have been made by many authors. Measurements by Klebanoff and Diehl (23) and recently by Tieleman (49) give experimental evidence which points out that local similarity exists

in a turbulent boundary layer with zero pressure gradient. A division of the turbulent boundary layer into two parts being admissible, it is assumed that, close to the wall, the velocity distribution is expressed by the law of the wall. The outer portion of the turbulent boundary layer, according to the general dimensional arguments, should follow the velocity defect law. As was shown particularly by Clauser (5), the velocity defect law collapses data onto a single curve quite satisfactorily.

However, presupposition of the existence of a universal function representing the mean velocity distribution imposes the conclusion that it cannot be singled out. Therefore, all mean quantities of the flow must be included in the similarity concept. Rotta (42) investigated the conditions required for similarity in the outer portion of the turbulent boundary layer. To obtain the required conditions, one has to introduce into the governing equation of motion the similarity forms of velocity and turbulent shear stress distribution. Rotta's investigations show that, for a turbulent boundary layer over a flat plate with zero pressure gradient, the ratio of shear velocity to free stream velocity must be a constant, and the displacement thickness of the boundary layer must vary linearly in the streamwise direction. He also demonstrated that an appropriate distribution of roughness may provide for the existence of conditions necessary for similarity. It should be pointed out at the outset that none of the similarity requirements is known to exist in the turbulent boundary layers. As has been mentioned, experimental data indicate similarity, although no one has attempted to prove the existence of the required conditions.

The present experiment was carried out in connection with a long-term project which had as its goal the modeling of atmospheric boundary layers in the wind tunnel. All experimental work was done in the large wind tunnel at Colorado State University and was supported by the Integrated Army Meteorological Wind Tunnel Research Program.

Chapter II

THEORETICAL BACKGROUND

2.1 Turbulent Boundary Layer

Since the time when the phenomenon occurring in the immediate neighborhood of a surface over which a certain fluid flows was observed and analyzed by Prandtl (37), the concepts of boundary layer phenomena have found application in a wide range of fields. As the flow in the boundary layer can be either laminar or turbulent, one must distinguish between laminar and turbulent boundary layers. Although both types of layer are subject to the same basic boundary layer concepts, the flat plate laminar boundary layer has been solved, but the turbulent boundary layer problem still remains to be solved.

In the turbulent boundary layer, the eddies introduce the turbulent shearing stress for which no reliable method of calculation exists. The two governing conditions for the boundary layer development are pressure gradient and surface roughness. These can be arbitrarily varied and thereby an infinite variety of boundary layers results. One has, therefore, to confine an investigation to some characteristic type of boundary layer. In this experiment the boundary layers developing on a smooth flat plate under a zero pressure gradient were investigated. Also, the following discussion is restricted to steady mean flow which deals with two-dimensional flows. Consequently, the Navier-Stokes equations reduce to:

$$U \frac{\partial U}{\partial x} + V \frac{\partial U}{\partial y} = \nu \frac{\partial^2 U}{\partial y^2} - \frac{\partial \overline{uv}}{\partial y} - \frac{\partial \overline{u^2}}{\partial x} - \frac{1}{\rho} \frac{\partial P}{\partial x} \quad (2-1)$$

$$\frac{\partial \overline{v^2}}{\partial y} = \frac{1}{\rho} \frac{\partial P}{\partial y} \quad . \quad (2-2)$$

The second equation can be directly integrated with respect to y (reference 42). When one differentiates the result with respect to x and introduces it into the first equation, the boundary layer equation for the mean flow is obtained:

$$U \frac{\partial U}{\partial x} + V \frac{\partial U}{\partial y} = - \frac{1}{\rho} \frac{dP_{\infty}}{dx} + \frac{\partial}{\partial y} (-\overline{uv} + v \frac{\partial U}{\partial y}) - \frac{\partial}{\partial x} (\overline{u^2} - \overline{v^2}) \quad . \quad (2-3)$$

In the case considered, the pressure gradient is zero; therefore equation (2-3) becomes

$$U \frac{\partial U}{\partial x} + V \frac{\partial U}{\partial y} = \frac{\partial}{\partial y} (-\overline{uv} + v \frac{\partial U}{\partial y}) - \frac{\partial}{\partial x} (\overline{u^2} - \overline{v^2}) \quad . \quad (2-4)$$

Equation (2-4), the momentum equation for the mean flow, describes the loss of momentum of the mean flow due to action of viscous stress and turbulent shear stress. This equation is used in combination with the continuity equation:

$$\frac{\partial U}{\partial x} + \frac{\partial V}{\partial y} = 0 \quad (2-5)$$

The boundary conditions are

$$\text{for } y = 0: \quad U = 0, \quad V = 0, \quad \overline{uv} = 0$$

$$\text{for } y \rightarrow \infty: \quad U = U_{\infty}, \quad \overline{uv} = 0.$$

In the system of equations (2-4) and (2-5), there are more unknowns than equations. The central problem is therefore to find additional relations in which the Reynolds stresses are related to the mean flow properties. Quite a few attempts have been made and a number

of hypothetical relations were proposed. However, one can say that a satisfactory solution to this problem has not yet been obtained.

Close examination of the turbulent boundary layer reveals a characteristic which allows division of the turbulent boundary layer into two parts. These parts can then be analyzed separately. It is an established fact that the total processes in the turbulent boundary layer are affected by the kinematic viscosity and wall roughness only in a very thin region in the neighborhood of the wall. In the remaining part of the boundary layer, the flow appears to be practically independent of the viscosity and the wall roughness. Consequently, this viscous sublayer being very thin, one should expect a velocity law to be affected only by viscosity and geometrical properties of the wall.

These assumptions make the separation of the influence of the viscosity and geometrical properties of the wall from the other influences possible. Thereby, one may assume the conditions in the viscous sublayer to be practically independent of the other flow conditions at the outer edge of the boundary layer. It then becomes possible to discuss various properties of the turbulent boundary layers. Furthermore, with the aid of similarity relations and experimental measurements, quantities needed may be determined for the development of approximate methods for calculation of turbulent boundary layers.

2.2 Law of the Wall

This investigation is concerned with measurements and similarity considerations of the outer portion of the turbulent boundary layer; however, it is necessary to inspect briefly the flow near the wall. This is necessary because the law of the wall and similarity considerations of the whole boundary layer are interconnected, as will become obvious from further analysis.

The law of the wall, attributed to Prandtl (39), pertains to the region close to the wall where viscosity effect is directly felt. The law is based on the assumption that the shear stress at the wall, τ_w , depends on velocity U at distance y from the wall, and on viscosity and density. Therefore, the relation may be written in the following general form:

$$F(\tau_w, U, y, \mu, \rho) = 0 \quad (2-6)$$

which can be expressed nondimensionally:

$$\frac{U}{U_\tau} = f\left(\frac{U_\tau y}{\nu}\right) \quad (2-7)$$

which is consistent with the earlier assumption that in the viscous sublayer the flow is determined by the conditions at the wall and is independent of the conditions existing at the outer edge of the boundary layer. The experimental evidence supports this conclusion (23,33,36,49). An examination of the momentum equation also supports the division of the boundary layer into two parts. Namely, very near the wall, $V \approx 0$; therefore, according to the continuity equation (2-4), $\frac{\partial U}{\partial x}$ also has to be very small. On the other hand, the viscous shear and the turbulent shear stress experience great changes in the same region as was shown by Tieleman (49). This leads to the assumption that for the considered part of the boundary layer one can write

$$\nu \frac{\partial^2 U}{\partial y^2} - \frac{\partial \overline{uv}}{\partial y} = \frac{1}{\rho} \frac{\partial \tau}{\partial y} \approx 0 \quad (2-8)$$

i.e., total shear stress in this region is constant, and since \overline{uv} goes to zero at the wall it is equal to the wall shear stress.

One integration gives

$$\nu \frac{\partial U}{\partial y} - \overline{uv} = \frac{1}{\rho} \tau \approx \frac{1}{\rho} \tau_w \quad (2-9)$$

Now if one takes equation (2-1), and if the term $\frac{\partial \overline{u^2}}{\partial x}$ is neglected on the basis of experimental evidence (43), it shows that normal turbulent stress terms in the equation of motion are an order of magnitude smaller than the other terms in equation (2-1). One obtains

$$U \frac{\partial U}{\partial x} + V \frac{\partial U}{\partial y} = \nu \frac{\partial^2 U}{\partial y^2} - \frac{\partial \overline{uv}}{\partial y} = \frac{1}{\rho} \frac{\partial \tau}{\partial y} \quad (2-10)$$

Introducing the law of the wall into equation (2-10), one obtains

$$\mu \frac{\partial U}{\partial x} \tau [f^2 - f'] \int_0^{\frac{\eta \nu}{U}} \tau f d\eta' = \frac{\partial \tau}{\partial \eta} \quad (2-11)$$

where $\eta = yU_\tau/\nu$ (reference 45).

If the law of the wall is to be a similarity law for the region near the wall, then equation (2-11) has to be independent of the x coordinate. Therefore $\partial U_\tau/\partial x$ must be constant. Now, if the outer portion of the turbulent boundary layer similarity condition (to be separately discussed later on), $U_\tau = \text{constant}$ is imposed, one obtains the same result as in equation (2-9). So there must exist a region of constant shear stress where the law of the wall is the similarity law. This is, therefore, one of the specific conditions which must be met to have similarity in the turbulent boundary layer. Division of the turbulent boundary into two parts being accepted, one can not expect to be able to represent the similarity form for the distribution of mean velocity of the whole boundary layer by a single universal function. As was shown, the similarity law in the viscous sublayer is the law of the wall, and experimental evidence supports this analysis.

One has to consider the outer portion of the turbulent boundary layer too. This is done in order to find out what the conditions of similarity are in the region which does not feel the effect of viscosity directly.

2.3 Outer Portion of the Turbulent Boundary Layer

The outer portion of the turbulent boundary layer is by far the larger of the two regions into which the boundary layer was at the outset divided. However, a large portion of the change in velocity from zero at the wall to the free stream velocity at the outer edge of the boundary layer takes place in the viscous sublayer. The momentum transport in the sublayer is constant while in the outer portion of the boundary layer the situation is different. If the turbulent shear stress is expressed by introducing the Boussinesq's concept of a turbulent exchange coefficient ϵ_{τ}

$$-\overline{\rho uv} = \rho \epsilon_{\tau} \frac{\partial U}{\partial y} \quad (2-12)$$

then the momentum transport of the outer portion corresponds to ϵ_{τ} , this coefficient of proportionality being called the "eddy viscosity." The ratio of kinematic viscosity and the eddy viscosity changes with change of Reynolds number based on the boundary layer thickness. This change consequently produces the change of the velocity profile. Therefore, the behavior of the turbulent boundary layer is quite different from the behavior of the laminar boundary layer. One concludes that the similarity of the velocity profile of the turbulent boundary layer will, accordingly, be of a more complex nature. One has to assume that there are no severe obstacles or disturbances if a similarity is to be expected in the velocity profile. The boundary layer should have

normal development and one should be able to describe the velocity profile by the local conditions.

2.3.1 The velocity defect law - The general dimensional arguments and experimental evidence indicate that in the outer portion of the turbulent boundary layer the similarity law is the velocity defect law. The general form of the velocity defect law was formulated by von Kármán (21).

In the preceding section it was stated that the boundary layer considered should have normal development, and the absence of any severe obstacles or disturbances was assumed. In such a case, considering also what was said before, i.e., that the turbulent boundary layer along the flat plate with the zero pressure gradient is investigated, it is experimentally justified to assume similarity of the velocity profile. This means that the mean velocity distribution $U(y)$, at any station along the plate, depends only on four parameters. These are: free stream velocity U_∞ , thickness of the boundary layer δ , kinematic viscosity ν , and the length scale of the surface roughness distribution k_r . Thus, the general form of the relationship would be

$$f(U, y, U_\infty, \delta, \nu, k_r) = 0 \quad (2-13)$$

This form can be rewritten in nondimensional form,

$$\frac{U}{U_\infty} = G\left(\frac{y}{\delta}, \frac{U_\infty \delta}{\nu}, \frac{U_\infty k_r}{\nu}\right) \quad (2-14)$$

If equation (2-13) is considered together with equation (2-7), i.e., with the law of the wall, then the shear velocity U_τ is introduced

$$U_\tau = \sqrt{\frac{\tau_w}{\rho}} \quad (2-15)$$

and the velocity distribution can be better specified since the following relation is implied:

$$g(U_\tau, V_\infty, \delta, \nu, k_r) = 0 . \quad (2-16)$$

Equations (2-16) and (2-13) may be used to eliminate U_∞ and replace (2-13) with

$$h(U, y, U_\tau, \delta, \nu, k_r) = 0 \quad (2-17)$$

which may be nondimensionalized as

$$\frac{U}{U_\tau} = H\left(\frac{yU_\tau}{\nu}, \frac{y}{\delta}, \frac{k_r U_\tau}{\nu}\right) . \quad (2-18)$$

This form in the region near the wall yields the similarity form for the case when geometrically similar roughnesses are considered. In other words, when $y \rightarrow 0$, equation (2-18) becomes

$$\frac{U}{U_\tau} = f\left(\frac{yU_\tau}{\nu}, \frac{k_r U_\tau}{\nu}\right) \quad (2-19)$$

which is the expanded law of the wall (42). To obtain the velocity defect law for the outer portion of the turbulent boundary layer, one has to inspect equations (2-16) and (2-17); this implies that one can write

$$l(U_\infty - U, y, U_\tau, \delta, \nu, k_r) = 0 . \quad (2-20)$$

Rotta (42) argues that beyond the sublayer $U_\infty - U$ is dependent on ν and k_r , only as far as through equation (2-16); there is a functional relation between $U_\tau, U_\infty, \delta, \nu$ and k_r . Therefore equation (2-20) becomes

$$L(U_\infty - U, y, U_\infty, U_\tau, \delta) = 0 \quad (2-21)$$

or in nondimensional form

$$\frac{U_{\infty} - U}{U_{\tau}} = \phi\left(\frac{y}{\delta}, \frac{U_{\tau}}{U_{\infty}}\right) \quad (2-22)$$

This universal velocity defect law extends into the region of the wall flow. Likewise, the law of the wall validity extends into the outer portion of the turbulent boundary layer. Thus, an overlap region exists where the law of the wall and the velocity defect law are valid simultaneously, as will be shown in the next paragraph.

2.3.2 The logarithmic region - An argument leading to the logarithmic form for the function f in equation (2-7) was given by Millikan (32). This argument is based on the law of the wall and the velocity defect law. Namely, from the law of the wall, differentiating with respect to y coordinate, one obtains, if the result is multiplied by y :

$$\frac{y}{U_{\tau}} \frac{\partial U}{\partial y} = \frac{yU_{\tau}}{\nu} f' \quad (2-23)$$

where prime denotes derivative with respect to y .

In the same manner from the velocity defect law one obtains

$$\frac{y}{U_{\tau}} \frac{\partial U}{\partial y} = -\frac{y}{\delta} \phi' \quad (2-24)$$

One can here assume ϕ to be a function of y/δ only, for flows satisfying the similarity conditions. If the existence of a region is now supposed, where the law of the wall and velocity defect law are valid simultaneously, equations (2-23) and (2-24) may be equated:

$$\frac{yU_{\tau}}{\nu} f' = -\frac{y}{\delta} \phi' = \frac{y}{U_{\tau}} \frac{\partial U}{\partial y} \quad (2-25)$$

Variables involved here are formally independent. Thus, their ratio may be chosen arbitrarily. It means that the expression (2-25) has to be equal to a constant, say $1/k$. Therefore, by integrating over this region it is found that

$$f\left(\frac{yU}{\nu}\right) = \frac{1}{k} \ln \frac{yU}{\nu} + \text{constant.} \quad (2-26)$$

Thus, this is an important consequence of the law of the wall and the velocity defect law in turbulent boundary layers where the similarity conditions are at least closely approached.

2.3.3 Contemporary treatments of the outer portion of the turbulent boundary layer - Until recently, no theories which would be equivalent to those for the viscous sublayer existed for the velocity distribution in the outer portion of the turbulent boundary layers. As has been shown, similarity laws for the boundary layers in question are the law of the wall in the viscous sublayer, and the velocity defect law in the outer portion of the turbulent boundary layer. Several authors (5, 42, 46, 49) have shown that, since the overlap region for these two laws exists, the functions f and ϕ in equations (2-7) and (2-22) respectively must be logarithmic. However, to be more specific they have the logarithmic form where they overlap, but not necessarily much beyond this region. Proposed extensions to the law of the wall will be considered herein. As two comprehensive approaches to the problem, Clauser's (5) and Cole's (6) treatments are briefly considered, since they are too extensive to be covered in detail.

Clauser (5) considered the outer 80 to 90 percent of the turbulent boundary layer. He used a new conceptual approach by making the laminar velocity profiles resemble the outer portion of the constant

pressure turbulent boundary layer velocity profile. The basis of his analysis was the universal plot of turbulent boundary layer velocity profiles at constant pressure in coordinates $U-U_\infty/U_\tau$ and y/δ . Clauser noted that the main difference in the shape of the constant pressure laminar velocity profiles and turbulent velocity profiles is that the turbulent profiles drop abruptly at the wall. The laminar velocity profiles approach zero gradually. Clauser observed that turbulent velocity profiles drop so abruptly that they extrapolate to non-zero velocity at the wall. The large change of velocity from the wall to the free stream velocity in the turbulent boundary layer occurs in the viscous sublayer. The same conditions would exist in a laminar boundary layer if a layer of fluid having a lower kinematic viscosity were to be placed adjacent to the wall. Clauser simulated this condition for laminar velocity profiles by solving the Blasius equation for slip velocities at the wall. He used different slip velocity to free stream velocity ratios and then collapsed this family to a single curve. The family of profiles obtained was collapsed on a single curve by dividing the $U-U_\infty/U_\tau$ and y/δ by suitable factors. He then related the laminar profiles to the turbulent profiles on the basis of the velocity defect law by an eddy viscosity which he assumed to be constant in the outer portion of the turbulent boundary layer. He obtained an almost universal curve which is in very good agreement with experimental data for the outer 80 to 90 percent of the boundary layer.

A similar treatment by Clauser (5) and Stratford (48) applies to the equilibrium layers with adverse pressure gradients. However, since the current experiment involves zero pressure gradient it will not be reviewed here.

Coles (6) started his investigation with a very extensive study of all available mean velocity profile measurements in various two-dimensional incompressible turbulent boundary layers. He accepted the law of the wall and then inquired about the information necessary to establish the velocity defect law.

Inspecting the mean velocity profiles of wide variation in environment, he decided not to try to determine the nature of the function ϕ , equation (2-22); but to find a function which would give the departure of the mean velocity profile from the logarithmic law of the wall. To begin with, he assumed that the mean velocity profile may be written in the form

$$\frac{U}{U_\tau} = f\left(\frac{yU_\tau}{\nu}\right) + \frac{\Pi}{k} w\left(\frac{y}{\delta}\right) \quad (2-27)$$

where Π is a profile parameter and $w(y/\delta)$ is a function supposedly common to all two-dimensional turbulent boundary layer flows. The function $w(y/\delta)$ is, therefore, by hypothesis a universal function, and is called the law of the wake. Since the departure of the mean velocity profile is not confined to equilibrium flows, Coles assumed the parameter Π to be a function of x .

Analyzing the experimental data, Coles found the form of $w(y/\delta)$, and using the normalizing conditions $w(0) = 0$, $w(1) = 2$, and $\int_0^2 y/\delta dw = 1$ he was able to tabulate the values of $w(y/\delta)$ as a function of y/δ . The equation of Coles (2-27) may be rewritten as

$$\frac{U}{U_\tau} = \frac{1}{k} \ln\left(\frac{yU_\tau}{\nu}\right) + C + \frac{\Pi(x)}{k} w\left(\frac{y}{\delta}\right) \quad (2-28)$$

where k and C have numerical values. Regarding the equation as a working form of equation (2-27) it is necessary to know $\Pi(x)$. Coles

obtained an expression for $\Pi(x)$ in terms of skin friction coefficient c_f . To test his hypothesis, he fitted the available experimental data on velocity distribution using the equation (2-28), and found that for unseparated flows the computed distributions represented observations well. It is not uncommon to find that the empirical formulas fit well the experimental results. However, it should be pointed out that equation (2-28) stands the test of wide variety of conditions but fails at the separation. As Coles himself states, the basis for his investigation from which the concept of the law of the wake resulted, was the work of Clauser (5). However, it is obvious that all his results stem from empirical data through analysis and observations.

It is necessary to note also the work of Mellor and Gibson (29). The work of these authors is an extension of the work of Clauser (5) and Townsend (50), i.e., they hypothesize eddy viscosity. On the basis of eddy viscosity information extracted from constant pressure flows, a family of velocity defect profiles are calculated for the range of equilibrium boundary layer parameter β , as proposed by Clauser $\beta = \frac{\delta^*}{\tau_0} \frac{dP}{dx}$. In his later work, Mellor (31) extended the work reported in reference (29), and applied the effective viscosity hypothesis to turbulent boundary layers with arbitrary pressure gradients. In both cases the hypothesized eddy viscosity is the basis for the numerical solution of the mean differential equation of motion. This method has been checked against the experimental data from the large wind tunnel at Colorado State University. It was found that the agreement is fairly good.

It should be noted here that all the mentioned approaches to treatment of the outer portion of the turbulent boundary layers are

based on the similarity concept expressed as the velocity defect law. Methods are deduced and the authors' discussion of the results and observed facts indicate some of the conditions necessary for existence of similarity. However, no one asks the question about the conditions to be fulfilled in the first place if similarity is to be expected. In the next section the similarity conditions for the turbulent boundary layer will be considered. However, the case of zero pressure gradient and the flow along the flat plate as pertinent to this experiment will be the type of turbulent boundary layer subject to this consideration.

2.4 Conditions for Local Similarity in the Turbulent Boundary Layer

In the first sections of this Chapter the viscous sublayer of the turbulent boundary layer was briefly considered. The examination of the governing equations of motion by introduction of the law of the wall was made. It has been shown that the existence of a constant shear stress region is required where similarity of the form

$$\frac{U}{U_{\tau}} = f\left(\frac{yU_{\tau}}{\nu}\right) \quad (2-7)$$

is to be expected.

Regarding the outer portion of the turbulent boundary layer, the preceding section shows that the existence of local similarity is indicated by experiment. Also Clauser(5) established that similarity in the form of a velocity defect law exists within the experimental precision. However, one has to examine the conditions under which this similarity is justified from the theoretical viewpoint. The similarity requirements were first investigated by Rotta (42). The requirement for similarity in the viscous sublayer was experimentally investigated by Tieleman (49), and its existence well established for high Reynolds

number boundary layers. This being the case in the current experiment, the consideration of similarity conditions here will be confined to the outer portion of the turbulent boundary layer. The aim is to find the conditions under which the generally accepted form of similarity, namely the velocity defect law, is compatible with the governing equations of motion.

However, if the existence of a universal function representing the mean velocity distribution is accepted, this imposes the conclusion that similarity can not be confined to the mean velocity profile. Therefore, all mean quantities of the flow must be included in the similarity concept. This means that one should be able to express nondimensionally the variation of any mean quantity of the flow at any station along the x-axis. This involves a corresponding scale for length and velocity, and the resulting expression will be a universal function of the nondimensional distance from the wall. The only quantities which are excluded are those which are directly affected by viscosity.

The velocity defect law could be checked simply by plotting $U_\infty - U/U_\tau$ versus y/δ , as is done by many authors. However, the boundary layer thickness δ cannot be exactly defined. Rotta (41) proposed for the length scale δ^*U_∞/U_τ , where δ^* is computed from

$$\delta^* = \int_0^\infty \left(1 - \frac{U}{U_\infty}\right) dy . \quad (2-29)$$

For the velocity profile given by equation (2-22), one obtains

$$\frac{\delta^*U_\infty}{\delta U_\tau} = \int_0^\infty \phi d\left(\frac{y}{\delta}\right) ; \quad (2-30)$$

therefore, δ is proportional to $\delta^* U_\infty / U_\tau$. Denoting $\delta^* U_\infty / U_\tau = \Delta$, and $U_\tau / U_\infty = \omega$, so U is the velocity scale, the velocity defect law can be written as

$$U = U_\infty - U_\tau F(\eta, \omega) \quad (2-31)$$

where $\eta = y/\Delta$. The similarity forms for Reynolds stresses would then be

$$\overline{u^2} = U_\tau^2 \psi_1(\eta, \omega) \quad (2-32)$$

$$\overline{v^2} = U_\tau^2 \psi_2(\eta, \omega) \quad (2-33)$$

and

$$-\overline{uv} = U_\tau^2 \psi_{12}(\eta, \omega). \quad (2-34)$$

To test the compatibility of the similarity concept of the outer portion of the turbulent boundary layer, the similarity forms for the velocity defect law and Reynolds stresses have to be introduced into the governing equations of motion. For the case considered we have $dP_\infty/dx = 0$, and the viscosity term in the equation (2-4) becomes negligible in the outer portion of the boundary layer, so the equations (2-4) and (2-5) become

$$U \frac{\partial U}{\partial x} + V \frac{\partial U}{\partial y} = \frac{\partial}{\partial y} (-\overline{uv}) - \frac{\partial}{\partial x} (\overline{u^2} - \overline{v^2}) \quad (2-35)$$

$$\frac{\partial U}{\partial x} + \frac{\partial V}{\partial y} = 0. \quad (2-36)$$

The expressions for flow quantities are given as functions of the variables η and ω . Therefore, the relation between the differential quotients must be found. Rotta (42) argues that to obtain

simple solutions one should discuss only the solutions for which all derivatives of the universal functions, with respect to ω , are negligible. One should point out that these experiment data show that the

($C_f = \text{Const}$) ratio of U_τ to free stream velocity U_∞ is very nearly constant.

Thus, applying the above assumption, one obtains differential quotients as follows:

$$\frac{\partial}{\partial x} = \frac{d}{d\eta} \frac{d\eta}{dx} \quad \text{where} \quad \frac{d\eta}{dx} = -\eta \frac{1}{\Delta} \frac{d\Delta}{dx}$$

or finally

$$\frac{\partial}{\partial x} = -\eta \frac{1}{\Delta} \frac{d\Delta}{dx} \frac{d}{d\eta} \quad (2-37)$$

and in the same manner

$$\frac{\partial}{\partial y} = \frac{1}{\Delta} \frac{d}{d\eta} \quad (2-38)$$

The vertical component of the mean velocity is calculated from the equation of continuity (2-36). Applying equation (2-37) to equation (2-31), one obtains

$$\frac{\partial U}{\partial x} = \eta \frac{d\Delta}{dx} \frac{1}{\Delta} \frac{dF}{d\eta} U_\tau + \eta \frac{d\Delta}{dx} \frac{1}{\Delta} \frac{dU_\tau}{d\eta} F. \quad (2-39)$$

Therefore, since equation (2-39) can also be written as

$$\frac{\partial U}{\partial x} = -\frac{\partial U_\tau}{\partial x} F + U_\tau \eta \frac{d\Delta}{dx} \frac{1}{\Delta} \frac{dF}{d\eta} \quad (2-40)$$

and

$$\frac{\partial U_\tau}{\partial x} = \frac{dU_\tau}{dx}, \quad \text{denoting} \quad \frac{dF}{d\eta} = F' \quad \text{one obtains the expression}$$

$$V = \Delta \frac{dU_\tau}{dx} \int_0^\eta F d\eta_1 + U_\tau \frac{d\Delta}{dx} \int_0^\eta F' \eta_1 d\eta_1. \quad (2-41)$$

Integrating the second term on the right hand side by the chain rule, and supposing that $F\eta \rightarrow 0$ when $\eta \rightarrow 0$ which follows from

$$\frac{U_\infty - U_\tau}{U_\tau} = -\frac{1}{k} \ln \frac{yU_\tau}{\delta^* U_\infty} + K \left(\frac{U_\tau}{U_\infty} \right) \quad (2-42)$$

as obtained by Rotta (42), the final expression for the vertical component of the mean velocity is obtained as

$$V = \left(\Delta \frac{dU_\tau}{dx} + U_\tau \frac{d\Delta}{dx} \right) \int_0^\eta F d\eta_1 - U_\tau \frac{d\Delta}{dx} F\eta . \quad (2-43)$$

Substituting equation (2-43) and $\partial U / \partial y = -U_\tau \frac{1}{\Delta} F'$ into equation (2-35), along with the expressions for the right hand side of the same equation (the latter obtained from equations (2-32), (2-33) and (2-34))

$$\frac{\partial(-\overline{uv})}{\partial y} = \frac{U_\tau^2}{\Delta} \psi'_{12}$$

$$\frac{\partial \overline{u^2}}{\partial x} = 2U_\tau \frac{dU_\tau}{dx} \psi_1 + \eta \frac{U_\tau^2}{\Delta} \frac{d\Delta}{dx} \psi'_1 \quad (2-44)$$

$$\frac{\partial \overline{v^2}}{\partial x} = 2U_\tau \frac{dU_\tau}{dx} \psi_2 + \eta \frac{U_\tau^2}{\Delta} \frac{d\Delta}{dx} \psi'_2 ,$$

one obtains

$$\begin{aligned} & (U_\infty - U_\tau F) \left(\eta \frac{d\Delta}{dx} \frac{1}{\Delta} F' U_\tau - \frac{dU_\tau}{dx} F \right) + (-U_\tau \frac{1}{\Delta} F') \left(\Delta \frac{dU_\tau}{dx} + U_\tau \frac{d\Delta}{dx} \right) \int_0^\eta F d\eta_1 - \\ & - U_\tau \frac{d\Delta}{dx} F\eta = U_\tau^2 \frac{1}{\Delta} \psi'_{12} - \left(2U_\tau \frac{dU_\tau}{dx} \psi_1 + \eta \frac{U_\tau^2}{\Delta} \frac{d\Delta}{dx} \psi'_1 - 2U_\tau \frac{dU_\tau}{dx} \psi_2 + \eta \frac{U_\tau^2}{\Delta} \frac{d\Delta}{dx} \psi'_2 \right) . \end{aligned} \quad (2-45)$$

If equation (2-45) is divided by U_∞^2 , and recalling that

$$w = \frac{U_\tau}{U_\infty} , \quad \frac{dw}{dx} = \frac{1}{U_\infty} \frac{dU_\tau}{dx} , \quad (2-46)$$

one finally obtains

$$\begin{aligned} & \omega(\eta - \omega \int_0^\eta F d\eta_1) F' \frac{d\Delta}{dx} - [F - \omega(F^2 - F' \int_0^\eta F d\eta_1)] \Delta \frac{d\omega}{dx} = \\ & = \omega^2 \psi'_{12} - 2\omega \frac{d\omega}{dx} (\psi_1 - \psi_2) + \omega^2 \frac{d\Delta}{dx} \eta (\psi'_1 - \psi'_2) . \end{aligned} \quad (2-47)$$

The boundary conditions for the function $F(\eta)$ are

$$\text{for } \eta \rightarrow \infty, \quad F(\infty) = F'(\infty) = 0 \quad (2-46a)$$

and since

$$\begin{aligned} \Delta &= \int_0^\infty \frac{U_\infty - U}{U_\tau} dy = \int_0^\infty \Delta F d\eta \\ \int_0^\infty F d\eta &= 1 . \end{aligned} \quad (2-47a)$$

For similarity in the x direction, equation (2-47) must be independent of the x coordinate. This is the case if

$$\omega = \text{constant}; \quad \frac{d\omega}{dx} = 0 \quad (2-48)$$

and Δ is a linear function of x , $\frac{d\Delta}{dx} = \text{constant}$.

The conditions (2-48) imply that

δ^* is a linear function of x
and $\frac{U_\tau}{U_\infty} = \text{constant}$; therefore $\tau_\omega = \text{constant}$,
since in the case considered the free stream velocity U_∞ and density ρ are constants. Further, since

$$\frac{2d\theta}{dx} = \frac{\tau_\omega}{\rho U_\infty^2} = \text{constant}, \quad (2-49)$$

the momentum thickness θ has also to be a linear function of x .

And finally, the form factor $H = \delta^*/\theta$ has to be constant in the

$$\frac{1}{\omega} = \frac{1}{k} \ln \frac{\Delta}{k_r} + C_r + K(\omega) \quad ; \quad (2-55)$$

therefore, ω would be constant for a constant ratio $\frac{\Delta}{k_r}$. As will be seen from the results of this experiment, even though the flat plate over which the turbulent boundary layer was developed is smooth, ω was very nearly constant for the whole length of the boundary layer. However, this will be discussed in the Chapter V.

2.5 Distribution and Order of Magnitude of the Individual Terms in the Momentum Equation of the Mean Flow

Equation (2-4) is called the momentum equation for the mean flow. Its terms describe the loss of momentum of the mean flow by the action of Reynolds and viscous stresses, since in the case of this experiment the pressure gradient is zero. The last term on the right hand side is usually neglected. This has been already mentioned in the preceding section; $\frac{\partial}{\partial x} (\overline{u^2 - v^2})$, as justified by experimental evidence, may be neglected, being much smaller than the other terms. Evaluation and analysis of the mean and turbulent terms in the equations of motion in a turbulent boundary layer have been done by Sandborn and Slogar (43). They investigated turbulent boundary layers in adverse pressure gradients. Their investigation included all terms of the equations (2-1, 2-2). The results show that it is justified to neglect terms not included in the equation (2-2). The distribution of terms appearing in the equations of motion was presented by Sandborn and Slogar (43) in nondimensional form, and the experimental difference between the left- and right-hand sides of the equation of motion was indicated. This difference is attributed mainly to uncertainty in determination of $U \frac{\partial U}{\partial x}$. Even so, agreement is very good, indicating that experimental

evaluation is a reliable approach to the problem. Of special importance is the insight into the distribution of the turbulent shear stress.

Turbulent velocities appear only in the energy equation if the term

$\frac{\partial}{\partial x} (\overline{u^2} - \overline{v^2})$ is neglected and the equation (2-51) is considered.

Chapter III

INSTRUMENTATION AND EXPERIMENTAL FACILITIES

The investigation was conducted in the U.S. Army Meteorological Wind Tunnel of the Fluid Dynamics and Diffusion Laboratory at Colorado State University. The purpose of this experimental work was to study the outer portion of a thick boundary layer, and to survey its development along the boundary layer length. The instrumentation, experimental facilities, and procedures used will be described and discussed in this chapter. The description and technical data of the commercial instruments which have been used during the experiment, are presented in Appendix A.

3.1 Wind Tunnel Facility

All mean velocity and turbulence measurements were taken in the thick turbulent boundary layer developed along the floor of the test section of the U.S. Army Meteorological Wind Tunnel (Figure 2). This facility is described by Plate and Cermak (35) in detail. The boundary layer is developed along the 80 foot long test section. The cross section of the test section is 6 x 6 feet. The first 40 feet of the floor are plywood and the rest is a 40 feet long aluminum plate. It is possible to heat or cool the aluminum plate. However, this was not done; only the cooling of the air stream was utilized in order to hold the ambient temperature constant. The wind tunnel is of the recirculating type with speed controlled by means of a variable speed, variable pitch propeller, and the temperature of the air is controlled by an air conditioning system.

As was mentioned above, the turbulent boundary layer investigated was 80 feet long and its thickness varied up to approximately 2 feet. To traverse the length and thickness of the boundary layer with probes the wind tunnel carriage was employed. The carriage moves along the wind tunnel on rails which are fixed to the vertical walls of the wind tunnel. The carriage boom, intended for mounting of probes and instrumentation, has independent movements, east-west and up-down. In this experiment only the up-down movement was used. A special probe carrier was designed and attached to the carriage boom. The wind tunnel carriage is provided with a remote control. The carriage movement is controlled by an outside control box, and the position of the carriage boom is determined from the output of potentiometers which are arranged for each separate movement. The power is supplied to the carriage by a 28 volt source.

Measurements were taken at 8 stations at 10 foot intervals along the test section, the first station being at 10 feet from the saw tooth fence which artificially trips the boundary layers along the tunnel walls. The saw tooth fence is preceded by four feet of 1/2 inch gravel fastened on the tunnel perimeter. The gravel and saw tooth section are at the entrance of the test section (Figure 1). This arrangement thickens the boundary layer. Furthermore, it provides the advantage of having the longest possible period of turbulence development toward the equilibrium.

In order to obtain a condition of zero pressure gradient, the tunnel ceiling was adjustable. The typical final pressure distribution employed is shown in Figure 3.

The turbulence level in the free stream is low, due to damping screens and entrance contraction. The free stream turbulence was measured at the entrance of the testing section. The measurement covers the range of used air stream velocities and the result is shown in Figure 4. The coordinate system used was so oriented that its x-axis was the center line of the tunnel floor, the y-axis was vertical to the tunnel floor, and the z-axis was normal to the tunnel centerline with positive direction westward. The origin of the system was the intersection of tunnel floor centerline and saw tooth fence at the test section entrance.

3.2 Instruments

3.2.1 Pitot static tube - The free stream velocity and mean velocity measurements were made with 0.125 inch diameter Pitot static tube (Figure 5). The Pitot static tube which was used throughout the entire experiment has been previously subjected to an elaborate calibration by Tieleman (49). This was done to obtain a Pitot static tube which can be used as a laboratory standard. The results of these calibrations show that the velocity head measured by this Pitot static tube needed a correction of 1.73%. Therefore, this correction factor was incorporated in the mean velocity formula.

3.2.2 Hot-wire probe actuator and carrier - Turbulence measurements in this experiment required covering of the full length of the Wind Tunnel. Also, it was necessary to move the probes in the vertical direction through the boundary layer. Since a rotating hot-wire was to be used, this movement also had to be provided. It was, therefore, necessary to develop special actuating equipment. Probes had to be moved approximately 80 feet along the tunnel, about 2 feet

in a vertical direction at each station, and the hot-wire had to be rotated at each chosen point.

The existing carriage of the wind tunnel provided the longitudinal and vertical movements. However, the necessary rotation of the hot-wire probe imposed an additional problem. To insure proper and reliable measurements a special probe carrier was designed (Figure 5). The carrier was designed so as to become a corporate part of the wind tunnel carriage. It consisted of a heavy gauge aluminum plate fixed to the wind tunnel carriage boom, hot-wire probe carrier boom, and hot-wire actuator.

The hot-wire probe holder was placed into a receptacle at the end of the hot-wire probe carrier boom, and the hot-wire probe was connected to the actuator motor by way of a flexible shaft. This arrangement provided for the necessary rotation of the hot-wire probe. The probe actuator consisted of the low-speed motor, a flexible shaft, and a potentiometer. The flexible shaft allowed the vertical adjustment of the hot-wire probe in order to bring the probe as near as possible to the wall. The low-speed motor provided the rotation of the hot-wire. The position of the hot wire was determined from the output of the potentiometer coupled to the low-speed motor through a set of gears.

The hot-wire probe carrier was designed in such a way that it was possible to place probes crosswise to the flow, and in the streamwise position as well. This was achieved by the ability to mount the hot-wire carrier boom and the low-speed motor in two positions with respect to the hot-wire probe carrier plate. In the crosswise to the flow position the hot-wire was rotated in the $x-y$ plane, and in the

streamwise position the rotation of the hot wire was in the x-y plane. The position of the hot-wire probe carrier with respect to the wind tunnel carriage is shown in Figures 6 and 7.

The vertical position of the hot wire was determined from the output of the potentiometer on the wind tunnel carriage boom. This potentiometer was connected through a gear to the gear rack fixed to the wind tunnel carriage frame. The position of the hot wire with respect to the x-axis was determined by the measured stations marked on the wind tunnel carriage rails.

To assure the reliable and non-drifting readings of the output of the potentiometer, the wind tunnel carriage was rewired so that a stable constant voltage source could be used. As a constant voltage source for the potentiometers an H Lab Model 6226A Power Supply was used. During the experiment the voltage of this power supply was monitored by a Hewlett-Packard 3440A Digital Voltmeter.

3.2.3 Hot-wire probes - In all turbulence and turbulent shear stress measurements the hot-wire technique was used. The hot wire was operated by a constant temperature hot-wire anemometer designed at Colorado State University (11). A rotating single wire was used. The streamwise velocity fluctuation, $\sqrt{u'^2}$, was measured with hot-wire positioned perpendicular to the tunnel floor. Since the wire could be rotated 360° in the x-y plane, it was possible to check the influence of wire position on the measurements. The wire used was platinum coated tungsten with a diameter of 0.0002 inch. A wire approximately 0.05 inch long was soldered to supports protruding from the 3/32 inch diameter ceramic probe. The ceramic probe was held by the sliding bearings of the hot-wire probe holder, which in turn was mounted on the hot-wire

carrier. The hot-wire carrier provided for alignment of the hot-wire and probe with the tunnel axes. The ceramic probe was fitted with a coupling at the end opposite to the hot wire. By means of this coupling and a flexible shaft, the hot wire-probe was connected to the low-speed electric motor. The low-speed electric motor provided the movement of the rotating wire. The position of the wire was determined from the output of a potentiometer which was rotated simultaneously with the hot wire through the connecting gears. The hot-wire probes are shown in Figure 8; the hot-wire probe mounted on the carrier is shown in Figures 6 and 7.

For the streamwise velocity fluctuation and the turbulent shear stress measurements, a hot wire soldered perpendicular to its supports was used. In the measurements of the lateral velocity fluctuation, $\sqrt{w'^2}$, an inclined hot wire was used. In this case the wire was inclined 45° with respect to the x-axis of the tunnel; i.e., the hot-wire carrier was in the streamwise position. The hot-wire supports were of different length so that the wire soldered across the tips was inclined at 45° . This was the only difference in the probes. With respect to the holder, bearings and rear end coupling, all hot-wire probes were identical. The hot-wire probe holder provided also a possibility to fix the hot-wire probe in any desired position when disconnected from the motor.

3.2.4 Integrator - In measurements of mean values of quantities which consist of a mean and fluctuating component, an integrating electronic circuit was used. This integrator was developed at the Fluid Dynamics and Diffusion Laboratory of Colorado State University, (Figures 9 and 10). The integrator was employed to obtain long time

period averages. The periods of averaging used were 3 minutes in the mean velocity measurements, and 100 seconds in the measurements of the mean of the hot-wire anemometer output.

The calibration of this integrating circuit was performed by using a non-fluctuating voltage from a power supply as the input for the required period of time of integration. A typical calibration curve is shown in Figure 11. Calibration of the circuit was checked frequently during the experiment, and was found to be very stable. The output voltage was corrected for zero input integrated voltage.

Chapter IV

DATA REDUCTION, CALIBRATION PROCEDURES AND
POSSIBLE SOURCES OF ERRORS4.1 Mean Velocity Measurements

To obtain accurate measurements of mean velocity in the turbulent boundary layer, it is necessary to employ some averaging method. A mean velocity is difficult to establish with high accuracy due to the fact that it is made up of mean and fluctuating components. Graphical averaging was not used, since it is not convenient for evaluation of great quantities of data. Moreover, graphical evaluation of averages would allow more possibility of error. Therefore, to improve the accuracy, an electronic integrating circuit was used (Figure 9).

The block diagram of the instrumentation used in the mean velocity measurements is given in Figure 12. As can be seen, the instrumentation used in measurements of the mean velocity consisted of a 0.125 inch diameter Pitot static tube, a Trans-Sonics Type 120 B Equibar Pressure Meter, a D.C. amplifier, an electronic integrating circuit that was developed at the Fluid Dynamics and Diffusion Laboratory of Colorado State University, and a Hewlett-Packard 3440A digital voltmeter as a read-out (Figure 12).

4.1.1 Calibration of mean velocity measurement instrumentation -

The above mentioned system consists of instruments which were previously described or are presented in Appendix A. Their calibration is also described in paragraphs 3.2.1 and 3.2.4, for the Pitot static tube and integrator, respectively, and in Appendix A for the commercial instruments. However, it is necessary to mention here that the pressure meter

output voltage had to be amplified before integration. The integrator requires input voltages of at least one volt magnitude to give good results at used integration times. Therefore, the amplifier-integrator circuit was calibrated by introducing a non-fluctuating voltage from a power supply. Integrating time was three minutes, and input voltage ranged from 0 to 30 mv. The integrating time of three minutes was chosen on the basis of experiment. The mean velocity was measured in the turbulent boundary layer using different integration times. These integration times were varied in range from one to five minutes. The three minutes integration time was chosen, since further extension of integration time did not improve this result. The measurements for three minute averages were repeatable within 0.5%. The input voltage range was dictated by the pressure meter D.C. output, which is 0 to 30 mv for each scale (see Appendix A). Amplifier gain of 100 was used through the entire experiment. Amplifier noise was calibrated out by integrating for three minutes with a zero input to the amplifier, and using the result as a correction for integrated voltages.

Calibration of the system was checked frequently during the experiment. A typical calibration curve for the amplifier-integrator circuit is given in Figure 11.

4.1.2 Possible sources of errors in the mean velocity measurements - As was already mentioned in the introduction to this Chapter, this experiment was conducted in order to study the outer portion of the thick boundary layers. This decreases considerably the possibility of errors due to shear and proximity of the solid boundary. However, these effects were taken into consideration and the order of

magnitude of errors which they might introduce was evaluated. Besides the effects of shear and proximity of the solid boundary, the effects of the turbulence were evaluated:

1) Effects of proximity of the solid boundary - In his experiments on Pitot tubes in shear flow, F. A. MacMillan (28) has found that where a tube is near the wall, a correction to the measured velocity must be added. MacMillan expressed the wall effect as a function of y/D , where D denotes the external diameter of the tube, and y is the distance of the geometrical center of the tube from the wall. The points nearest to the floor of the tunnel, for which the mean velocity measurements were made, were examined. This shows that the ratio y/D never drops below 1.4. One concludes, entering the values into the MacMillan correction diagram (Figure 14), that the correction necessary is always less than $0.001U$, and therefore negligible.

2) Effects of shear - The above mentioned reference (28) gives the effect of shear expressed as displacement d , of the effective center of the tube toward the region of higher velocity. The value of d/D is given as 0.15 regardless of Reynolds number and velocity gradient. Therefore, in the case of this experiment this displacement would be 0.0063 inch. This is again well within the scatter of data.

3) Turbulence effects - The effect of turbulence can not be overlooked when one considers the inner portion of the turbulent boundary layer where the turbulence intensities are very high. However, it is necessary to investigate this effect also in the outer portion of the turbulent boundary layer. The importance of this effect decreases with the distance from the wall. Even so, this effect might be considerable up to $0.025 y/\delta$, as data of this experiment show. To get an insight

into the order of magnitude of the possible error due to turbulence effect, the expression suggested by Goldstein (13) was used:

$$p = p_s + \frac{1}{2} \rho U^2 + \frac{1}{2} \rho (\overline{u^2} + \overline{v^2} + \overline{w^2}) \quad (4-1)$$

where p is dynamic pressure, p_s ambient pressure, U mean velocity, and u , v and w are the velocity fluctuations in the direction of the x , y and z axes respectively. When the mean velocity measurements were made, turbulence was not measured for all cases of free stream velocity. One, therefore, can only make an estimate of this effect and apply it as such to uncertainty interval considerations. Turbulence measurements show that one can use as an approximation the following ratios:

$$\sqrt{\overline{w^2}} = 0.75 \sqrt{\overline{u^2}} \quad \text{and} \quad \sqrt{\overline{v^2}} = 0.6 \sqrt{\overline{u^2}} \quad . \quad (4-2)$$

The pressure meter gives $\Delta h = p - p_s$, and starting from

$$U = 2.36 \sqrt{\frac{\Delta h \cdot 1.0173}{\rho}} \quad (4-3)$$

accepting the suggestion of Goldstein, the following expression for actual mean velocity is obtained:

$$U_a = \sqrt{5.67 \frac{\Delta h}{\rho} - 1.9 \overline{u^2}} \quad . \quad (4-4)$$

This was applied to mean velocity measurements at free stream velocity of $U_\infty = 60$ ft/sec, at the station $X = 80$ feet. The results show that the error varies from 1.7 to 0.1% of the local velocity (Figure 15).

The expression suggested by Goldstein is subject to criticism by Hinze (17). Hinze points out that due to the finite dimensions of Pitot tube dynamic port, a deviation might be expected. Also he maintains that the static pressure at the static pressure ports will be

lower than the ambient pressure and that is in conflict with the correction suggested by Goldstein. No systematic investigation along these lines has been done. Therefore, in this experiment the results illustrated by Figure 15 are used as an estimate of the order of magnitude of this effect and its influence on the uncertainty intervals of these measurements.

4) Non-linear averaging - The measured Δh obtained from the pressure meter is not the true representation of the mean velocity, but is affected by the mean velocity fluctuations as well. A non-linear relation causes the Δh average to shift toward the higher values. If one starts with equation (4-3), a relationship is obtained:

$$\Delta h = 0.177\rho U^2 \quad (4-5)$$

or

$$\Delta h = 0.0003297U^2$$

for the same station along the tunnel floor and the same U_∞ as in the preceding paragraph. The corresponding mean velocity fluctuations were added to mean velocity and the shift of Δh was evaluated. It was found that it is considerable near the wall, 2.7%, and that with the increase of the distance from the wall it drops quite quickly to an approximately constant value of about 0.6% in the outer region (Figure 16) from $y/\delta \geq 0.05$. In this investigation the evaluation of this effect was used as information for evaluation of the uncertainty intervals, and correction was not applied to data.

4.1.3 Mean velocity calculations - According to the system of instruments used and correction necessary for Pitot static tube, the mean velocity is obtained through a procedure consisting of the

following steps:

- 1) The pressure difference in mm Hg is obtained from the amplifier-integrator circuit output versus pressure meter reading calibration curve (Figures 11 and 17).
- 2) A correction is applied according to the pressure meter reading versus Merriam micromanometer calibration curve (Figure 13);
- 3) Mass density is determined from ambient temperature and atmospheric pressure data, and velocity is then calculated by means of

$$U = 2.36 \sqrt{\frac{1,0173\Delta h}{\rho}} \quad (\text{ft/sec})$$

where the coefficient 1,0173 is a correction implied by the Pitot static tube calibration. Step 1 involves actually two calibration curves. The first one is the pressure meter D.C. output versus amplifier-integrator output. And the second is the pressure meter D.C. output versus pressure difference in mm Hg calibration, obtained for each scale of pressure meter separately.

4.2 Turbulence Measurements

To obtain turbulence data, measurements with the hot-wire anemometer were employed. The hot-wire anemometer as a basic instrument has become the accepted standard for experimental studies of fluctuating velocities. A large number of hot-wire anemometers are available at the present time. During this experiment the measurement of fluctuating velocity components was done by the constant-temperature hot-wire anemometer designed at Colorado State University by C. L. Finn and V. A. Sandborn (11). This hot-wire anemometer has a distinct advantage in measurements of the type involved here; namely, a long and thick

boundary layer was covered. The majority of instruments have the problem of critical cable length. Usually the hot-wire anemometer must be used with a special cable which is calibrated to be used between the hot wire and anemometer. The advantage of the Colorado State University instrument is that it does not have any critical cable length. A cable of 47 foot length was used in these measurements. This was a great advantage since it was possible to group all the instruments at one position and perform the measurements along the whole length of the boundary layer without interruption.

To be able to interpret data obtained during the experiment from the hot-wire anemometer it is necessary to consider briefly the principles involved. Only the essential principles of hot-wire anemometry will be presented.

4.2.1 The hot-wire anemometer - The hot-wire anemometer basically consists of a detecting element and a control unit. The output of a constant-temperature hot-wire anemometer depends on the total velocity of the flow, angle of yaw with respect to flow direction, and the temperature difference between the wire and the local fluid temperature, for the fixed dimensions of the wire. The selection of hot-wires, i.e., of detecting elements, which are to be used for a certain experiment, depends upon the turbulent quantities required. In the present experiment the measurements of velocity fluctuations were required. For this purpose two types of hot wires were used, a single wire soldered perpendicularly to its support and a wire inclined at 45° . Both types were used on probes which could be rotated.

The hot-wire anemometer responds to both velocity changes and temperature changes. In this experiment all measurements were made in

flows of constant temperature and fluid properties. The mean heat loss from hot wires in subsonic flow can be written in the form

$$\frac{I^2 R}{R - R_a} = A + BU^m \quad (4-6)$$

and it was found that m varies with Reynolds number. The constant temperature operation being the case in this experiment, one can rewrite equation (4-6) and obtain the form

$$E^2 - E_0^2 = B_1 U^m \quad (4-7)$$

where E_0 is the output voltage for no-flow condition. For very low velocities the free convection problems arise; however, these are insignificant for velocities above 2.5 ft/sec, and therefore, of no consequence in this experiment.

4.2.2 Hot-wire sensitivity to velocity and yaw - In hot-wire anemometry applications it has been found (3) that the heat loss from a circular cylinder is a function of velocity, temperature, density, and angle of attack. As was already stated, in this experiment temperature and fluid properties were considered constant. No problems of frequency response were considered since it was assumed that the hot wire is ideally operated by the electronic circuit. General relations for sensitivity and response for hot wire, derived from considerations of heat transfer from small cylinders, have been reported by various researchers. However, helpful as these relations are for the basic understanding of the physical phenomena, in practice their use involves complexities. The direct use of calibration is considered more reliable. When measurement of transient velocities is required, one has to consider the heat transfer from the hot wire in the transient state.

It is assumed in hot-wire anemometry that the fluctuations can be evaluated from a calibration between the hot-wire mean heat loss and the mean quantity to be measured. The output of the constant-temperature hot-wire anemometer is an indication of the hot-wire heat loss. This must be known very accurately, since the first derivative of heat loss, with respect to the quantity changing it, has to be obtained. One can assume now that the output of a constant temperature hot-wire anemometer is a function of velocity and angle of yaw. Assuming that the hot-wire output and the calibration curves are known, one has now to develop a technique for determination of turbulent intensities.

According to the previous assumption

$$E_{\text{OUT}} = E(U_{\text{TOT}}, \xi) \quad (4-8)$$

where angle of yaw ξ , in general, can be constructed of two angles ϕ and ψ . The angle ϕ is the angle which the hot wire makes with the x-axis when rotated in the x-y plane, while angle ψ is the angle between the hot wire and x-axis in the x-y plane (Figure 18). Following now the development given in references (49) and (44), and assuming that a perturbation in the velocity field produces a corresponding voltage perturbation, one can write the following basic response equation for the hot wire:

$$e = \frac{\partial E}{\partial U} u + \frac{\partial E}{\partial \phi} \frac{v}{u} + \frac{\partial E}{\partial \psi} \frac{w}{U} \quad (4-9)$$

This equation is used for the evaluation of turbulence quantities when yawed hot wires are employed. In this experiment one encounters two cases. The first case is when the hot-wire probe carrier holds the probe crosswise to the flow position. In this position, the hot wire

is rotated in the x-y plane, and the value of $\frac{\partial E}{\partial \psi} = 0$. However, small deviations from the alignment with the x-y plane may cause a heat loss to change (44). This imposes a problem with which one deals when probes and hot wires are designed and made. The second case is when the hot-wire probe is held and rotated in the streamwise position. In this position the hot wire during the measurement is aligned with the x-y plane and accordingly $\frac{\partial E}{\partial \phi} = 0$. Therefore, for each of the mentioned cases one obtains an equation which expresses the hot-wire anemometer output in terms of the velocity fluctuations, mean local velocity, and sensitivities of the hot wire with respect to velocity and yaw.

To utilize equation (4-9) in calculation of the values of velocity fluctuations, this equation must be rewritten and obtained in terms of measured quantities. Considering the first case, $\frac{\partial E}{\partial \psi} = 0$, the hot wire rotated in the x-y plane, one obtains:

$$e = \frac{\partial E}{\partial U} u + \frac{\partial E}{\partial \phi} \frac{v}{U} \quad . \quad (4-10)$$

Squaring this equation and averaging an expression for mean square results in

$$\overline{e^2} = \left(\frac{\partial E}{\partial U} \right)^2 \overline{u^2} + 2 \frac{\partial E}{\partial U} \frac{\partial E}{\partial \phi} \frac{\overline{uv}}{U} + \left(\frac{\partial E}{\partial \phi} \right)^2 \frac{\overline{v^2}}{U^2} \quad . \quad (4-11)$$

If one denotes sensitivities with respect to velocity and angle of yaw as:

$$S_U = \frac{\partial E}{\partial U} \quad \text{and} \quad S_V = \frac{1}{U} \frac{\partial E}{\partial \phi} \quad , \quad (4-12)$$

equation (4-11) becomes

$$\overline{e^2} = S_U^2 \overline{u^2} + 2S_U S_V \overline{uv} + S_V^2 \overline{v^2} \quad . \quad (4-13)$$

One can see immediately that the hot wire has to be calibrated with respect to angle and velocity. The hot-wire sensitivities S_U and S_V vary with velocity and angle. However, it would be convenient if one can have such conditions that S_U and S_V are of the same magnitude. This was investigated (49) and it was found that for $\phi = 40^\circ$ the condition is approximately satisfied. On the basis of the experiments described in reference (49), it was decided to operate the hot wire in the x-y plane at $\pm 40^\circ$ yaw. This gives two equations:

$$\begin{aligned} (\overline{e^2})_{+40} &= (S_U^2)_{+40} \overline{u^2} + 2(S_U)_{+40} (S_V)_{+40} \overline{uv} + (S_V^2)_{+40} \overline{v^2} \\ (\overline{e^2})_{-40} &= (S_U^2)_{-40} \overline{u^2} + 2(S_U)_{-40} (S_V)_{-40} \overline{uv} + (S_V^2)_{-40} \overline{v^2} \end{aligned} \quad (4-14)$$

for $+40^\circ$ and -40° yawed hot wire, respectively. Here S_V is a positive quantity for positive angles, and a negative quantity for negative angles (49). This gives, together with specific conditions imposed by the hot-wire calibration, a possibility to construct a calculation method suitable for use with an electronic digital calculator (see Appendix B).

When the second case is considered, $\frac{\partial E}{\partial \phi} = 0$, the hot wire aligned with the x-z plane, one obtains through the same steps as in the first case, the following expressions:

$$\begin{aligned} (\overline{e^2})_{+45} &= (S_U^2)_{+45} \overline{u^2} + 2(S_U)_{+45} (S_W)_{+45} \overline{uw} + (S_W^2)_{+45} \overline{w^2} \\ (\overline{e^2})_{-45} &= (S_U^2)_{-45} \overline{u^2} + 2(S_U)_{-45} (S_W)_{-45} \overline{uw} + (S_W^2)_{-45} \overline{w^2} \end{aligned} \quad (4-15)$$

for $+45^\circ$ and -45° yawed hot wires, respectively. In this case a

hot wire inclined at 45° was used for the following reasons: The change from the straight rotating hot wire to an inclined one was dictated by the available facility. It was impractical to adapt the hot-wire carrier in such a way that the hot wire could be rotated in the x-z plane with the probe axis perpendicular to the x-z plane, i.e., use of a non-inclined wire was not practical. To use a non-inclined wire would require further rewiring of the carriage control and would in fact disrupt the whole existing system. Therefore, the hot-wire carrier was adapted in such a way that the use of an inclined hot wire facing the flow was possible. The probe rotation is in this case around the x-axis with which the probe was aligned. Further, the angle of 45° was chosen, since it was very important in this case to be able to produce a "perfect" hot wire; that is, a hot wire whose calibration will be exactly the same for $\pm 45^\circ$. The angle of 45° was the one which could be exactly controlled during the making of the hot wire, and therefore it was chosen. The necessity of having a "perfect" hot wire in this case will be clear after the discussion of the calibration procedure for the hot wires.

Both systems of equations (4-14) and (4-15) require another additional equation, to be solved for values of $\overline{v^2}$, \overline{uv} and/or $\overline{w^2}$ when one has $\overline{e^2}$ measurements for positive and negative angles of yaw. In other words one has to know $\overline{u^2}$. When the hot wire is perpendicular to the mean flow, then the angle sensitivity is zero (44,49) and equation (4-11) becomes

$$\overline{e^2} = \left(\frac{\partial E}{\partial U}\right)_{90}^2 \overline{u^2} = (S_U)_{90}^2 \overline{u^2} \quad . \quad (4-16)$$

Subscript 90 here means that the hot wire is at an angle of 90° with respect to the mean flow direction, i.e., x-axis in this experiment.

Therefore, one obtains $\overline{u^2}$ from equation

$$\overline{u^2} = \frac{\overline{e^2}}{(S_U^2)_{90}} \quad (4-17)$$

knowing $\overline{e^2}$ from the measurements and S_{U90} from the calibration of the hot wire.

4.2.3 Hot-wire calibrations - To obtain accurate calibration curves, the calibration of the hot wires was done near the test section entrance. The wind tunnel carriage was brought to the forward end of the test section and the hot-wire probe carrier was brought into its highest position. In this way the hot-wire probes and the Pitot static probe, against which the hot wires were calibrated, were held in the free stream outside of the boundary layer.

Prior to the hot-wire calibration in the wind tunnel, each hot wire was subjected to the "cooking" process. During the cooking process the hot wire was subject to operational condition of no flow with an overheat ratio of 1.7, for at least 24 hours. This operation stabilized the hot-wire characteristics very satisfactorily. In all cases the calibration curves before and after each run were the same (Figure 19), and the value of E_0 did not show any detectable change. Even the calibrations after prolonged periods of time gave the same calibration curve. Furthermore, the "cooking" process, calibration, measurement run and check calibration sequence were always carried out without interruption of power to the wire. During the turbulence measurements, the mean velocity and mean hot-wire output voltage were measured at each

measurement point. These were checked against the calibration curves. Since the measurement runs were of very long duration, these checks provided the hot-wire calibration control throughout the run. After the run, check calibrations were again made covering the whole range of velocities. The straight hot wires were calibrated for angles of yaw of 90° and $\pm 40^\circ$, the inclined hot wires were calibrated for positions of $\pm 45^\circ$. The output voltage from the wires in these positions was obtained for a range of mean velocities. The velocity was varied from 10 ft/sec to 80 ft/sec. The velocity sensitivity $\frac{\partial E}{\partial U}$ was obtained from the calibration curves. First the values of $\frac{\partial E}{\partial U}$ were obtained by determining the slope of the calibration curve of the hot-wire voltage versus velocity for a range of velocities. With these values a curve of $\frac{\partial E}{\partial U}$ vs U was plotted (Figures 20 and 21). To check the accuracy of this method, the velocity sensitivity was also determined by another method: the relation given by equation (4-7) was plotted on log-log paper, $E^2 - E_0^2$ versus U . And it was possible to fit a straight line for the range of velocities of interest. From this plot B was determined as the intercept on the ordinate, and m as the slope. From the equation (4-7) one obtains

$$\frac{\partial E}{\partial U} = \frac{Bm}{2E} U^{m-1} \quad . \quad (4-18)$$

Values of $\frac{\partial E}{\partial U} = S_V$ were calculated for the same range of velocities and these were checked against those obtained from slope reading. The result is shown in Figures 20 and 21. The agreement is very good; therefore the equation (4-18) was employed in one of the turbulence calculation methods, see Appendix B. This same procedure was used to obtain the velocity sensitivity for all angles of yaw.

If the hot wire is perfectly symmetrical one should expect that it would have the same calibration curves for $+40^\circ$ and -40° . Also one would expect the velocity sensitivity curves to be the same for these angles. Practically it is very difficult, if not impossible, to make an absolutely symmetrical wire. In making the wires for this experiment much care was taken to solder the wires right across the tips of the wire supports, so that the only remaining asymmetry was the cut-off end of the wire at one of the supports. One would expect that the velocity sensitivity would in this manner be unaffected by change of angle from $+40^\circ$ to -40° . Even if the wire output voltage would change slightly, the calibration curve slopes would not change perceptibly. Figures 20 and 21 show the sensitivities for $\pm 40^\circ$ and $\pm 45^\circ$. In the case of the wire inclined at 45° , the curves are identical. The angle sensitivity of the hot wires was obtained by rotating the wire for about $\pm 5^\circ$ around the angle of yaw used. This rotation was done in steps of approximately 1° and the hot-wire output voltage was measured at each step. From these data the plot E vs ϕ resulted and $\frac{\partial E}{\partial \phi}$ was obtained. This was done for the range of velocities encountered and the angle sensitivity versus mean velocity curve was constructed.

During this experiment it was found that one can expect to obtain two kinds of angle sensitivity for hot wires. One kind is the hot wire with the same angle sensitivity curve for $\pm 40^\circ$ (Figure 22), this indicating a perfectly symmetrical wire. In the rest of this study, this kind of a hot wire will be called a "perfect" wire. The other kind of the hot wire is the one having two distinct angle sensitivity curves for $\pm 40^\circ$ yaw (Figure 23). The second is more frequently the case; this

kind of the hot wire will be called a "real" wire, throughout the rest of this study.

It is known that $\frac{\partial E}{\partial U}$ and $\frac{1}{U} \frac{\partial E}{\partial \phi}$ are not independent of each other. It was observed by Tieleman (49) from actual calibrations that at angles close to $\pm 40^\circ$ the velocity and angle sensitivity should be the same. In this experiment the "perfect" wire confirmed this, $\frac{\partial E}{\partial U} = \frac{1}{U} \frac{\partial E}{\partial \phi}$ for angle of yaw of $\pm 40^\circ$, and for a wide range of velocities (Figure 22). For angles close to $\pm 45^\circ$ it was observed that angle and velocity sensitivities differed only by a constant factor $C \cot \phi$ (1). Webster (52) explored carefully Hinze's suggestion that besides the component of the total velocity which is normal to the wire, the parallel one also affects the heat transfer from the wire. Arya and Plate also explored this problem. In Reference (1) starting with the expression suggested by Hinze for "effective velocity"

$$U_{\text{eff}}^2 = U^2(\sin^2 \phi + a \cos^2 \phi) \quad (4-19)$$

they arrive at an expression which relates $\frac{\partial E}{\partial U}$ and $\frac{1}{U} \frac{\partial E}{\partial \phi}$ in the manner mentioned:

$$\frac{1}{U} \frac{\partial E}{\partial \phi} = \frac{(1-a^2) \cot \phi}{(1+a^2 \cot^2 \phi)} \frac{\partial E}{\partial U} \quad (4-20)$$

therefore

$$C = \frac{1-a^2}{(1+a^2 \cot^2 \phi)} \quad (4-21)$$

If a is known, then for a given angle of yaw, values of C can be calculated. Webster carried out a very elaborate experiment (52) to determine a . He made measurements for different mean flow

velocities and a wide range of wire length-to-diameter ratios. And he was not able to detect any trend in the change of a . However, the scatter of Webster's values of a lies in range of 0.11 to 0.28. The mean value is $a = 0.20$. It is not difficult to conclude that direct calibration which is done carefully, will give more reliable values. However, the direct calibrations indicate that this kind of relation exists. Therefore, if $\frac{\partial E}{\partial U}$ and $\frac{1}{U} \frac{\partial E}{\partial \phi}$ calibration curves are known, the determination of C is not difficult. If $\frac{\partial E}{\partial U}$ and $\frac{1}{U} \frac{\partial E}{\partial \phi}$ calibration curves are obtained by the methods described previously, then the possibility of determining C enables one to set up a convenient calculation method for computing the turbulence components and the turbulent shear stress. This calculation method can be used in the case of a "perfect" or "real" hot wire and is given in Appendix B.

In the case of the inclined hot wire it is not possible to measure the angle sensitivity directly. Therefore equation (4-21) can be used, provided that a good estimate of value for a can be made.

4.2.4 Possible sources of error in turbulence measurements -

Various possible sources of error will be briefly considered here. Detailed discussion of these will be found in Reference 49; however, the considerations necessary to calculate the uncertainty intervals for the measurements of turbulence show that errors resulting from instrumentation and accuracy of calibrations are, by far, more significant.

1) The solid boundary effect - The solid boundary near to the hot wire affects the rate of heat loss from the hot wire. The wire temperature is much higher than the temperature of the solid boundary, i.e., tunnel wall. However, without use of experimental methods no

exact correction for this effect can be obtained. Tieleman in his discussion of this effect refers to the investigations of Piercy, Richardson and Winny (34) and Wills (53), stating that at distances which are greater than 0.02 inch from the solid boundary this effect is negligible. In this experiment all points of measurement were at much greater distances; thus no corrections for the effect of the solid boundary were necessary.

2) Effect of the hot-wire length - It is possible that velocity fluctuations on one part of the hot wire are not completely correlated with the velocity fluctuations on another part of the hot wire. This is because of hot-wire finite length. So if the dominating eddies are of the same size or smaller than the wire length, then the measurements of turbulence will be in error. Depending on the correlation curve of the turbulence in the direction of the wire, the rms voltage is reduced. For the hot wires of the same size this correction was evaluated (49) for a free stream velocity of 40 ft/sec. It was found to be 15% at 0.015 inch above the tunnel floor. However, the same reference offers information about the change of integral scale of turbulence with increase of the distance from the tunnel floor. One can therefore expect that this correction will rapidly decrease with increase of the distance from the floor, since the integral scale of turbulence is also increasing. All measurement points in this experiment were more than ten times higher, above the tunnel floor, than the mentioned measurement for which the correction was determined. Furthermore, this was the only measurement available and was not sufficient to predict the magnitude of the correction. Thus no correction was applied for the effect of the hot-wire length.

3) Effect of velocity and turbulence intensity gradients -

When a hot wire is placed in a flow where a velocity gradient exists, the heat transfer along the wire is non-uniform. If a turbulence-intensity gradient also exists, i.e., if the hot wire is working in a turbulent boundary layer, the situation is still more complicated. A mathematical solution for the temperature distribution has not been obtained explicitly. However, one can say that the general effect would be a shift of the effective center of the wire toward the region of the higher heat transfer. One problem which can be expected during the turbulence measurements is, therefore, the possible difference in hot-wire voltage output for the wire aligned with the y-axis and wire aligned with the z-axis, i.e., between the vertical and horizontal wire. However, this problem does not affect the measurement of the velocity fluctuation component, u , in the direction of the x-axis. In this case the hot wire can be held horizontal and therefore would not experience any velocity and turbulence gradients in a two-dimensional flow. But when the turbulent shear stress and vertical component of velocity fluctuations are to be measured with yawed hot wires, a projection in the y-direction can not be avoided.

In order to evaluate this effect, and be able to apply the corrections if necessary, measurements with a horizontal and vertical hot wire were made. These measurements were made in the region close to the tunnel floor, and at two stations along the aluminum-plate part of the tunnel floor. The stations were 20 feet apart. The results of these measurements are presented in Figures 24 and 25. Scatter of points is approximately 1.5% and no systematic trend can be detected. It was concluded that the measurement points in this experiment are

above the region where this effect is strong enough to be detected. This is also in agreement with the measurements done by Tieleman (49). Tieleman's measurements were made very near the floor and indicate that this effect is felt up to approximately 0.175 inches above the floor. The height of 0.175 was approximately the lower limit of the present measurements. Therefore, no corrections for this effect were necessary.

4) Effect of turbulence on the hot-wire output voltage - As was already mentioned in 3.3.7., during the turbulence measurements, the mean velocity and mean hot-wire output voltage were monitored at all measurement points. These values are in good agreement with the hot-wire calibrations. It was, therefore, assumed that the heat transfer from the hot wire was not affected by the turbulence intensity in these measurements. Accordingly there is no need for corrections.

5) Linearization effect on turbulence calculation - The assumption that the hot-wire calibration curve is linear around the point of operation will introduce an error for high intensities of turbulence. The highest turbulence intensities encountered in this experiment were in the neighborhood of 15%. The graphical check on the calibration curve shows that the maximum error to be expected is of the order of 0.5%. This led to the conclusion that this effect is negligible.

4.3 Uncertainty Intervals

The results of experiments are never free of all errors. Therefore, one must provide the results with some measure of reliability. In cases when measurements can be repeated enough times and data can be taken by diverse instruments, one can use statistics to obtain the measure of reliability of the results. However, in the case described here, it was not possible to use repetition to resolve uncertainties.

Therefore, it is the case of the so-called single-sample experiment. In the case of single-sample experiments, it is unavoidable that the statements of reliability will be based in part on estimates. This is true because by definition, statistics can not be applied to all of the errors.

In the further parts of this study the following terms will be used: "Uncertainty" will mean a possible value the error might have. For a single observation, the error is a certain fixed number. Uncertainty, therefore, may vary considerably depending upon the particular circumstances of the observation. "Variable" will mean a basic quantity observed directly in the laboratory. This term is opposed to the "result", which is obtained by making correction to, or calculations with, the recorded values of variables. Recorded values of the variables will be referred to as "data".

The uncertainty of each variable may be described by specifying the mean and an uncertainty interval based on specified odds. The uncertainty interval, therefore, is not a variable but a fixed value. The second power equation given by Kline and McClintock (25) will be used for prediction of uncertainties. So if R is a linear function of n variables V_i , and each of them is normally distributed, then the relation between the intervals for the variables W_i , and the uncertainty interval for the result W_R , which gives the same odds for each of the variables and for the result, is given by the relation:

$$W_R = \left[\left(\frac{\partial R}{\partial V_1} W_1 \right)^2 + \left(\frac{\partial R}{\partial V_2} W_2 \right)^2 + \dots + \left(\frac{\partial R}{\partial V_n} W_n \right)^2 \right]^{1/2} \quad (4-22)$$

This equation is used directly as an approximation for calculating the uncertainty interval in the result.

The methods for calculating the uncertainty intervals are given, and uncertainty intervals are calculated in detail in Appendix C. The results are given below.

The mean velocity measurements in this experiment are within the uncertainty interval of ± 1 percent. Considering also the effects which were discussed in section 4.1.2, one can claim that the results of the mean velocity measurements are within an uncertainty interval which is less than ± 2 percent, except very close to the wall where it might be up to ± 3 percent of the correct value. The calculation of uncertainty intervals for the turbulence quantities shows that for this experiment the uncertainty intervals are:

$$\frac{w\sqrt{u^2}}{\sqrt{u^2}} = 11.65\%$$

$$\frac{w\sqrt{v^2}}{\sqrt{v^2}} = 10.0\%$$

$$\frac{w\overline{uv}}{\overline{uv}} = 20.1\%$$

and since in the calculation of $\overline{w^2}$ the method is the same, and constants involved are of the same order of magnitude as in the case of calculation of $\overline{v^2}$, it was assumed that the uncertainty interval for $\sqrt{\overline{w^2}}$ is

$$\frac{w\sqrt{\overline{w^2}}}{\sqrt{\overline{w^2}}} = 10.0\% .$$

Chapter V

RESULTS AND DISCUSSION

5.1 The Character of the Measured Turbulent Boundary Layer

The development of measurement techniques in general, and especially the development of hot-wire anemometer as a tool for turbulence research, has directed attention to the quantitative measurements in turbulent boundary layer research. In order to facilitate the use of hot-wire probes and minimize errors due to wire length, the boundary layer should be as thick as possible. The wind tunnel facility disposition is shown in Figure 1, and the boundary layer definition is given in Figure 2. As Figure 2 shows, at the entrance of the test section the gravel is placed to increase the boundary layer thickness at the higher rate. It is expected that downstream from the gravel roughness the boundary layer will return to "normal" within reasonable distance. The stations, at which the measurements were made, were 10 feet apart along the x-axis, the first one being about 10 feet from the gravel roughness. With this arrangement it was possible to observe the effect of the artificial thickening of the boundary layer. As can be observed from the mean velocity measurements (Figures 26, 27, 28, 29, 30, 31), the boundary layer returned to "normal" after 25 to 30 feet. It should be mentioned also that for the first 20 feet of the test section, it was not possible to adjust conditions to zero pressure gradient.

The artificial thickening of the boundary layer involved the setting up of criteria by which to establish the identity of a fully developed boundary layer. In this experiment the turbulence quantities were measured beside the mean velocity measurements. As a consequence

it is possible to show how all these quantities are affected in the front part of the wind tunnel test section, and when the layer is no longer influenced by the conditions at the entrance of the test section.

Figures 26, 27, 28, and 29 show the mean velocity distributions downstream from the entrance of the test section at the free stream velocities of 60, 75, 85 and 95 ft/sec. The nondimensional velocity profiles are given in Figures 32 and 33. Nondimensional velocity profiles are not presented for all free stream velocities since these graphs show the same general character. One can see that data from the first station are distinctly off the universal curve, and that data from the second station, though already in the band covered by the data points from the subsequent stations, show a definite trend in their slight deviation. Data from the subsequent stations cover the narrow band caused by the experimental scatter but no systematic trend is detectable. The data are consistent, so one can conclude that from the second station downstream, the boundary layer investigated in this experiment can be considered as an equilibrium turbulent boundary layer on a smooth flat plate, with a zero pressure gradient. Furthermore, it was possible to make another check to establish from which point along the x-axis one can consider the developed boundary layer to be an equilibrium turbulent boundary layer. For this purpose the numerical integration of the mean differential equations of motion by the method developed by Mellor (31) for calculation of equilibrium turbulent boundary layers without secondary flows was used. This method calculates the boundary layer development, using, as input data, the measurements at an initial point. The calculated boundary layer is an equilibrium turbulent boundary layer. Therefore, data from this experiment measured

at Station 1 were used as input, and the resulting calculated equilibrium boundary layer was compared with the actually measured one. Comparison is shown in Figures 34 and 35. Again it is seen that the measured values approach closely the equilibrium boundary layer values already at Station 2 (Figure 34). At the stations further downstream the measured values are practically identical with those obtained by Mellor's method, Figure 35. The previous discussion shows that as was expected, the investigated turbulent boundary mean velocity distributions assume "normal" character within the first 20 feet of the wind tunnel test section.

The lack of knowledge concerning the relationship between the mean flow and the turbulence quantities does not allow the use of the mean velocity distribution development as evidence that the turbulence is fully developed as well. However, the experimental evidence of measurements of turbulence quantities at the same stations along the x-axis show that this is the case. The results of measurements of the turbulence quantities will be discussed later on, but let it be stated here that they show that the distributions of the turbulence quantities also assume universal character from Station 2 downstream.

In conclusion to this section one can say that the artificial thickening of the turbulent boundary layer is successful since the layer becomes free of distortion within reasonable distance. This distance in this experiment is accepted as approximately 20 feet.

5.2 Mean Velocity Measurements and Similarity in Outer Portion of the Turbulent Boundary Layer

The test of the compatibility of the similarity concept of the outer portion of the turbulent boundary layer by introduction of the similarity form for the velocity defect law and Reynolds stresses,

as suggested by Rotta (42), has been considered in Section 2.4. The similarity requirements were consequently deduced from these considerations. However, it has to be pointed out at the outset that the similarity requirements have not been known to exist in the turbulent boundary layers.

In this experiment the mean velocity distributions were measured along the centerline of the test section floor (Figures 26, 27, 28, 29, 30, 31) and from these the velocity profile parameters were calculated. The parameters are listed in Table II. Equations (2-48) and (2-49) imply that the displacement thickness and momentum thickness should be linear functions of x coordinate. Therefore, the mean velocity profile parameters were plotted as functions of x coordinate. This was done for each free stream velocity and the results are shown in Figures 37, 38, 39, 40, 41, 42. In all cases the displacement thickness and momentum thickness show linear growth with x . The form factor change with respect to x coordinate is also shown on Figures 37, 38, 39, 40, 41, 42, and it is very nearly constant except within the first 20 feet of the test section. This is consistent with the discussion in Section 4.1, where it was stated that for the first 20 feet of the test section it was not possible to adjust conditions for zero pressure gradient.

The results shown in Figures 37, 38, 39, 40, 41, 42, cast no doubt on consistency with the requirements for similarity implied by Equations (2-48) and (2-49). These requirements may be expressed as

$$\delta^* = ax$$

and

$$\theta = bx$$

(5-1)

One notices immediately that the form factor, which is the ratio

$$H = \frac{\delta^*}{\theta} \quad (5-2)$$

has a constant value which is universal. The value of the form factor H in Figures 41 and 42, is equal within experimental precision to the value obtained by van Doenhoff and Tetervin (8) for the case of zero pressure gradient. Namely, van Doenhoff and Tetervin obtained for the case of constant dynamic pressure, consequently

$$\frac{dq}{dx} = 0,$$

and

$$\frac{dH}{dx} = 0, \quad (5-3)$$

the value

$$H = 1.286$$

which is in agreement with Figures 41 and 42 as stated previously. Clauser (5) points out that originally it was thought that H expresses solely the effect of the pressure gradient on the shape of the velocity profile, but that H is affected as much by skin friction as by pressure gradient. The results of this experiment show the presence of still another factor. As was already pointed out, the value of H shown in Figures 41 and 42, is consistent with results of van Doenhoff and Tetervin (8). These authors do not indicate that the data which they have used were influenced by any secondary flows. Data shown in Figures 41 and 42, though affected by secondary flow, show that this

effect was very small (Figures 34, 35 and 46). On the contrary data shown in Figures 37, 38, 39 and 40, were obtained under relatively strong secondary flow influence. The comparison of values of H shows considerable difference. Since all the conditions were the same under which the measurements represented in Figures 37, 38, 39 and 40, and Figures 41 and 42 were made, one has to conclude that the secondary flow effect on the form factor H is prominent.

Equation (2-48) states, besides the requirements expressed in Equation (5-1), the most difficult requirement of similarity, which is that the wall shear stress has to be constant. In this experiment it was not possible to measure the wall shear stress directly. Measurement was taken along the entire length of the test section, as it was unpracticable to make direct measurements at each station. Therefore, the values of the wall shear stress were computed from empirical relations. As a first approximation the Ludwig-Tillmann relation

$$\frac{\tau_w}{\frac{1}{2}\rho U_\infty^2} = 0.246 \times 10^{-0.678H} \left(\frac{U_\infty \theta}{\nu}\right)^{-0.268} \quad (5-4)$$

was used. One should immediately point out that Equation (5-4) is not compatible with similarity requirements; θ has to vary linearly with x according to similarity requirements; and cannot give constant value for τ_w . Values for τ_w , U_τ and c_f which are given in Table II are computed from Equation (5-4). It was expected that discrepancy would be rather great; however, the Ludwig and Tillmann relation gives a small but systematic variation of U_τ and x . This variation is along the entire test section floor up to 9 percent. If one observes the variation of the ratio U_τ/U_∞ it is found that its variation is relatively much smaller, not even 5 percent along the entire length of

the test section. This justifies the assumption made in Chapter II, according to which the derivatives with respect to $\omega = U_\tau/U_\infty$ were neglected when Equation (2-47) was derived. It is difficult to answer explicitly why ω is exhibiting almost universality. However, one may say that the wall similarity prescribes the slope of the velocity defect law near the wall and deviations are less probable. As the relation (5-4) was utilized, it provided means to go a step further and use also the similarity relation suggested by Rotta (42)

$$\frac{\tau_w}{\rho U_\infty^2} = A^2 \left(1 - \frac{1}{H}\right)^2 \quad (5-5)$$

where $A = 1/I_1$, and shape parameter I_1 is given by

$$I_1 = \int_0^\infty \left(\frac{U_\infty - U}{U_\tau}\right)^2 d\left(\frac{yU_\tau}{\delta^* U_\infty}\right) . \quad (5-6)$$

The value of I_1 was determined from experimental data, and was found to be in this case $I_1 = 6.85$ (values measured after the wind tunnel screens imperfections were removed). Comparison of values calculated from Equations (5-4), (5-5) and values obtained from Mellor's calculation of equilibrium boundary layers (31) is given in Figure 46. As further check and comparison, the skin friction was obtained by Clauser's method and included in Figure 46. This shows that the relation (5-5) gives almost constant values for skin friction coefficient. However, one should recall that the values of U_τ on the basis of which the value of I_1 was obtained, are those calculated from Equation (5-4). Therefore, the values shown on Figure 46 may be considered as first iteration values.

Nevertheless, the values of c_f , in Figure 46, and the values in Table II, vary very slightly. As was mentioned previously, the actual

variation of U_τ/U_∞ is very small. This indicates a very close approach to similarity. The Equation (2-11) shows that near the wall similarity exists even for a linear variation of U_τ with x . Therefore, a slight variation of U_τ should not affect the outer flow. This also further explains the weak influence of the parameter ω . The requirement of a constant shear at the wall, therefore, is not critical for the approach of the turbulent boundary layer, with zero pressure gradient, to similarity. When the law of the wall was considered in Section 2.2 it was shown that the existence of a constant shear stress region is required where similarity of the form (2-7) is to be expected. In his investigation of the viscous sublayer, Tieleman (49) measured viscous and turbulent shear stress near the wall. His results confirm the existence of the region of constant shear, though the uncertainty limit is quite wide. Further support for the existence of this similarity requirement is offered by recent measurements of Arya (2), to be reported yet, which show existence of constant shear stress region in thermally stratified flows. In this experiment measurements were not taken close enough to the wall to provide data for proof of the existence of this similarity requirement. However, the consistency of the turbulent shear stress measurements with the calculated values of the wall shear, τ_w , was checked. Figures 70 to 77 show the turbulent shear stress distribution across the boundary layer thickness, with τ_w value indicated. The uncertainty limits were calculated for the turbulent shear stress in Section 4.3.2, and the uncertainty interval was found to be 20 percent. Inspection of results of Tieleman's (49) investigation of the viscous region of the turbulent boundary layer indicates that one should expect $\overline{\rho u v}$ values slightly higher than τ_w

in the region adjacent to the wall at high velocities. This actually occurs, as shown on Figures 70 to 77; however, within the uncertainty limits agreement is good. Once again these figures show that for the first 20 feet the boundary layer is still distorted by the gravel roughness effect.

Figure 47 suggests universality of the plot U/U_∞ vs y/δ . One may say that this can be expected if one recalls the comparison of data obtained by various authors on a flat plate with zero pressure gradient presented by Clauser (5), plotted U/U_∞ vs y/δ . Clauser compared data by Klebanoff and Diehl (23) and Hama (15) for a range of Reynolds numbers based on boundary layer thickness. This comparison is reproduced on Figure 48. One notices that the nondimensional profiles tend asymptotically to some final form. In the case of data from this experiment the Reynolds number based on the boundary layer thickness is approximately three to eight times higher than for the data presented by Clauser, and if these data are presented on the same graph, they appear to be asymptotic values (Figure 48). This in other words means that for very high Reynolds numbers one should expect similarity in the outer portion of the boundary layer of the form

$$\frac{U}{U_\infty} = \phi\left(\frac{y}{\delta}\right); \quad (5-7)$$

δ is not easily defined, and since it has been proved already in Equation (2-30) that δ is proportional to δ^*U_∞/U_τ , one can replace δ with $\Delta = \delta^*U_\infty/U_\tau$ in Equation (5-7), and obtain

$$U = U_\infty \phi\left(\frac{y}{\Delta}\right). \quad (5-8)$$

Now one can ask the same question as in Section 2.4, what are conditions required for similarity of this form to exist? If the same notation is used

$$\eta = \frac{y}{\Delta} \text{ , then } \frac{\partial}{\partial x} = -\eta \frac{d\Delta}{dx} \frac{1}{\Delta} \frac{d}{d\eta} \quad (5-9)$$

$$\frac{\partial}{\partial y} = \frac{1}{\Delta} \frac{d}{d\eta} \text{ ,}$$

since it was already established that the influence of w parameter is weak. Introducing (5-8) and (5-9) into (2-35) and (2-36), and also in this case assuming that similarity cannot be confined to mean velocity distribution but must be extended to all mean quantities

$$\overline{u^2} = U_{\infty}^2 \psi_1(\eta)$$

$$\overline{v^2} = U_{\infty}^2 \psi_2(\eta) \quad (5-10)$$

$$\overline{uv} = U_{\infty}^2 \psi_{12}(\eta)$$

one obtains for individual terms of equations (2-35) and (2-36)

$$\frac{\partial U}{\partial x} = -U_{\infty} \eta \frac{1}{\Delta} \frac{d\Delta}{dx} \phi' \quad (5-11)$$

$$\frac{\partial U}{\partial y} = U_{\infty} \frac{1}{\Delta} \phi' \quad (5-12)$$

$$\frac{\partial(-\overline{uv})}{\partial y} = U_{\infty}^2 \frac{1}{\Delta} \psi'_{12} \quad (5-13)$$

$$\frac{\partial \overline{u^2}}{\partial x} = U_{\infty}^2 \eta \frac{1}{\Delta} \frac{d\Delta}{dx} \psi_2' \quad (5-14)$$

$$\frac{\partial \overline{v^2}}{\partial x} = -U_{\infty}^2 \eta \frac{1}{\Delta} \frac{d\Delta}{dx} \psi_2' \quad (5-15)$$

The vertical component of the mean velocity is calculated from the equation of continuity (2-36). One obtains

$$V = - U_{\infty} \frac{d\Delta}{dx} \int_0^{\eta} \phi' \eta_1 d\eta_1 \quad (5-16)$$

Using the chain rule of integration and argument expressed by Equation (2-42), Equation (5-16) becomes

$$V = - U_{\infty} \frac{d\Delta}{dx} [\phi\eta - \int_0^{\eta} \phi d\eta_1] \quad (5-17)$$

Introducing expressions (5-11) to (5-17) into Equation (2-35) one obtains

$$\frac{d\Delta}{dx} [\phi' \int_0^{\eta} \phi d\eta_1 - 2\phi\phi'\eta] = \psi'_{12} + \eta \frac{d\Delta}{dx} (\psi'_1 - \psi'_2) \quad (5-18)$$

Boundary conditions for the function ϕ are

$$\begin{aligned} \text{for } \eta \rightarrow \infty \quad \phi(\infty) = 1, \quad \phi'(\infty) = 0 \\ \eta \rightarrow 0 \quad \phi(0) = 0, \quad \phi'(0) = 0 \end{aligned} \quad (5-19)$$

Equation (5-18) is somewhat simpler than Equation (2-47). If similarity in the x-direction is required, then equation (5-18) must be independent of the x coordinate. This is satisfied if

$$\frac{d\Delta}{dx} = \text{constant}, \quad (5-20)$$

i.e., Δ must be a linear function of x . Therefore,

$$\frac{U_{\infty}}{U_{\tau}} \cdot \delta^* = D_1 x \quad (5-21)$$

Experimental evidence shows that δ^* is a linear function of x , and it is a requirement consistent with requirements for the case of the velocity defect law validity. So U_{∞}/U_{τ} must be constant. The obtained similarity requirements are essentially the same as for similarity of

the mean velocity defect law form; however, the form (5-8) requires practically infinite Reynolds numbers. Therefore, the following conclusion is implied: turbulent boundary layers of the type investigated in this experiment approach similarity very closely. The highest Reynolds numbers achieved based on δ , the boundary layer thickness, are of the order of 10^6 . When such high Reynolds numbers are obtained, then a complete similarity can be expected, and the similarity of the form (5-8) may be also expected as an asymptotic form corresponding to infinite Reynolds numbers.

In all cases of the mean velocity distribution measurements it was found that when data are plotted in coordinates, $U_\infty - U/U_\tau$ versus y/Δ , data points fall on a single universal curve, within experimental precision. As experimental precision in this case, one can assume that it is equal to the uncertainty interval calculated for the mean velocity measurement. The uncertainty interval for the mean velocity measurements is calculated in Section 4., and is found to be ± 1 percent. To this value uncertainty resulting from possible errors due to turbulence effect and to non-linear averaging must be superimposed. Finally the uncertainty interval for the mean velocity measurements becomes ± 2.7 percent at the most. With this value accepted as the uncertainty limit, the best average values of the $U_\infty - U/U_\tau$ versus y/Δ experimentally obtained curve, were tabulated and are given in Table III.

5.3 Turbulence Measurements and Similarity in the Outer Portion of the Turbulent Boundary Layer

In Section 2.4 similarity requirements were considered. It was assumed that Reynolds stresses would be expressed in the forms (2-32), (2-33) and (2-34) if similarity exists. It should be pointed out that

previously no data were available in support of this assumption. In this experiment turbulence quantities were measured across the boundary layer at eight stations along the test section of the wind tunnel. The arrangement of these stations has been already described. The hot-wire techniques and uncertainty intervals were considered in Chapter IV and Appendix C. The present method of measurement reduced the errors and calculated uncertainty intervals have set more reliable uncertainty limits for results.

The similarity of Reynolds stresses distribution across the outer part of the boundary layer is a requirement of the analysis in Section 2.4, Equation (2-47). Figures 49, 50, 51 and 68 give a plot of \overline{uv}/U^2 , $\sqrt{\overline{u^2}}/U$, $\sqrt{\overline{v^2}}/U$ and $\sqrt{\overline{w^2}}/U$ versus y/δ respectively, each one containing data from eight stations along the boundary layer length. The measurements of \overline{uv} , $\sqrt{\overline{u^2}}$, and $\sqrt{\overline{v^2}}$ were taken with a single rotating wire probe, while $\sqrt{\overline{w^2}}$ measurements were made with a 45° inclined wire probe. Considering the uncertainty intervals for the quantities measured, Figures 49, 50, 51 and 68 suggest similarity of Reynolds stresses distributions across the outer portion of the turbulent boundary layer. In Figure 49, stations 1 and 2 are omitted and therefore the curve represents data from Station 3 downstream. This region was found to be free from distortions caused by gravel roughness at the entrance, according to considerations in Section 5.1. In Figures 50, 51 and 68 the first two stations are not omitted. The high level of intensities of turbulence at Stations 1 and 2 is apparently the result of the diffusion of the high turbulence generated by the roughness at the test section entrance. Therefore, Figures 49, 50, 51 and 68 show that the distributions of the turbulence quantities assume universal character from Station 3 downstream. This is the

same region in which the mean velocity distributions are similar. One can therefore conclude that in large scale turbulent boundary layers, turbulence quantities closely approach similarity conditions, and that the assumptions of similarity for all mean quantities of the flow in the analysis in Section 2.4 are verified. As supporting experimental evidence one should also point out recent, yet unpublished, measurements by Kawatani (20). These measurements were made in the canopy flow field at very low velocities of flow, and they show distinctly the existence of similarity for turbulence intensity distributions in the fully developed flow region, Figure 69.

Bradshaw (4) suggests that $\sqrt{\overline{u^2}}$, $\sqrt{\overline{v^2}}$, and \overline{uv} distributions across the boundary layer thickness should collapse on a single curve when nondimensionalized by constant scales U_∞ and δ . This was done on Figures 70, 71, 72 and 73. Data were plotted as \overline{uv}/U_∞^2 vs. y/δ , $\sqrt{\overline{u^2}}/U_\infty$ vs. y/δ , $\sqrt{\overline{v^2}}/U_\infty$ vs. y/δ and $\sqrt{\overline{w^2}}/U_\infty$ vs. y/δ . When the data points are closely examined, one finds that there is a systematic shift toward lower values in the ordinate as one proceeds from station to station along the boundary layer length. However, this shift seems to be toward an asymptotic universal curve which is achieved at high Reynolds numbers. This tendency supports the considerations from Section 5.2 where similarity of the form (5-8) was assumed for very high Reynolds numbers, and where the velocity scale was U_∞ . Figures 72 to 77 show that turbulent shear stress near the wall has a value very close to the wall shear stress. Within the uncertainty limits which can be set for turbulent shear stress measurements at the present time, there appears to be good agreement between the two. As was stated before and discussed in the light of the results of this

experiment, a constant wall shear is a necessary requirement if the boundary layer momentum thickness is a linear function of the x coordinate. This has been found to be the case.

Observing Figures 72 to 77 one comes to the conclusion that if a constant wall shear stress is a similarity requirement, and since the turbulent shear stress goes practically to zero at the outer edge of the boundary layer, i.e., for $y/\delta = 1.0$, then a linear function can be fitted to the turbulent shear stress distribution in the outer portion of the boundary layer as a first approximation. If one takes as an approximation that at the wall $\rho\overline{uv} \approx \tau_w$ and that at $y/\delta = 1.0$, $\rho\overline{uv} \approx 0$, a linear function of the form

$$-\rho\overline{uv} = a \frac{y}{\delta} + b \quad (5-22)$$

can be fitted to the turbulent shear stress distribution. The assumed boundary conditions

$$\text{for } \frac{y}{\delta} = 0 \quad -\rho\overline{uv} = \tau_w$$

and (5-23)

$$\text{for } \frac{y}{\delta} = 1.0 \quad -\rho\overline{uv} = 0$$

yield the values of the constants, and one obtains

$$-\rho\overline{uv} = \tau_w \left(1 - \frac{y}{\delta}\right) \quad (5-24)$$

or

$$-\overline{uv} = \frac{\tau_w}{\rho} \left(1 - \frac{y}{\delta}\right) . \quad (5-25)$$

If in accordance with the Equation (2-34), δ is substituted by Δ , the value of the constant b is changed and Equation (5-25) becomes

$$-\overline{uv} = u_\tau^2 \left(1 - \frac{1}{.25} \eta\right) . \quad (5-26)$$

Therefore, the universal function ψ_{12} becomes

$$\psi_{12} = 1 - \frac{1}{.25} \eta \quad . \quad (5-27)$$

In this manner from Equation (2-47) one of the similarity variables is eliminated. The method of solution of this equation should be the subject of a separate study.

The experimental results of this investigation are evidence that the large scale turbulent boundary layers developed on a flat plate with a zero pressure gradient closely approach similarity conditions. However, it has to be mentioned that in the test section of the wind tunnel, secondary flow exists. Secondary currents are formed whenever the wall conditions along the circumference of the cross-section of a conduit are not uniform, either because of geometry or roughness non-uniformity. Extensive measurements of this effect were made by various authors, the most detailed being those of Hoagland (19) and Gessner and Jones (12), and the most recently reported being the experiments of Hinze (18). From these sources one can summarize the following: the region exists where the law of the wall applies, but it is affected in such a way that it becomes thicker if the secondary flow is directed away from the wall. It can be concluded that the secondary currents are mainly present outside of the viscous sublayer part of the boundary layer. The measurements now in progress in the large wind tunnel at CSU indicate that the effect on the outer portion of the boundary layer is the thickening of the boundary layer in the region close to the center line and the decreasing of thickness toward the corners. The measurements indicate the secondary flow velocities are, at the most, about 2 percent of the free stream velocity of the flow. One might

conclude that the secondary flow affects the terms of the mean flow equation of motion. However, at present it is not possible to apply any corrections to the obtained data. In this experiment it was found that the variation of the momentum thickness is too great to give a wall shear stress value of a magnitude close to values obtained from Equations (5-4) and (5-5). During the experiment the secondary flow conditions were changed, but the similarity trend did not change. Therefore, it does not appear that the secondary flow affects similarity.

Chapter VI

CONCLUSIONS

The subject of this experimental study was a zero pressure gradient, large scale turbulent boundary layer developed along the floor of the large CSU wind tunnel. The results of measurements have been discussed in Chapter V. It was ascertained that the boundary layer assumes "normal" character within the first 20 to 25 feet of the test section. The compatibility of the similarity concept of the outer portion of the turbulent boundary layer with a zero pressure gradient was tested. To summarize the results and discussion given in the preceding chapter, the following conclusions can be drawn:

1. The experimental results show that the similarity requirements for the existence of local similarity of the form

$$\frac{U_{\infty} - U}{U_{\tau}} = F\left(\frac{y}{\Delta}, \frac{U_{\tau}}{U_{\infty}}\right)$$

are found in the large scale turbulent boundary layers.

2. The boundary layer displacement and momentum thickness grow in a linear manner with increase of the x coordinate. Their ratio, the form factor H, is very nearly constant along the boundary layer length. The value of form factor H = 1.286 obtained by van Doenhoff and Tetervin for conditions pertinent to the investigated boundary layer is confirmed.
3. A constant wall shear stress requirement is found to be very closely approached. The weak influence of the parameter ω is explained. For very large Reynolds numbers the wall shear stress approaches a constant value.

4. The mean velocity measurements suggest an approach to universality of the form

$$\frac{U}{U_{\infty}} = \phi \left(\frac{y}{\delta} \right) .$$

The requirements for this were considered. The comparison of experimental data and introduction of the suggested form into the governing equation of motion suggest that this might be the case reached at practically infinite Reynolds numbers. In this case one expects (45), that in the overlap region the relation

$$\frac{U}{U_{\infty}} = \left(\frac{y}{\delta} \right)^m$$

applies.

5. The best average universal velocity profile of the form

$$\frac{U_{\infty} - U}{U_{\tau}} = F \left(\frac{y}{\Delta} \right)$$

is tabulated.

6. The experimental measurements of turbulence quantities show that the similarity assumed actually exists. The similarity conditions are very closely approached. When U_{∞} is used as a velocity scale for turbulence quantities the influence of the increase of Reynolds number supports the considered approach to similarity of the form $U/U_{\infty} = \phi(y/\delta)$.

7. The turbulent shear stress distributions across the boundary layer thickness are approximated by a linear function of the form

$$-\overline{uv} = U_{\tau}^2 \left(1 - \frac{1}{.25} \eta\right),$$

the function ψ_{12} being defined as

$$\psi_{12} = 1 - \frac{1}{.25} \eta .$$

8. The methods for calculating uncertainty limits for turbulence quantities measurements are given, and the uncertainty intervals are calculated.
9. The influence of the secondary flow is considered and its prominent effect on the form factor H is indicated.

BIBLIOGRAPHY

1. Arya, S.P.S. and Plate, E.J. Hot-wire measurements of turbulence in a thermally stratified flow. U.S. Army Grant DA-AMC-28-043-65-G20, CEM67-68SPSA-EJP11, Colorado State University, February 1968.
2. Arya, S.P.S. Structure of stably stratified turbulent boundary layer. Ph. D. Dissertation, CED68-69SPSA15, Colorado State University, December 1968.
3. Baldwin, L.V., Sandborn, V.A. and Lawrence, J.C. "Heat Transfer from Transverse and Yawed Cylinders in Continuum, Slip and Free Molecule Flow." Journal of Heat Transfer, ASME Trans. Ser. C, vol. 82, No. 2, 1960.
4. Bradshaw, P. The turbulence structure of equilibrium boundary layers. J. Fluid Mech., 29, part 4, pp. 625-645, 1967.
5. Clauser, F.H. The Turbulent Boundary Layer. Advances in Applied Mechanics, vol. IV, Academic Press Inc., 1956.
6. Coles, D. The law of the wake in the turbulent boundary layer. J. Fluid Mech., 1, Part 2, pp. 191-226, 1956.
7. Coles, D. Remarks on the Equilibrium Turbulent Boundary Layer. J. Aero. Sci., Vol. 24, No. 7, July 1957, p. 495-506.
8. van Doenhoff, A.E. and Tetervin, N. Determination of General Relations for the Behavior of Turbulent Boundary Layers. NACA T Rep. 772 (1943).
9. van Driest, E.R. On turbulent flow near a wall. Journal of the Aeronautical Sciences, 23: 1007-1011, 1956.
10. Elias, F. The transference of heat from a hot plate in an air stream. NACA TM 614 (1931).
11. Finn, C.L. and Sandborn, V.A. The design of a constant temperature hot-wire anemometer. U.S. Army Research Grant DA-AMC-28-043-65-G20 and NACA NGR-06-002-038. CER66-67CLF36, Colorado State University, Fort Collins, March 1967.
12. Gessner, F.B. and Jones, J.B. On some aspects of fully-developed turbulent flow in rectangular channels. J. Fluid Mech., 23, p. 689, 1965.
13. Goldstein, S. A note on the measurement of total head and static pressure in a turbulent stream. Proc. Roy. Soc., London, A155, p. 570 (1936).
14. Gruschwitz, E. Die turbulente Reibungsschicht in ebener Stromung bei Druckabfall und Druckansteig. Ingenieur-Archiv., Band II, Heft 3, pp. 321-346, Sept. 1931.

15. Hama, F.R. Boundary Layer Characteristics for Smooth and Rough Surfaces. Trans. Soc. Naval Arch. Marine Engr. 62, pp. 333-358 (1954).
16. van der Hegge Zijnen, B.G. Heat transfer from horizontal cylinders to a turbulent airflow. Applied Scientific Research, Section A, 7:205-223, 1958.
17. Hinze, J.O. Turbulence. McGraw-Hill Book Co. Inc., 1959.
18. Hinze, J.O. Secondary Currents in Wall Turbulence. The Physics of Fluids Supplement, 1967.
19. Hoagland, L.C. Fully developed flow in straight rectangular ducts--Secondary flow, its cause and effect on the primary flow. Ph.D. Thesis, Massachusetts Institute of Technology, 1960.
20. Kawatani, T. Structure of a canopy fluid flow. Masters Thesis, CET67-68TK33, Colorado State University, 1968.
21. von Kármán, Th. Turbulence and skin friction. J. Aero. Sci., vol. 1, No. 1, Jan. 1934, p. 1-20.
22. von Kármán, T. Über laminare und turbulente Reibung. Z. angew. Math. Mech. 1, 233-252 (1921); also NACA TM 1092.
23. Klebanoff, P.S. and Diehl, Z.W. Some features of artificially thickened fully developed turbulent boundary layers with zero pressure gradient. NACA Rept. 1110, 1952.
24. Klebanoff, P.S. Characteristics of Turbulence in a Boundary Layer with Zero Pressure Gradient. NACA TN 3178 (1954).
25. Kline, S.J. and McClintock, F.A. Describing uncertainties in single sample experiment. Mechanical Engineering, Jan. 1953.
26. Kovasznay, L.S.G. Structure of the Turbulent Boundary Layer. The Physics of Fluids Supplement, 1967, vol. 10, No. 9, Part II.
27. Ludwig, H. and Eillmann, W. Investigation of the wall shearing stress in turbulent boundary layer. NACA TM 1285 (1950).
28. MacMillan, F.A. Experiments on Pitot-tubes in Shear Flow. Aeronautical Research Council Reports and Memoranda No. 3028, February, 1956.
29. Mellor, G.L. and Gibson, D.M. Equilibrium turbulent boundary layers. J. Fluid Mech., vol. 24, part 2, pp. 225-253, 1955.
30. Mellor, G.L. The effects of pressure gradients on turbulent flow near a smooth wall. J. Fluid Mech., vol. 24, part 2, pp. 255-274, 1966.

31. Mellor, G.L. Incompressible, turbulent boundary layers with arbitrary pressure gradients and divergent or convergent cross flows. *AIAA Journal*, vol. 5, no. 9, 1967.
32. Millikan, C. A critical discussion of turbulent flows in channels and circular tubes. *Proc. 5th Int. Cong. Appl. Mech.*, Cambridge, p. 386-392.
33. Nedderman, R.M. The measurement of velocities in the wall region of turbulent liquid pipe flow. *Chemical Engineering Science*, Vol. 16, pp. 120-126, Pergamon Press, Ltd., London, 1961.
34. Piercy, N.A.V., Richardson, E.G., and Winny, H.F. On the convection of heat from a wire moving through air close to a cooling surface. *The Proceedings of the Physical Society*, 69B: 731-742, 1956.
35. Plate, E.J. and Cermak, J.E. Micrometeorological Wind Tunnel Facility, Description and Characteristics. CSU Report, CER63EJP-JEC9, Feb. 1963.
36. Popovich, A.T. and Hummel, R.L. Experimental study of the viscous sublayer in turbulent pipe flow. *AIChE Journal*, September 1967.
37. Prandtl, L. Über Flüssigkeitsbewegung bei sehr kleiner Reibung. *I.M.K.*, 1904.
38. Prandtl, L. Über den Reibungswiderstand strömender Luft. *Ergeb. Aerodyn. Versuchsanst. Göttingen* 3, 1-5, München, 1927.
39. Prandtl, L. Recent results of turbulence research. *NACA Tech. Memo.* 720, (1933).
40. Prandtl, L. *Aerodynamic Theory*. Vol. 3, Durand, W.F. ed. Durand Reprinting Committee, Calif. Inst. Technol., 1943.
41. Rotta, J. Über die theorie der turbulenten Grenzschichten. *NACA TM* 1344 (1953).
42. Rotta, J.C. Turbulent boundary layers in incompressible flows. *Prof. in Aero. Sci.* Vol. 2, ed. Ferri, Küchemann and Sterne, Pergamon Press, N.Y., 1962.
43. Sandborn, V.A. and Slogar, R.J. Study of momentum distribution of turbulent boundary layers in adverse pressure gradients. *NACA Technical Note* 3264 (1955).
44. Sandborn, V.A. Hot-wire anemometer measurements in large scale boundary layers. U.S. Army Research Grant DA-AMC-28-043-65-G20, CER66-67VAS32, Colorado State University, March 1967.

45. Sandborn, V.A., Tieleman, H.W. and Liu, C.Y. The similarity of large scale turbulent boundary layers. Colorado State University, CER67-68VAS-HWT-CYL39, March 1968. Submitted to Journal of Fluid Mechanics.
46. Schubauer, G.B. and Tchen, C.M. Turbulent flow. Princeton University Press, 1961.
47. Schubauer, G.B. Turbulent Processes as Observed in Boundary Layer and Pipe. Journal of Applied Physics, Vol. 25, No. 2.
48. Stratford, B.S. An experimental flow with zero skin friction throughout its region of pressure raise. J. Fluid Mech., 5, 17-35, (1956).
49. Tieleman, H.W. Viscous Region of Turbulent Boundary Layer. U.S. Army Research Grant DA-AMC-28-043-65-G20, CER67-68HWT21, Colorado State University, Fort Collins, December 1967.
50. Townsend, A.A. The Structure of Turbulent Shear Flow. Univ. Press, Cambridge, 1956.
51. Townsend, A.A. The properties of equilibrium boundary layers. J. Fluid. Mech., Vol. 1, 561-573, 1956.
52. Webster, C.A.G. A note on the sensitivity to yaw of a hot-wire anemometer. Jour. Fluid. Mech., Vol. 13, 1962.
53. Wills, J.A.B. The correction of hot-wire readings for proximity to a solid boundary. Jour. Fluid Mech., 12:388-396, 1962.

APPENDIX A

COMMERCIAL EQUIPMENT

Pressure Meter

For pressure measurements a Trans-Sonics 120B Equibar pressure meter was used. The instrument utilizes a capacitance type transducer. This instrument is a portable differential micro-manometer with the following manufacturer's specifications:

Range: 0.001 mm Hg to 3 mm Hg full scale, in 8 steps.

D.C. output: 0-30 millivolts \pm 2%, proportional to pressure.

Accuracy of meter readings: \pm 3% full scale of selected range.

Response time: 10 milliseconds to 63% of a step change in pressure, at atmospheric pressure.

The pressure meter was used for measurements in the turbulent boundary layer. To obtain an accurate reading of dynamic pressure, which was subject to fluctuations, an integration procedure was employed. The D.C. output of the pressure meter was amplified 100 times by means of a D.C. amplifier, and then integrated for 3 minutes. The time span of integration was determined experimentally so that repeated measured values were within \pm 0.5%. Amplifier noise was calibrated by integrating for 3 minutes with a zero input to the amplifier, and using the result as a correction for integrated voltages. A calibration curve of pressure in mm Hg versus integrator output voltage was obtained for each scale range of the pressure meter (Figure 13).

True RMS Meter

To measure rms of the constant temperature hot-wire anemometer output, a DISA Type 55D35 True RMS Voltmeter was used. This voltmeter permits the integrator time constant to be varied for the best possible response time. The integration time depends on the wave form and frequency of the voltage under measurement.

Technical data:

Range: 12 full scale ranges from 1 mv to 300 mv in 1, 3, 10 sequence.

Frequency response: 1 Hz to 400 kHz.

Crest factor: 5 to 1 at full scale, inversely proportional to pointer deflection; e.g., 10 to 1 at half-scale deflection.

Input impedance: 1 megohm.

Time constant: 6 ranges from 0.1 to 30 seconds in a 1, 3, 10 sequence.

Amplifier

In the integration procedure which was used in the mean velocity measurements, a Dynamics Instrumentation Co., Model 3184 Amplifier was used. For the mentioned purpose this amplifier was used in combination with the Trans-Sonics Type 120B Equibar Pressure Meter, and an electronic integrating circuit, as described in 3.3.1 and 3.3.2.

Technical data:

Voltage gain: 0, 25, 50, 75, 100, 150, 250, 350, 500, 750, 1000
(changed in feedback circuit for optimum signal-to-noise ratio).

Maximum output voltage: ± 50 volts.

Gain accuracy: $\pm 1.0\%$ of set value.

Equivalent drift referred to the input: ± 2.0 microvolts in 40 hours operation after warm up.

Linearity: Better than 0.3% from dc to 5.0 kc.

Frequency response: Down 3.0 db at 30 kc.

Input impedance: 100,000 ohms.

Voltmeter

In all measurements a Hewlett-Packard 3440A Digital Voltmeter was used with a 3443A High Gain Auto Range Unit.

Technical data:

Sample rate: 5 samples per second to 1 per second.

Voltage range: 4 digit presentation in four steps from 99.99 mV to 999.9 volts full scale.

Range control: This control provides Manual Range selection for the five ranges provided. Automatic ranging from 100 mv to 1000 volts and Remote Ranging.

Accuracy: $\pm 0.05\%$ of reading ± 1 digit in voltage range to $\pm 0.1\%$ of reading ± 1 digit in millivolt range.

Input impedance: 10.2 Mohms all ranges.

Power Supply

As a constant voltage source for the potentiometers indicating the position of the hot-wire probes and wind tunnel carriage, a HLab Model 6226A Power Supply was used.

Technical data:

Input: 105-125/210-250 VAC, single phase 50-70 cps.

Output: 0-36 volts, 0-1, 5 amps.

Load regulation:

Constant voltage: Less than 0.02% or 2 mv for 1.5 amp load change.

Constant current : Less than 0.05% or 300 μ a for 36 volt load change.

Line regulation:

Constant voltage: Less than 0.02% or 2 mv from 105 to 125 VAC or from 125 to 105 VAC.

Constant current: Less than 0.03% or 250 μ a from 105 to 125 VAC or 125 to 105 VAC.

Operating temperature range: 0 - 50^oC.

Stability: As a constant voltage source, the total drift for 8 hours (after 30 minutes warmup) at a constant ambient is less than 0.05% or 5 mv.

APPENDIX B

CALCULATION OF THE TURBULENCE QUANTITIES FROM THE HOT-WIRE ANEMOMETER DATA, USING THE WANG ELECTRONIC CALCULATOR

In Section 4.2.2, the hot-wire anemometer techniques and calibration procedures were described and discussed. Here, only the direct use of the Wang Electronic Calculator will be described, and the calculator programs will be given.

1. Calculation of $\overline{u^2}$ and related quantities.

To obtain the values of $\overline{v^2}$, \overline{uv} , and $\overline{w^2}$ from the systems of Equations (4-14) and (4-15), the knowledge of $\overline{u^2}$ beforehand is required. Therefore, a program was written for calculation of $\overline{u^2}$. As the operating formula, Equation (4-17) was used:

$$\overline{u^2} = \frac{\overline{e^2}_{90}}{(S_U^2)_{90}} \quad (3-1)$$

Since the presentation of experimental results required the calculation of turbulence quantities, the program was extended so as to give these additional quantities. Therefore, Program No. 1 gives the following information: $\overline{u^2}$, $\sqrt{\overline{u^2}}$, $\sqrt{\overline{u^2}}/U$ and $\sqrt{\overline{u^2}}/U_\infty$.

The necessary input data are: $\sqrt{\overline{e^2}}$, root mean square of the hot-wire voltage output fluctuation; E_0 , the hot-wire mean voltage output for no flow conditions; S_U , velocity sensitivity of the hot-wire at the velocity U ; U , the local mean velocity of the flow; and U_∞ , the free stream velocity of the flow. The value of S_U can be obtained from the hot-wire

calibration curve by direct slope reading. It can also be obtained from the equation

$$\frac{\partial E}{\partial U} = \frac{mB}{2E} U^{m-1} \quad (B-2)$$

As described in Section 4.2.3, the values of m , E_0 and B may be obtained from the hot-wire calibration data. Since U is measured at each measurement point, one may include in a calculator program the calculation of S_U as well. Program No. 1 assumes that S_U is already known.

2. Calculation of $\overline{v^2}$, \overline{uv} and related quantities.

a) "Perfect" hot-wire.--In Section 4.2.2 the hot-wire with the characteristic

$$S_{U+40} = S_{U-40} ; S_{V+40} = S_{V-40} \quad (B-3)$$

was called a "perfect" hot-wire. When these characteristics are introduced into the system of Equations (4-14), one finds that the calculation of values of \overline{uv} and $\overline{v^2}$ becomes quite simple, provided that the value of $\overline{u^2}$ is already known.

Denoting

$$S_{U\pm 40} = S_U \quad \text{and} \quad S_{V\pm 40} = S_V \quad (B-4)$$

and rearranging the system of Equations (4-14), one obtains

$$\overline{e^2}_{+40} - S_U^2 \overline{u^2} = 2S_U S_V \overline{uv} + S_V^2 \overline{v^2} \quad (B-5)$$

$$\overline{e^2}_{-40} - S_U^2 \overline{u^2} = - 2S_U S_V \overline{uv} + S_V^2 \overline{v^2} .$$

Adding these two equations and rearranging, the operating formula for $\overline{v^2}$ is obtained:

$$\overline{v^2} = \frac{\overline{e^2}_{+40} + \overline{e^2}_{-40} - 2S_U^2 \overline{u^2}}{2S_V^2} \quad (\text{B-6})$$

Introduction of another relation known from the previous considerations simplifies the calculation further. If the constant

$$C = \frac{1 - a^2}{(1 + a^2 \cot^2 \theta)} \cdot \cot \theta \quad (\text{B-7})$$

has been determined, then Equation (B-6) becomes

$$\overline{v^2} = \frac{\overline{e^2}_{+40} + \overline{e^2}_{-40} - 2S_U^2 \overline{u^2}}{2C^2 S_U^2} \quad (\text{B-8})$$

In a similar manner, Equation (B-5) yields

$$\overline{uv} = \frac{\overline{e^2}_{+40} - \overline{e^2}_{-40}}{4C S_U^2} \quad (\text{B-9})$$

Obviously, the calculation program No. 2 is now necessarily more elaborate and needs more input information. Input informations are: S_U^2 , square of velocity sensitivity; $\sqrt{\overline{e^2}_{-40}}$ and $\sqrt{\overline{e^2}_{+40}}$, the root mean squares of hot-wire output voltage fluctuations at respective angles; and $\overline{u^2}$.

For the velocity sensitivity, S_U , an addition to the program can be made as for the program for the "perfect" hot wire.

b) "Real" hot-wire.--It was pointed out in the Section 4.2.2 that, in the case of the "real" hot-wire, S_U is the same for

$\pm 40^0$; however, this is not true for S_V , and $S_{V+40} \neq S_{V-40}$. Therefore, the system of equations to be solved for \overline{uv} and $\overline{v^2}$ is

$$\overline{e^2}_{+40} - S_U^2 \overline{u^2} = 2S_U S_{V+40} \overline{uv} + S_{V+40}^2 \overline{v^2} \quad (\text{B-10})$$

$$\overline{e^2}_{-40} - S_U^2 \overline{u^2} = -2S_U S_{V-40} \overline{uv} + S_{V-40}^2 \overline{v^2} .$$

Let A denote

$$\overline{e^2}_{+40} - S_U^2 \overline{u^2} = A_{+40} \quad (\text{B-11})$$

$$\overline{e^2}_{-40} - S_U^2 \overline{u^2} = A_{-40} .$$

Introducing (B-11) into the system of equations (B-10), and solving for \overline{uv} and $\overline{v^2}$, one obtains

$$\overline{v^2} = \frac{A_{-40}}{S_{V-40}(S_{V+40} + S_{V-40})} + \frac{A_{+40}}{S_{V+40}(S_{V+40} + S_{V-40})} \quad (\text{B-12})$$

and

$$\overline{uv} = \frac{A_{+40} S_{V-40}^2 - A_{-40} S_{V+40}^2}{2S_U (S_{V+40}^2 S_{V-40} + S_{V-40}^2 S_{V+40})} . \quad (\text{B-13})$$

It is convenient to tabulate values of S_U , S_{V+40} , and S_{V-40} . Also, since the Wang Calculator card can handle a total of 79 operations, A_{+40} and A_{-40} have to be calculated beforehand and tabulated, together with sensitivities. With these data available, it is possible to condense the calculation program on one card. Program No. 3 is composed on this basis. Since the program for calculation of $A_{\pm 40}$ makes the calculation

still faster, however, it is not included in this Appendix, being a simple one easily written when necessary.

c) Calculation of $\overline{w^2}$.--In section 4.2.2, it was found that in the case of this experiment the hot wire inclined at 45° behaved as a "perfect" hot-wire. Therefore, one can assume

$$S_{U+45} = S_{U-45} \quad \text{and} \quad S_{W+45} = - S_{W-45} \quad (\text{B-14})$$

and also

$$S_U = CS_W$$

In such a case, the system of equations (4-15) yields

$$\overline{w^2} = \frac{\overline{e^2}_{+45} + \overline{e^2}_{-45} - 2S_U^2 \overline{u^2}}{2C^2 S_U^2} \quad (\text{B-15})$$

which is the same form as Equation (B-8). Consequently, Program No. 2 can be used in this case, too; one may ignore \overline{uw} or use it as a check of two-dimensionality of the flow.

The constant C for an average value of $a = 0.20$ and $\vartheta = 45^\circ$ has the value $C = 0.925$.

CALCULATOR PROGRAM

No. 1

Date:

No.	Cmd	Code	Comment	No.	Cmd	Code	Comment
00	R ₁	15		40			
01	x ²	45		41			
02	+R	52		42			
03	R ₀	14		43			
04	x ²	45		44			
05	Enter	41		45			
06	R _R	51		46			
07	÷	47		47			
08	Stop	01	$\overline{u^2}$; cont.	48			
09	\sqrt{x}	44		49			
10	Stop	01	$\sqrt{u^2}$; cont.	50			
11	+L	56		51			
12	Enter	41		52			
13	R ₂	16		53			
14	÷	47		54			
15	Stop	01	$\sqrt{u^2/U}$; contd.	55			
16	R _L	55		56			
17	Enter	41		57			
18	R ₃	17		58			
19	÷	47		59			
20	Stop	01	$\sqrt{u^2/U_\infty}$	60			
21				61			
22				62			
23				63			
24				64			
25				65			
26				66			
27				67			
28				68			
29				69			
30				70			
31				71			
32				72			
33				73			
34				74			
35				75			
36				76			
37				77			
38				78			
39				79			

$\overline{u^2}$ program; No. 1

1. Store $\sqrt{e^2}$ in S₀
2. Store S_U in S₁
3. Store U in S₂
4. Store U_∞ in S₃

Clear all; Start.

1., 2., 3. repeated at each point.

Record values obtained at:

- 08 - $\overline{u^2}$
- 10 - $\sqrt{u^2}$
- 15 - $\sqrt{u^2/U}$
- 20 - $\sqrt{u^2/U_\infty}$

List of operations.

00		40	
01	Stop	41	Enter
02		42	Log _e x
03		43	e ^x
04		44	\sqrt{x}
05		45	x ²
06		46	x-
07		47	+-
10	Store	0	50 Clear Adder Right
11	Store	1	51 Recall Adder Right
12	Store	2	52 + Adder Right
13	Store	3	53 - Adder Right
14	Recall	0	54 Clear Adder Left
15	Recall	1	55 Recall Adder Left
16	Recall	2	56 + Adder Left
17	Recall	3	57 - Adder Left
20		60	0
21		61	1
22		62	2
23		63	3
24		64	4
25		65	5
26		66	6
27		67	7
30		70	8
31		71	9
32		72	.
33		73	÷
34		74	←
35		75	→
36		76	Clear Display
37		77	Change Sign

Blank indicates not assigned.



Wang Laboratories, Inc.

836 NORTH STREET

700 1201 12/67
TEWKSBURY, MASSACHUSETTS

CALCULATOR PROGRAM

No. 2

Date:

No.	Cmd	Code	Comment	No.	Cmd	Code	Comment
00	R ₁	15		40	Enter	41	
01	x ²	45		41	R _R	51	
02	-R	53		42	÷	47	
03	-L	57		43	Stop	01	\sqrt{z} cont.
04	+L	56		44	\sqrt{x}	44	
05	R ₂	16		45	Stop	01	$\sqrt{\sqrt{z}}$
06	x ²	45		46			
07	+R	52		47			
08	+L	56		48			
09	R _R	51		49			
10	Enter	41		50			
11	R _O	14		51			
12	÷	47		52			
13	Enter	41		53			
14	4	64		54			
15	÷	47		55			
16	Enter	41		56			
17	Stop	01	in C. Cont.	57			
18	S ₁	11		58			
19	÷	47		59			
20	Stop	01	\overline{uv} cont.	60			
21	Clear R	50		61			
22	R ₁	15		62			
23	x ²	45		63			
24	Enter	41		64			
25	2	62		65			
26	x	46		66			
27	Enter	41		67			
28	R _O	14		68			
29	x	46		69			
30	+R	52		70			
31	R ₃	17		71			
32	Enter	41		72			
33	2	62		73			
34	x	46		74			
35	Enter	41		75			
36	R _O	14		76			
37	x	46		77			
38	-L	57		78			
39	R ₁			79			

\overline{uv} , \sqrt{z} program; No. 2

1. Store S_U^2 in S_0
2. Store $\sqrt{e^2_{-40}}$ in S_1
3. Store $\sqrt{e^2_{+40}}$ in S_2
4. Store $\overline{u^2}$ in S_3

Clear all. Start.

Type in C. Continue

Record values obtained at:

- 20 - \overline{uv}
- 43 - \sqrt{z}
- 45 - $\sqrt{\sqrt{z}}$

List of operations.

00	Stop	40
01	Stop	41 Enter
02		42 Log _a x
03		43 e ^x
04		44 \sqrt{x}
05		45 x ²
06		46 X=
07		47 +=
10	Store 0	50 Clear Adder Right
11	Store 1	51 Recall Adder Right
12	Store 2	52 + Adder Right
13	Store 3	53 - Adder Right
14	Recall 0	54 Clear Adder Left
15	Recall 1	55 Recall Adder Left
16	Recall 2	56 + Adder Left
17	Recall 3	57 - Adder Left
20		60 0
21		61 1
22		62 2
23		63 3
24		64 4
25		65 5
26		66 6
27		67 7
30		70 8
31		71 9
32		72
33		73
34		74
35		75
36		76 Clear Display
37		77 Change Sign

Blank indicates not assigned.



Wang Laboratories, Inc.

836 NORTH STREET

700 1201 12/67
TEWKSBURY, MASSACHUSETTS

CALCULATOR PROGRAM

No. 3

Date:

No.	Cmd	Code	Comment	No.	Cmd	Code	Comment
00	Enter	41		40	x	46	
01	R ₂	16		41	-L	57	
02	x ²	45		42	Enter	41	
03	x	46		43	R ₂	16	
04	-L	57		44	:	47	
05	R ₀	14		45	Stop	01	\overline{uv} ; cont.
06	+L	56		46	S ₂	12	
07	S ₃	13		47	Clear L	54	
08	Stop	01	in A ₊₄₀ ; cont.	48	R ₀	14	
09	R ₀	14		49	Enter	41	
10	-L	57		50	R _R	51	
11	R ₁	15		51	x	46	
12	+L	56		52	+L	56	
13	+R	52		53	R ₁	15	
14	Stop	01	in A ₋₄₀ ; 4., 5.	54	Enter	41	
15	Clear L	54		55	R ₃	17	
16	R ₀	14		56	x	46	
17	+L	56		57	+L	56	
18	Enter	41		58	S ₃	13	
19	R ₁	15		59	Clear L	54	
20	+L	56		60	R ₀	14	
21	Enter	41		61	+L	56	
22	R ₂	16		62	R ₁	15	
23	Enter	41		63	+L	56	
24	R ₁	15		64	Enter	41	
25	Enter	41		65	R ₀	14	
26	2	62		66	Enter	41	
27	x	46		67	R ₁	15	
28	S ₂	12		68	x	46	
29	Clear L	54		69	S ₀	10	
30	R ₃	17		70	R ₃	17	
31	Enter	41		71	Enter	41	
32	R ₁	15		72	R ₀	14	
33	x ²	45		73	:	47	
34	x	46		74	Stop	01	$\overline{v^2}$
35	+L	56		75	\sqrt{x}	44	
36	R _R	51		76	Stop	01	$\sqrt{\overline{v^2}}$
37	Enter	41		77			
38	R ₀	14		78			
39	x ²	45		79			

\overline{uv} ; $\overline{v^2}$ program; No. 3

1. Store $e^{\overline{2}_{+40}}$ in S₀
2. Store $e^{\overline{2}_{-40}}$ in S₁
3. Store S_U in S₂

Clear all type in $\overline{u^2}$

Start

Type in A₊₄₀; continue

4. Store S_{V+40} in S₀
5. Store S_{V-40} in S₁

Type in A₋₄₀; continue

Record values obtained at:

$$45 - \overline{uv}$$

$$74 - \overline{v^2}$$

$$77 - \sqrt{\overline{v^2}}$$

List of operations.

00		40	Enter
01	Stop	41	Enter
02		42	Log _e x
03		43	e ^x
04		44	\sqrt{x}
05		45	x ²
06		46	x =
07		47	÷ =
10	Store	0	50 Clear Adder Right
11	Store	1	51 Recall Adder Right
12	Store	2	52 + Adder Right
13	Store	3	53 - Adder Right
14	Recall	0	54 Clear Adder Left
15	Recall	1	55 Recall Adder Left
16	Recall	2	56 + Adder Left
17	Recall	3	57 - Adder Left
20		60	0
21		61	1
22		62	2
23		63	3
24		64	4
25		65	5
26		66	6
27		67	7
30		70	8
31		71	9
32		72	
33		73	
34		74	
35		75	
36		76	Clear Display
37		77	Change Sign

Blank indicates not assigned.



Wang Laboratories, Inc.

836 NORTH STREET

700 1201 12/67
TEWKSBURY, MASSACHUSETTS

APPENDIX C

UNCERTAINTY INTERVALS

Mean Velocity Measurements

In the case of mean velocity measurements one has to consider the measurement of the velocity with a Pitot static tube in an air stream. The formula used for calculation of mean velocity is:

$$u = 2.36 \sqrt{\frac{\Delta h}{\rho_a}} \quad . \quad (C-1)$$

Δh in this case is measured by a Trans-Sonic Type 120 B Equibar pressure meter. This instrument has $\pm 2\%$ accuracy in D.C. output of the instrument, i.e., Δh was calibrated against a Meriam Model 34FB2 TM Micromanometer. This micromanometer is maintained as the laboratory standard. The micromanometer accuracy is 0.001 in $H_2O \cong 0.001868$ mm Hg. The uncertainty of $\pm 2\%$ in D.C. output causes an uncertainty of $\pm 1.9\%$ in the Δh value. In turn the D.C. output was determined through the integration procedure for averaging; however, these measurements were repeated within 0.5%. Therefore, an uncertainty of $\pm 2\%$ for Δh was assumed.

Density Measurements

To determine the uncertainty interval for density, Clapeyron's equation of state was used:

$$pv = RT$$

$$\therefore \rho = \frac{p}{RT} = \frac{1}{53,3 \times 32,2} \cdot \frac{p}{T} = A \frac{p}{T} \quad (C-2)$$

where

$$A = 0.000583 \left[\frac{^{\circ}F \text{ sec}^2}{ft^2} \right] \quad .$$

From here one obtains:

$$\frac{\partial \rho}{\partial p} = \frac{A}{T} \quad ; \quad \text{and} \quad \frac{\partial \rho}{\partial T} = - \frac{Ap}{T^2} \quad . \quad (C-3)$$

Therefore,

$$w_{\rho} = \left[\left(\frac{\partial \rho}{\partial p} w_p \right)^2 + \left(\frac{\partial \rho}{\partial T} w_T \right)^2 \right]^{1/2}$$

or

$$w_{\rho} = \left[\left(\frac{A}{T} w_p \right)^2 + \left(- \frac{Ap}{T^2} w_T \right)^2 \right]^{1/2} \quad . \quad (C-4)$$

Temperature was measured by mercury-in-glass thermometer. Therefore, one can assume:

$$w_T = \pm 0.5^{\circ} F_{\text{abs}} \quad .$$

Pressure was measured by a bellows-type barometer made by Frieze Instruments, Baltimore. Accuracy of this instrument is 0.05 in Hg , or 3.537 lb/ft , or 0.0246 psi. Therefore,

$$w_p = \pm 3,537 \text{ lb/ft}^2 \quad .$$

The equation (C-4) may be nondimensionalized; one obtains, using the above given values:

$$\frac{w_{\rho}}{\rho} = \left[\left(\frac{3.537}{\rho} \right)^2 + \left(- \frac{0.5}{T} \right)^2 \right]^{1/2} \quad . \quad (C-5)$$

The results for the range of changes in p and T as applies to these measurements are listed below:

Range of change

P	24.62 - 24.94 in Hg or 1741.45 - 1764.08 lb/ft ²
T	25 - 30°C or 536.4 - 545.4 °F abs
w _ρ /ρ	0.00223 - 0.002205

According to the assumption of uncertainty for h of ± 2%:

$$w_{\Delta h} = \pm 0.068 \text{ mm Hg for the highest value of } \Delta h$$

and

$$w_{\Delta h} = \pm 0.001 \text{ mm Hg for the lowest value of } \Delta h.$$

From equation (C-1) one obtains

$$\frac{\partial u}{\partial \rho} = - 1.18 \sqrt{\Delta h / \rho_a^3}$$

and

$$\frac{\partial u}{\partial \Delta h} = 1.18 / \sqrt{\Delta h \rho_a}$$

Therefore

$$w_u = \left[\left(\frac{\partial u}{\partial \rho} w_{\rho} \right)^2 + \left(\frac{\partial u}{\partial \Delta h} w_{\Delta h} \right)^2 \right]^{1/2}$$

or if this equation is nondimensionalized:

$$\frac{w_u}{u} \left[\left(-0.5 \frac{w_{\rho}}{\rho} \right)^2 + \left(0.5 \frac{w_{\Delta h}}{\Delta h} \right)^2 \right]^{1/2} \quad (C-6)$$

The results for the given range of changes in ρ and h are listed below:

	Range of change
ρ	1.865 - 1.905 x 10 ⁻³ slug/cu ft
Δh	0.1 - 3.5 mm Hg
w _u /u	0.005123 - 0.00978

Therefore, one can claim that the mean velocity measurements in this experiment are within the uncertainty interval of ± 1 percent. Now one has to consider also the effects which were discussed in section 4.1.2. The above calculated uncertainty intervals are obtained on the basis of known or estimated uncertainties of the instrumentation. The errors introduced by the effects that were discussed in section 4.1.2 are reflected in the result so that the calculated uncertainty is superimposed. Accounting for the possible uncorrected errors, one can therefore claim that the results of the mean velocity measurements are within an uncertainty interval which is less than ± 2 percent, except very close to the wall where it might be up to ± 3 percent of the correct value.

Turbulence Measurements

1) Uncertainty intervals for U and E.

In the preceding section the uncertainty intervals for mean velocity measurements were determined for the applicable range of changes in Δh . The obtained values, therefore, can be used in the process of determining the uncertainty intervals for turbulence measurements. However, for the mean voltage, the output of the hot-wire uncertainty interval must be determined. Direct measurement of the output mean voltage was done, during the calibration of the hot wires, with Hewlett-Packard 3440A Digital Voltmeter. The calibrations were performed in the free stream at Station 1 of the wind tunnel test section. Free stream turbulence was very low (Figure 4). Therefore, the following value is assumed to be true for mean voltage measurements where the value of E is obtained by direct measurement:

$$\frac{w_E}{E} = 0.05\% . \quad (C-7)$$

If we consider values of the mean voltage obtained from the calibration curve, then the relation given by equation (4-7) allows us to determine the uncertainty interval for E since the uncertainty interval for U was determined in the first section of this Appendix. The value of exponent m in Equation (4-7) is very close to 0.5. Therefore, one can with confidence assume that

$$\frac{w_E^2}{E^2} \sim \frac{1}{2} \frac{w_U}{U} \quad \text{or} \quad \frac{w_E^2}{E^2} \sim 0.5\%$$

which means that $\frac{w_E}{E} \sim 0.25\% . \quad (C-8)$

2) Uncertainty interval for $\sqrt{u^2}$.

The mean square of the x-direction component of the velocity fluctuation is obtained from Equation (4-17):

$$\overline{u^2} = \frac{\overline{e^2}_{90}}{(S_U^2)_{90}} . \quad (C-9)$$

Therefore, applying Equation (4-22) and nondimensionalizing one obtains

$$\frac{w_{\overline{u^2}}}{\overline{u^2}} = \left[\left(\frac{\partial \overline{u^2}}{\partial \overline{e^2}} w_{\overline{e^2}} \right)^2 + \left(\frac{\partial \overline{u^2}}{\partial S_U^2} w_{S_U^2} \right)^2 \right]^{1/2} \frac{1}{\overline{u^2}}$$

or

$$\frac{w_{\overline{u^2}}}{\overline{u^2}} = \left[\left(\frac{w_{\overline{e^2}}}{\overline{e^2}} \right)^2 + \left(- \frac{w_{S_U^2}}{S_U^2} \right)^2 \right]^{1/2} . \quad (C-10)$$

A DISA Type 55D35 True RMS Voltmeter was used for the measurement of rms of the hot-wire anemometer output. Manufacturer gives the

accuracy of this instrument for the mean square output as 10%. Therefore, it was assumed that

$$\frac{\overline{w e^2}}{\overline{e^2}} = 0.10 .$$

For hot-wire sensitivity to velocity if one assumes that the data point scatter is within the uncertainty interval, one can assume the uncertainty interval of

$$\frac{w S_U^2}{S_U^2} = 0.20 ,$$

Introducing these values into Equation (C-10) the uncertainty interval for \overline{u} is obtained as

$$\frac{\overline{w u^2}}{\overline{u^2}} = 0.223$$

or

$$\frac{w \sqrt{\overline{u^2}}}{\sqrt{\overline{u^2}}} = 0.1165 = 11.65\% .$$

- 3) Uncertainty interval for \overline{v} and for turbulent shear stress measurement.

The values of the mean square of y-direction component of the velocity fluctuation and of the turbulent shear stress were obtained from the system of Equations (4-14). Denoting

$$A_{+40} = \overline{e^2}_{+40} - S_U^2 \overline{u^2}$$

and

(C-11)

$$A_{-40} = \overline{e^2}_{-40} - S_U^2 \overline{u^2}$$

the final formulas for calculation may be written in the following forms:

$$\overline{uv} = \frac{A_{+40} S_{V-40}^2 - A_{-40} S_{V+40}^2}{2S_U S_{V+40} S_{V-40} (S_{V+40} + S_{V-40})} \quad (C-12)$$

and

$$\overline{v^2} = \frac{1}{S_{V+40} S_{V-40}} \left(\frac{A_{-40}}{S_{V-40}} + \frac{A_{+40}}{S_{V+40}} \right) . \quad (C-13)$$

Recalling now the considerations of the hot-wire calibrations in Section 3, in connection with references (1 and 52), one can introduce the relations between the hot-wire sensitivity to the change of velocity and the hot-wire sensitivity to the change of angle of yaw. One obtains

$$S_{V+40} = CS_U ; \quad S_{V-40} = DS_U$$

and consequently (C-14)

$$S_{V+40} = \frac{C}{D} S_{V-40}$$

where C and D are known constants for a certain hot-wire. With introduction of relations (C-14), the Equations (C-12) and (C-13) become

$$\overline{uv} = \frac{A_{+40} - A_{-40} \left(\frac{C}{D}\right)^2}{2S_U^2 \left(\frac{C}{D}\right) (C+D)} \quad (C-15)$$

and

$$\overline{v^2} = \frac{1}{S_U^2} \left(\frac{A_{-40}}{\frac{C}{D} + 1} + \frac{A_{+40}}{\frac{D}{C} + 1} \right) . \quad (C-16)$$

To proceed to find the uncertainty intervals for \overline{uv} and $\overline{v^2}$ using the equations (C-15) and (C-16), one has to find the uncertainty interval for $A_{\pm 40}$. The Equation (C-11) yields

$$\frac{\partial A}{\partial \theta^2} = 1; \quad \frac{\partial A}{\partial S_U^2} = -\overline{u^2}; \quad \frac{\partial A}{\partial u^2} = -S_U^2 . \quad (C-17)$$

Introducing the expressions (C-17) into Equation (4-22), the following form is obtained

$$w_A = [(1 \cdot \overline{w_{e^2}})^2 + (-\overline{u^2} w_{S_U^2})^2 + (-S_U^2 \overline{w_{u^2}})^2]^{\frac{1}{2}} \quad (C-18)$$

and by nondimensionalizing

$$\frac{w_A}{A} = \left[\left(\frac{\overline{w_{e^2}}}{A} \right)^2 + \left(-\frac{\overline{u^2}}{A} w_{S_U^2} \right)^2 + \left(-\frac{S_U^2}{A} \overline{w_{u^2}} \right)^2 \right]^{\frac{1}{2}} \quad (C-19)$$

which is valid for $\pm 40^\circ$.

With known uncertainties for involved variables, listed below

Variable, V_i	$\overline{e^2} \pm 40$	S_U^2	$\overline{u^2}$
$\frac{w_i}{V_i}$	0.10	0.20	0.1165

one obtains

$$w_{A \pm 40} = 0.014 \quad \text{at the most,} \quad (C-20)$$

or

$$\frac{w_A}{A} = \begin{cases} 0.006 & \text{for } + 40^\circ \\ 0.028 & \text{for } - 40^\circ \end{cases}$$

at the highest values of turbulence intensity.

4) Uncertainty interval for \overline{uv} ,

With previously obtained uncertainty intervals for S_U^2 , and $A_{\pm 40}$, it is now possible to determine the uncertainty interval for the turbulent shear stress. Equation (C-15), when partially differentiated, yields

$$\frac{\partial \overline{uv}}{\partial A_{+40}} = \frac{1}{2S_U^2 \left(\frac{C}{D}\right) (C+D)}$$

$$\frac{\partial \overline{uv}}{\partial A_{-40}} = - \frac{C/D}{2S_U^2 (C+D)} \quad (C-21)$$

and

$$\frac{\partial \overline{uv}}{\partial S_U^2} = \frac{A_{-40} \left(\frac{C}{D}\right)^2 - A_{+40}}{2S_U^2 \frac{C}{D} (C+D)} .$$

Therefore, the uncertainty interval for \overline{uv} is obtained by introduction of expressions (C-21) into Equation (4-22):

$$w_{\overline{uv}} = \left[\left(\frac{D/C}{2S_U^2 (C+D)} w_{A_{+40}} \right)^2 + \left(- \frac{C/D}{2S_U^2 (C+D)} w_{A_{-40}} \right)^2 + \left(\frac{A_{-40} \left(\frac{C}{D}\right)^2 - A_{+40}}{2(S_U^2)^2 \frac{C}{D} (C+D)} w_{S_U^2} \right)^2 \right]^{1/2} \quad (C-22)$$

or in nondimensionalized form

$$\frac{w_{\overline{uv}}}{\overline{uv}} = \left\{ \left[\frac{w_{A_{+40}}}{A_{+40} - A_{-40} \left(\frac{C}{D}\right)^2} \right]^2 + \left[- \frac{\left(\frac{C}{D}\right)^2 w_{A_{-40}}}{A_{+40} - A_{-40} \left(\frac{C}{D}\right)^2} \right]^2 + \left(\frac{w_{S_U^2}}{S_U^2} \right)^2 \right\}^{1/2} . \quad (C-23)$$

In the case of this experiment, for the hot-wires used in the turbulence measurements, the average values for the constants C and D were:

$$C = 1.18 \quad D = 0.846$$

therefore

$$\frac{C}{D} = 1.39 \quad \frac{D}{C} = 0.717 .$$

Introduction of these values, and values for previously determined uncertainties, gives the uncertainty interval for turbulent shear stress

$$\frac{w_{\overline{uv}}}{\overline{uv}} = 0.201 \quad (C-24)$$

where values for $A_{\pm 40}$ were those corresponding to the highest values of turbulence intensity.

5) Uncertainty interval for $\overline{v^2}$,

Using Equation (C-16), and partially differentiating it with respect to involved variables one obtains

$$\frac{\partial \overline{v^2}}{\partial A_{-40}} = \frac{1}{S_U^2} \frac{1}{\frac{C}{D} + A}$$

$$\frac{\partial \overline{v^2}}{\partial A_{+40}} = \frac{1}{S_U^2} \frac{1}{\frac{D}{C} + 1} \quad (C-25)$$

$$\frac{\partial \overline{v^2}}{\partial S_U^2} = - \frac{1}{(S_U^2)^2} \left[\frac{1}{\frac{C}{D} + 1} + \frac{1}{\frac{D}{C} + 1} \right]$$

By introduction of expressions (4-46), one obtains

$$\begin{aligned} w_{\overline{v^2}} = & \left\{ \left(\frac{1}{S_U^2} \frac{1}{\frac{C}{D} + 1} w_{A-40} \right)^2 + \left(\frac{1}{S_U^2} \frac{1}{\frac{D}{C} + 1} w_{A+40} \right)^2 \right. \\ & \left. + \left[- \left(\frac{A_{-40}}{\frac{C}{D} + 1} + \frac{A_{+40}}{\frac{D}{C} + 1} \right) \frac{w_{S_U^2}}{(S_U^2)^2} \right]^2 \right\}^{1/2} \quad (C-26) \end{aligned}$$

or in nondimensional form

$$\begin{aligned} \frac{w_{\overline{v^2}}}{\overline{v^2}} = & \left\{ \left[\frac{w_{A-40}}{A_{-40} + \frac{\frac{C}{D} + 1}{\frac{D}{C} + 1} A_{+40}} \right]^2 + \right. \\ & \left. + \left[\frac{w_{A+40}}{A_{+40} + \frac{\frac{D}{C} + 1}{\frac{C}{D} + 1} A_{-40}} \right]^2 + \left[\frac{w_{S_U^2}}{S_U^2} \right]^2 \right\}^{1/2} \quad (C-27) \end{aligned}$$

Using the same average values for constants C and D in Equation (C-27) and previously obtained values for the uncertainty intervals w_{A+40} and $w_{S_U^2}$, one obtains

$$\frac{w_{\overline{v^2}}}{\overline{v^2}} = 0.2001 = 20\%$$

or

$$\frac{w\sqrt{\overline{v^2}}}{\sqrt{\overline{v^2}}} = 10\% .$$

Obtained values are of the same order of magnitude as the values estimated by other authors (44, 49). However, one might say that they can be claimed with more confidence when calculated.

The uncertainty interval for $\overline{w^2}$ was not calculated, the assumption being made that it has to be of the same order of magnitude as the uncertainty interval for $\overline{v^2}$. The assumption is based on the fact that in the calculation of $\overline{w^2}$, the constants of the same order of magnitude are involved, and the uncertainty intervals of the variables involved are the same. Therefore, it was assumed that the uncertainty interval for $\overline{w^2}$ is

$$\frac{w\sqrt{\overline{w^2}}}{\sqrt{\overline{w^2}}} = 10\% .$$

TABLE I — MEAN VELOCITY DISTRIBUTIONS

Run No. 1

Station 1, x = 7 ft, 11 in.

 $U_{\infty} = 62.10$ ft/sec $\rho = 1.869 \times 10^{-3}$ slug/cu ft

y in.	U ft/sec
0.1563	35.80
0.400	39.22
0.69	41.54
0.90	43.33
1.20	44.30
1.625	46.14
2.30	48.21
2.91	49.73
4.48	54.73
6.63	60.56
7.10	60.817
9.80	62.10

Station 2, x = 17 ft, 11 in.

 $U_{\infty} = 61.330$ ft/sec $\rho = 1.873 \times 10^{-3}$ slug/cu ft

y in.	U ft/sec
0.0625	31.06
0.316	38.61
0.496	40.69
0.772	44.32
1.131	44.72
1.526	46.47
2.226	48.73
2.906	49.11
4.386	51.11
6.536	53.27
8.646	56.88
9.576	57.51
11.866	59.38
13.096	60.37
15.35	61.330

Run No. 1

Station 3, x = 27 ft, 11 in.

 $U_{\infty} = 61.600$ ft/sec $\rho = 1.87 \times 10^{-3}$ slug/cu ft

y in.	U ft/sec
0.125	33.65
0.300	39.22
0.560	41.78
0.805	43.38
1.425	46.04
2.155	48.24
3.255	50.08
5.395	52.44
8.780	55.72
10.850	56.81
12.895	58.24
15.09	59.87
16.130	60.49
18.995	61.08

Station 4, x = 37 ft, 11 in.

 $U_{\infty} = 62.20$ ft/sec $\rho = 1.873 \times 10^{-3}$ slug/cu ft

y in.	U ft/sec
0.1875	34.39
0.271	36.70
0.691	41.63
1.151	44.20
2.165	47.13
3.361	48.97
5.521	51.66
8.721	53.93
10.821	54.99
13.036	57.32
15.541	58.67
17.751	59.87
19.081	60.63
21.41	62.20

TABLE I - Continued:

Run No. 1

Station 5, x = 47 ft, 11 in.

$$U_{\infty} = 67.62 \text{ ft/sec}$$

$$\rho = 1.873 \times 10^{-3} \text{ slug/cu ft}$$

y in.	U ft/sec
0.0938	30.49
0.247	35.64
1.052	42.34
2.283	45.60
3.383	47.91
6.417	51.24
9.667	53.36
12.911	55.91
16.287	57.42
18.487	58.86
20.027	59.24
22.117	60.51
23.860	61.62

Run No. 1

Station 7, x = 67 ft, 11 in.

$$U_{\infty} = 61.10 \text{ ft/sec}$$

$$\rho = 1.873 \times 10^{-3} \text{ slug/cu ft}$$

y in.	U ft/sec
0.0938	28.37
0.5238	36.93
1.614	42.81
3.164	45.55
6.490	49.31
10.524	52.58
15.028	54.94
19.524	59.50
21.824	58.72
23.494	59.73
23.98	58.86
26.67	60.63
29.63	61.10

Station 6, x = 57 ft, 11 in.

$$U_{\infty} = 62.4 \text{ ft/sec}$$

$$\rho = 1.873 \times 10^{-3} \text{ slug/cu ft}$$

y in.	U ft/sec
0.0938	30.47
0.2038	34.03
0.994	41.70
2.138	45.01
4.374	48.55
7.474	51.52
12.94	54.80
17.574	57.94
20.713	59.50
22.134	60.51
23.523	61.08
26.12	62.40

Station 8, x = 77 ft, 11 in.

$$U_{\infty} = 60.68 \text{ ft/sec}$$

$$\rho = 1.885 \times 10^{-3} \text{ slug/cu ft}$$

y in.	U ft/sec
0.0938	14.99
0.5538	37.05
1.634	42.22
3.144	45.26
6.514	48.97
10.774	51.75
15.101	54.87
20.437	56.85
23.524	58.83
24.30	58.41
26.53	59.61
29.74	60.3
33.90	60.68

TABLE I - Continued:

Run No. 2

Station 2, x = 17 ft, 11 in.

 $U_{\infty} = 75.20$ ft/sec $\rho = 1.896 \times 10^{-3}$ slug/cu ft

Station 3, x = 27 ft, 11 in.

 $U_{\infty} = 75.33$ ft/sec $\rho = 1.885 \times 10^{-3}$ slug/cu ft

Station 4, x = 37 ft, 11 in.

 $U_{\infty} = 75.40$ ft/sec $\rho = 1.869 \times 10^{-3}$ slug/cu ft

y in.	U ft/sec	y in.	U ft/sec	y in.	U ft/sec
0.438	54.19	0.250	45.95	0.250	43.52
0.7345	56.82	0.574	52.67		
0.9994	58.45	0.8906	54.87	1.0947	54.50
1.323	59.99	1.513	61.49	2.8419	63.05
1.676	60.79	2.177	61.88	4.605	65.57
2.911	63.55	4.158	64.91	7.255	67.79
3.222	64.20	7.701	67.96	11.848	70.42
4.547	65.58	12.909	71.47	15.361	72.63
5.254	66.65	16.355	73.51	18.375	72.93
7.377	68.79			18.794	73.36
9.737	71.14	18.699	74.49		
11.007	72.37	21.10	75.33	25.40	75.40
13.263	74.18				
14.283	74.61				
15.673	74.98				
17.00	75.2				

Run No. 2

Station 5, x = 47 ft, 11 in.

 $U_{\infty} = 75.50$ ft/sec $\rho = 1.882 \times 10^{-3}$ slug/cu ft

Station 6, x = 57 ft, 11 in.

 $U_{\infty} = 75.40$ ft/sec $\rho = 1.879 \times 10^{-3}$ slug/cu ft

y in.	U ft/sec	y in.	U ft/sec
0.125	43.05	0.0625	38.06
0.323	46.96	0.1854	43.82
1.442	58.67	1.1181	53.76
2.5148	61.09	2.5310	60.55
3.6678	63.18	4.7953	63.10
7.0179	66.60	8.1082	66.63
10.491	69.13	14.0428	69.77
14.0939	71.31	17.2560	71.92
17.982	73.61	20.656	73.29
18.448	73.15	22.920	74.57
19.567	71.50	29.30	75.40
20.640	74.29		
21.695	74.90		
27.80	75.50		

TABLE I - Continued:

Run No. 2

Station 7, x = 67 ft 11 in.

 $U_{\infty} = 75.50$ ft/sec $\rho = 1.879 \times 10^{-3}$ slug/cu ft

y in.	U ft/sec
0.125	38.25
0.5560	47.49
1.7896	54.68
3.3405	60.99
7.2219	65.40
11.5183	68.06
16.4531	75.90
17.0471	75.85
21.4655	73.53
25.3469	75.06
29.6735	76.07
31.827	75.50
35.20	76.89

Station 8, x = 77ft, 11 in.

 $U_{\infty} = 75.50$ ft/sec $\rho = 1.879 \times 10^{-3}$ slug/cu ft

y in.	U ft/sec
0.250	43.46
1.1513	52.30
3.3572	57.31
7.0042	64.26
11.5978	67.43
18.375	70.94
21.4822	72.74
25.1292	74.01
29.7238	75.32
34.5252	75.50
36.180	75.50

Run No. 3

Station 1, x = 7 ft, 11 in.

 $U_{\infty} = 83.75$ ft/sec $\rho = 1.891 \times 10^{-3}$ slug/cu ft

y in.	U ft/sec
0.3438	59.10
0.5410	62.07
0.8579	64.58
1.5238	66.67
2.1297	68.46
3.7143	72.28
4.7583	74.43
7.1247	79.02
8.5237	81.40
9.4308	82.89
11.10	83.75

Station 2, x = 17 ft, 11 in.

 $U_{\infty} = 84.54$ ft/sec $\rho = 1.872 \times 10^{-3}$ slug/cu ft

y in.	U ft/sec
0.250	55.63
0.5834	60.66
0.9360	65.73
1.3712	67.78
1.6448	68.63
2.7368	71.26
3.2541	72.12
4.4327	74.03
5.2911	74.97
7.6877	77.71
10.3858	80.70
12.258	82.81
14.1489	84.13
16.40	84.54

TABLE I - Continued:

Run No. 3

Station 3, x = 27 ft, 11 in.

 $U_{\infty} = 84.00$ ft/sec $\rho = 1.872 \times 10^{-3}$ slug/cu ft

y in.	U ft/sec
0.250	54.93
0.465	60.15
0.8606	63.75
1.1564	65.36
1.4798	65.66
2.3057	68.69
3.4857	71.60
6.1142	74.85
8.6477	76.50
10.9329	78.84
14.4175	81.27
16.0946	82.38
18.590	83.51
20.40	84.00

Station 4, x = 37 ft, 11 in.

 $U_{\infty} = 84.10$ $\rho = 1.891 \times 10^{-3}$ slug/cu ft

y in.	U ft/sec
0.3125	50.83
0.7811	60.68
1.2697	63.36
2.4627	67.57
4.2259	70.99
6.1515	73.33
9.9679	76.46
12.8493	78.40
16.8003	81.19
18.3941	82.48
18.4375	81.88
18.9061	81.89
23.60	84.10

Run No. 3

Station 5, x = 47 ft, 11 in.

 $U_{\infty} = 83.9$ ft/sec $\rho = 1.891 \times 10^{-3}$ slug/cu ft

y in.	U ft/sec
0.1563	51.30
0.3679	56.76
1.1187	63.04
2.3845	67.54
3.9737	70.41
6.9177	73.76
9.9407	76.02
14.068	78.74
18.5403	81.11
19.2437	81.73
20.5095	83.09
22.193	83.86
26.65	83.90

Station 6, x = 57 ft, 11 in.

 $U_{\infty} = 83.9$ ft/sec $\rho = 1.891 \times 10^{-3}$ slug/cu ft

y in.	U ft/sec
0.09375	47.72
0.4369	56.94
0.9688	61.92
2.0555	66.07
4.5556	70.72
8.0077	74.12
12.889	77.46
15.3992	78.96
20.1805	81.39
22.6806	82.68
31.014	84.01

TABLE I - Continued:

Run No. 3

Station 7, x = 67 ft, 11 in.

 $U_{\infty} = 83.6$ ft/sec $\rho = 1.891 \times 10^{-3}$ slug/cu ft

y in.	U ft/sec
0.125	48.60
0.5988	57.15
1.7397	63.34
3.4329	67.33
6.7876	71.44
11.7733	75.53
16.3762	78.16
19.8647	79.63
21.5579	80.77
24.9126	82.57
29.8983	83.49
33.70	83.60

Station 8, x = 77 ft, 11 in.

 $U_{\infty} = 83.5$ ft/sec $\rho = 1.891 \times 10^{-3}$ slug/cu ft

y in.	U ft/sec
0.1875	49.53
0.7939	58.53
2.9044	64.46
5.5724	69.58
10.3888	73.46
15.6366	77.17
18.8568	78.81
21.0294	79.80
23.6974	81.18
28.5138	83.09
33.7616	83.55
36.9818	83.46

Run No. 4

Station 1, x = 7 ft, 11 in.

 $U_{\infty} = 95.00$ ft/sec $\rho = 1.885 \times 10^{-3}$ slug/cu ft

y in.	U ft/sec
0.3438	65.45
0.4998	68.74
0.7999	71.50
1.2629	73.96
1.6730	75.79
2.1173	77.33
3.2554	81.26
4.9355	84.73
6.9218	88.32
8.1837	93.80
10.302	95.00

Station 2, x = 17 ft, 11 in.

 $U_{\infty} = 94.70$ ft/sec $\rho = 1.885 \times 10^{-3}$ slug/cu ft

y in.	U ft/sec
0.2813	64.77
0.4943	69.31
0.9615	73.67
1.4455	76.10
1.6676	76.85
2.7233	79.95
3.320	81.35
4.4007	83.17
5.2604	84.45
7.2914	86.92
9.9655	90.60
11.8064	92.66
13.1545	93.94
15.70	94.70

TABLE I - Continued:

Run No. 4

Station 3, x = 27 ft, 11 in.

 $U_{\infty} = 94.5$ ft/sec $\rho = 1.885 \times 10^{-3}$ slug/cu ft

y in.	U ft/sec
0.250	61.59
0.5228	69.16
0.9648	73.03
1.5960	75.94
2.2055	78.01
3.2203	80.18
5.8480	84.23
7.8458	86.41
10.1376	88.39
13.7510	91.43
14.7123	92.52
16.4803	93.79
20.1895	94.50

Station 4, x = 37 ft, 11 in.

 $U_{\infty} = 94.4$ ft/sec $\rho = 1.882 \times 10^{-3}$ slug/cu ft

y in.	U ft/sec
0.3125	61.09
0.4921	65.30
0.7725	69.37
1.2941	72.64
2.5655	76.91
3.8539	80.03
5.4413	82.50
8.1545	85.32
11.4608	87.77
14.3227	89.80
17.03	92.30
19.5869	93.83
20.1588	94.00
20.4392	94.16
20.9608	93.93
22.2322	94.40

Run No. 4

Station 5, x = 47 ft, 11 in.

 $U_{\infty} = 94.1$ ft/sec $\rho = 1.882 \times 10^{-3}$ slug/cu ft

y in.	U ft/sec
0.0605	52.40
0.3128	62.36
0.9952	70.21
2.0891	75.20
3.7808	78.36
6.7096	83.18
9.1119	85.50
13.4589	88.54
16.1308	90.30
20.6619	92.51
21.7486	93.29
23.1475	93.70
25.7975	94.10

Station 6, x = 57 ft, 11 in.

 $U_{\infty} = 95.0$ ft/sec $\rho = 1.882 \times 10^{-3}$ slug/cu ft

y in.	U ft/sec
0.1563	57.49
0.4339	65.08
0.9035	69.65
1.8776	74.09
3.5478	78.44
6.0009	82.45
7.9214	84.37
12.4762	87.70
15.1193	89.75
20.5720	91.90
21.5443	92.86
23.2145	93.94
25.6676	95.00

TABLE I - Continued:

Run No. 4

Station 7, x = 67 ft, 11 in.

 $U_{\infty} = 94.9$ ft/sec $\rho = 1.882 \times 10^{-3}$ slug/cu ft

y in.	U ft/sec
0.1563	56.46
0.5318	64.28
1.4657	70.98
2.5038	74.85
5.4188	79.92
9.3415	84.57
13.2002	87.07
15.1008	88.34
21.1318	91.06
22.1705	92.03
25.0855	94.33
29.0082	94.90

Station 8, x = 77 ft, 11 in.

 $U_{\infty} = 94.5$ ft/sec $\rho = 1.882 \times 10^{-3}$ slug/cu ft

y in.	U ft/sec
0.250	58.37
0.6118	64.53
1.9203	72.15
3.2136	75.87
6.4314	80.60
10.6635	84.59
14.2658	86.77
21.587	90.18
22.8803	91.09
26.0981	92.77
30.3302	94.13
33.9325	94.50

TABLE I - MEAN VELOCITY DISTRIBUTIONS* (Cont'd)

Run No. 1'

Station 1, x = 10 ft

 $U_{\infty} = 61.80$ ft/sec $\rho = 1.895 \times 10^{-3}$ slug/cu ft

y in.	U ft/sec
0.250	35.96
0.515	39.17
0.804	40.85
1.054	41.85
1.491	43.46
2.121	45.32
2.724	47.22
4.263	52.03
6.315	58.19
7.162	60.05
7.873	61.07
8.348	61.51
8.780	61.67

Station 2, x = 20 ft

 $U_{\infty} = 61.33$ ft/sec $\rho = 1.900 \times 10^{-3}$ slug/cu ft

y in.	U ft/sec
0.250	33.73
0.496	39.40
0.756	41.97
1.500	45.52
2.927	49.06
4.645	51.81
7.153	55.75
9.537	58.83
10.725	60.07
12.906	61.15
14.337	61.33

TABLE I - Continued:

Run No. 1'

Station 3, x = 30 ft

 $U_{\infty} = 61.08$ ft/sec $\rho = 1.900 \times 10^{-3}$ slug/cu ft

y in.	U ft/sec
0.0938	32.17
0.3411	38.33
0.7371	42.16
1.4276	45.35
2.3434	47.84
3.9993	50.70
5.8866	52.70
9.4942	56.72
14.030	60.33
17.6305	61.08
20.013	60.92
20.859	61.08

Station 4, x = 40 ft

 $U_{\infty} = 60.90$ ft/sec $\rho = 1.900 \times 10^{-3}$ slug/cu ft

y in.	U ft/sec
0.250	36.31
0.6420	40.60
1.0713	43.09
2.3514	46.95
3.4871	49.03
5.8802	52.26
9.5165	55.49
11.788	57.54
14.434	59.32
17.822	60.47
20.860	60.82
21.894	60.89

Run No. 1'

Station 5, x = 50 ft

 $U_{\infty} = 60.90$ ft/sec $\rho = 1.900 \times 10^{-3}$ slug/cu ft

y in.	U ft/sec
0.125	33.26
0.3130	37.13
1.0111	42.603
2.3487	46.45
4.5343	50.03
7.0754	53.00
15.777	58.39
17.927	60.20
20.263	60.76
21.940	60.92

Station 6, x = 60 ft

 $U_{\infty} = 60.94$ ft/sec $\rho = 1.905 \times 10^{-3}$ slug/cu ft

y in.	U ft/sec
0.0938	29.58
0.8048	40.62
2.0956	45.43
4.0712	48.55
6.7913	51.97
9.750	54.45
14.391	57.70
17.657	59.74
20.117	60.42
21.599	60.35
22.805	
25.764	

TABLE I - Continued:

Run No. 1'

Station 7, x = 70 ft

 $U_{\infty} = 60.85$ ft/sec $\rho = 1.905 \times 10^{-3}$ slug/cu ft

y in.	U ft/sec
0.1875	33.85
0.3736	36.90
1.330	42.42
2.497	45.07
4.263	48.20
7.163	50.76
10.278	54.15
14.224	56.85
18.510	59.24
20.277	60.12
22.299	60.51
23.177	60.85

Station 8, x = 80 ft

 $U_{\infty} = 60.90$ ft/sec $\rho = 1.900 \times 10^{-3}$ slug/cu ft

y in.	U ft/sec
0.1563	31.54
0.5596	37.99
1.574	43.04
2.755	45.42
6.914	50.43
10.354	53.44
14.525	56.40
18.729	58.65
22.928	60.82
26.368	60.85

Run No. 5

Station 1 & 2, x = 18 ft

 $U_{\infty} = 60.38$ ft/sec $\rho = 1.875 \times 10^{-3}$ slug/cu ft

y in.	U ft/sec
0.3332	34.049
0.3833	35.589
0.4446	36.591
0.6181	38.453
0.9760	46.014
1.717	44.047
2.801	46.714
4.656	50.306
6.083	52.838
9.866	58.799
11.70	60.38
15.53	60.655

Station 3, x = 28 ft

 $U_{\infty} = 61.06$ ft/sec $\rho = 1.870 \times 10^{-3}$ slug/cu ft

y in.	U ft/sec
0.3037	33.432
0.3668	35.660
0.4788	37.562
0.6225	39.324
1.032	42.197
1.655	44.900
3.074	48.322
4.875	51.248
6.380	53.014
10.053	57.493
12.295	59.441
16.421	61.124
19.56	61.055

TABLE I - Continued:

Run No. 5

Station 4, x = 38 ft

 $U_{\infty} = 61.20$ ft/sec $\rho = 1.850 \times 10^{-3}$ slug/cu ft

y in.	U ft/sec
0.2651	33.686
0.3354	35.276
0.4182	36.515
0.5521	38.071
0.9229	40.824
1.564	43.818
2.486	46.276
3.943	48.975
5.430	51.017
8.386	54.504
11.93	57.728
15.72	60.486
18.76	60.611
20.86	60.912

Station 5, x = 48 ft

 $U_{\infty} = 61.51$ ft/sec $\rho = 1.860 \times 10^{-3}$ slug/cu ft

y in.	U ft/sec
0.1778	27.563
0.2483	31.191
0.3226	33.194
0.4693	36.192
0.7749	39.191
1.512	43.251
2.393	48.899
3.910	48.717
5.355	51.409
8.918	54.833
11.883	57.676
15.75	60.005
18.83	61.236
22.10	61.509

Run No. 5

Station 6, x = 58 ft

 $U_{\infty} = 61.28$ ft/sec $\rho = 1.850 \times 10^{-3}$ slug/cu ft

y in.	U ft/sec
0.2949	32.36
0.3361	33.75
0.4285	35.60
0.6234	37.82
1.386	42.65
2.911	46.57
4.940	49.746
6.732	52.027
9.670	54.99
12.94	57.80
17.27	60.24
21.53	66.13
23.65	61.28

Station 7, x = 68 ft

 $U_{\infty} = 60.90$ ft/sec $\rho = 1.850 \times 10^{-3}$ slug/cu ft

y in.	U ft/sec
0.2515	31.28
0.3028	32.62
0.3848	34.33
0.4997	35.94
0.8643	39.16
1.525	42.26
2.871	45.58
7.006	51.39
9.637	53.55
12.84	56.17
16.96	58.83
20.54	60.57
23.49	60.90

Station 8, x = 78 ft

 $U_{\infty} = 60.90$ ft/sec $\rho = 1.850 \times 10^{-3}$ slug/cu ft

y in.	U ft/sec
0.0956	28.97
0.2807	29.06
0.4345	33.13
0.6394	36.16
0.8728	38.59
1.460	41.57
2.190	43.60
5.173	48.60
8.123	51.91
11.820	55.08
15.53	57.57
20.00	59.63
23.59	60.90

TABLE I - Continued:

Run No. 3'

Station 1, x = 10 ft

 $U_{\infty} = 83.36$ ft/sec $\rho = 1.870 \times 10^{-3}$ slug/cu ft

y in.	U ft/sec
0.375	50.15
0.552	52.74
1.5531	58.85
3.4789	67.32
4.6358	72.70
6.8500	80.58
9.1615	83.19
9.9087	83.31
10.511	83.36

Station 2, x = 20 ft

 $U_{\infty} = 82.32$ ft/sec $\rho = 1.870 \times 10^{-3}$ slug/cu ft

y in.	U ft/sec
0.1875	48.58
0.5490	50.90
0.8877	58.75
1.5438	62.31
3.1096	66.93
5.0204	71.32
7.4905	76.81
11.3642	81.81
13.6345	82.30
15.2062	82.32

Run No. 3'

Station 3, x = 30 ft

 $U_{\infty} = 82.42$ ft/sec $\rho = 1.870 \times 10^{-3}$ slug/cu ft

y in.	U ft/sec
0.125	47.41
0.3751	53.72
0.6321	56.99
1.2887	61.50
2.0358	64.23
3.0365	67.00
5.7148	72.32
8.3071	76.47
10.5733	79.51
13.6116	81.98
15.2055	82.27
16.150	82.42

Station 4, x = 40 ft

 $U_{\infty} = 81.45$ ft/sec $\rho = 1.870 \times 10^{-3}$ slug/cu ft

y in.	U ft/sec
0.1875	46.91
0.4506	53.789
0.9645	57.931
2.0830	63.137
4.1801	67.56
5.8412	71.289
10.446	77.686
13.589	80.344
17.211	81.446

TABLE I - Continued:

Run No. 3'

Station 5, x = 50 ft

 $U_{\infty} = 82.50$ ft/sec $\rho = 1.880 \times 10^{-3}$ slug/cu ft

y in.	U ft/sec
0.125	43.714
0.3174	50.374
0.9604	57.846
2.1309	62.778
3.7451	66.545
4.7186	68.402
8.0648	73.969
13.042	79.251
17.954	81.909
19.111	81.569
19.340	82.246
20.085	81.621
20.684	82.296

Station 6, x = 60 ft

 $U_{\infty} = 81.86$ ft/sec $\rho = 1.880 \times 10^{-3}$ slug/cu ft

y in.	U ft/sec
0.0935	41.291
0.301	49.661
0.937	56.878
1.956	61.436
4.248	66.76
8.490	73.219
13.197	78.069
15.127	79.773
19.614	81.569
23.856	81.809
28.563	81.861

Run No. 3'

Station 7, x = 70 ft

 $U_{\infty} = 81.74$ ft/sec $\rho = 1.890 \times 10^{-3}$ slug/cu ft

y in.	U ft/sec
0.157	43.549
0.541	50.157
1.777	58.981
3.678	64.107
6.992	69.762
12.089	75.883
16.572	80.035
19.044	80.575
22.358	81.668
27.455	81.739

Station 8, x = 75 ft

 $U_{\infty} = 81.96$ ft/sec $\rho = 1.890 \times 10^{-3}$ slug/cu ft

y in.	U ft/sec
0.0938	39.960
0.3521	49.605
1.6920	59.441
3.7044	64.688
7.035	69.995
12.0526	75.598
16.824	79.912
19.070	80.698
22.401	81.835
27.419	81.956

* Clean Screens

TABLE II - TURBULENT BOUNDARY LAYER PARAMETERS

Station	x ft	U_∞ ft/sec	U_τ ft/sec	c_f	τ_w lb/ft ²	δ in	δ^* in	θ in	H	ν ft ² /sec	R_θ
Run No. 1											
1	7'11"	62.00	1.949	1.972×10^{-3}	7.10×10^{-3}	8.30	1.340	0.990	1.353	2.05×10^{-4}	24991
2	17'11"	61.33	1.945	2.013×10^{-3}	7.085×10^{-3}	14.50	1.740	1.350	1.289	2.05×10^{-4}	33657
3	27'11"	61.60	1.947	1.999×10^{-3}	7.092×10^{-3}	18.30	2.130	1.700	1.253	2.05×10^{-4}	42569
4	37'11"	62.20	1.946	1.959×10^{-3}	7.095×10^{-3}	21.50	2.525	2.050	1.232	2.05×10^{-4}	51833
5	47'11"	61.62	1.930	1.915×10^{-3}	6.980×10^{-3}	24.20	2.925	2.400	1.219	2.05×10^{-4}	60878
6	57'11"	62.40	1.910	1.876×10^{-3}	6.836×10^{-3}	26.00	3.325	2.750	1.209	2.05×10^{-4}	69756
7	67'11"	61.10	1.867	1.862×10^{-3}	6.527×10^{-3}	27.50	3.720	3.110	1.196	2.05×10^{-4}	77370
8	77'11"	60.68	1.850	1.848×10^{-3}	6.411×10^{-3}	28.40	4.110	3.475	1.183	2.05×10^{-4}	85717
Run No. 2											
2	17'11"	75.2	2.53	2.26×10^{-3}	1.215×10^{-2}	13.90	1.438	1.200	1.1983	2.01×10^{-4}	36683
3	27'11"	75.3	2.43	2.15×10^{-3}	1.115×10^{-2}	18.40	1.710	1.425	1.200	2.02×10^{-4}	44267
4	37'11"	75.4	2.437	2.08×10^{-3}	1.111×10^{-2}	20.90	1.978	1.656	1.1944	2.02×10^{-4}	51511
5	47'11"	75.5	2.43	2.02×10^{-3}	1.112×10^{-2}	22.70	2.250	1.890	1.1905	2.03×10^{-4}	58578
6	57'11"	75.4	2.35	1.939×10^{-3}	1.039×10^{-2}	24.80	2.530	2.111	1.1985	2.03×10^{-4}	65427
7	67'11"	75.5	2.32	1.882×10^{-3}	1.010×10^{-2}	26.40	2.810	2.340	1.200	2.03×10^{-4}	72525
8	77'11"	75.5	2.28	1.829×10^{-3}	0.980×10^{-2}	27.00	3.100	2.578	1.202	2.03×10^{-4}	79901
Run No. 3											
1	7'11"	83.75	2.83	2.280×10^{-3}	1.512×10^{-2}	9.40	1.181	0.975	1.211	2.03×10^{-4}	33521
2	17'11"	84.54	2.79	2.175×10^{-3}	1.455×10^{-2}	13.30	1.440	1.194	1.206	2.06×10^{-4}	40834
3	27'11"	84.00	2.70	2.070×10^{-3}	1.368×10^{-2}	17.40	1.706	1.410	1.210	2.06×10^{-4}	47913
4	37'11"	84.10	2.66	1.999×10^{-3}	1.337×10^{-2}	20.00	1.975	1.640	1.204	2.03×10^{-4}	56619
5	47'11"	83.90	2.62	1.949×10^{-3}	1.297×10^{-2}	21.60	2.230	1.860	1.199	2.03×10^{-4}	64062
6	57'11"	83.90	2.56	1.866×10^{-3}	1.242×10^{-2}	23.40	2.506	2.075	1.208	2.03×10^{-4}	71466
7	67'11"	83.60	2.52	1.823×10^{-3}	1.205×10^{-2}	26.10	2.775	2.300	1.206	2.03×10^{-4}	78933
8	77'11"	83.50	2.49	1.773×10^{-3}	1.169×10^{-2}	27.00	3.050	2.525	1.208	2.03×10^{-4}	86557
Run No. 4											
1	7'11"	95.0	3.184	2.246×10^{-3}	1.911×10^{-2}	8.375	1.060	0.870	1.218	2.04×10^{-4}	33762
2	17'11"	94.7	3.041	2.062×10^{-3}	1.743×10^{-2}	12.96	1.330	1.075	1.237	2.04×10^{-4}	41586
3	27'11"	94.5	3.038	2.067×10^{-3}	1.740×10^{-2}	11.65	1.600	1.335	1.1985	2.04×10^{-4}	51535
4	37'11"	94.4	3.025	2.049×10^{-3}	1.722×10^{-2}	18.80	1.749	1.565	1.176	2.03×10^{-4}	60711
5	47'11"	94.1	2.947	1.954×10^{-3}	1.635×10^{-2}	21.70	2.130	1.800	1.183	2.03×10^{-4}	69680
6	57'11"	95.0	2.916	1.884×10^{-3}	1.600×10^{-2}	23.60	2.400	2.025	1.185	2.03×10^{-4}	78972
7	67'11"	94.9	2.876	1.841×10^{-3}	1.557×10^{-2}	25.30	2.670	2.260	1.181	2.03×10^{-4}	87951
8	77'11"	94.5	2.845	1.807×10^{-3}	1.522×10^{-2}	27.00	2.940	2.500	1.176	2.03×10^{-4}	97085

TABLE II - TURBULENT BOUNDARY LAYER PARAMETERS* (Cont'd)

Station	x	U_∞	U_t	c_f	τ_w	δ	δ^*	θ	H	ν	R_θ
	ft	ft/sec	ft/sec		lb/ft ²	in	in	in		ft ² /sec	
Run No. 5											
1&2	18	60.38	1.910	2.007×10^{-3}	6.839×10^{-3}	10.83	1.725	1.325	1.302	2.09×10^{-4}	31890
3	28	61.06	1.912	1.961×10^{-3}	6.815×10^{-3}	13.53	1.950	1.513	1.289	2.01×10^{-4}	37100
4	38	61.20	1.937	2.004×10^{-3}	6.980×10^{-3}	16.20	2.175	1.740	1.250	2.07×10^{-4}	42910
5	48	61.51	1.921	1.950×10^{-3}	6.863×10^{-3}	17.90	2.373	1.899	1.250	2.05×10^{-4}	47500
6	58	61.28	1.857	1.837×10^{-3}	6.382×10^{-3}	19.00	2.533	1.976	1.282	2.05×10^{-4}	49280
7	68	60.90	1.885	1.917×10^{-3}	6.576×10^{-3}	19.90	2.733	2.213	1.235	2.05×10^{-4}	55320
8	78	60.90	1.801	1.748×10^{-3}	5.999×10^{-3}	21.50	2.967	2.315	1.286	2.03×10^{-4}	57900
Run No. 1'											
1	10	61.8	1.945	1.981×10^{-3}	7.17×10^{-3}	7.95	1.450	1.088	1.333	2.03×10^{-4}	27611
2	20	61.33	1.930	1.981×10^{-3}	7.08×10^{-3}	11.65	1.687	1.294	1.304	2.02×10^{-4}	32728
3	30	61.08	1.994	2.129×10^{-3}	7.55×10^{-3}	14.00	1.850	1.500	1.233	2.02×10^{-4}	37797
4	40	60.90	1.925	1.997×10^{-3}	7.04×10^{-3}	16.80	2.100	1.672	1.256	2.02×10^{-4}	41995
5	50	60.90	1.811	1.772×10^{-3}	6.23×10^{-3}	18.40	2.430	1.850	1.314	2.01×10^{-4}	46642
6	60	60.94	1.904	1.955×10^{-3}	6.91×10^{-3}	19.50	2.576	2.094	1.230	2.01×10^{-4}	52905
7	70	60.85	1.806	1.760×10^{-3}	6.21×10^{-3}	20.80	2.850	2.213	1.288	2.01×10^{-4}	55826
8	80	60.90	1.818	1.790×10^{-3}	6.28×10^{-3}	22.90	3.038	2.400	1.266	2.01×10^{-4}	60597
Run No. 3'											
1	10	33.36	2.448	1.725×10^{-3}	1.121×10^{-2}	8.37	1.413	1.0225	1.381	2.04×10^{-4}	34819
2	20	32.32	2.568	1.946×10^{-3}	1.233×10^{-2}	11.00	1.513	1.180	1.282	2.04×10^{-4}	39667
3	30	32.42	2.605	1.998×10^{-3}	1.269×10^{-2}	12.95	1.650	1.325	1.245	2.04×10^{-4}	44604
4	40	31.45	2.538	1.9425×10^{-3}	1.205×10^{-2}	14.40	1.800	1.437	1.252	2.05×10^{-4}	47599
5	50	32.30	2.498	1.843×10^{-3}	1.173×10^{-2}	16.25	2.067	1.640	1.260	2.04×10^{-4}	55149
6	60	31.86	2.508	1.877×10^{-3}	1.182×10^{-2}	17.13	2.200	1.780	1.236	2.04×10^{-4}	59509
7	70	31.74	2.360	1.668×10^{-3}	1.053×10^{-2}	18.25	2.540	1.960	1.295	2.05×10^{-4}	65112
8	75	31.96	2.437	1.768×10^{-3}	1.122×10^{-2}	19.20	2.550	2.030	1.256	2.05×10^{-4}	67647

* Clean Screens

TABLE III - UNIVERSAL VELOCITY PROFILE $\Delta = \frac{\delta^* U_\infty}{U_t}$

$\frac{U_\infty - U}{U_t}$	$\frac{y}{\Delta}$
18.00	0.001
15.90	0.002
13.70	0.004
12.36	0.006
11.52	0.008
10.87	0.010
9.77	0.015
9.02	0.020
8.45	0.025
7.98	0.030
7.55	0.035
7.17	0.040
6.81	0.045
6.50	0.050
5.94	0.060
5.44	0.070
4.97	0.080
4.14	0.100
3.36	0.120
2.63	0.140
1.97	0.160
1.35	0.180
1.07	0.190
0.81	0.200
0.56	0.210
0.36	0.220
0.20	0.230
0.11	0.240
0.05	0.250
0.00	0.260

TABLE IV - TURBULENCE QUANTITIES

Run No. 4

Station 1, $x = 17$ ft $U_{\infty} = 60.2$ ft/sec $\rho = 1.850 \times 10^{-3}$ slug/cu ftStation 2, $x = 22$ ft $U_{\infty} = 60.0$ ft/sec $\rho = 1.855 \times 10^{-3}$ slug/cu ft

y in.	U	$\sqrt{u^2}$	$\frac{\overline{uv}}{x(-1)}$	$\sqrt{v^2}$	y in.	U	$\sqrt{u^2}$	$\frac{\overline{uv}}{x(-1)}$	$\sqrt{v^2}$
.2115	31.27	4.411	3.269	1.785	.1841	30.85	4.160	3.333	2.131
.2728	33.79	4.386	3.762	2.141	.2366	32.99	4.169	3.565	2.293
.3248	35.10	4.366	4.000	2.311	.3063	35.36	4.232	3.474	2.284
.3550	35.66	4.394	3.684	2.219	.4071	37.48	4.263	4.063	2.401
.4793	37.87	4.295	4.063	2.559	.6065	40.15	4.255	4.071	2.447
.5917	39.27	4.297	3.933	2.544	.7912	41.62	4.188	4.000	2.498
.7352	40.86	4.263	4.536	2.607	1.251	44.12	4.064	3.909	2.490
1.0123	42.04	4.174	4.250	2.576	1.729	45.55	3.859	4.000	2.515
1.459	44.04	4.061	4.000	2.679	2.259	46.74	3.763	4.111	2.976
2.100	45.74	4.005	4.100	2.651	3.735	49.47	3.521	4.500	2.712
3.400	48.22	3.867	4.556	2.896	5.301	57.85	3.387	4.286	2.761
4.901	50.96	3.917	5.714	2.909	7.001	53.49	3.306	4.500	2.520
7.253	54.95	3.838	4.333	2.443	8.831	56.09	3.018	2.667	2.180
9.430	55.00	2.665	2.333	2.040	10.572	58.22	2.417	2.000	1.852
12.319	60.12	.916	2.000	1.016	12.343	59.29	1.458	.800	1.238
14.102	59.91	.457	0		14.410	59.74	.664	.200	.721
					15.914	59.87	.429	0	

Station 3, $x = 32$ ft $U_{\infty} = 60.36$ ft/sec $\rho = 1.860 \times 10^{-3}$ slug/cu ftStation 4, $x = 42$ ft $U_{\infty} = 59.20$ ft/sec $\rho = 1.860 \times 10^{-3}$ slug/cu ft

y in.	U	$\sqrt{u^2}$	$\frac{\overline{uv}}{x(-1)}$	$\sqrt{v^2}$	y in.	U	$\sqrt{u^2}$	$\frac{\overline{uv}}{x(-1)}$	$\sqrt{v^2}$
.1391	30.85	3.850	3.963	2.779	.1712	30.19	4.170	3.571	2.239
.1889	32.62	4.193	3.870	2.394	.2234	31.41	4.193	3.720	2.287
.2474	34.64	4.312	3.750	2.344	.2851	33.92	4.289	3.714	2.310
.3408	36.60	4.314	4.059	2.423	.3480	35.16	4.274	4.211	2.463
.4517	38.22	4.320	4.063	2.446	.4619	37.34	4.331	3.824	2.470
.6908	40.64	4.205	4.846	2.463	.7994	40.43	4.232	4.214	2.604
.9981	42.37	4.107	4.083	2.591	1.006	41.58	4.229	3.615	2.286
1.742	45.38	3.848	3.900	2.449	1.748	44.78	3.880	3.600	2.560
2.472	47.66	3.624	3.444	2.330	2.480	46.54	3.588	3.889	2.406
3.949	50.04	3.331	3.375	2.414	3.966	48.85	3.276	3.125	2.224
5.485	51.92	3.113	3.143	2.380	5.443	50.70	3.087	2.875	2.259
6.930	53.49	3.100	2.167	1.779	6.950	52.49	2.959	2.857	2.192
9.911	56.40	2.710	2.167	1.950	9.966	54.88	2.557	2.167	1.899
12.85	60.41	1.923	1.200	1.580	12.88	57.12	2.158	1.400	1.516
15.82	60.68	.922	.250	.807	15.97	58.84	1.395	.600	.962
17.66	60.36	.529	0		18.94	59.14	.659	.200	.626

TABLE IV - TURBULENCE QUANTITIES - Continued

Run No. 4 - Cont'd.

Station 5, $x = 52$ ft $U_{\infty} = 59.75$ ft/sec $\rho = 1,860 \times 10^{-3}$ slug/cu ftStation 6, $x = 62$ ft $U_{\infty} = 60.20$ ft/sec $\rho = 1,865 \times 10^{-3}$ slug/cu ft

y in.	U	$\sqrt{u^2}$	$\frac{\overline{uv}}{x(-1)}$	$\sqrt{v^2}$	y in.	U	$\sqrt{u^2}$	$\frac{\overline{uv}}{x(-1)}$	$\sqrt{v^2}$
.1840	29.87	4.036	3.034	2.049	.1785	33.98	4.403	3.571	2.155
.2359	31.84	4.068	3.480	2.272	.2408	35.50	4.341	3.842	2.385
.3213	34.58	4.093	3.900	2.454	.3336	36.82	4.312	3.882	2.443
.4530	36.84	4.094	3.882	2.468	.4980	38.78	4.237	4.067	2.499
.9575	41.05	4.041	3.769	2.429	.9286	41.41	4.110	3.154	2.174
1.702	43.80	3.867	3.273	2.052	1.671	44.07	3.905	3.182	2.134
2.736	46.30	3.529	2.900	2.216	2.914	46.50	3.470	3.444	2.264
4.548	48.96	3.280	3.000	2.076	4.978	49.39	3.252	3.000	2.076
6.597	51.23	3.059	2.857	2.100	7.004	51.68	3.003	2.571	2.012
9.848	53.95	2.207	2.333	1.813	10.25	54.24	2.768	2.333	1.889
12.83	55.73	2.175	1.666	1.746	13.55	56.74	2.296	2.000	1.697
16.10	57.95	1.638	1.000	1.252	17.79	58.73	1.530	.800	1.234
19.37	58.85	.903	.200	1.114	21.24	59.87	.872	.200	.694
20.90	59.75	.608	.200	.671	23.14	60.12	.555	.200	.602

Station 7, $x = 72$ ft $U_{\infty} = 59.63$ ft/sec $\rho = 1,865 \times 10^{-3}$ slug/cu ftStation 8, $x = 80$ ft $U_{\infty} = 60.60$ ft/sec $\rho = 1,865 \times 10^{-3}$ slug/cu ft

y in.	U	$\sqrt{u^2}$	$\frac{\overline{uv}}{x(-1)}$	$\sqrt{v^2}$	y in.	U	$\sqrt{u^2}$	$\frac{\overline{uv}}{x(-1)}$	$\sqrt{v^2}$
.1578	32.69	4.344	3.521	2.206	.1688	32.92	4.345	3.783	2.242
.2332	35.05	4.420	3.421	2.185	.2308	34.66	4.387	3.900	2.288
.3121	36.39	4.357	3.611	2.308	.3151	35.98	4.304	3.666	2.226
.4764	37.98	4.302	4.375	2.581	.4485	37.57	4.190	3.938	2.399
1.039	41.48	4.070	3.615	2.420	1.082	41.72	4.042	3.307	2.187
1.778	43.82	3.091	3.182	2.200	1.822	43.97	3.744	3.182	2.309
3.050	46.12	3.566	3.300	2.277	3.162	46.89	3.512	3.333	2.303
5.156	48.80	3.272	3.125	2.096	5.253	49.34	3.177	2.875	2.265
6.920	50.10	3.088	2.625	2.108	7.020	51.09	3.080	2.857	2.140
10.20	53.37	2.841	2.286	2.002	10.271	53.43	2.842	1.857	1.800
13.45	56.00	2.380	1.833	1.876	13.57	56.03	2.513	1.666	1.778
17.64	58.42	1.865	.800	1.209	20.05	59.77	1.494	.600	1.050
21.25	59.59	1.132	.400	.806	23.64	60.46	.892	.200	.717
23.58	59.63	.745	.200	.664					

TABLE IV - TURBULENCE QUANTITIES - Continued

Run No. 5.

Station 1 and 2, x = 18 ft

 $U_{\infty} = 60.38$ ft/sec $\rho = 1.875 \times 10^{-3}$ slug/cu ft

Station 3, x = 28 ft

 $U_{\infty} = 61.055$ ft/sec $\rho = 1.870 \times 10^{-3}$ slug/cu ft

y in.	U	$\sqrt{u^2}$	$\sqrt{w^2}$	y in.	U	$\sqrt{u^2}$	$\sqrt{w^2}$
.3332	34.049	5.18	3.384	.3037	33.432	5.656	3.571
.3833	35.589	4.91	4.382	.3668	35.666	5.991	2.402
.4446	36.591	5.13	3.953	.4788	37.562	5.890	2.497
.6181	38.453	5.04	4.027	.6225	39.324	5.440	3.095
.9760	41.014	4.77	4.038	1.032	42.197	4.828	3.357
1.717	44.047	4.41	3.885	1.655	44.900	4.450	3.532
2.801	46.714	4.32	4.178	3.074	48.322	3.860	3.612
4.656	50.306	4.42	3.937	4.875	51.248	3.630	3.395
6.083	52.833	4.09	3.987	6.380	53.014	3.440	3.288
9.866	58.799	2.99	3.558	10.053	57.493	3.040	2.625
11.70	60.380	1.689	1.378	12.295	59.441	2.350	2.093
15.53	60.655	.369	.428	16.421	61.129	0.845	.629
				19.560	61.055	0.338	.500

Station 4, x = 38 ft

 $U_{\infty} = 61.20$ ft/sec $\rho = 1.850 \times 10^{-3}$ slug/cu ft

Station 5, x = 48 ft

 $U_{\infty} = 61.509$ ft/sec $\rho = 1.860 \times 10^{-3}$ slug/cu ft

y in.	U	$\sqrt{u^2}$	$\sqrt{w^2}$	y in.	U	$\sqrt{u^2}$	$\sqrt{w^2}$
.2651	33.686	5.360	3.404	.1778	27.563	6.01	
.3359	35.276	5.316	3.389	.2483	31.192	5.162	3.457
.4182	36.515	5.299	3.415	.3226	33.194	5.293	3.220
.5521	38.071	5.148	3.243	.4693	36.192	5.190	3.824
.9229	40.824	4.871	3.436	.7749	39.191	4.899	3.647
1.564	43.818	4.432	3.542	1.512	43.251	4.423	3.547
2.486	46.276	3.950	3.704	2.393	45.899	4.234	3.456
3.943	48.975	3.659	3.331	3.910	48.717	3.739	3.267
5.430	51.017	3.533	3.152	5.355	51.409	3.634	3.189
8.386	54.504	3.563	2.177	8.918	54.833	3.166	2.882
11.93	57.728	2.532	3.063	11.883	57.676	2.760	2.743
15.72	60.486	1.577	1.273	15.750	60.005	1.987	1.874
18.76	60.611	.738	.580	18.830	61.236	1.115	1.121
20.86	60.912	.438	.339	22.100	61.509	0.542	.461

TABLE IV - TURBULENCE QUANTITIES - Continued

Run No. 5

Station 6, x = 58 ft

 $U_{\infty} = 61.280$ ft/sec $\rho = 1.860 \times 10^{-3}$ slug/cu ft

Station 7, x = 68 ft

 $U_{\infty} = 60.90$ ft/sec $\rho = 1.850 \times 10^{-3}$ slug/cu ft

y in.	U	$\sqrt{u^2}$	$\sqrt{w^2}$	y in.	U	$\sqrt{u^2}$	$\sqrt{w^2}$
.2949	32.36	5.177	3.301	.2515	31.28	5.390	3.012
.3361	33.75	5.125	3.583	.3028	32.62	5.145	3.334
.4285	35.60	5.094	3.602	.3848	34.33	5.092	3.536
.6234	37.82	4.902	3.708	.4997	35.94	5.047	3.690
1.386	42.65	4.589	3.444	.8643	39.16	4.849	3.758
2.911	46.57	4.028	3.126	1.525	42.26	4.485	3.419
4.940	49.75	3.647	3.203	2.871	45.58	4.111	3.249
6.732	52.03	3.454	2.986	7.006	51.39	3.453	3.079
9.670	54.99	3.145	2.864	9.639	53.55	3.225	2.962
12.940	57.80	2.736	2.307	12.840	56.17	2.732	2.718
17.270	60.24	1.906	1.698	16.960	58.83	2.147	2.064
21.530	61.13	.892	.752	20.540	60.57	1.426	1.230
23.650	61.28	.438	.510	23.490	60.90	.808	.865

Station 8, x = 78 ft

 $U_{\infty} = 60.90$ ft/sec $\rho = 1.850 \times 10^{-3}$ slug/cu ft

y in.	U	$\sqrt{u^2}$	$\sqrt{w^2}$
.0956	28.97	5.134	3.08
.1883	28.86	5.852	4.365
.2807	29.06	5.072	2.614
.4345	33.13	4.989	3.622
.6394	36.16	4.976	3.738
.8728	38.59	4.826	3.376
1.460	41.57	4.465	3.509
2.190	43.60	4.151	3.563
5.173	48.60	3.652	3.225
8.123	51.91	3.500	2.817
11.820	55.08	2.972	2.781
15.530	57.57	2.597	2.334
20.00	59.63	1.777	2.564
23.59	60.90	1.044	2.690

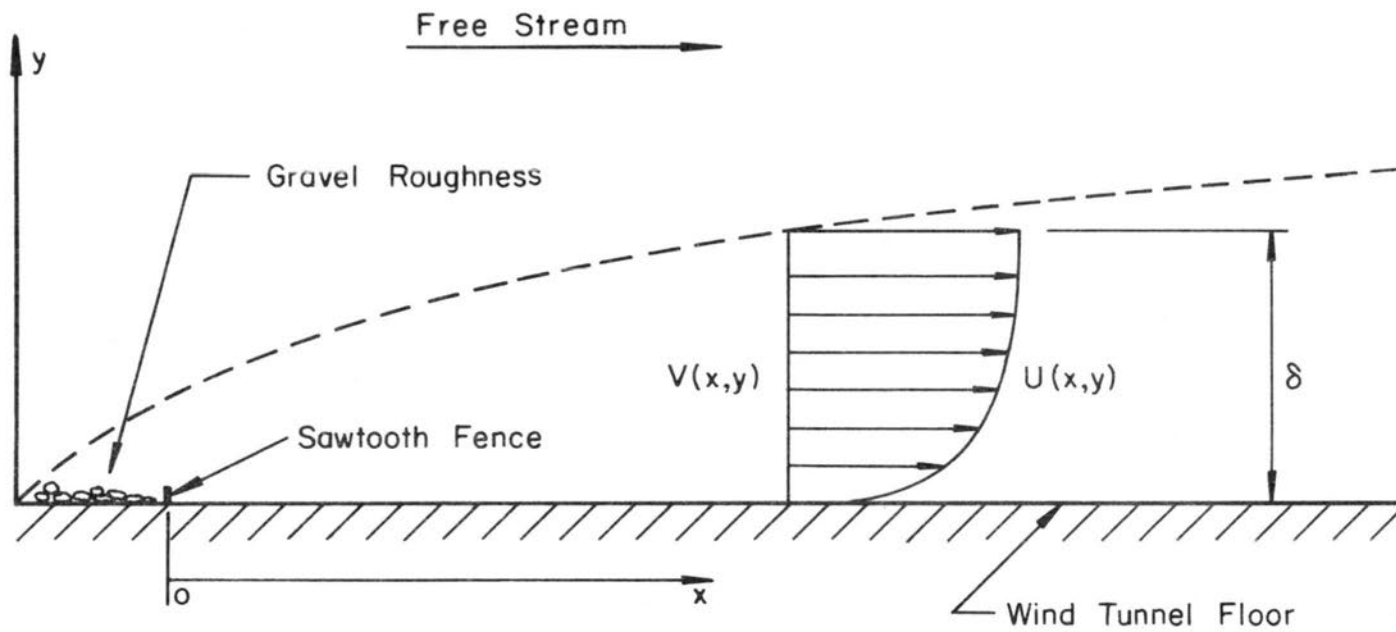
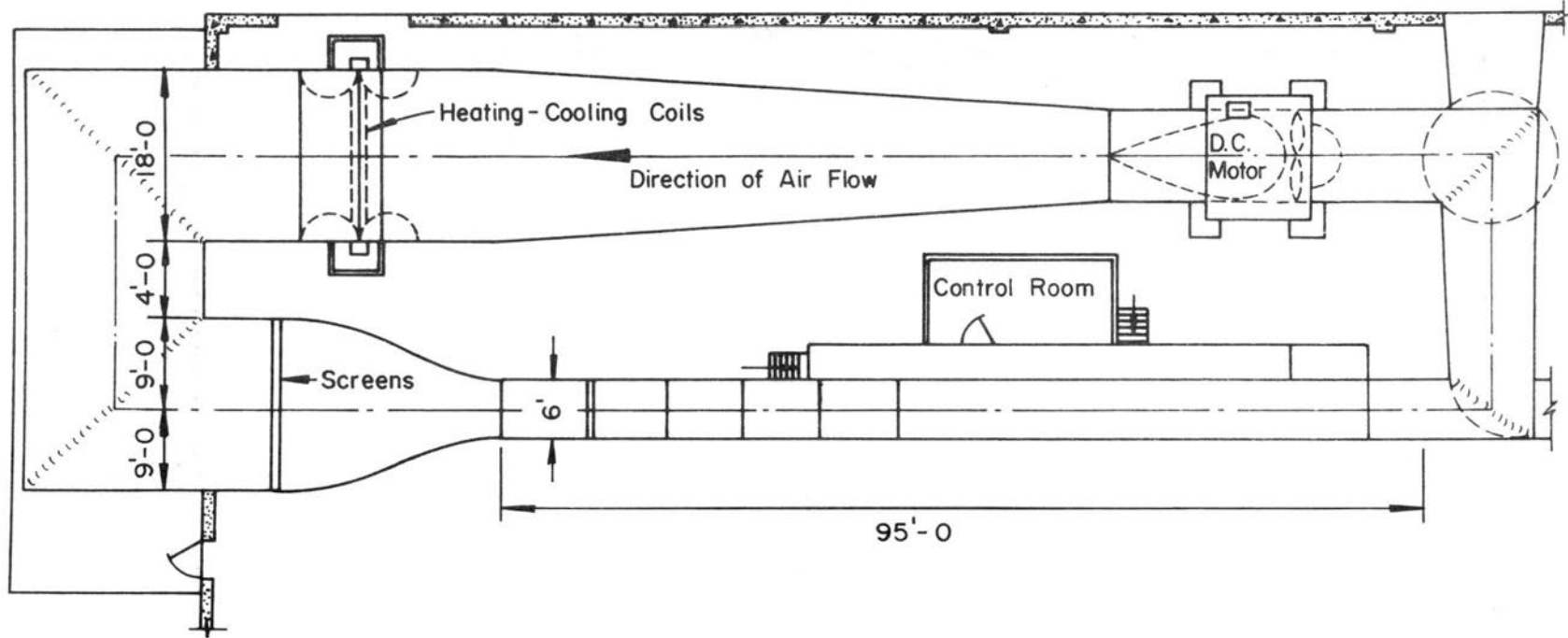


Fig. 1. Definition sketch of the boundary layer.



Plan View

Fig. 2. Wind tunnel.

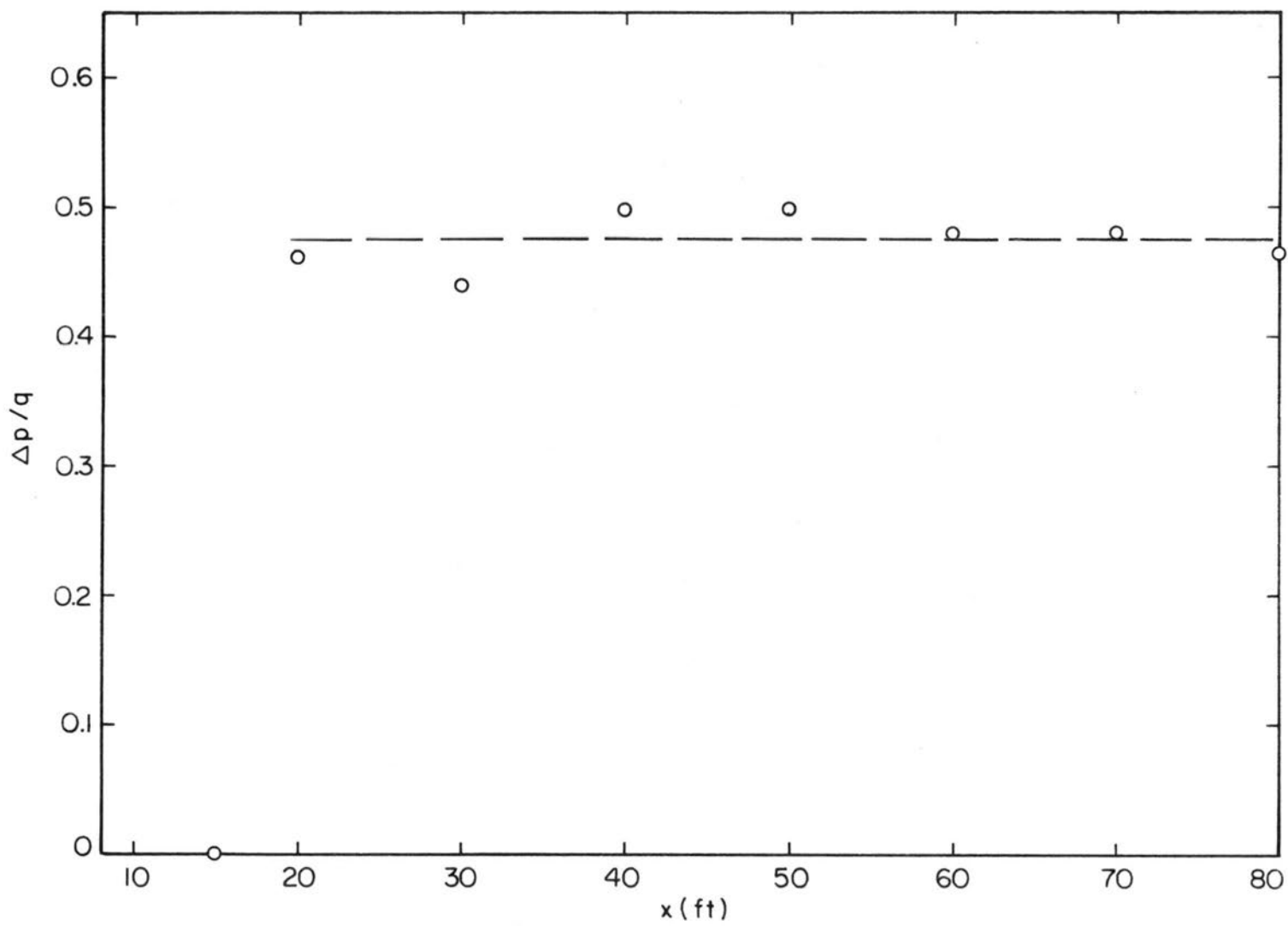


Fig. 3. The pressure distribution.

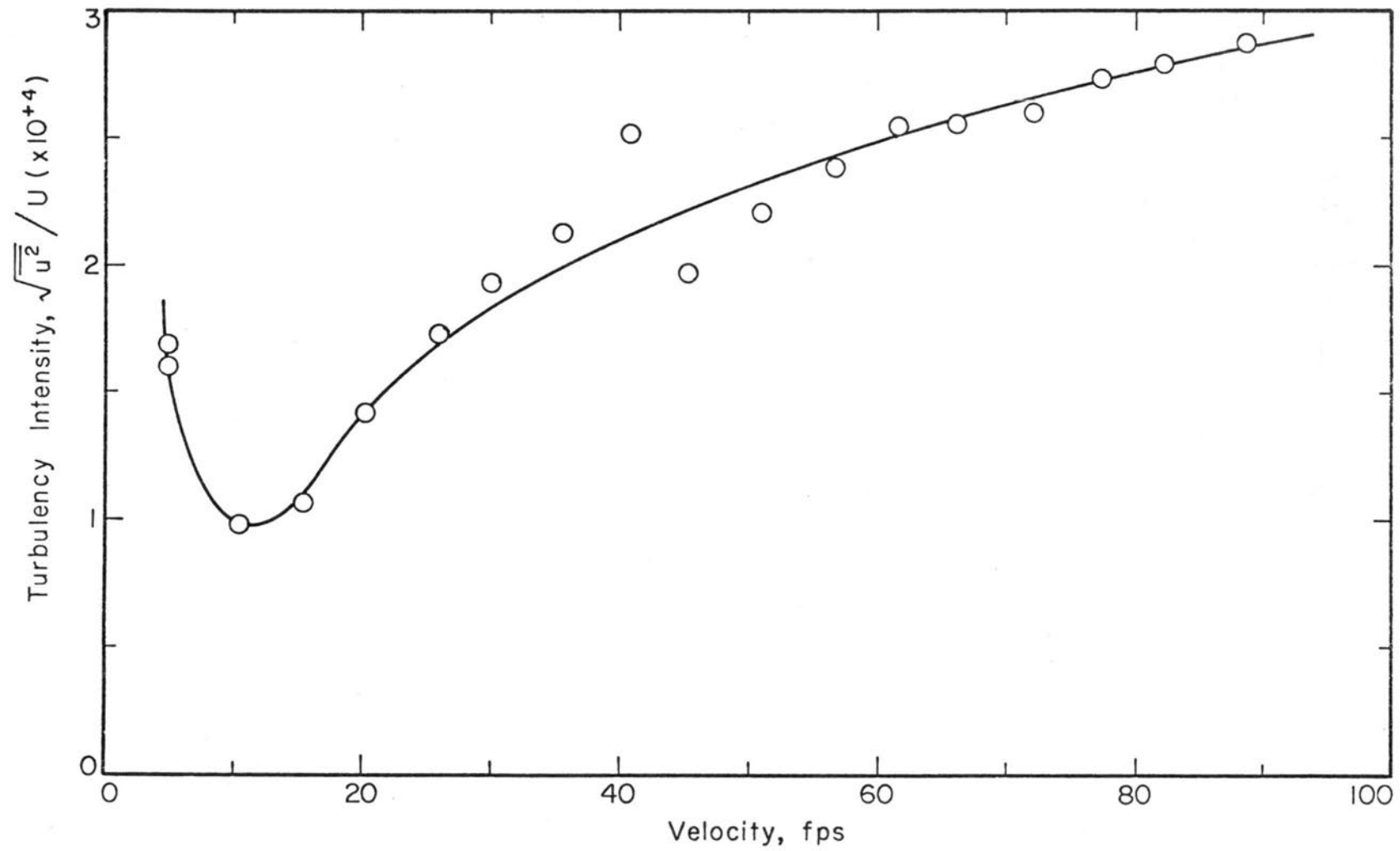


Fig. 4. Free stream turbulence intensity at the entrance of the test section.

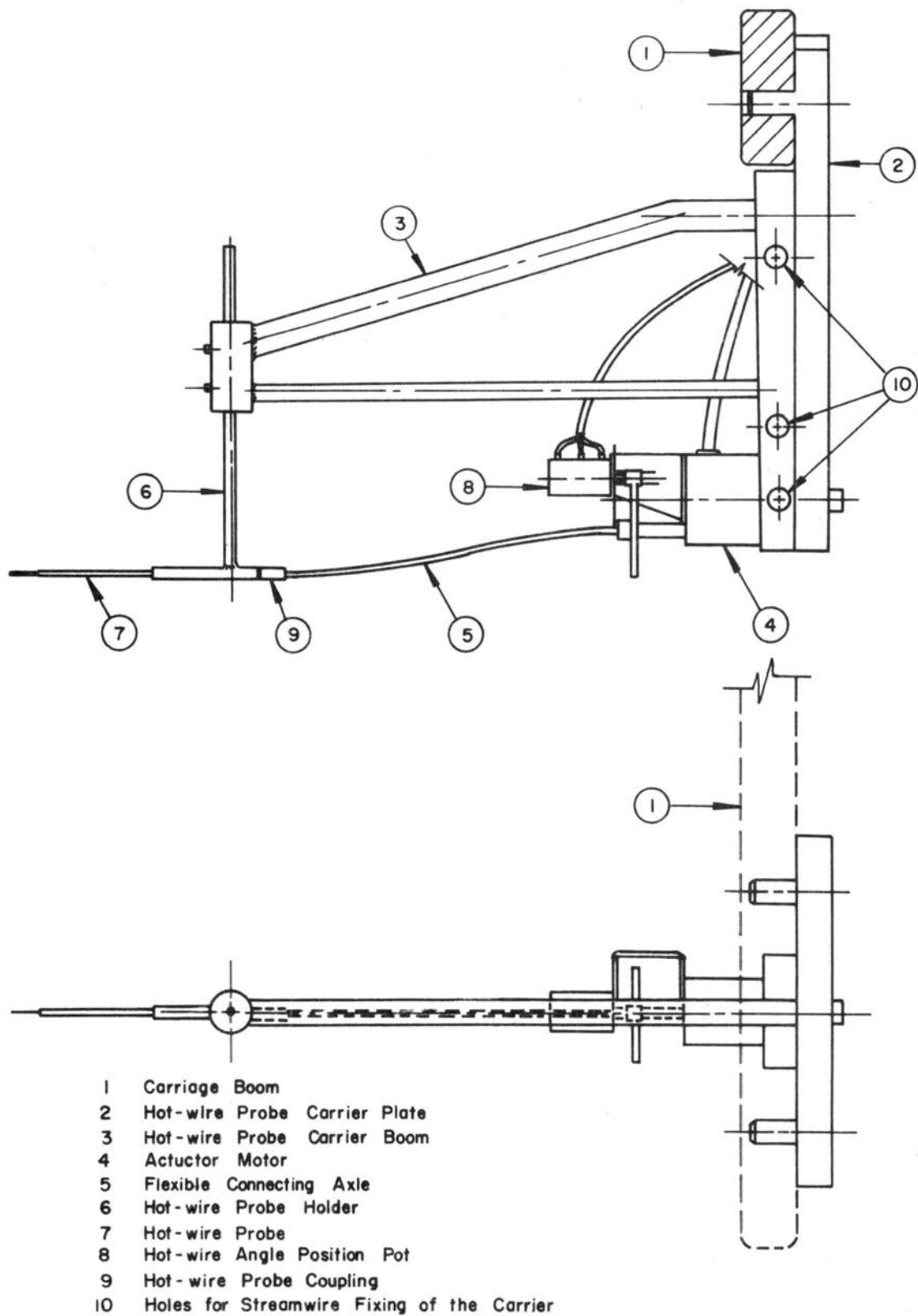


Fig. 5. Schematic of the hot-wire probe carrier.

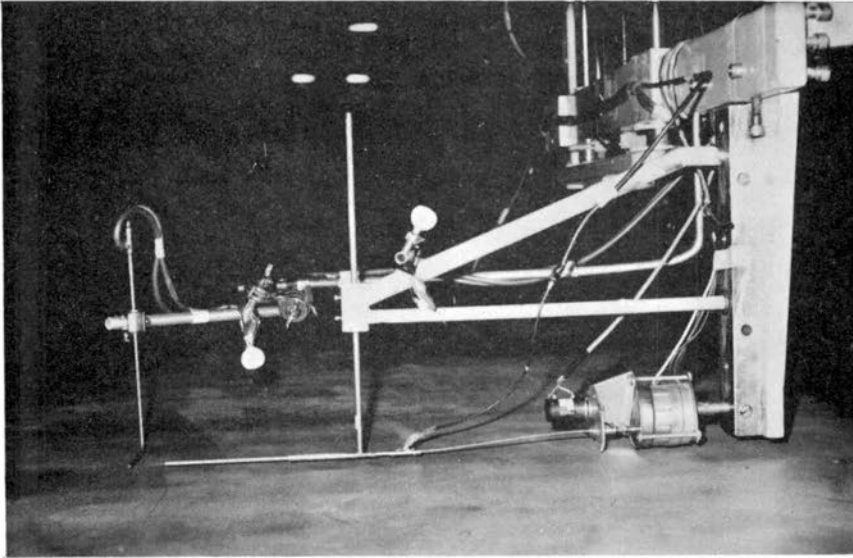


Fig. 6. Hot-wire probe carrier, crosswise probe position.

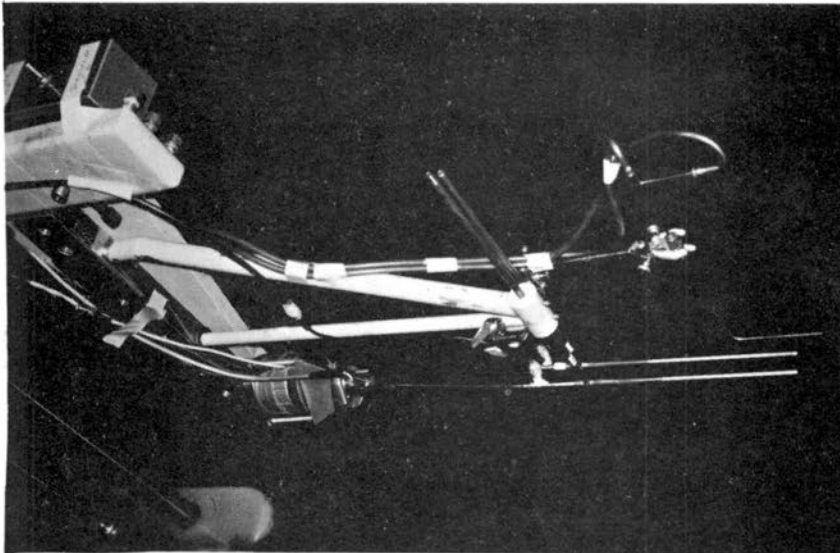


Fig. 7. Hot-wire probe carrier, streamwise probe position.

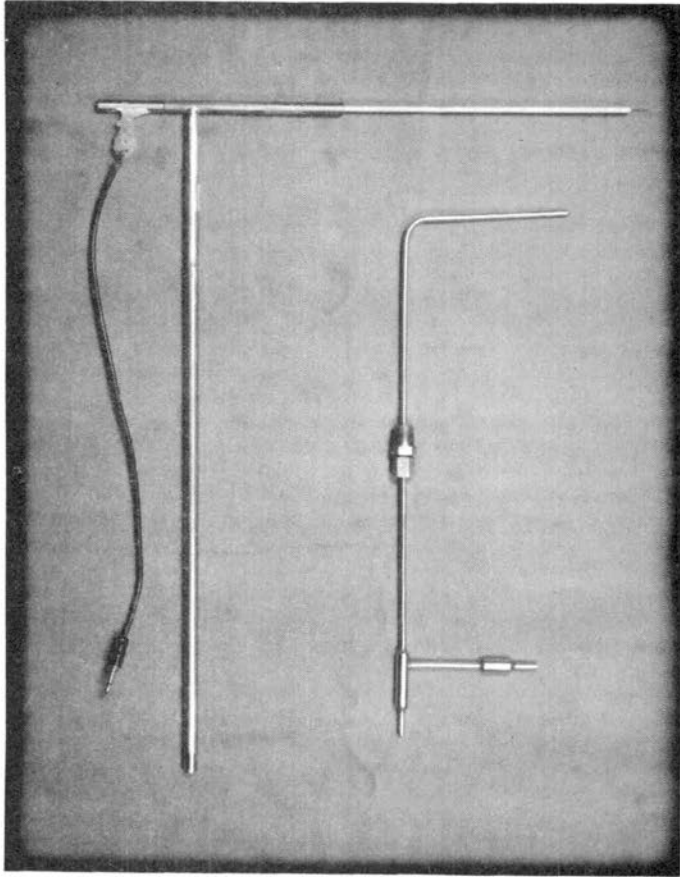


Fig. 8. Probes.

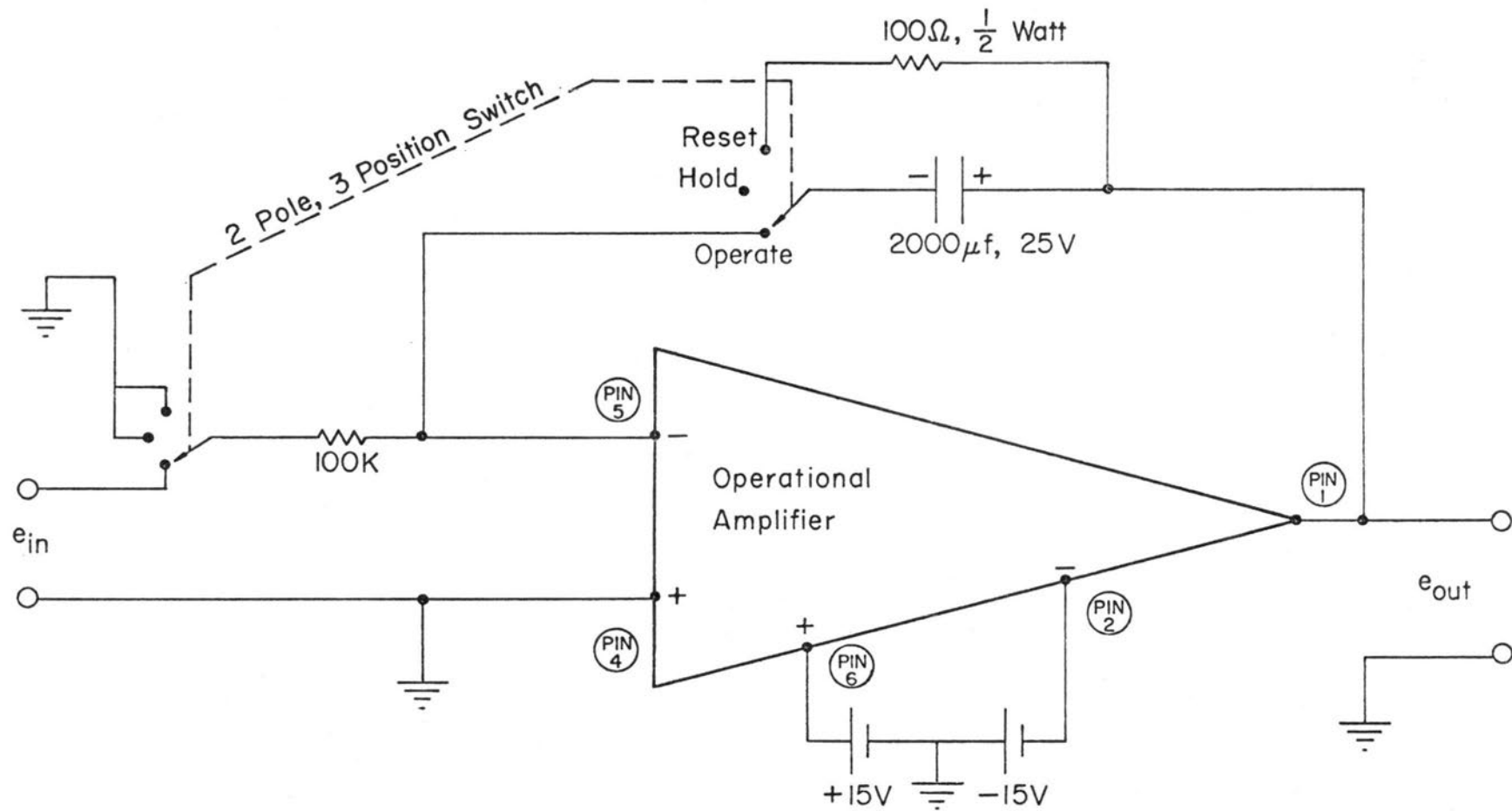


Fig. 9. Integrating circuit.

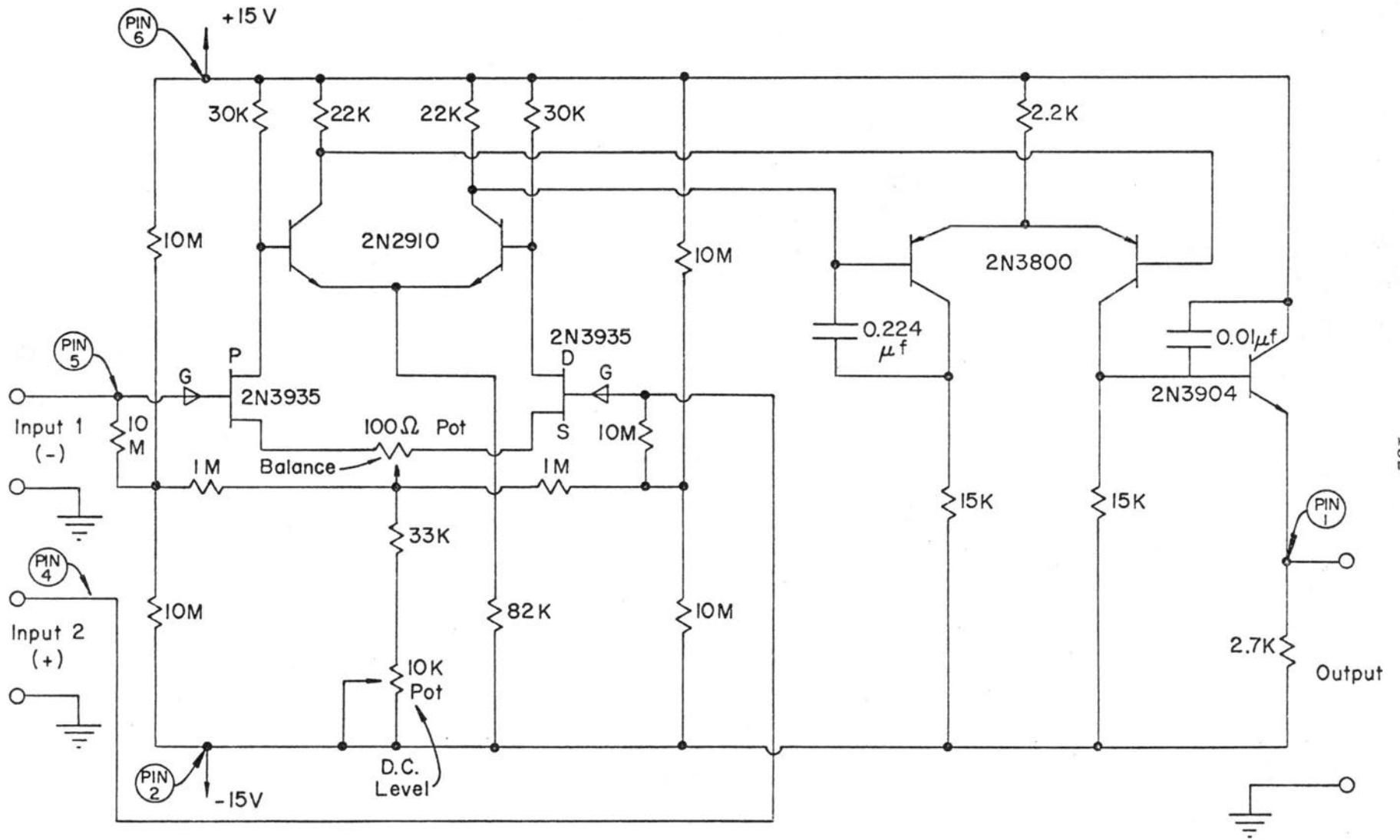


Fig. 10. Operational amplifier of the integrating circuit.

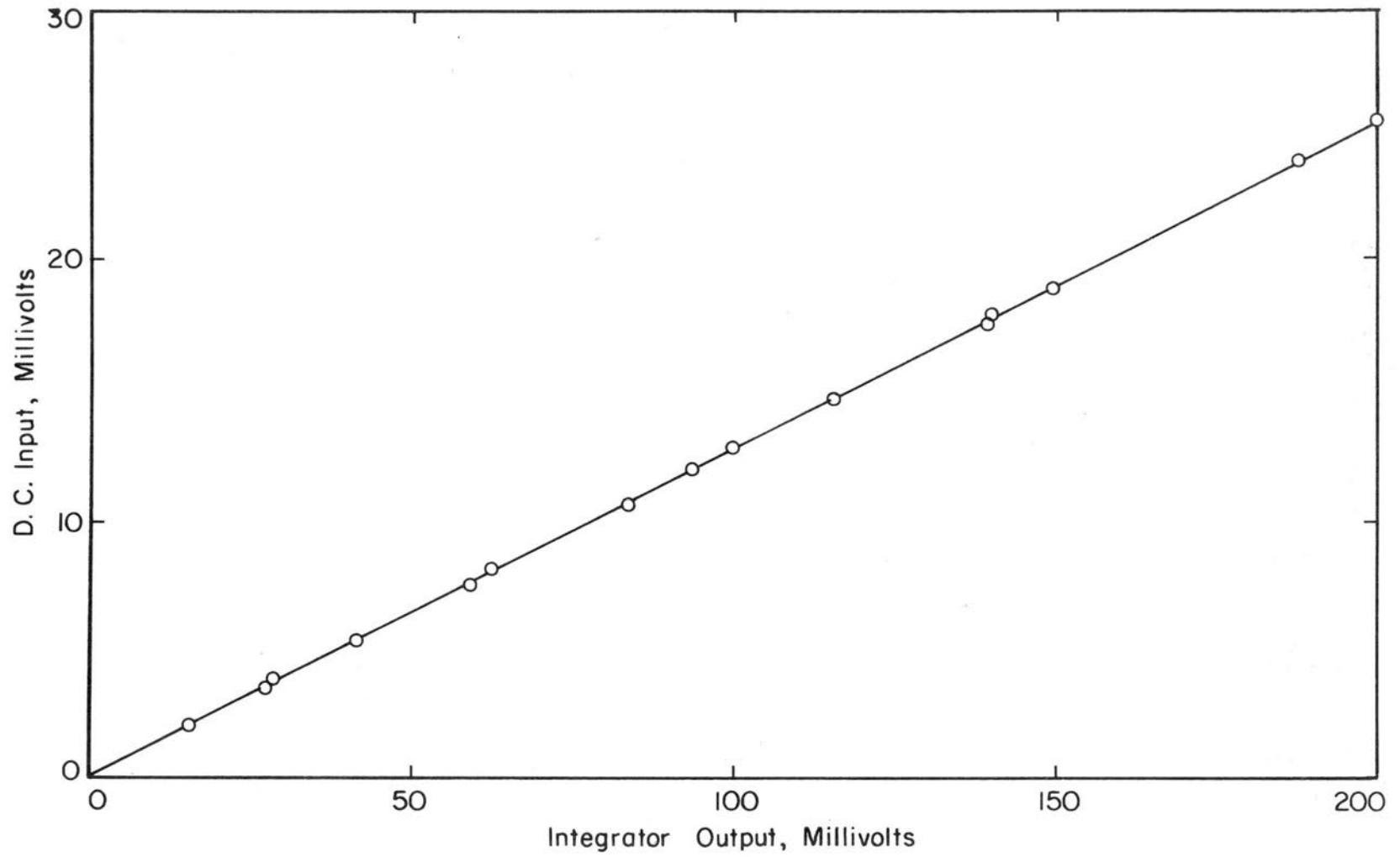


Fig. 11. Integrating circuit calibration curve.

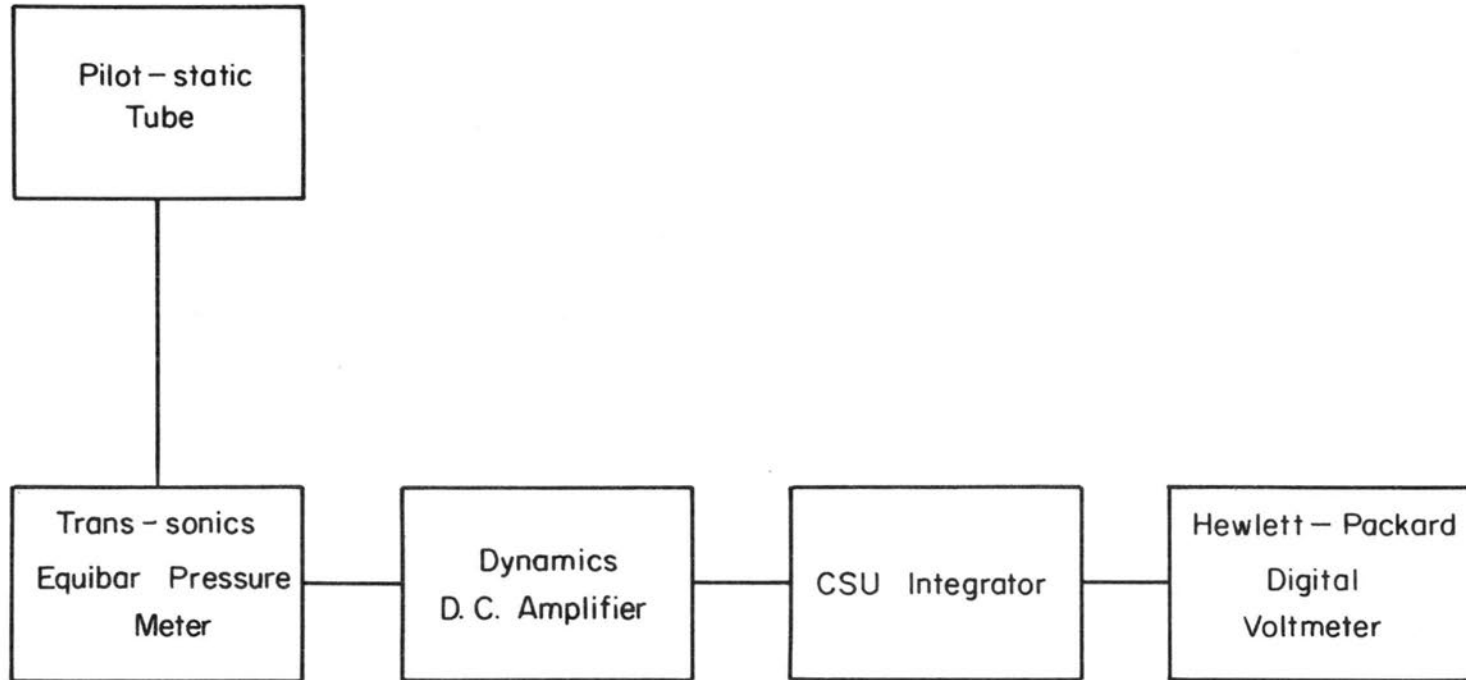


Fig. 12. Block diagram of the mean velocity measurement instrumentation.

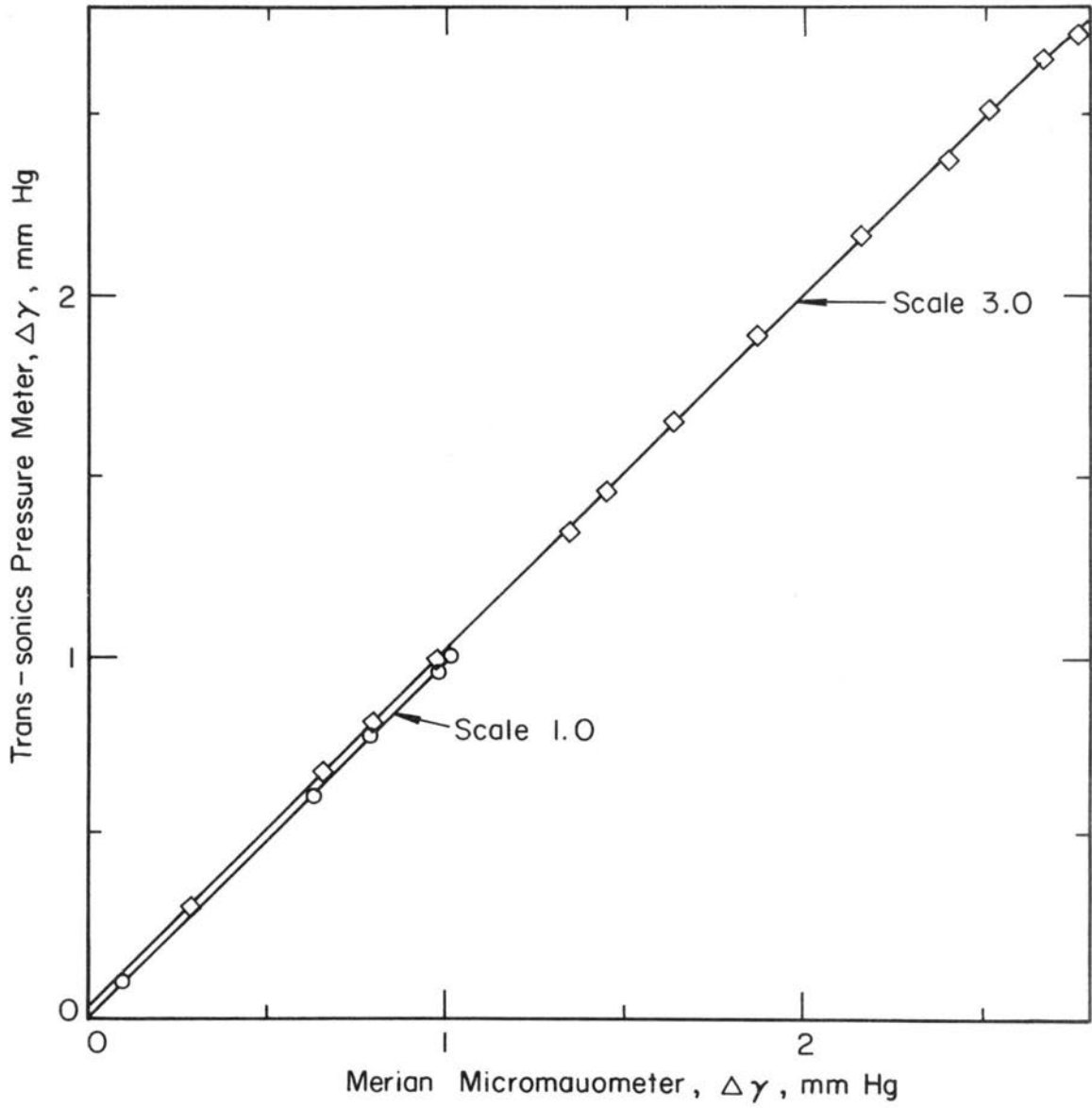


Fig. 13. Calibration of Trans-Sonics pressure meter against the Merriam micromanometer.

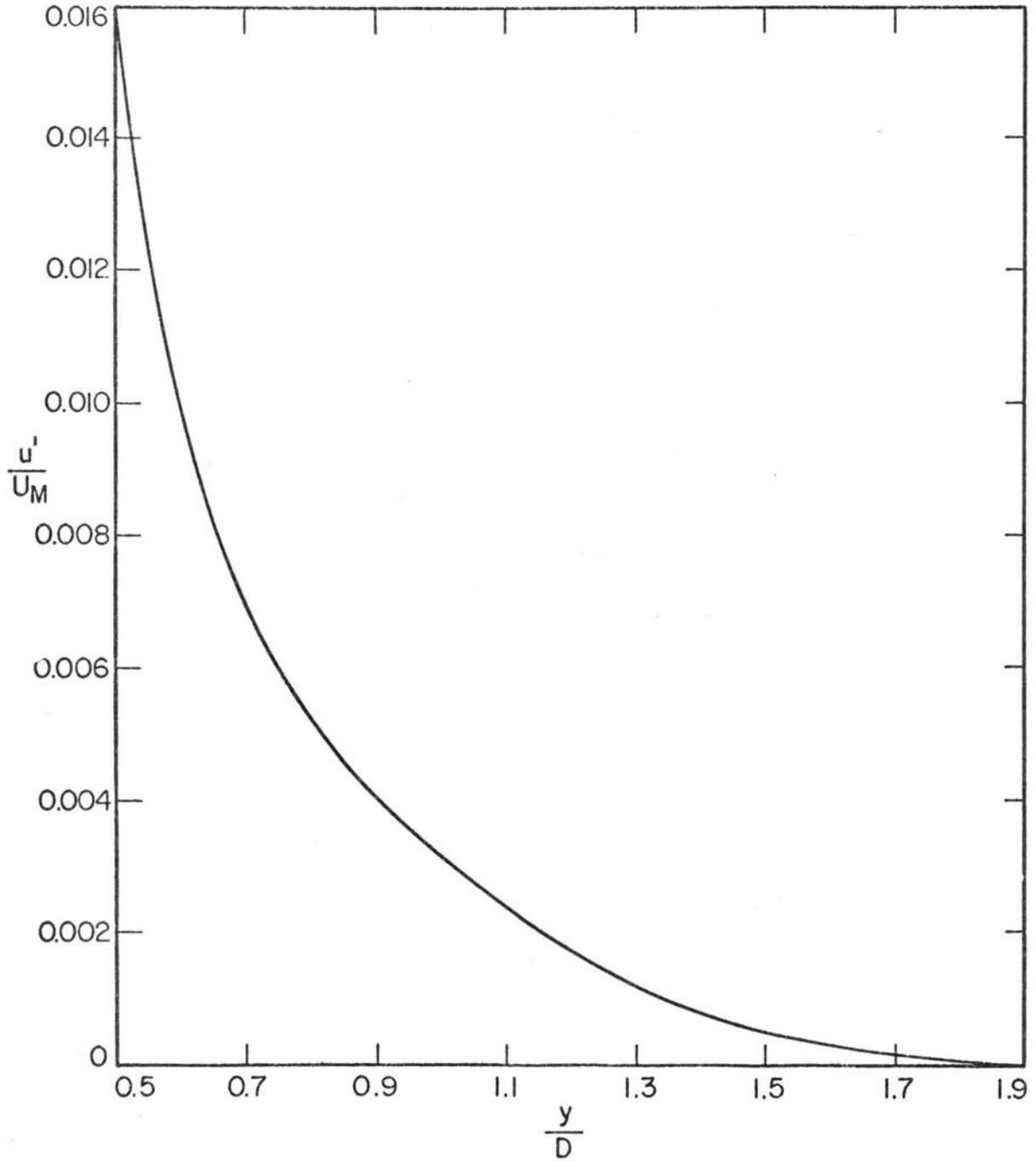


Fig. 14. The wall effect expressed as a function of y/D after MacMillan.

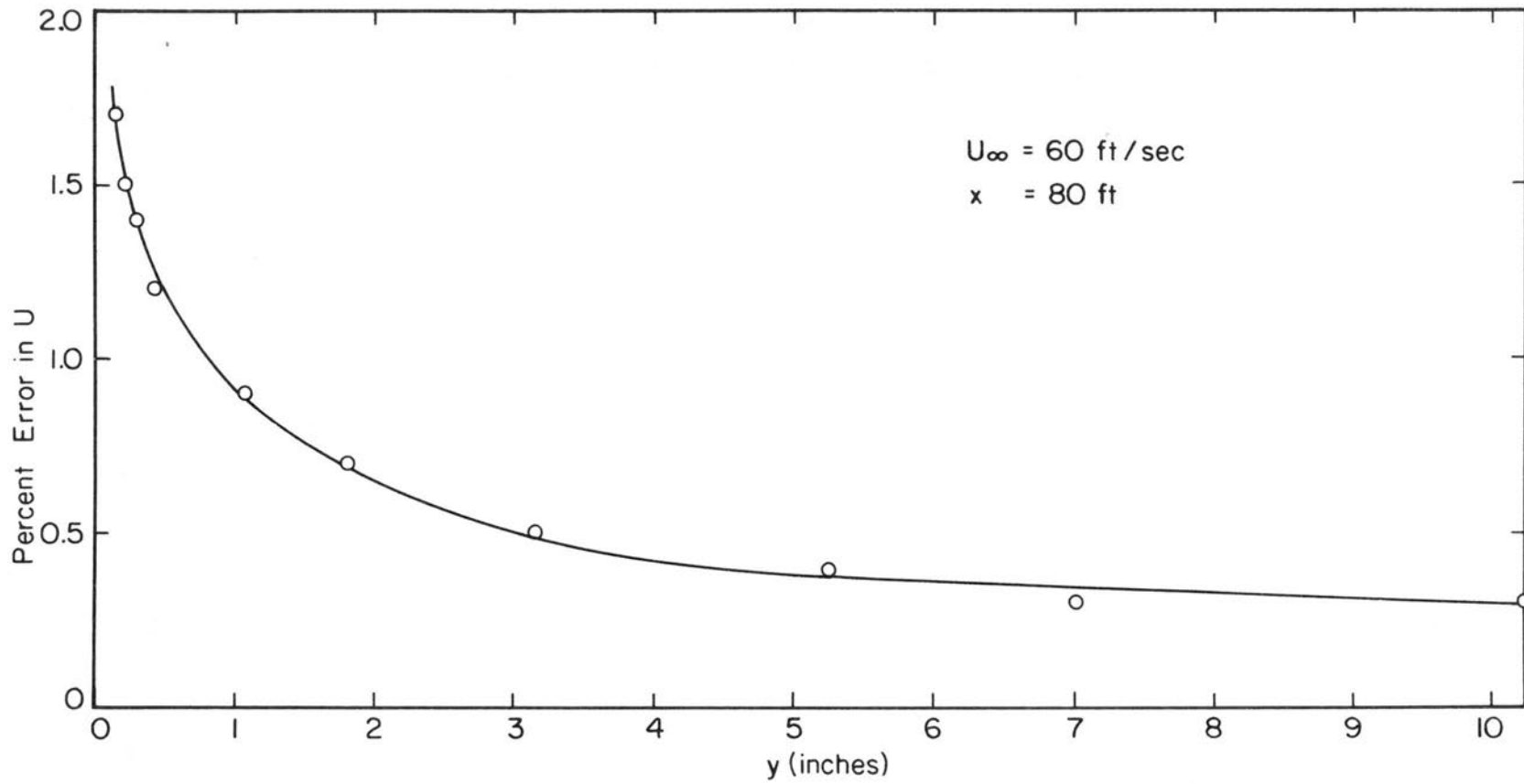


Fig. 15. Turbulence effect on mean velocity measurement.

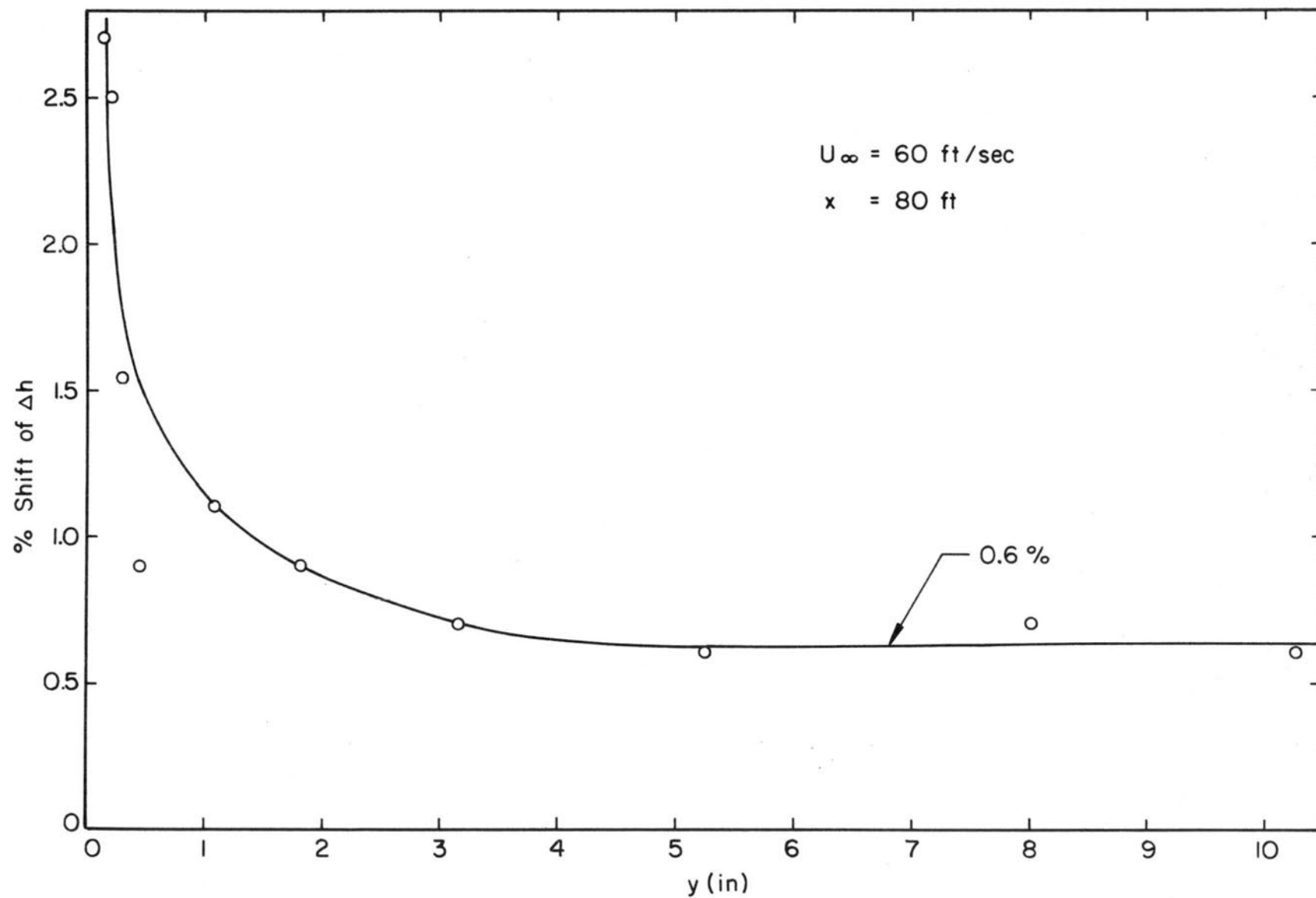


Fig. 16. Turbulence effect on Δh shift-nonlinear averaging.

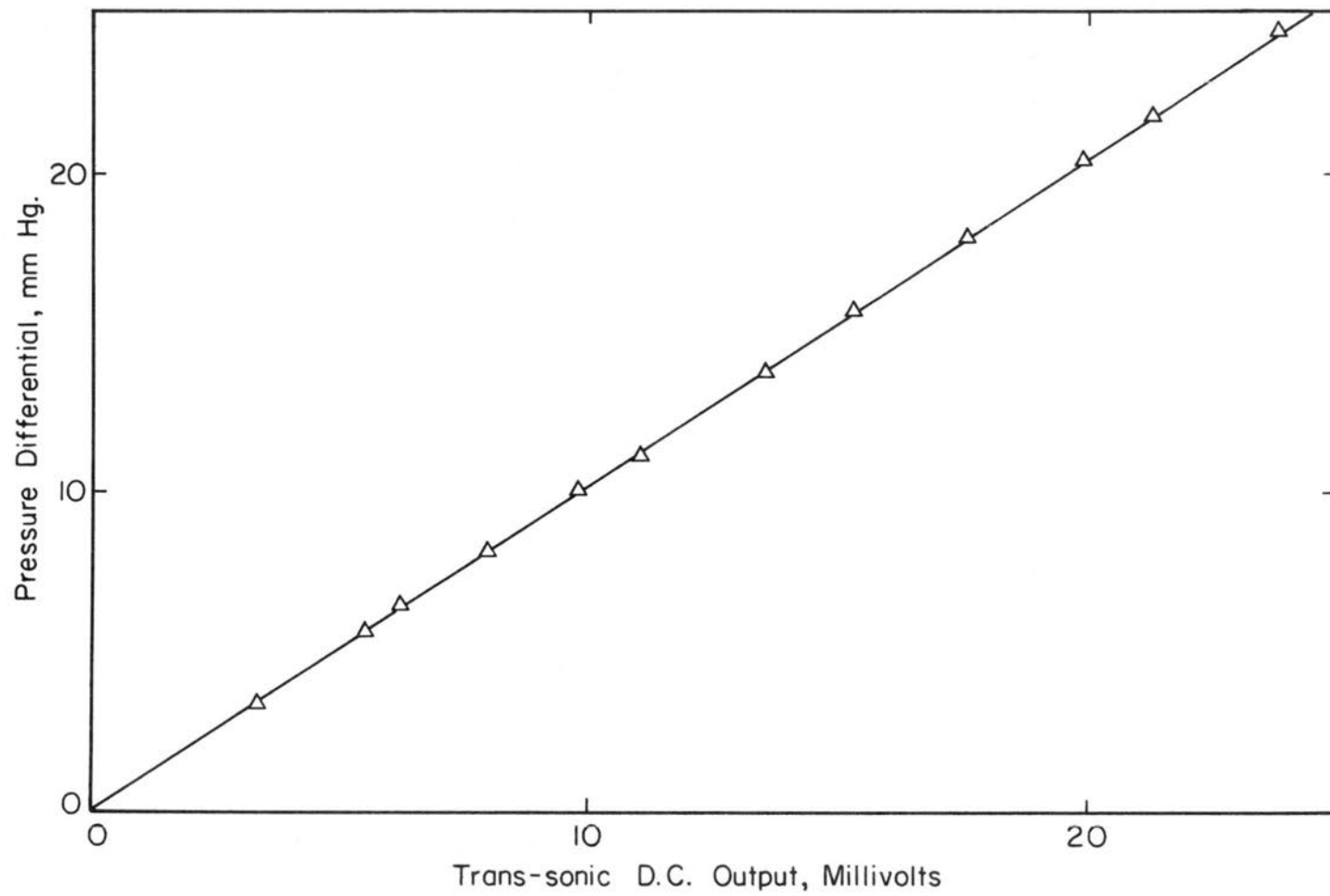


Fig. 17. Typical calibration curve of Trans-Sonics pressure meter versus pressure differential.

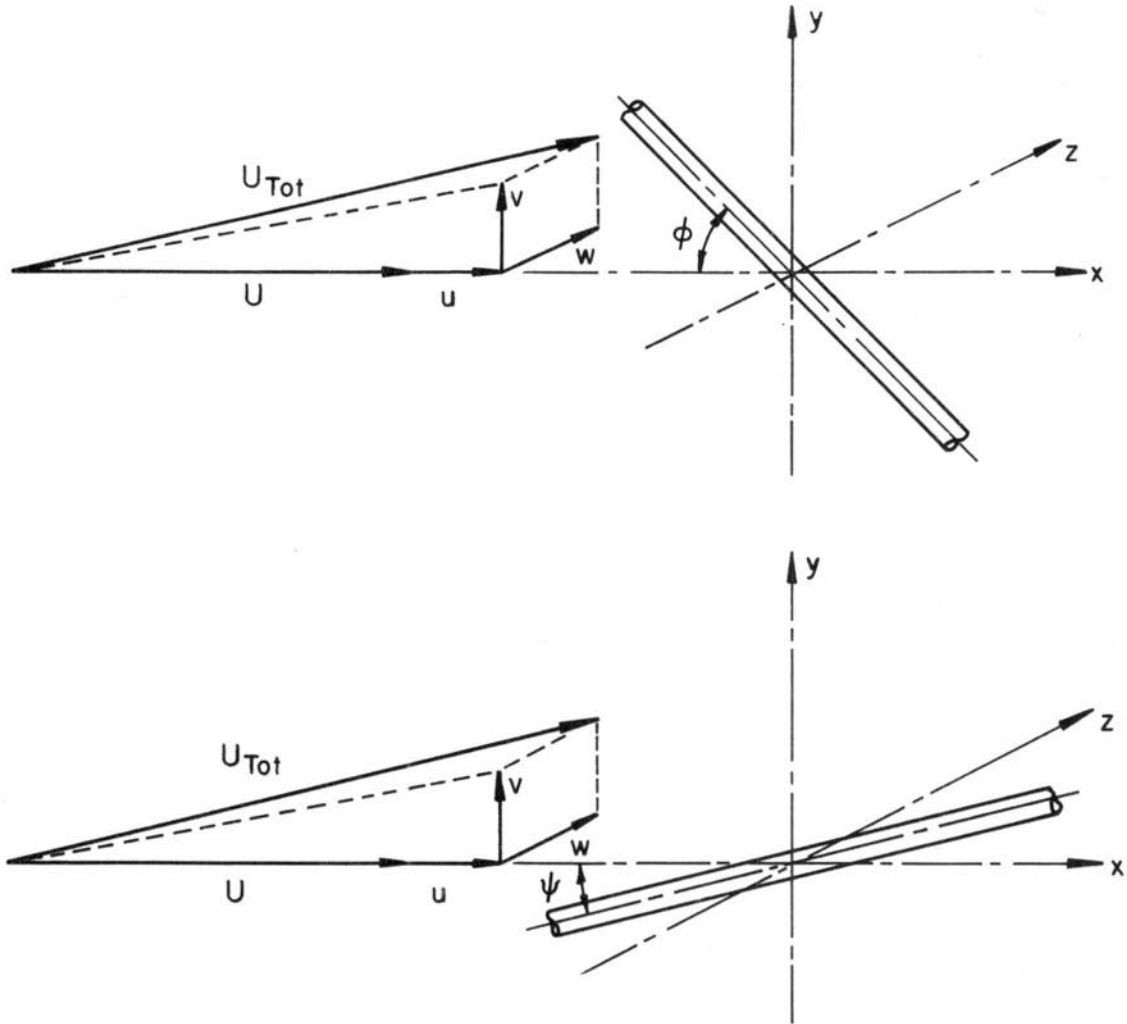


Fig. 18. Hot-wire with respect to the coordinate system.

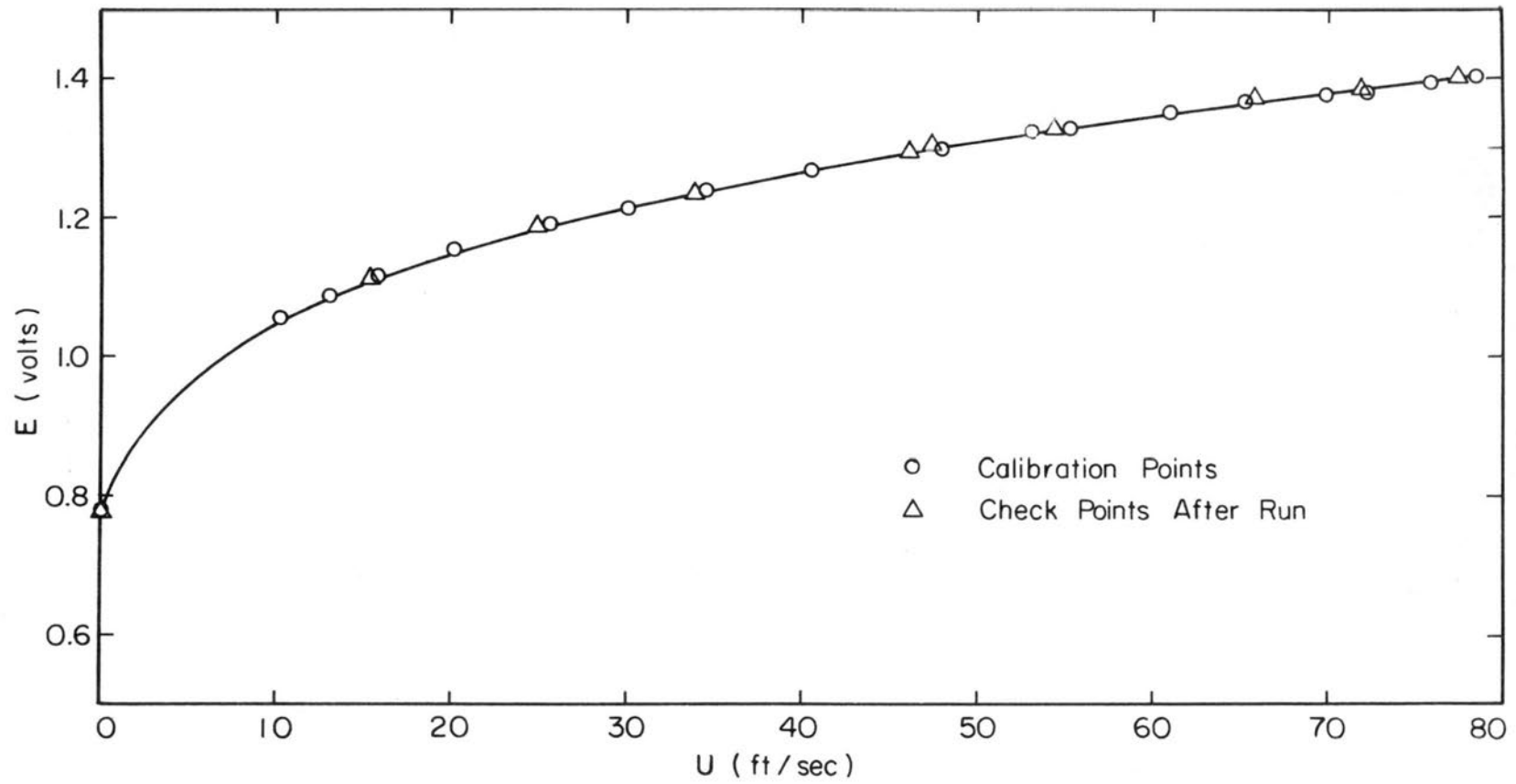


Fig. 19. Typical hot-wire calibration curve.

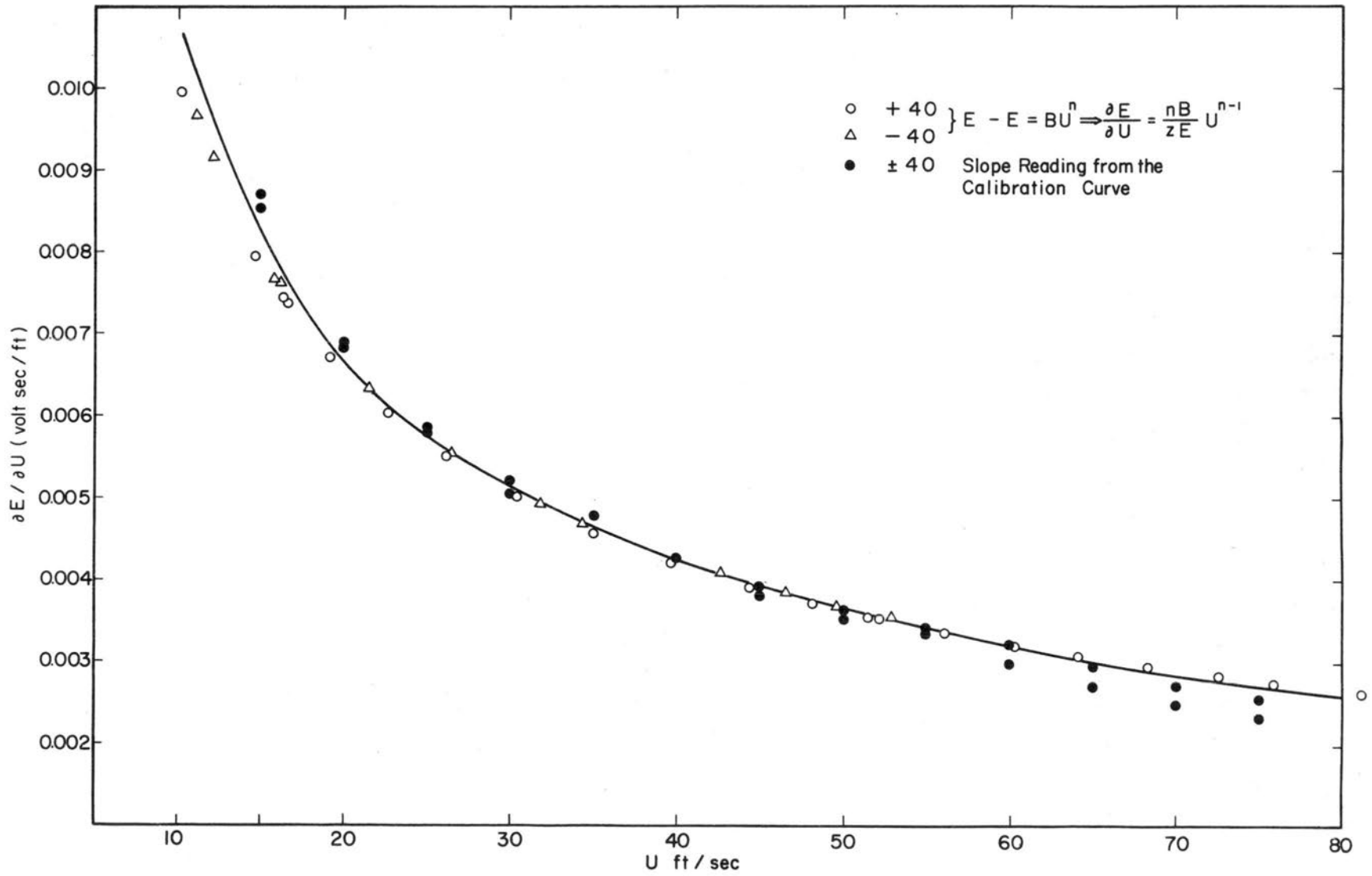


Fig. 20. Velocity sensitivity for $\pm 40^\circ$ angle of yaw.

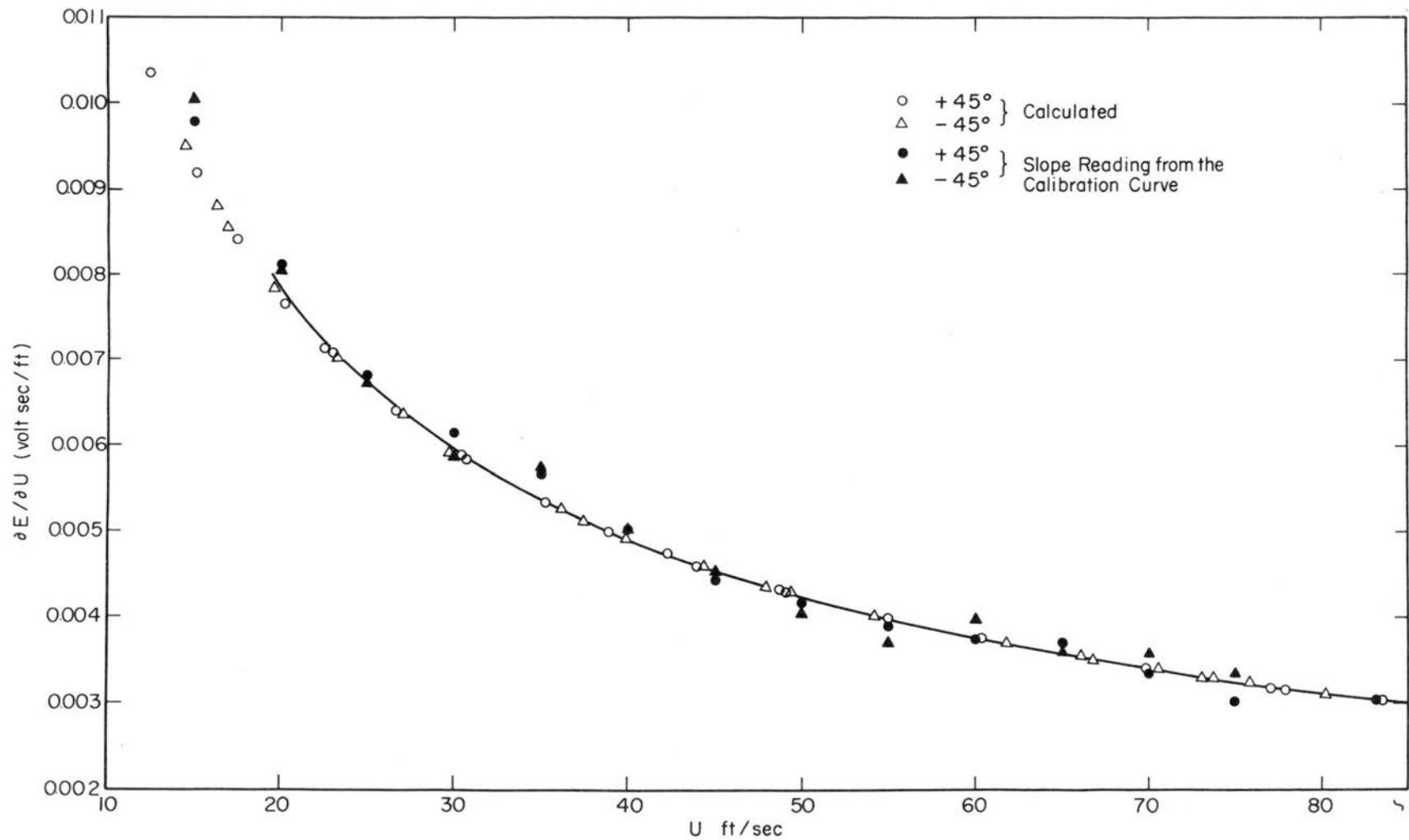


Fig. 21. Velocity sensitivity for $\pm 45^\circ$ angle of yaw.

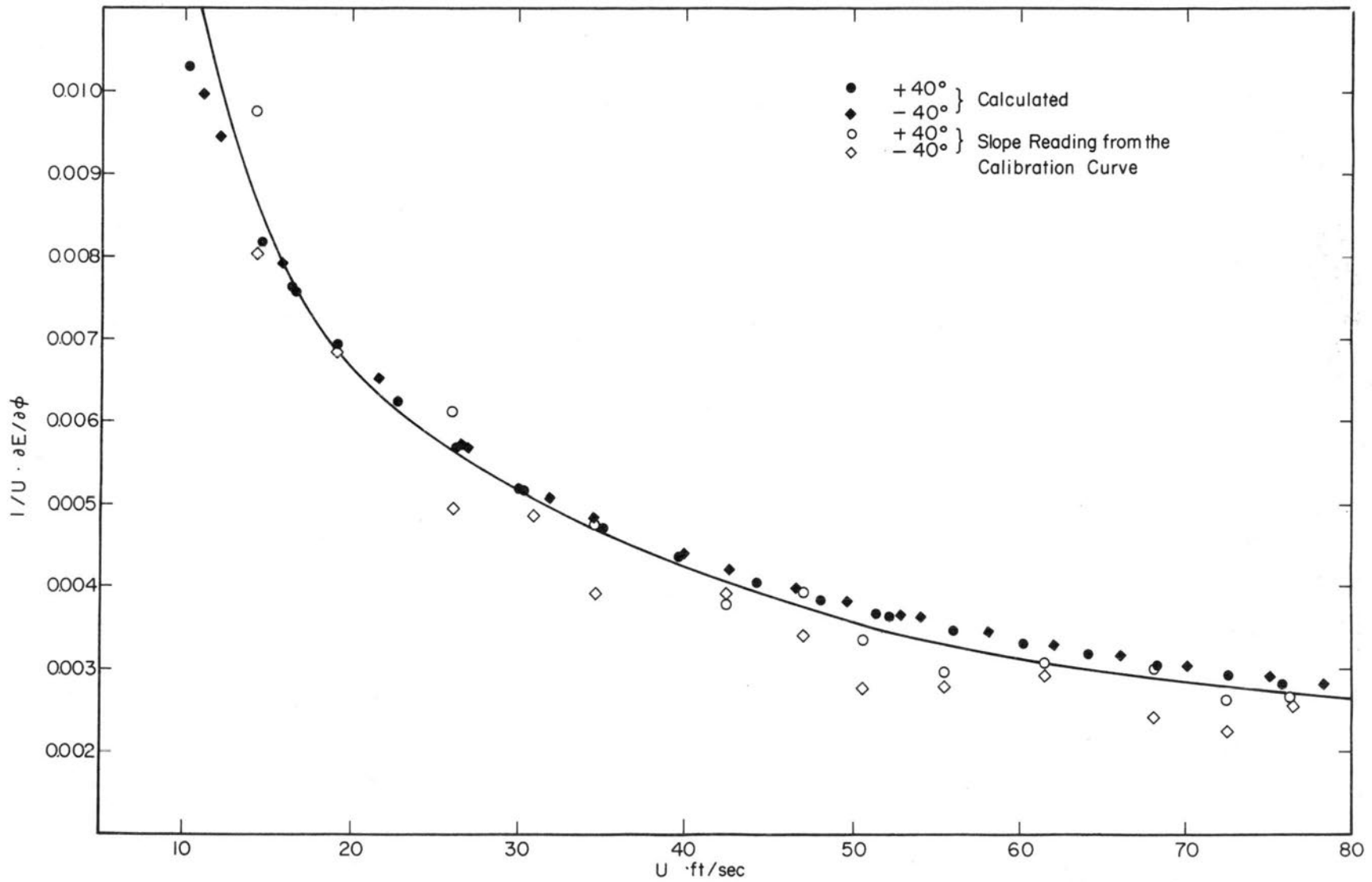


Fig. 22. Angle sensitivity for $\pm 40^\circ$ yaw for a "perfect" hot-wire.

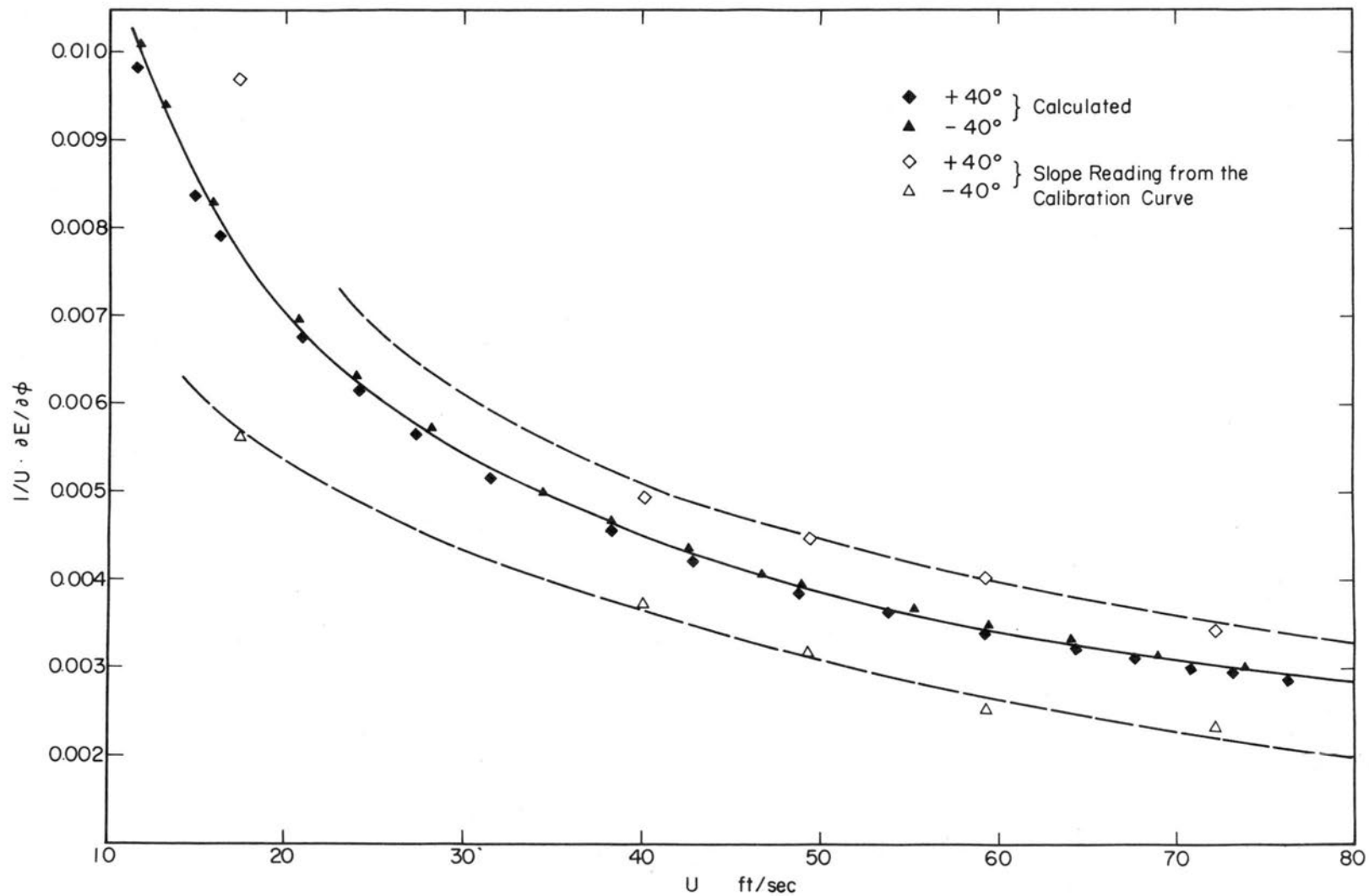


Fig. 23. Angle sensitivity for $\pm 40^\circ$ yaw for a "real" hot-wire.

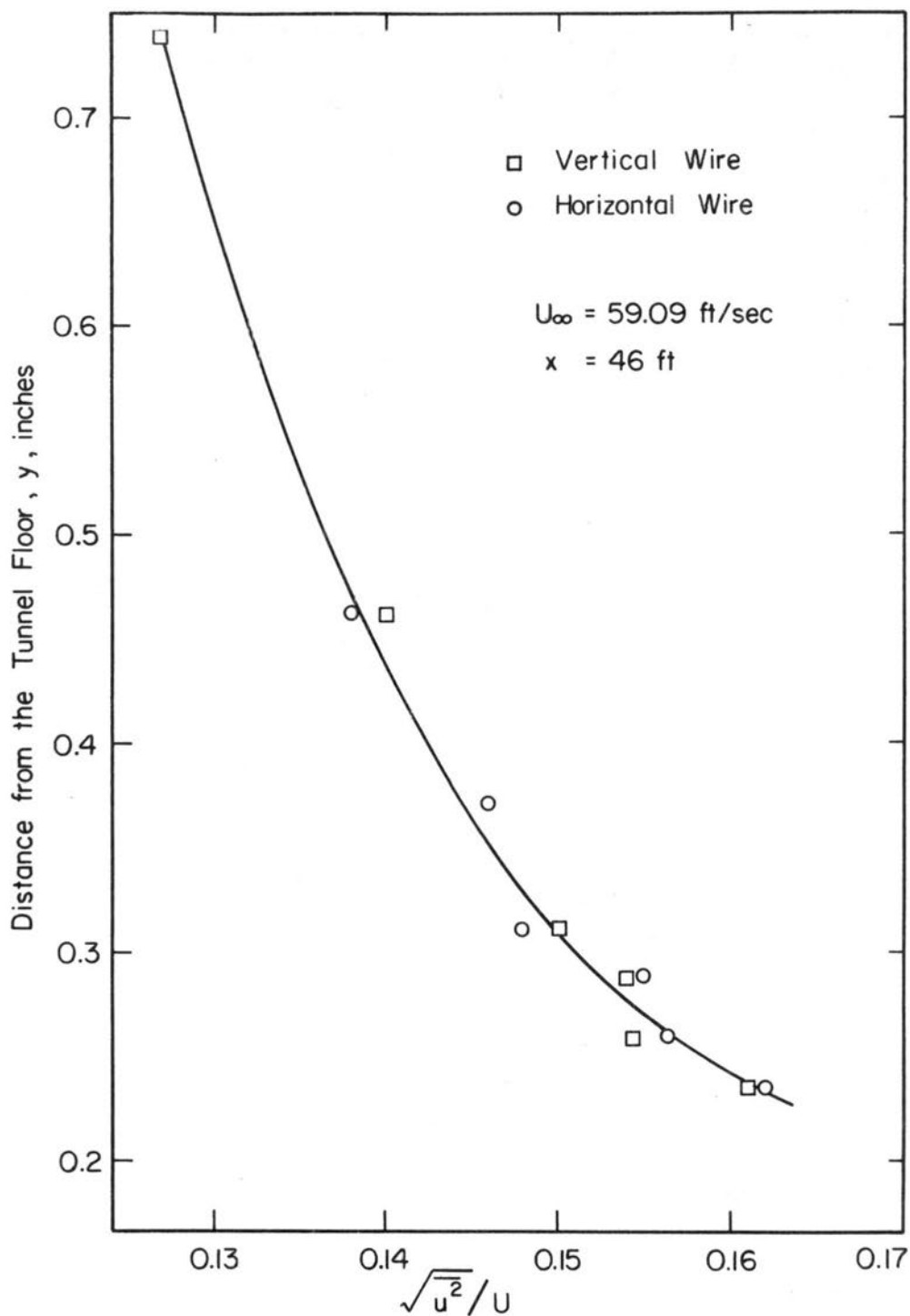


Fig. 24. Comparison of turbulence measurement with a horizontal and vertical hot-wire near the tunnel floor. Station 46 ft.

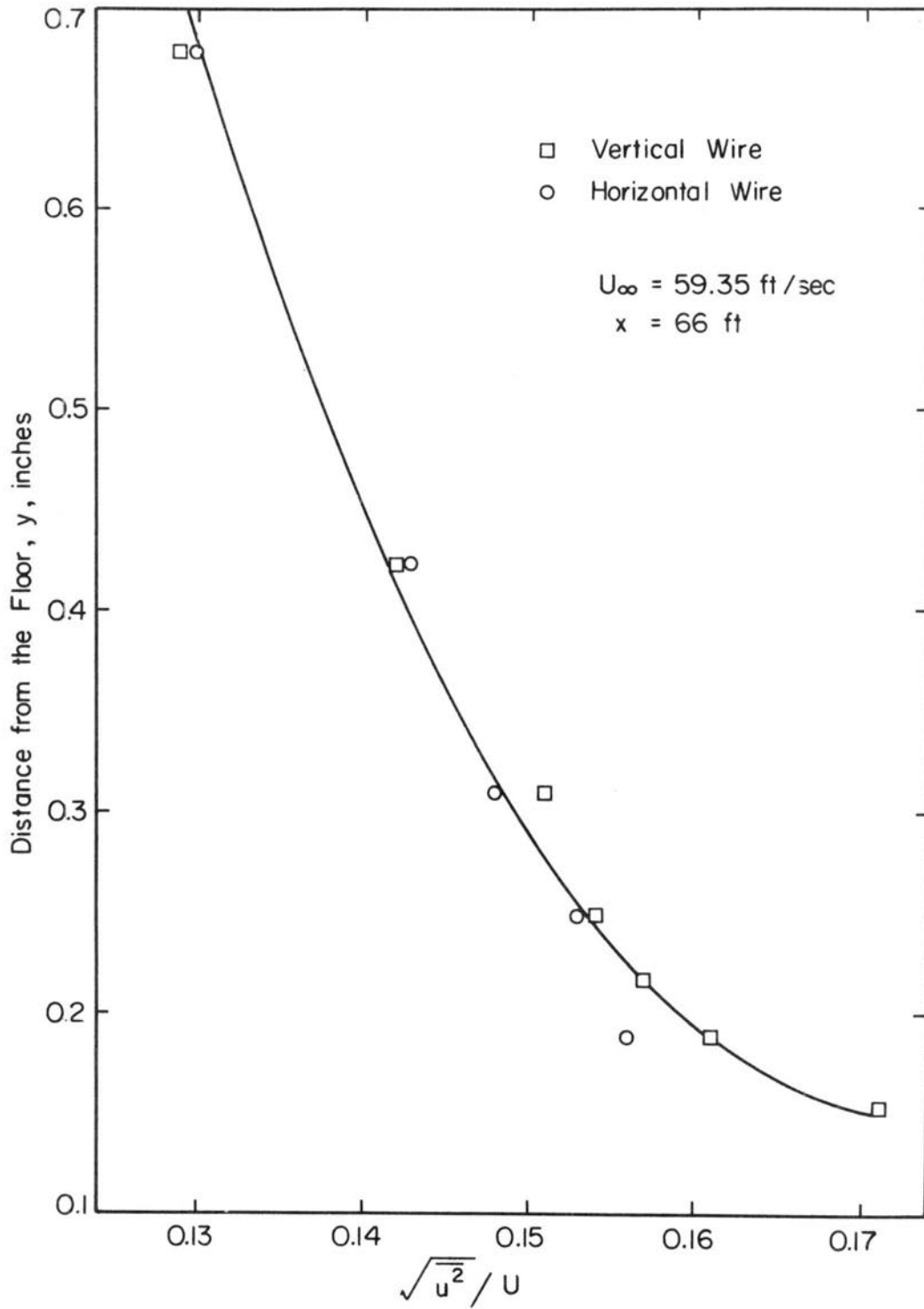


Fig. 25. Comparison of turbulence measurement with a horizontal and vertical hot-wire near the tunnel floor. Station 66 ft.

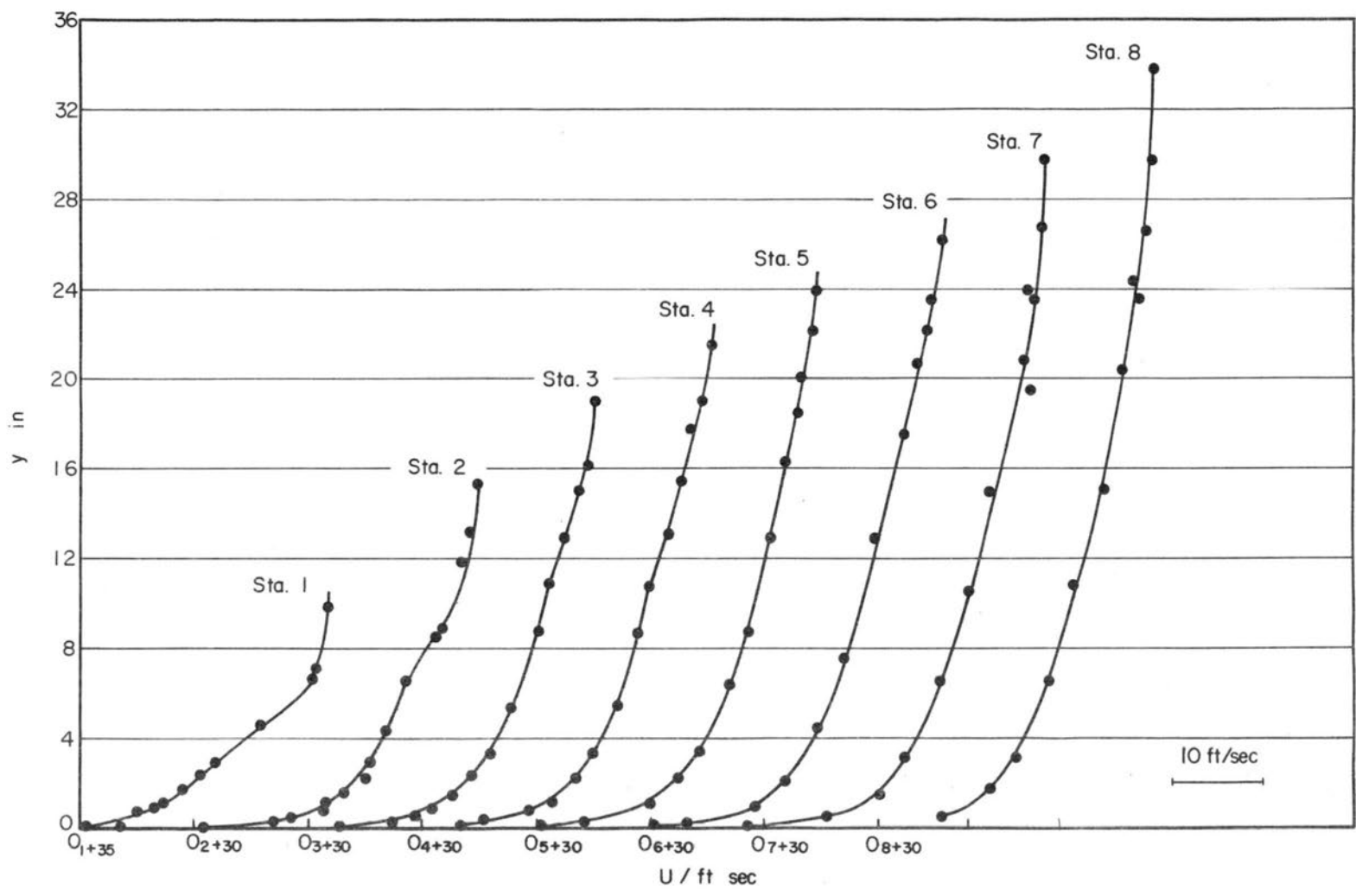


Fig. 26. Mean velocity distributions. $U_{\infty} \approx 60$ ft/sec.
Origins: (0+30) ft/sec.

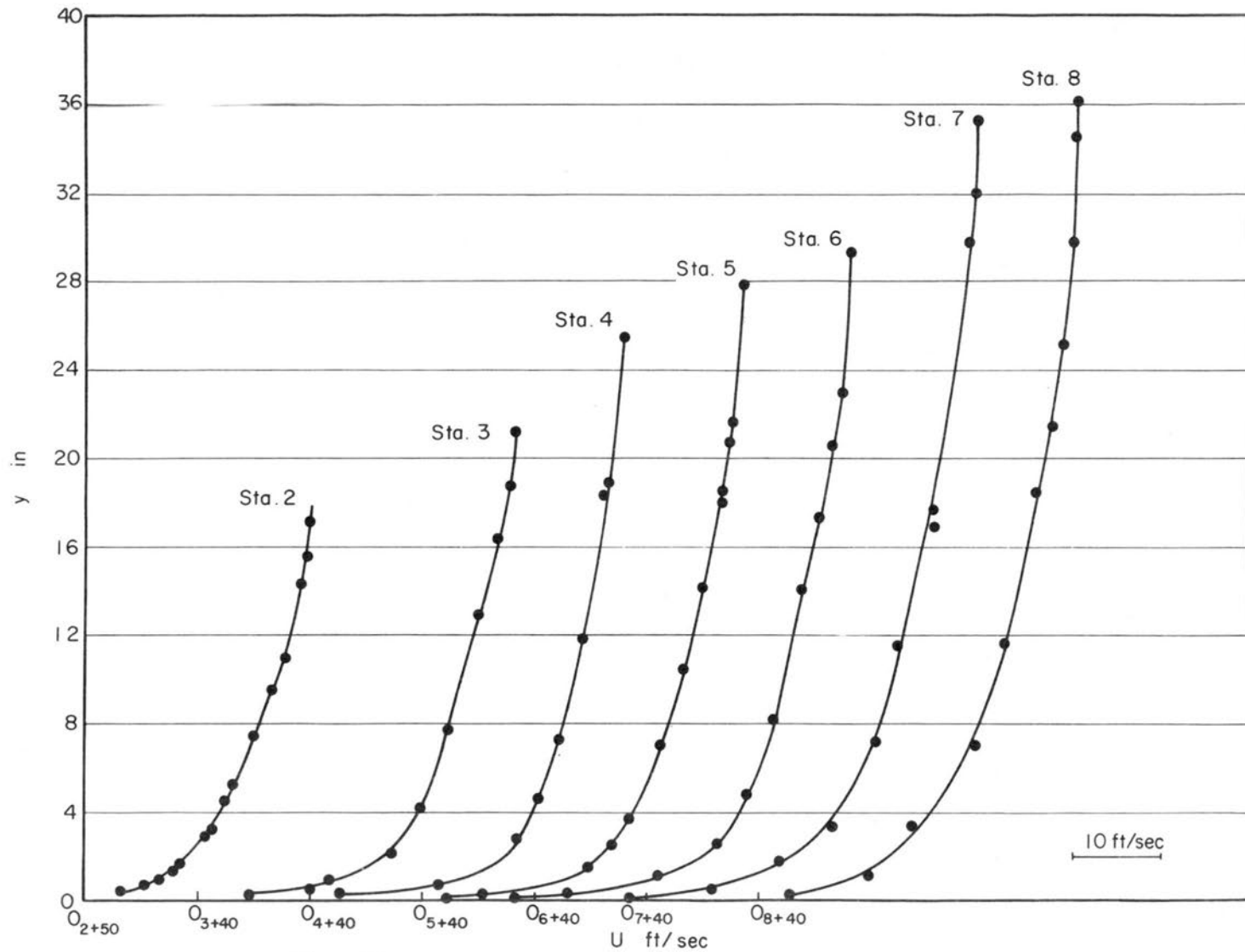


Fig. 27. Mean velocity distributions. $U_{\infty} \approx 75$ ft/sec.
Origins: (0+40) ft/sec.

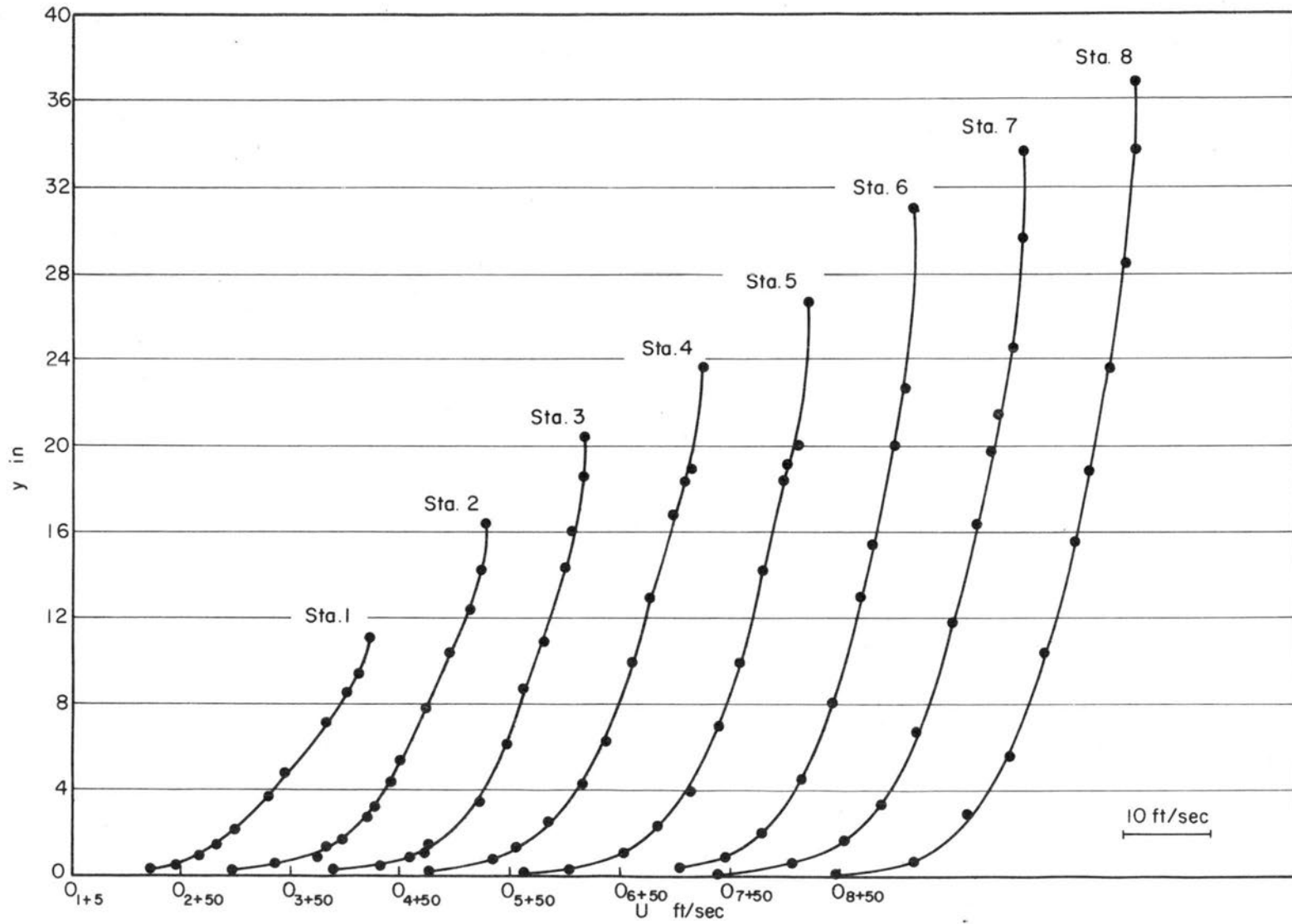


Fig. 28. Mean velocity distributions. $U_{\infty} \approx 84$ ft/sec.
Origins: $(0+50)$ ft/sec.

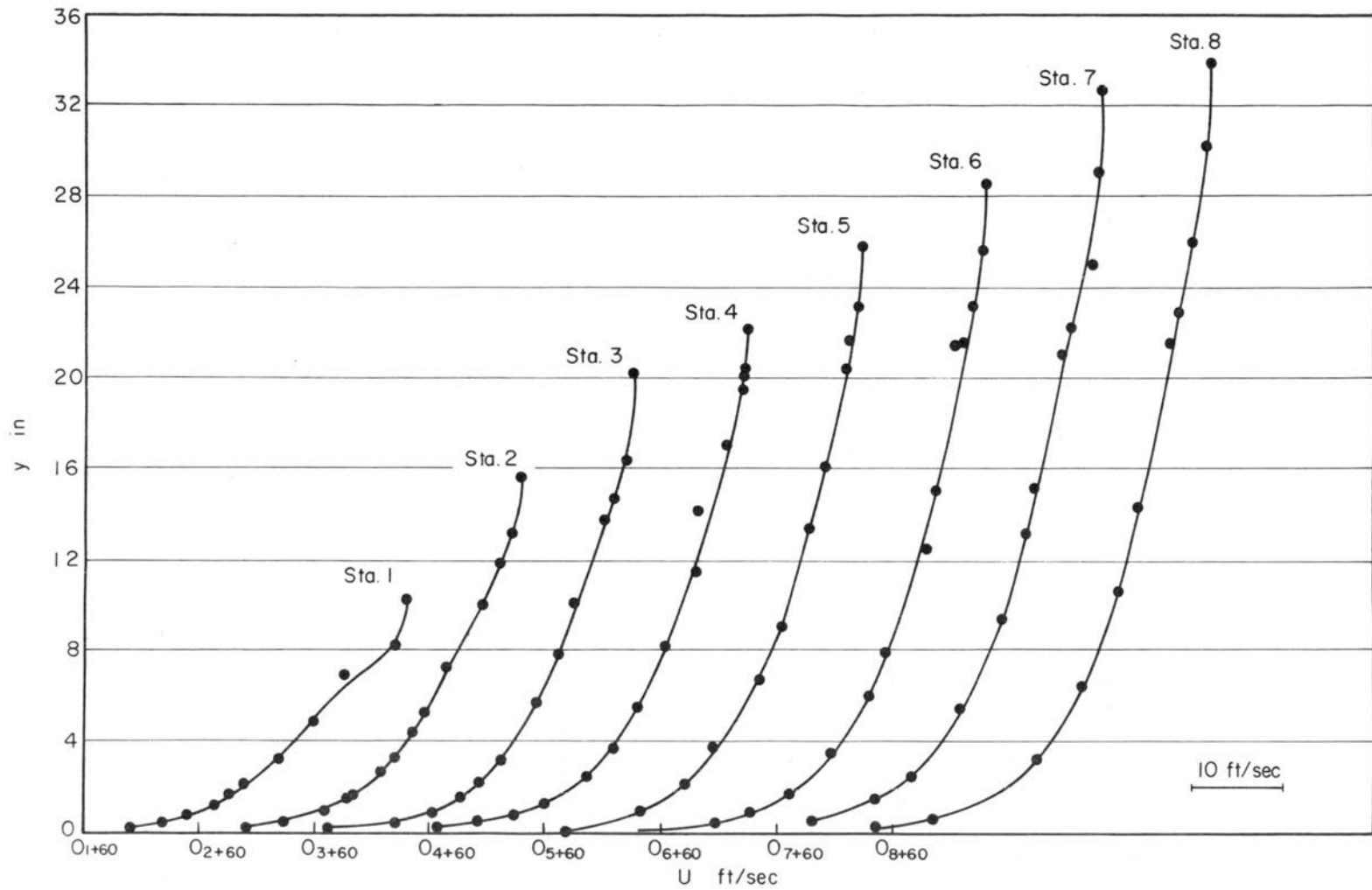


Fig. 29. Mean velocity distributions. $U_{\infty} \approx 95$ ft/sec.
Origins: (0+60) ft/sec.

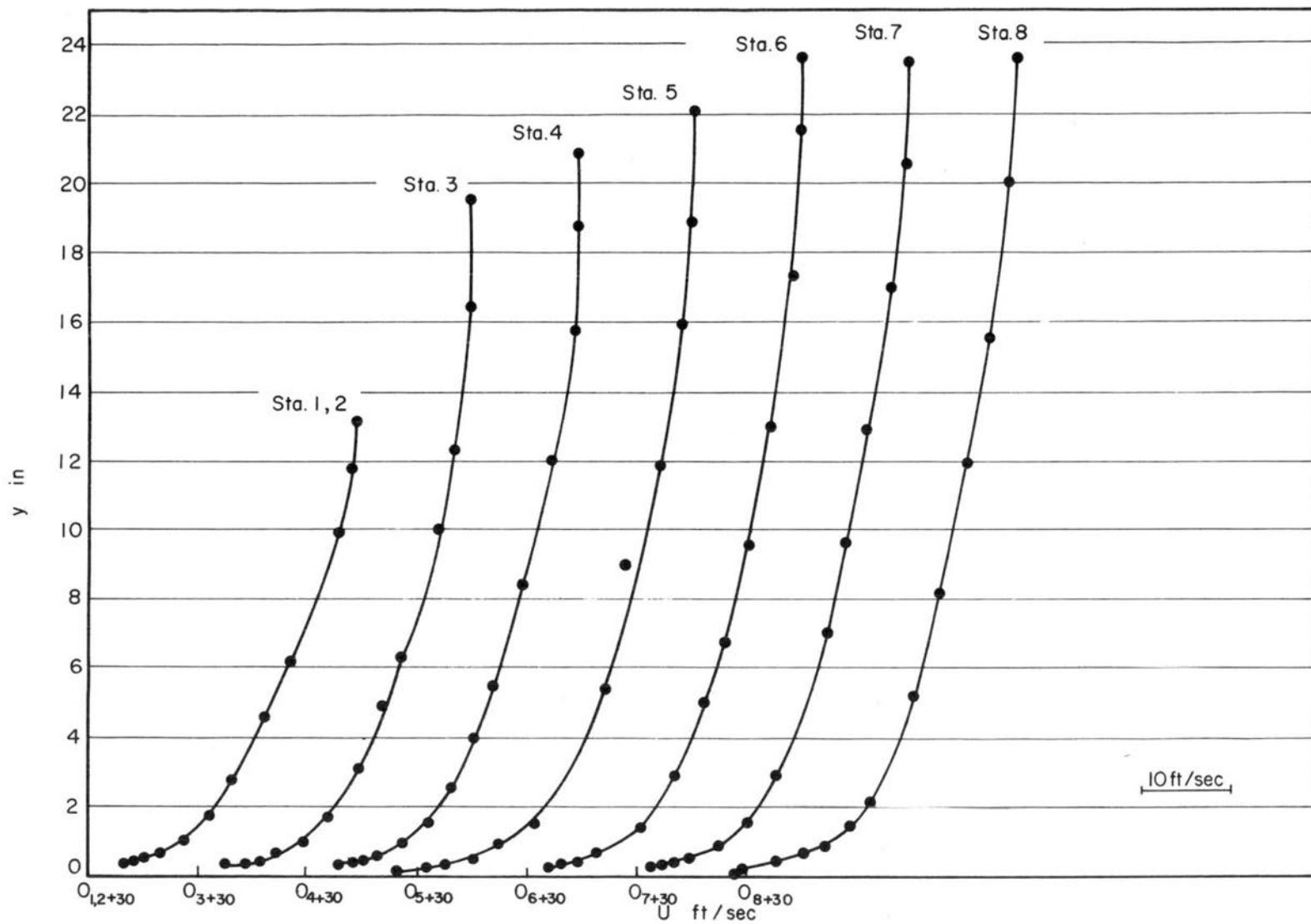


Fig. 30. Mean velocity distributions. $U_{\infty} \approx 61$ ft/sec.
Origins: (0+30) ft/sec.

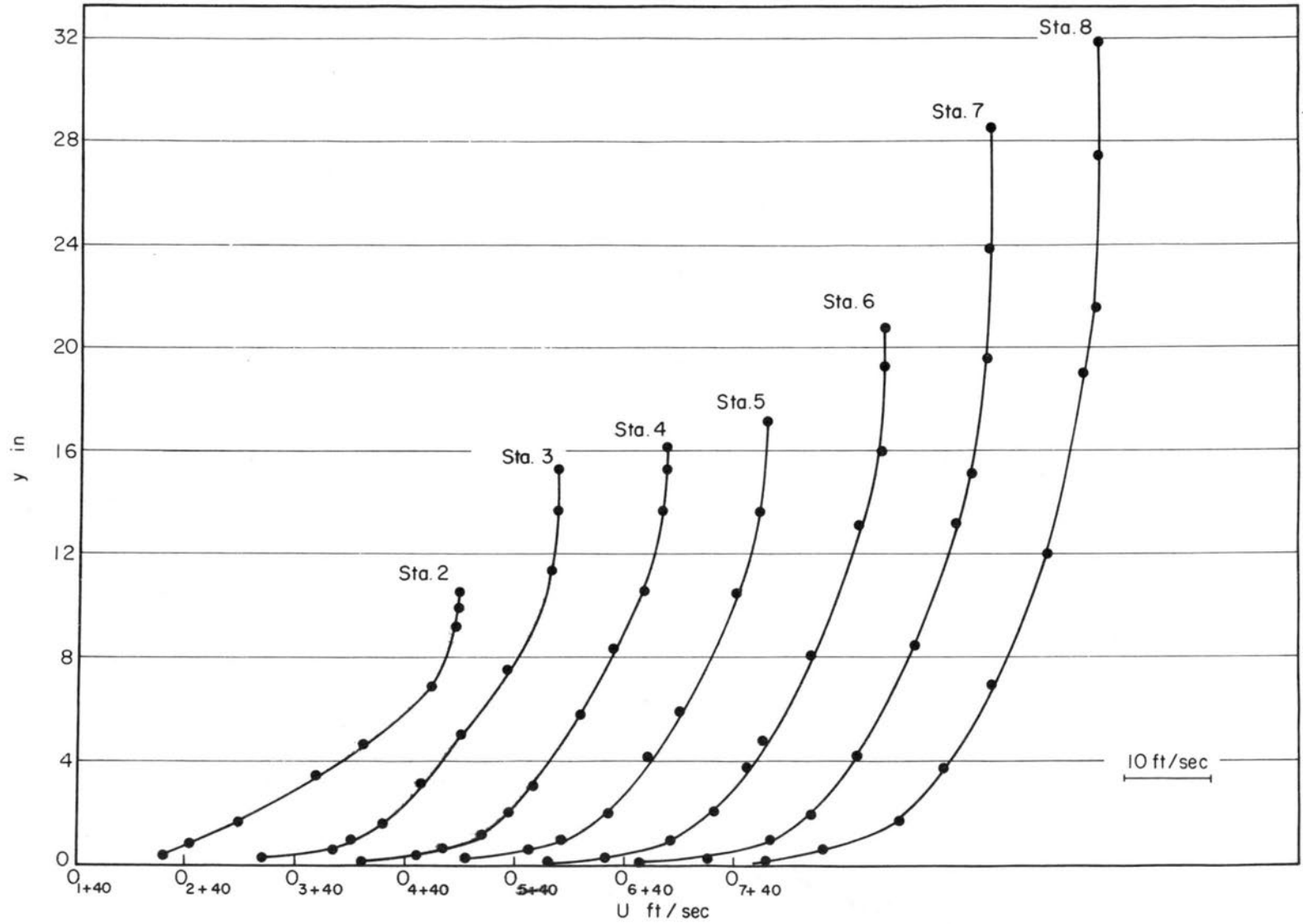


Fig. 31. Mean velocity distributions. $U_{\infty} \approx 82$ ft/sec.
Origins: (0+40) ft/sec.

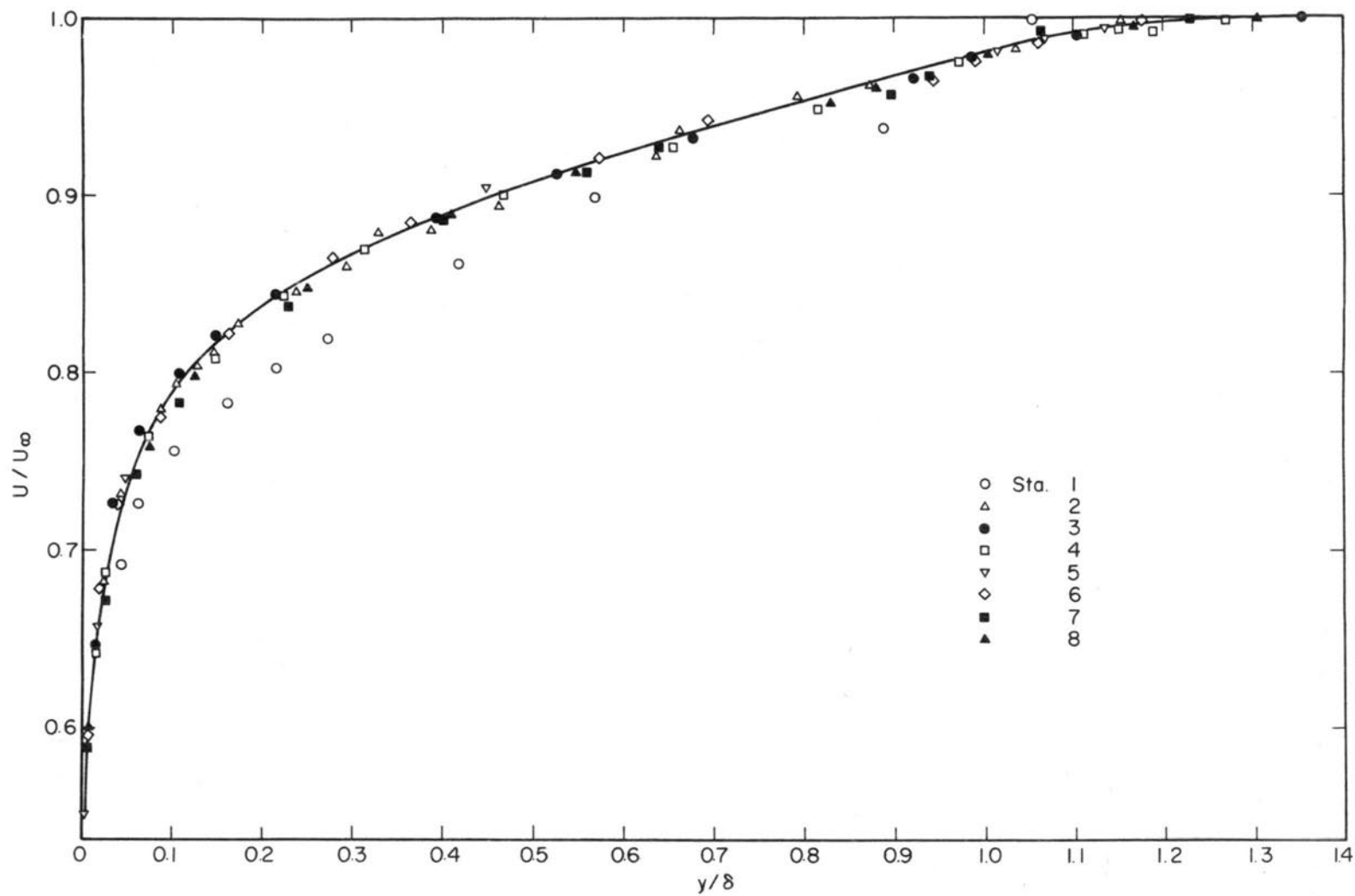


Fig. 32. Nondimensional velocity profile. $U_\infty \approx 95$ ft/sec.

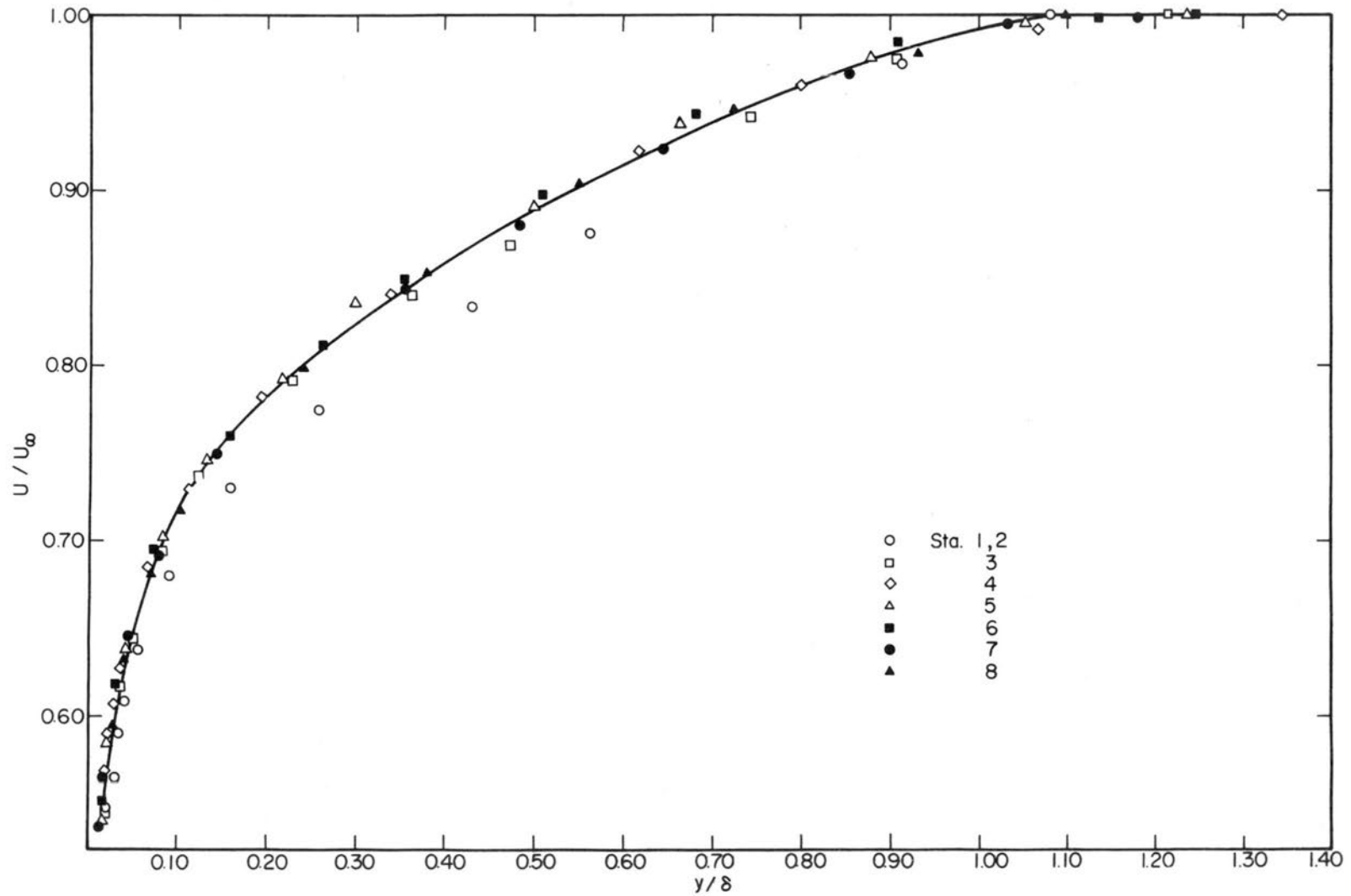


Fig. 33. Nondimensional velocity profile. $U_\infty \approx 60$ ft/sec.

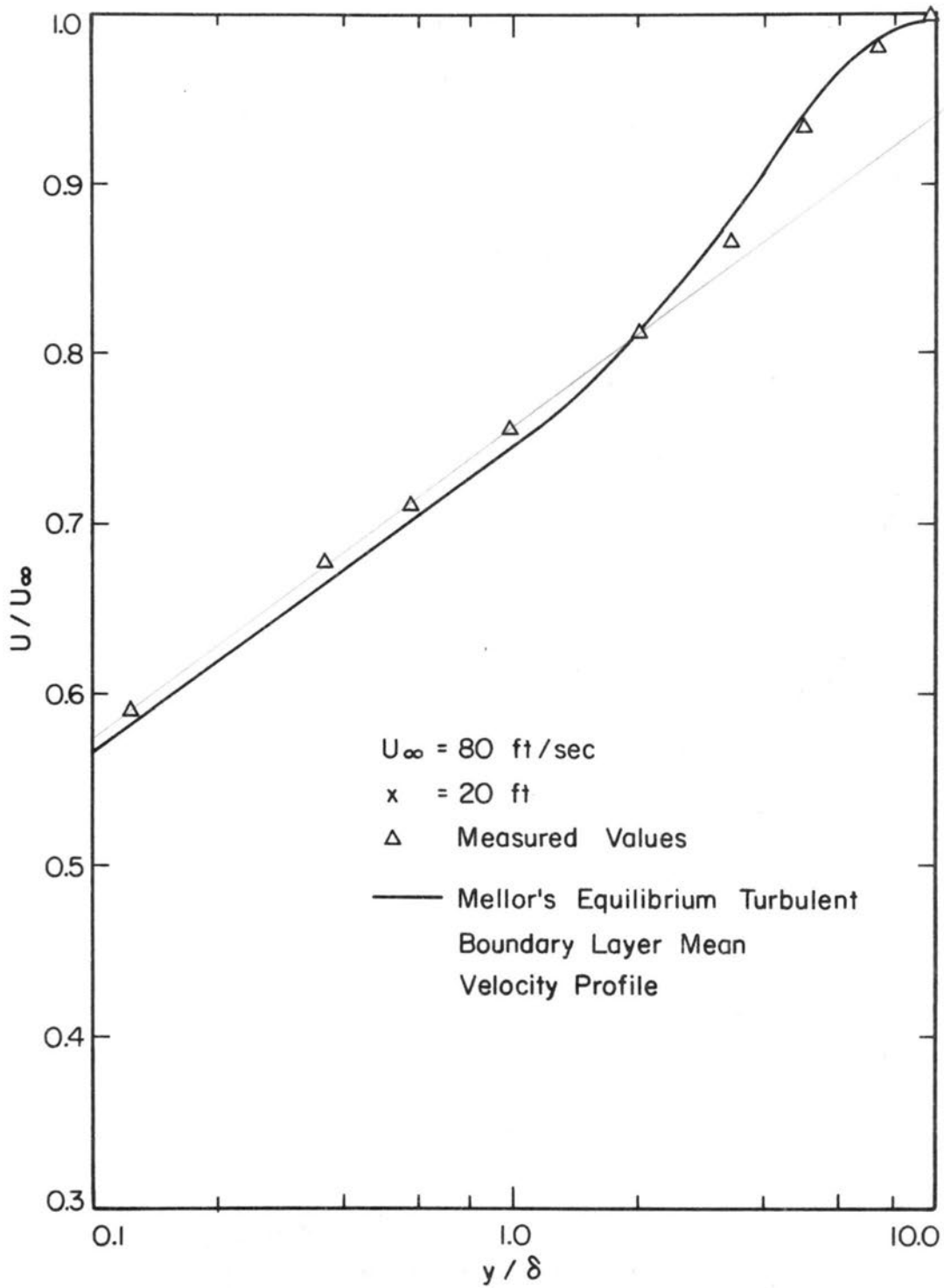


Fig. 34. Comparison of measured mean velocity profile and velocity profile calculated by Mellor's method. $U_{\infty} \approx 81 \text{ ft/sec}$. $x = 20 \text{ ft}$.

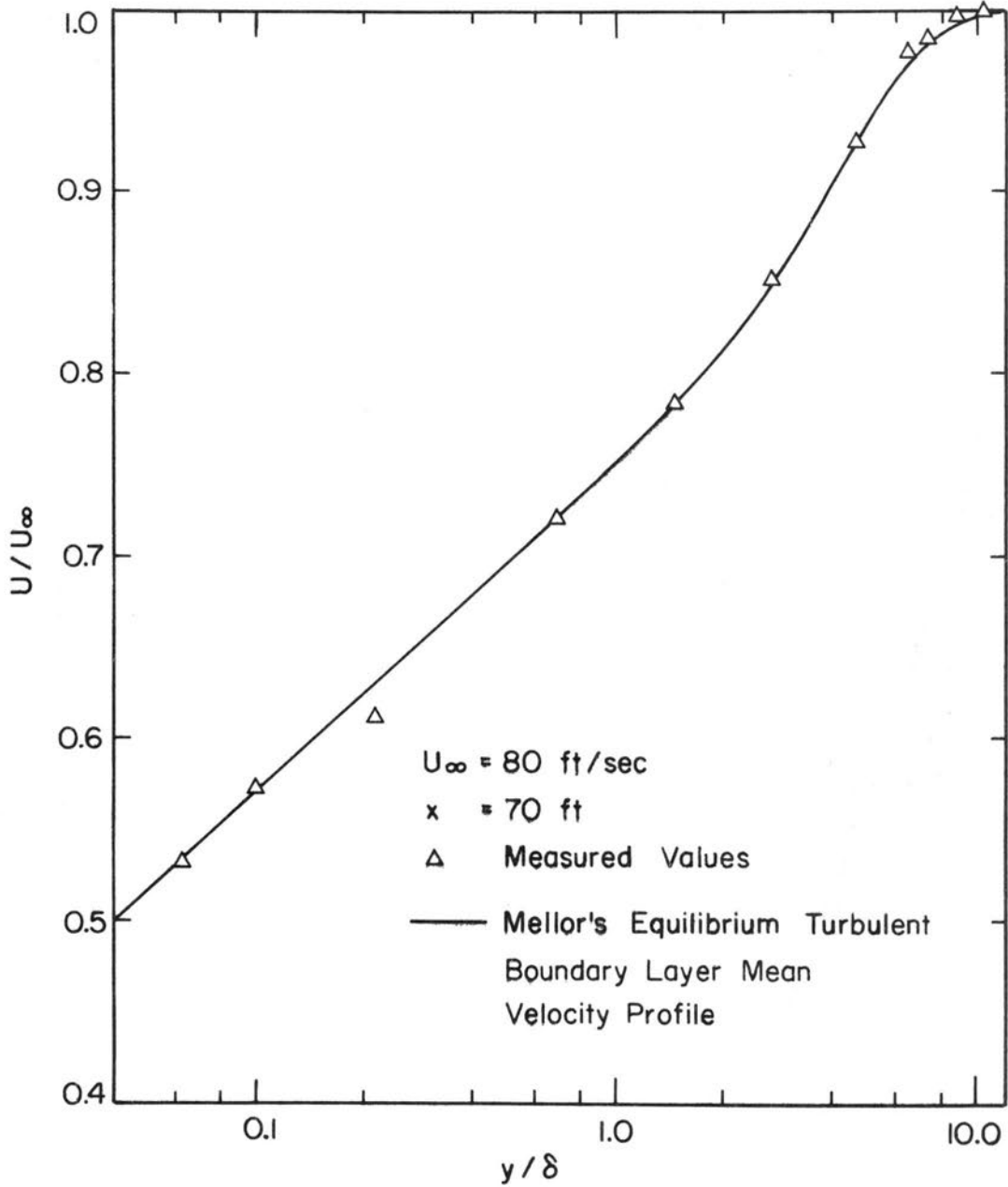


Fig. 35. Comparison of measured mean velocity profile and velocity profile calculated by Mellor's method. $U_\infty \approx 81 \text{ ft/sec}$. $x = 70 \text{ ft}$.

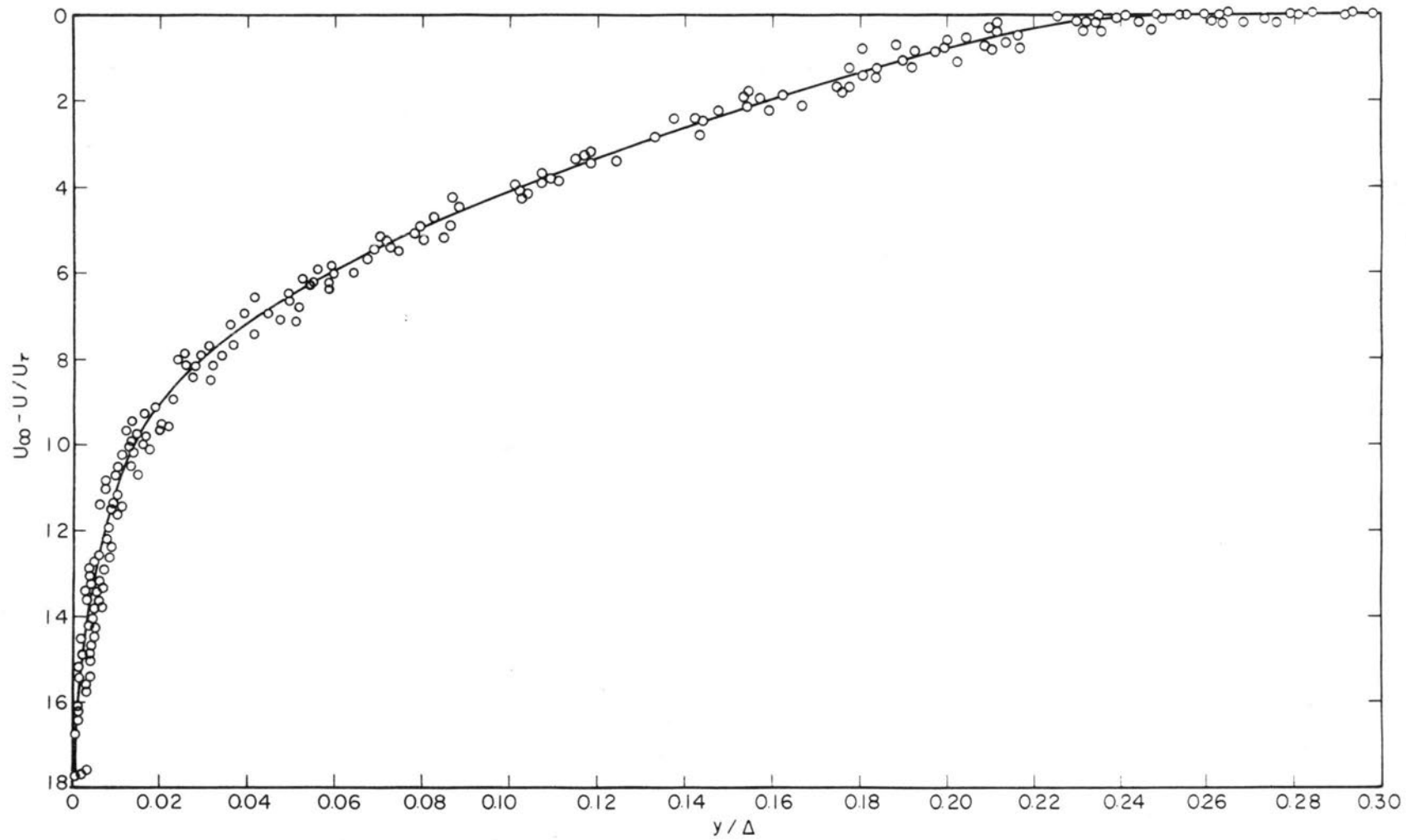


Fig. 36. Universal velocity profile A.

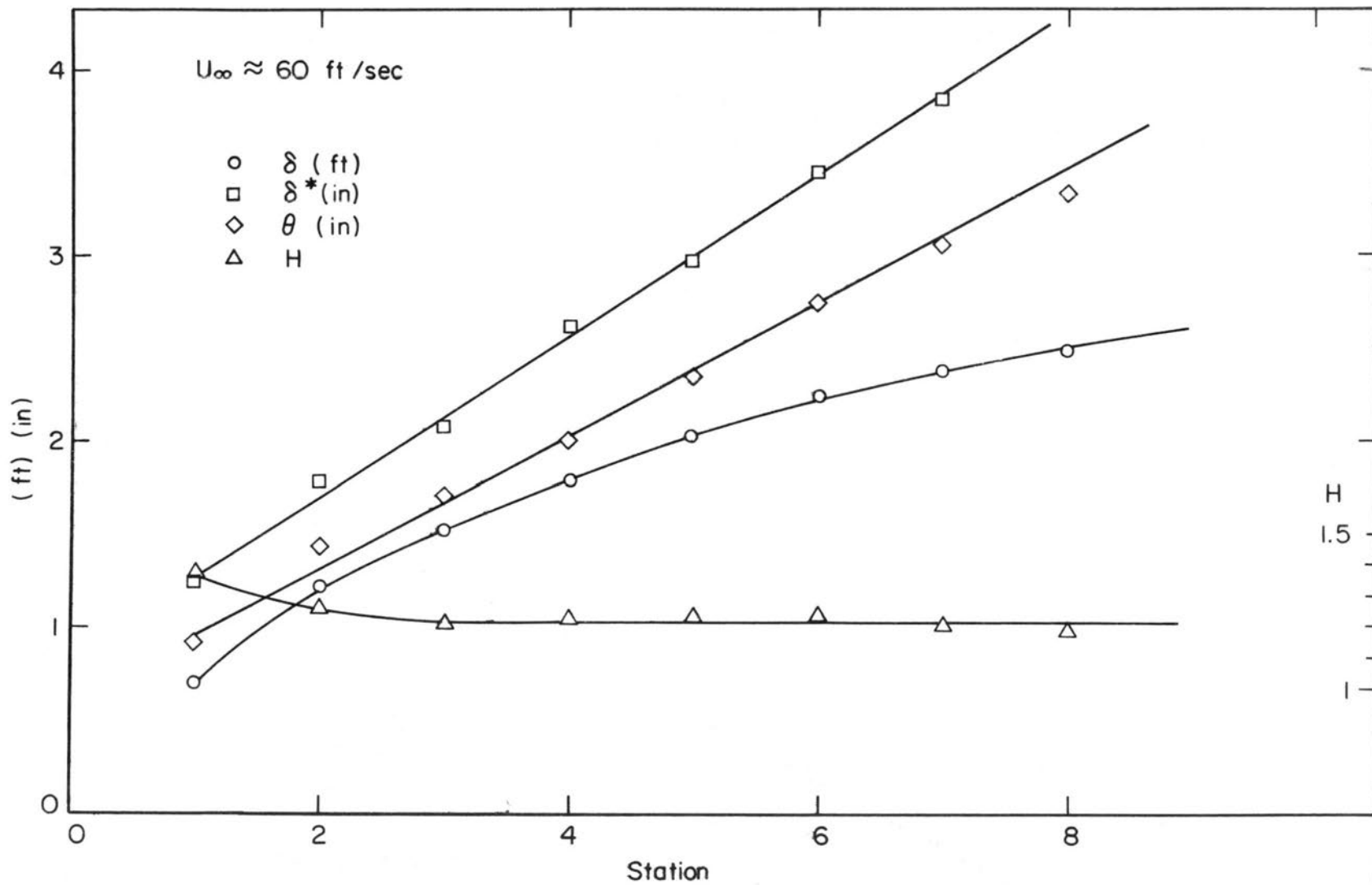


Fig. 37. Boundary layer development. $U_\infty \approx 60$ ft/sec. $x_1 = 7$ ft 11 in.

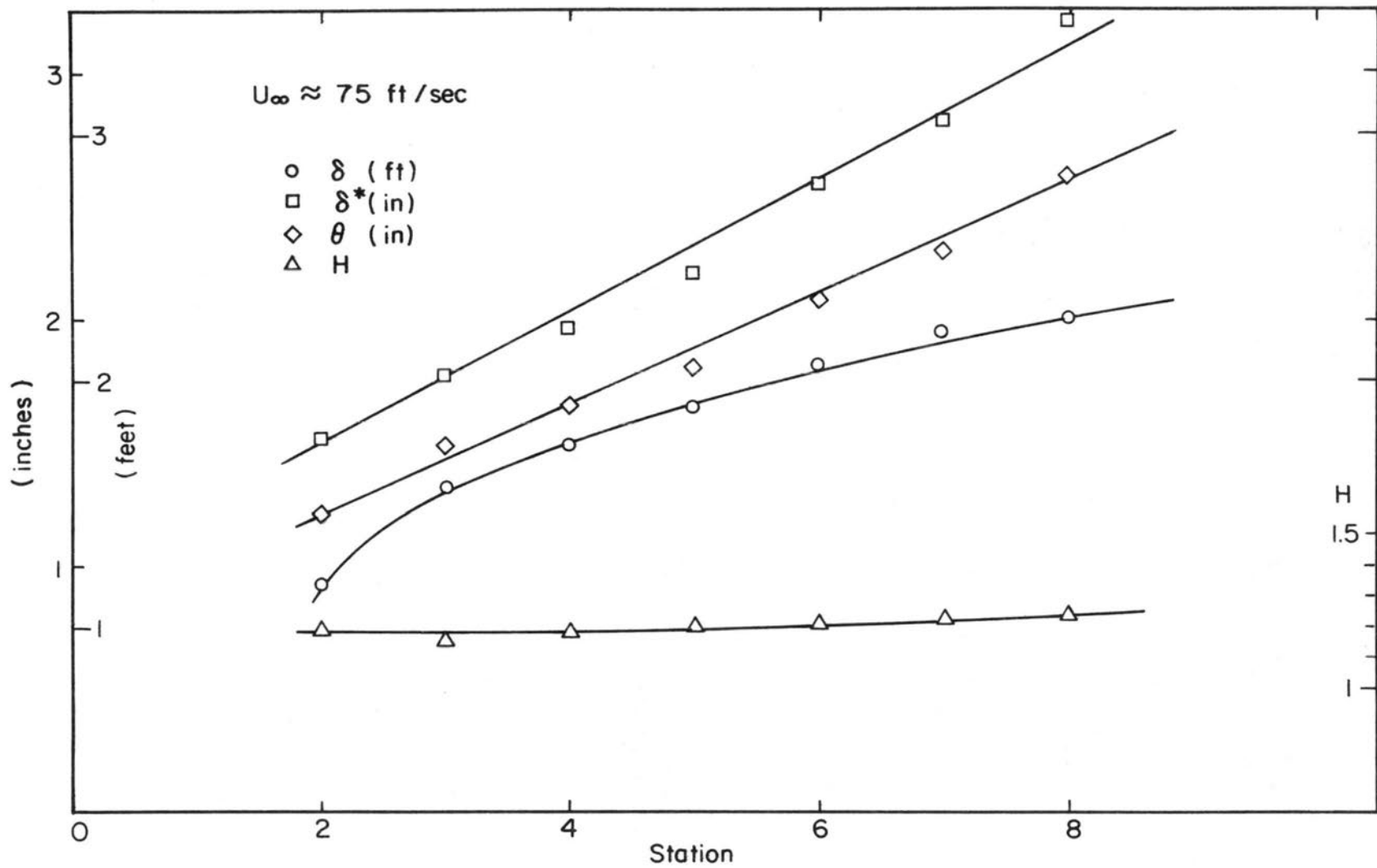


Fig. 38. Boundary layer development. $U_{\infty} \approx 75 \text{ ft/sec}$. $x_1 = 7 \text{ ft } 11 \text{ in.}$

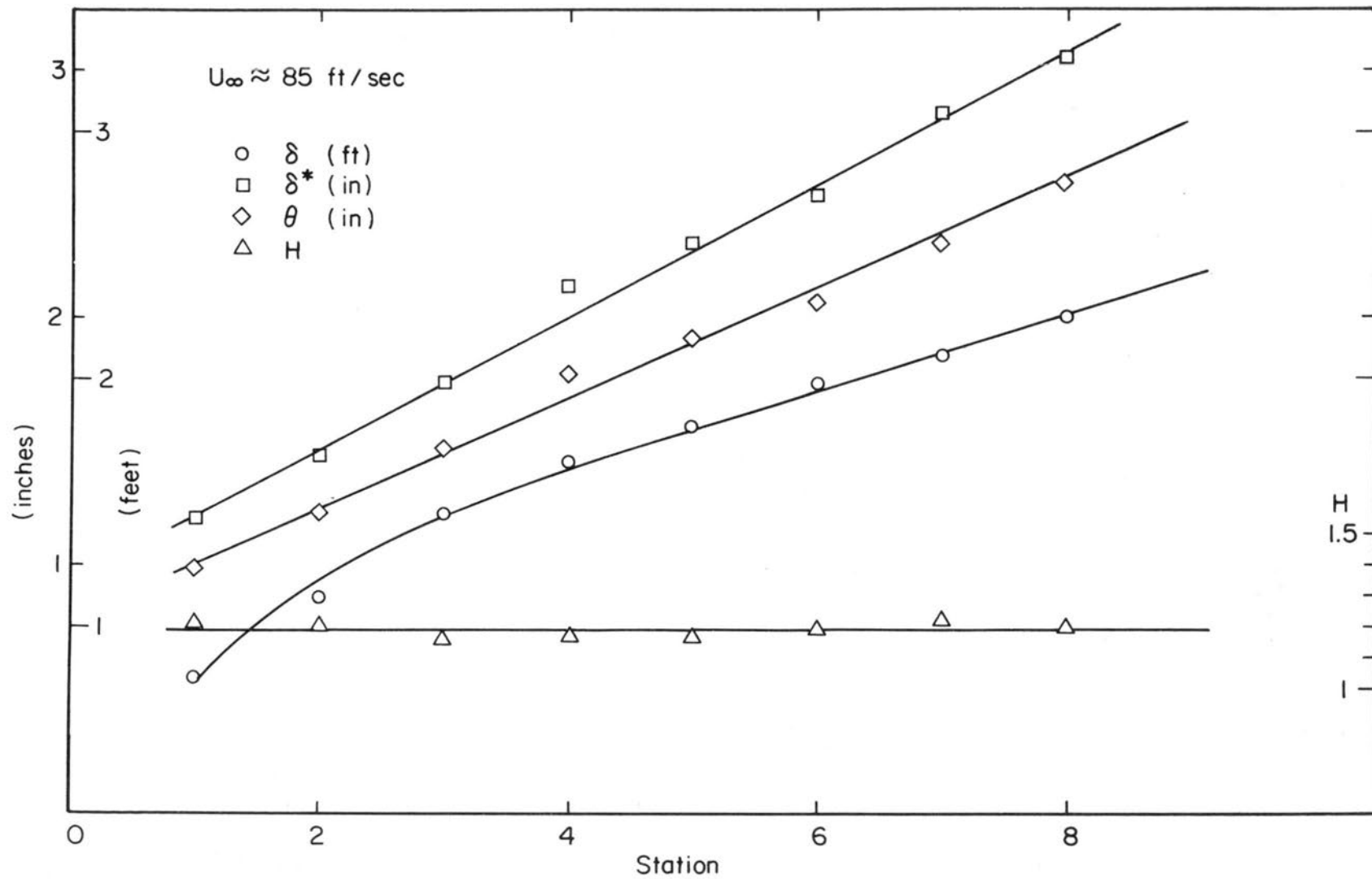


Fig. 39. Boundary layer development. $U_{\infty} \approx 85 \text{ ft/sec}$. $x_1 = 7 \text{ ft. } 11 \text{ in.}$

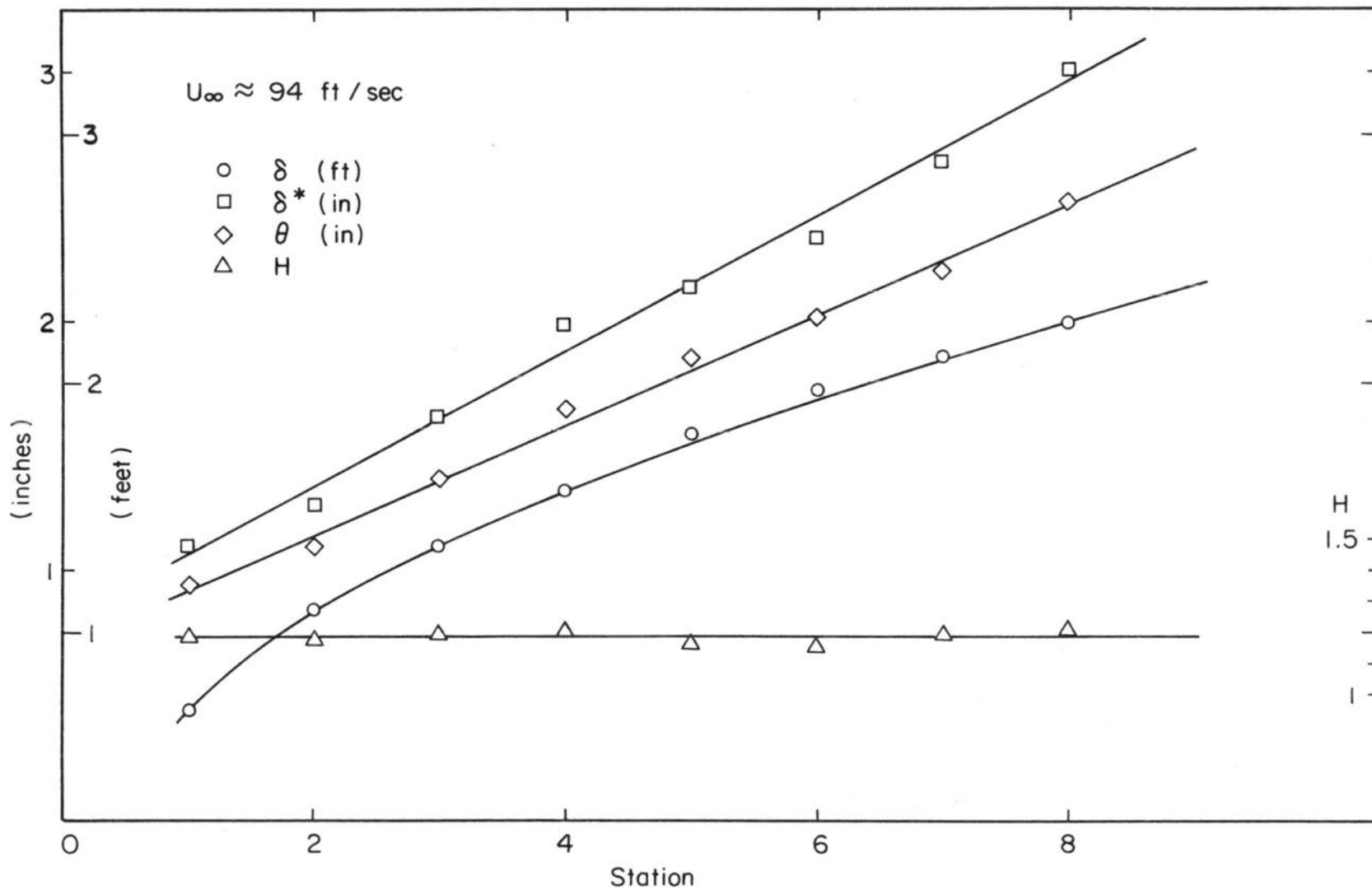


Fig. 40. Boundary layer development. $U_{\infty} \approx 95 \text{ ft/sec}$. $x_1 = 7 \text{ ft. } 11 \text{ in.}$

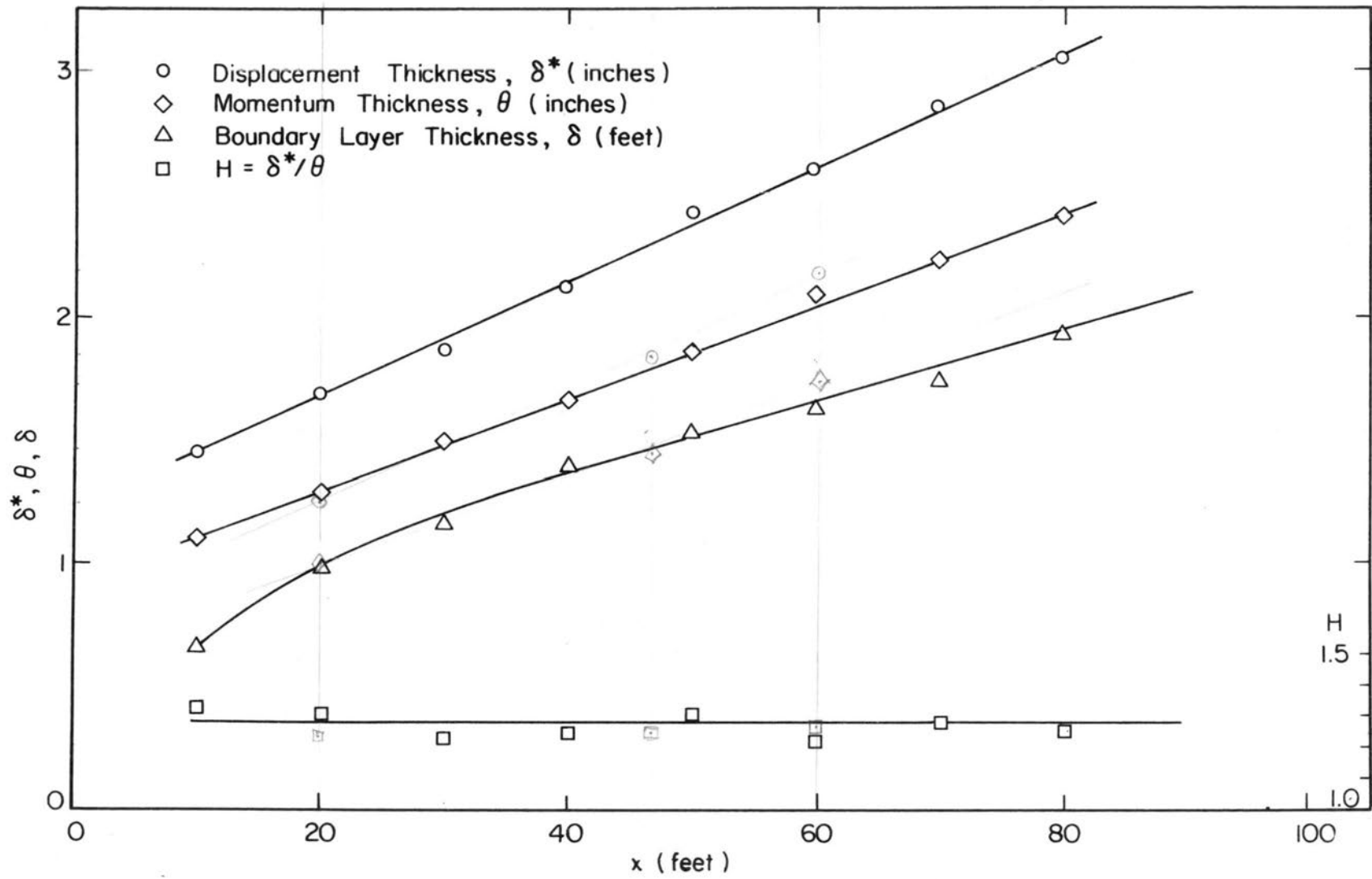


Fig. 41. Boundary layer development. $U_\infty \approx 61$ ft/sec.

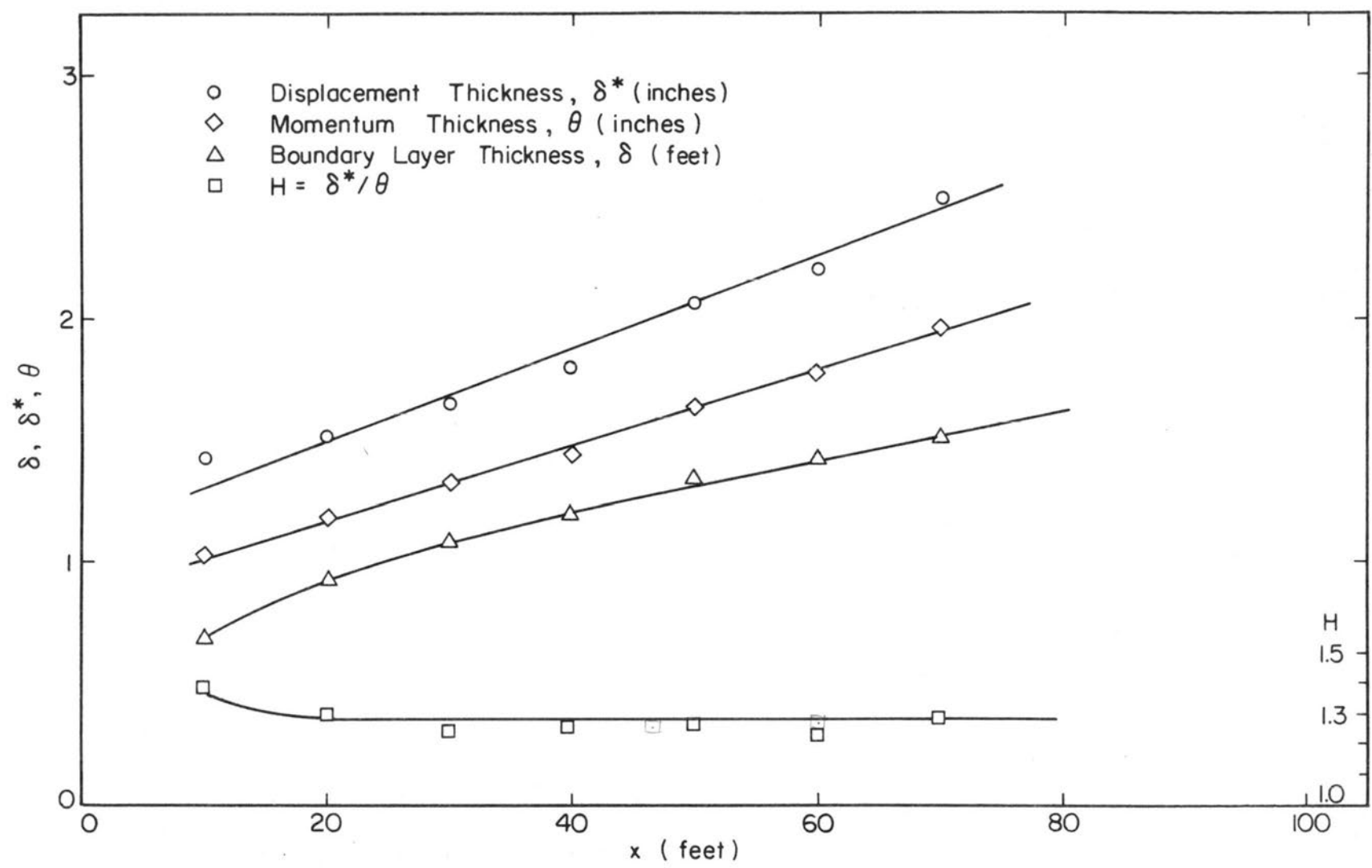


Fig. 42. Boundary layer development. $U_\infty \approx 82$ ft/sec.

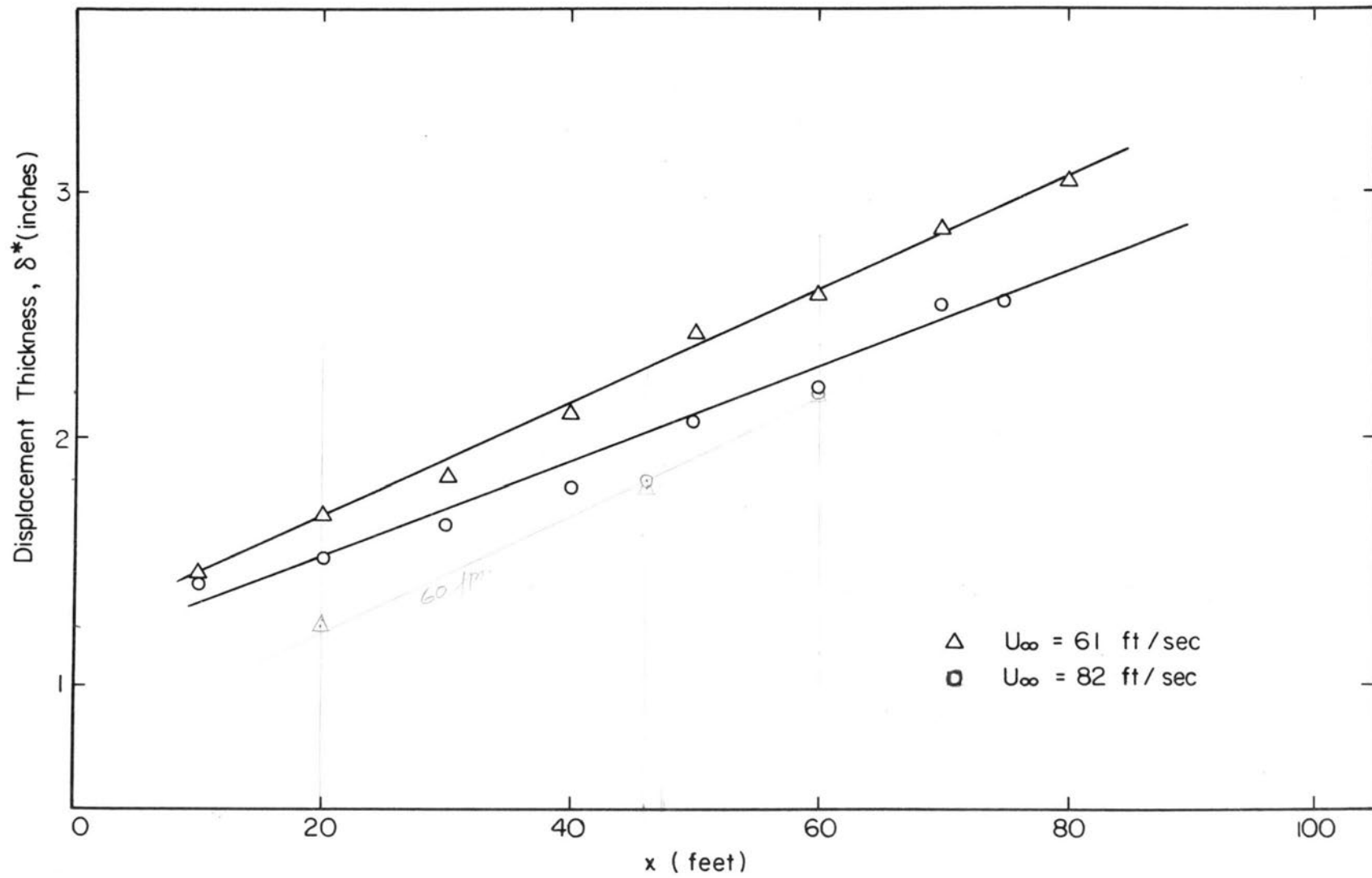


Fig. 43. Displacement thickness comparison.

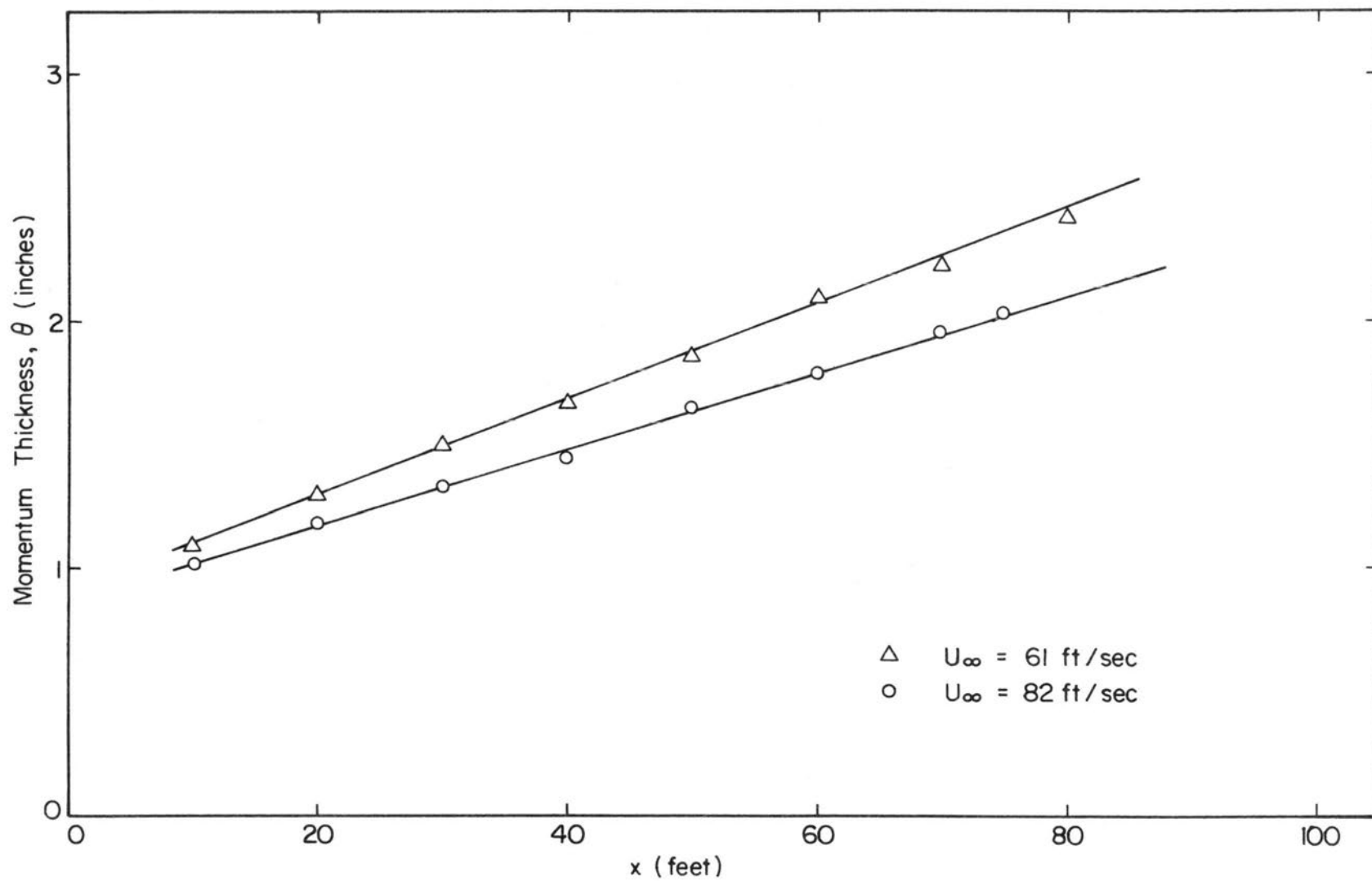


Fig. 44. Momentum thickness comparison.

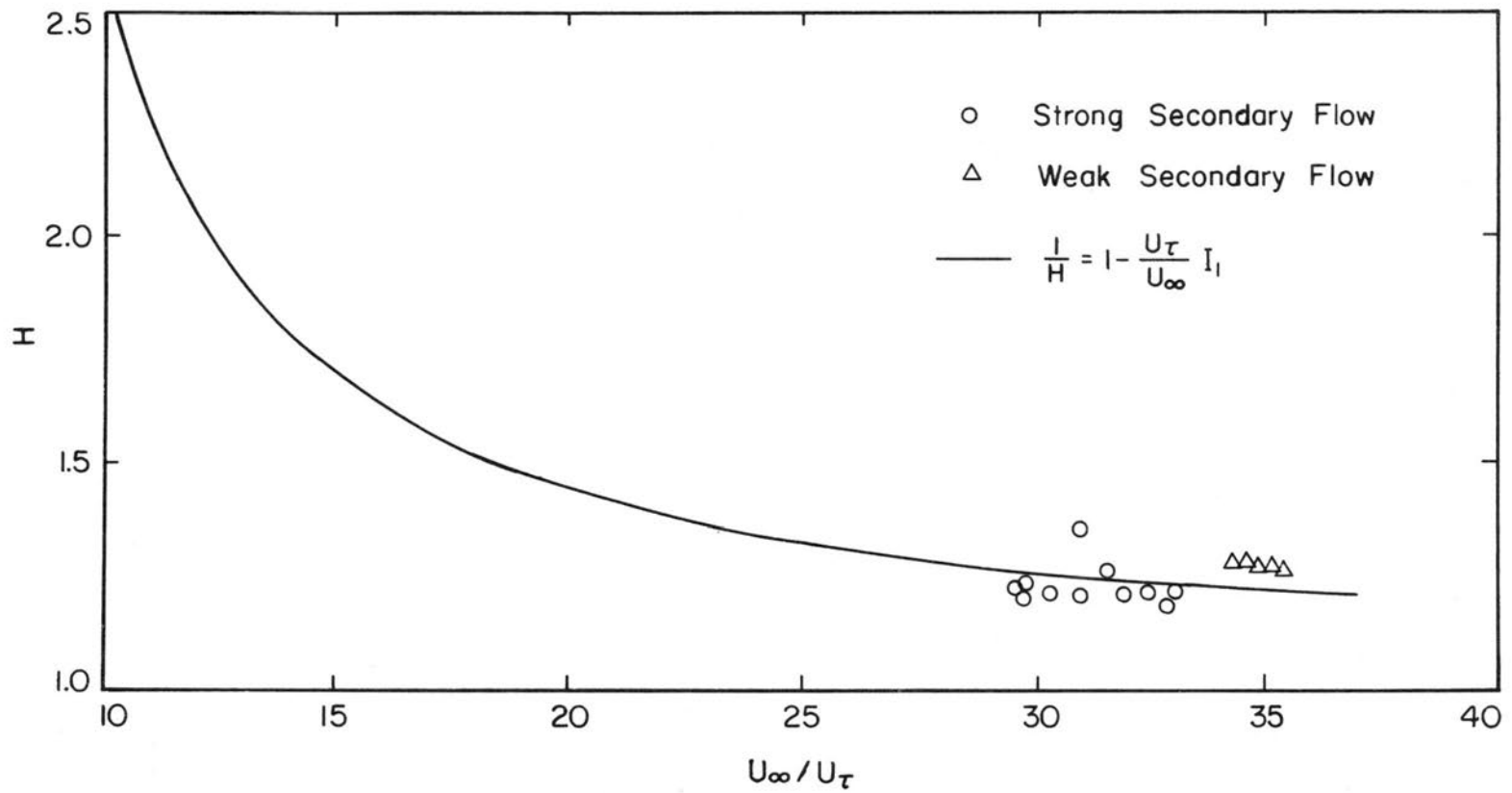


Fig. 45. Effect of skin friction on form factor H .

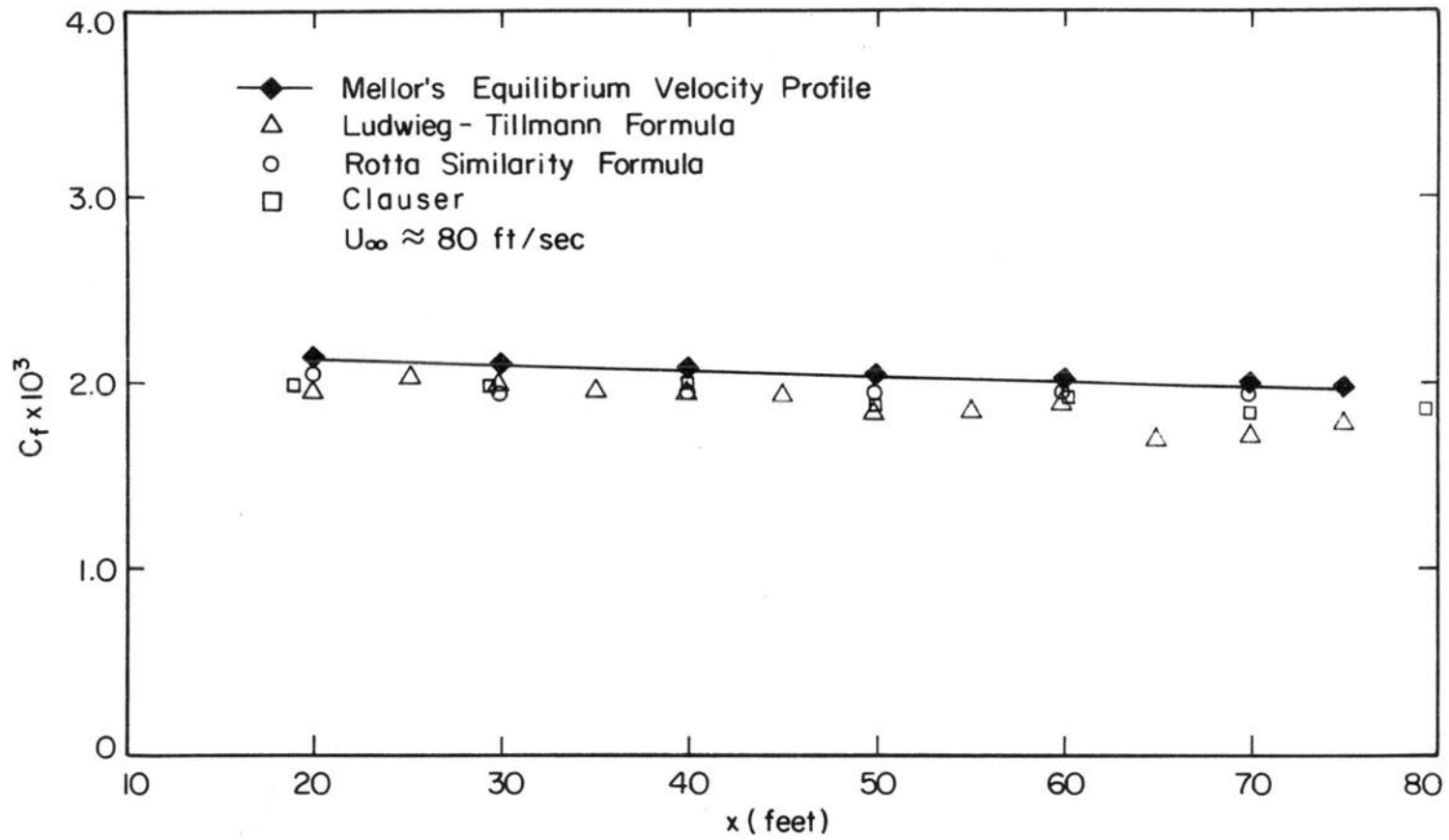


Fig. 46. Comparison of friction coefficient values.

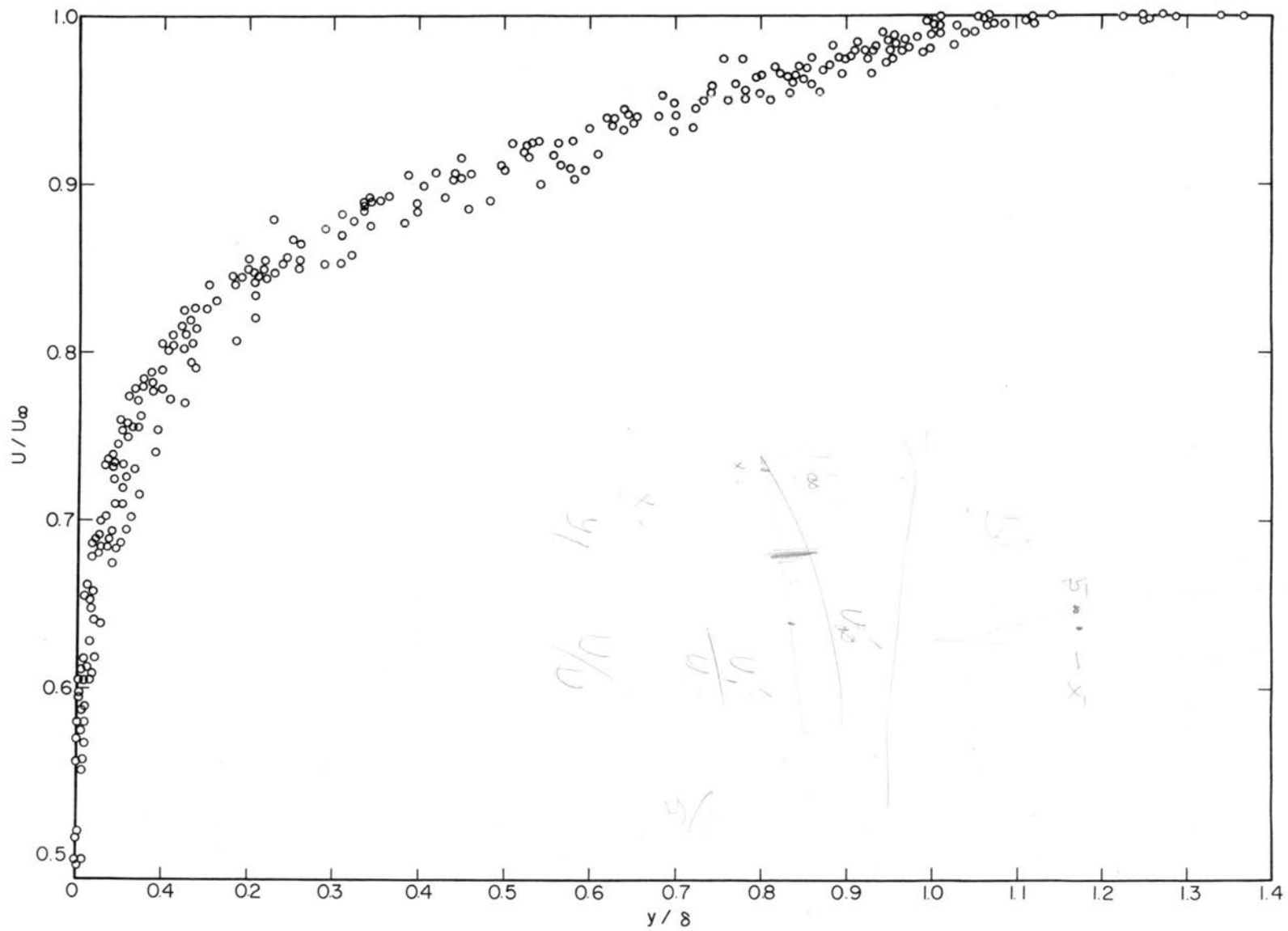


Fig. 47. Universal velocity profile B.

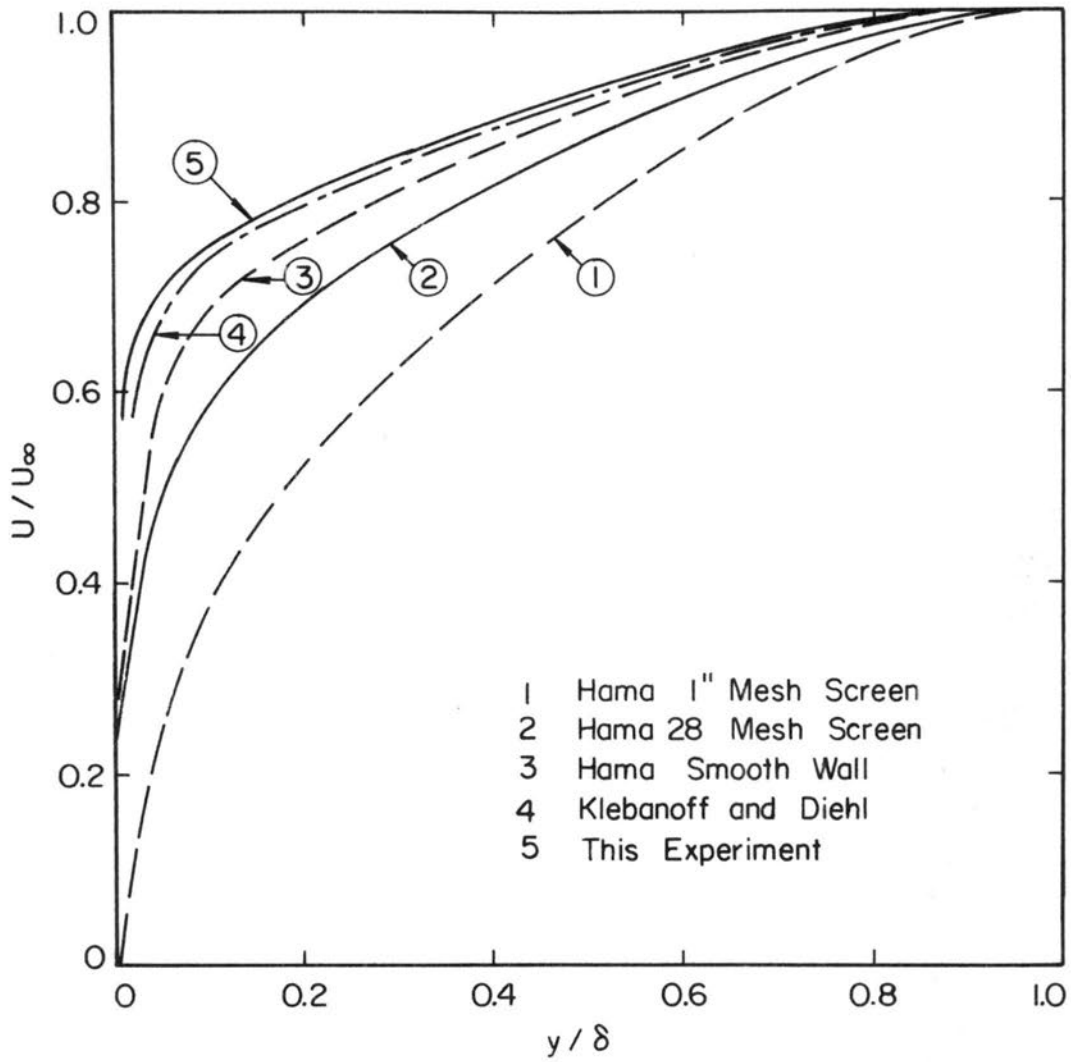


Fig. 48. Turbulent boundary layer velocity distributions at zero pressure gradient on a flat plate.

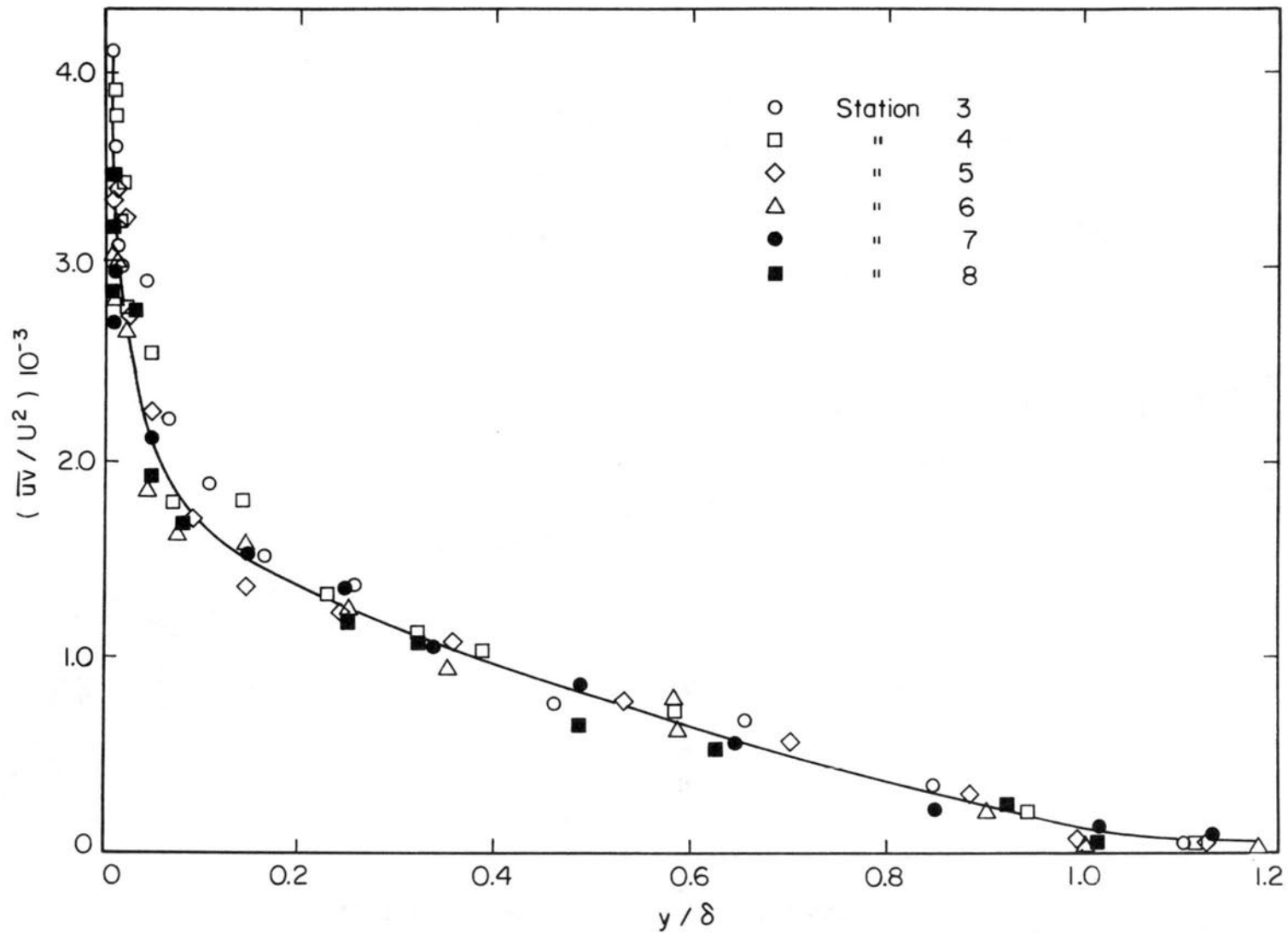


Fig. 49. Comparison of turbulent shear stress distribution along the boundary layer length. $U_{\infty} \approx 60$ ft/sec.

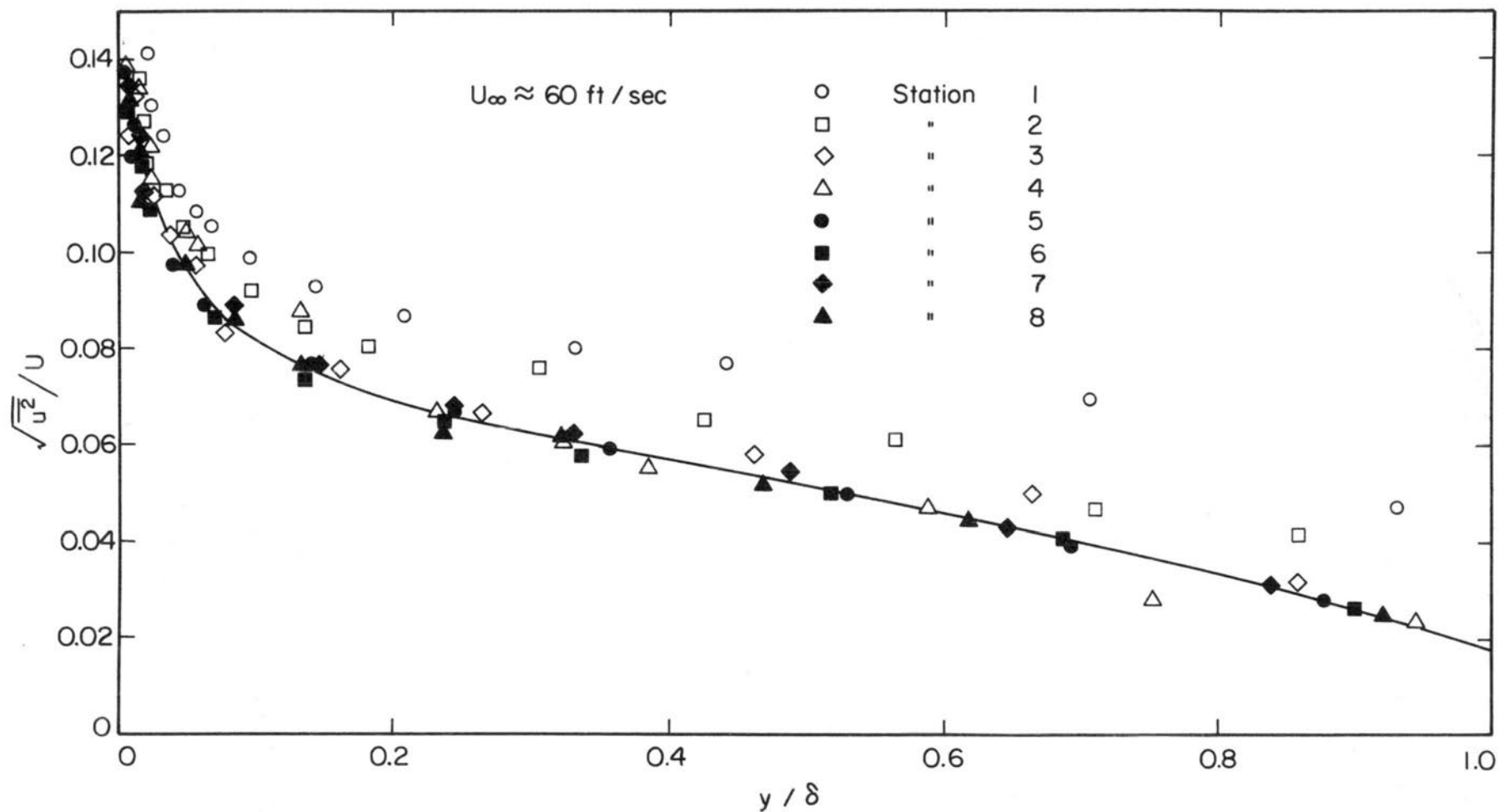


Fig. 50. Comparison of u-component of turbulence distributions along the boundary layer length.

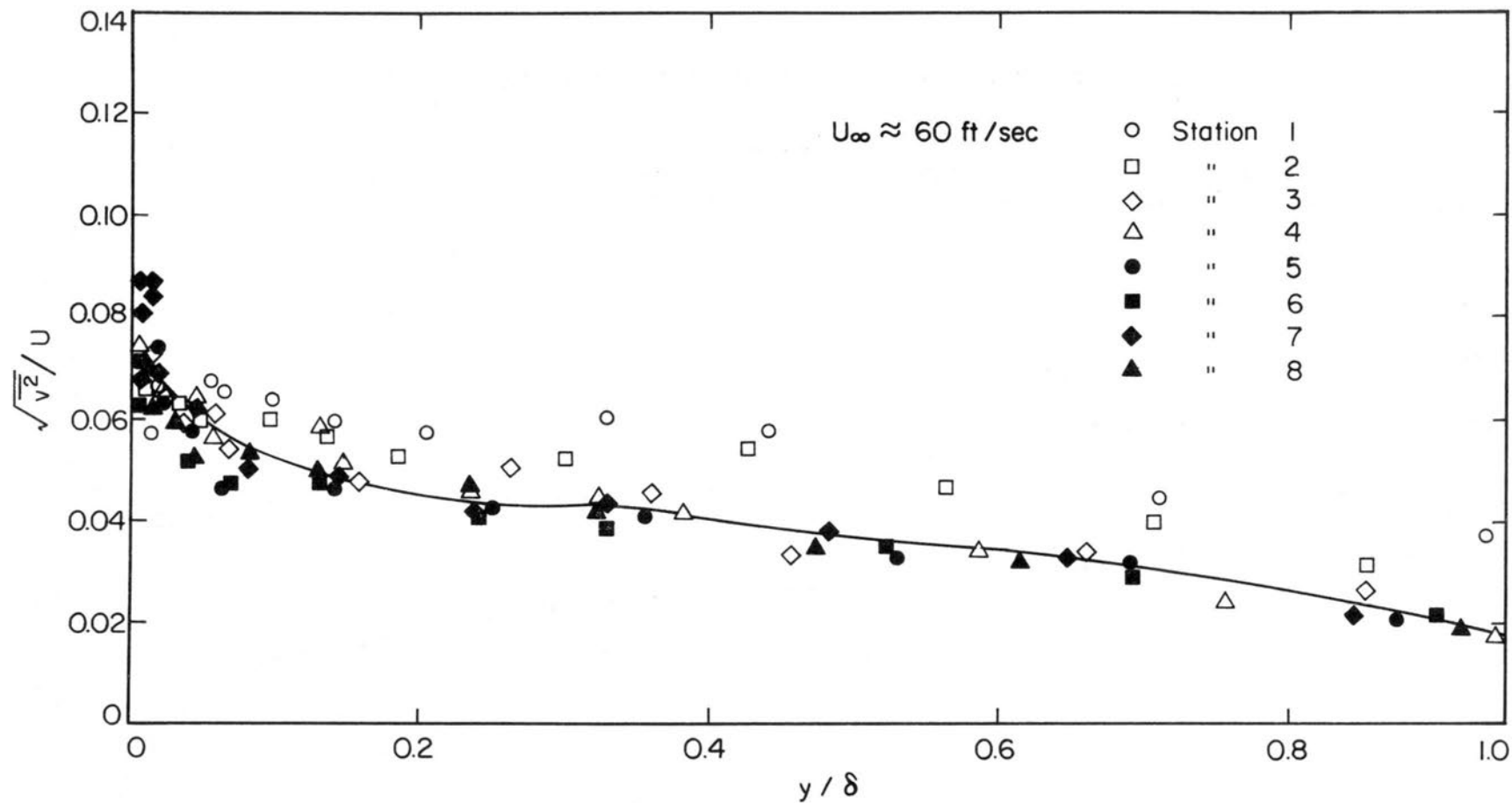


Fig. 51. Comparison of v-component of turbulence distributions along the boundary layer length.

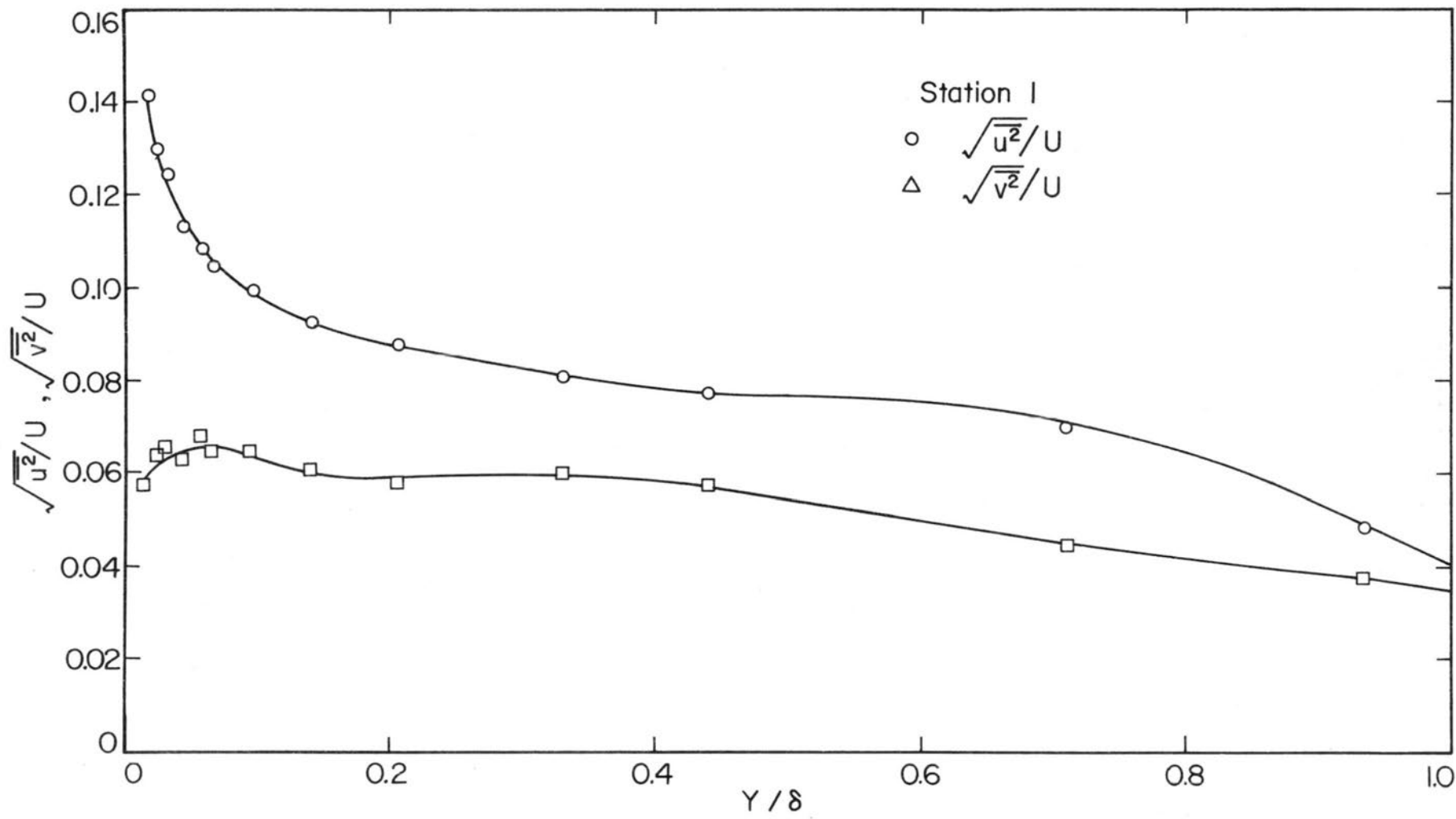


Fig. 52. Turbulence intensities, $U_\infty \approx 60$ ft/sec, $x = 10$ ft.

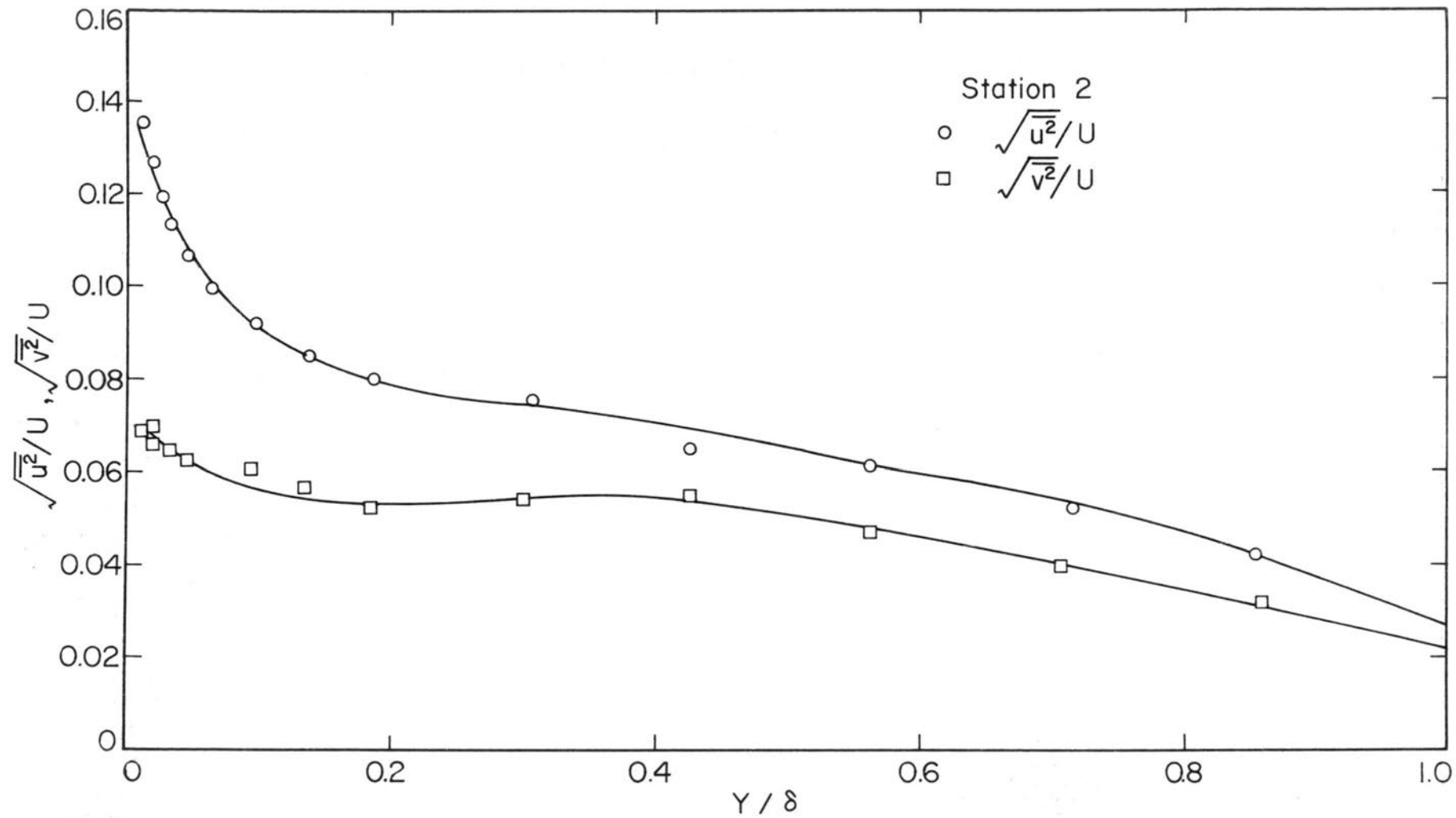


Fig. 53. Turbulence intensities, $U_\infty \approx 60$ ft/sec, $x = 20$ ft.

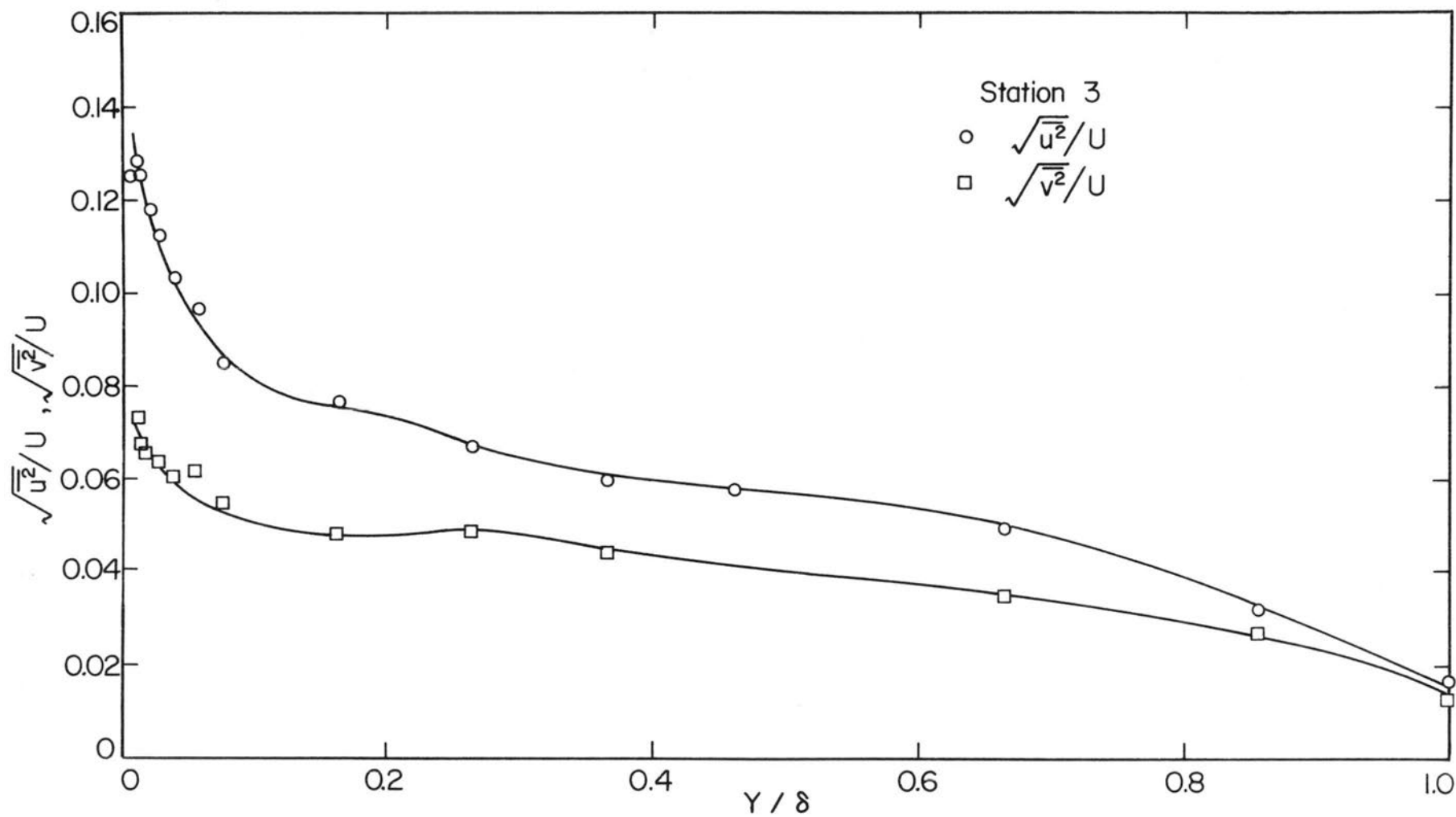


Fig. 54. Turbulence intensities, $U_\infty \approx 60$ ft/sec, $x = 30$ ft.

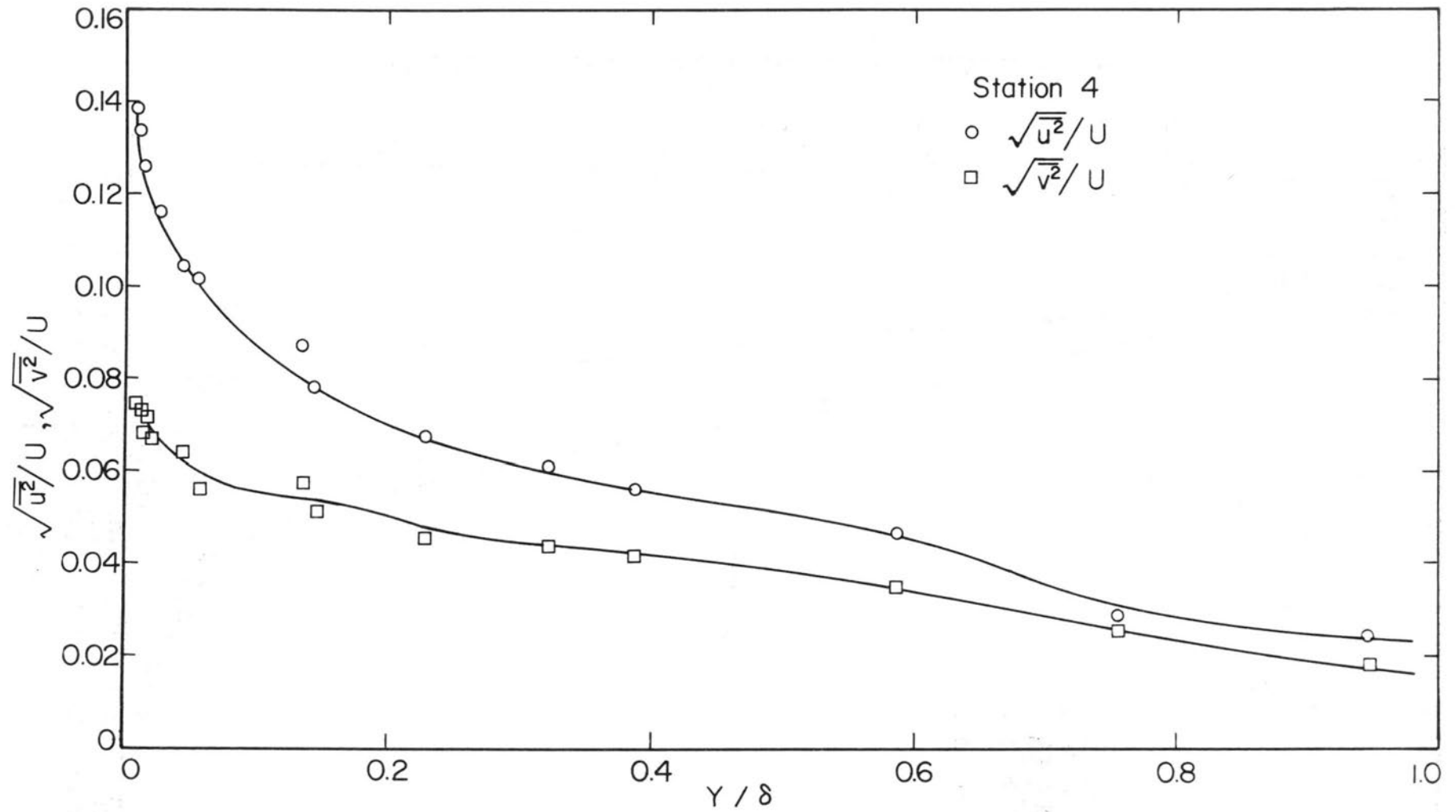


Fig. 55. Turbulence intensities, $U_\infty \approx 60$ ft/sec, $x = 40$ ft.

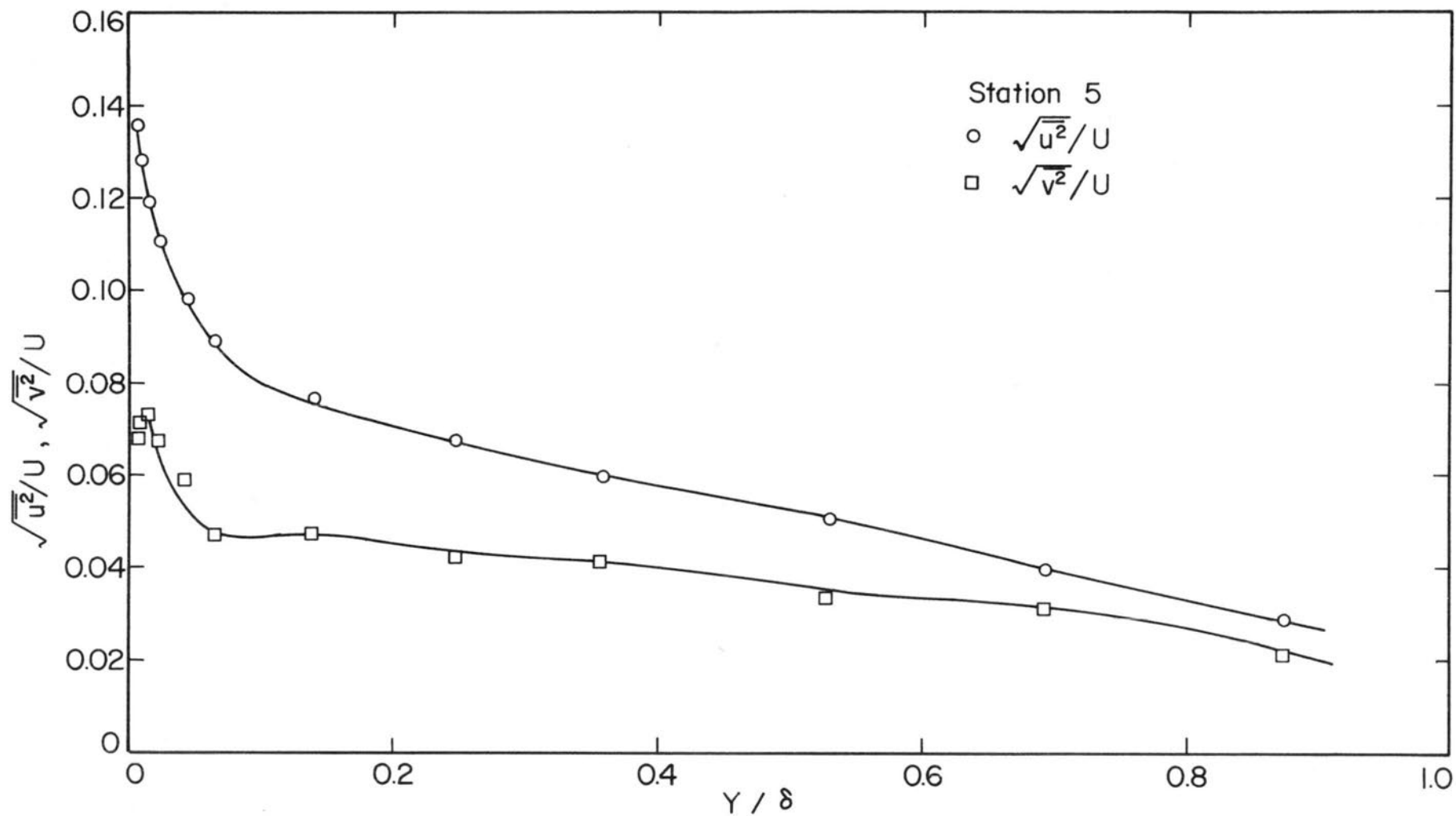


Fig. 56. Turbulence intensities, $U_\infty \approx 60$ ft/sec, $x = 50$ ft.

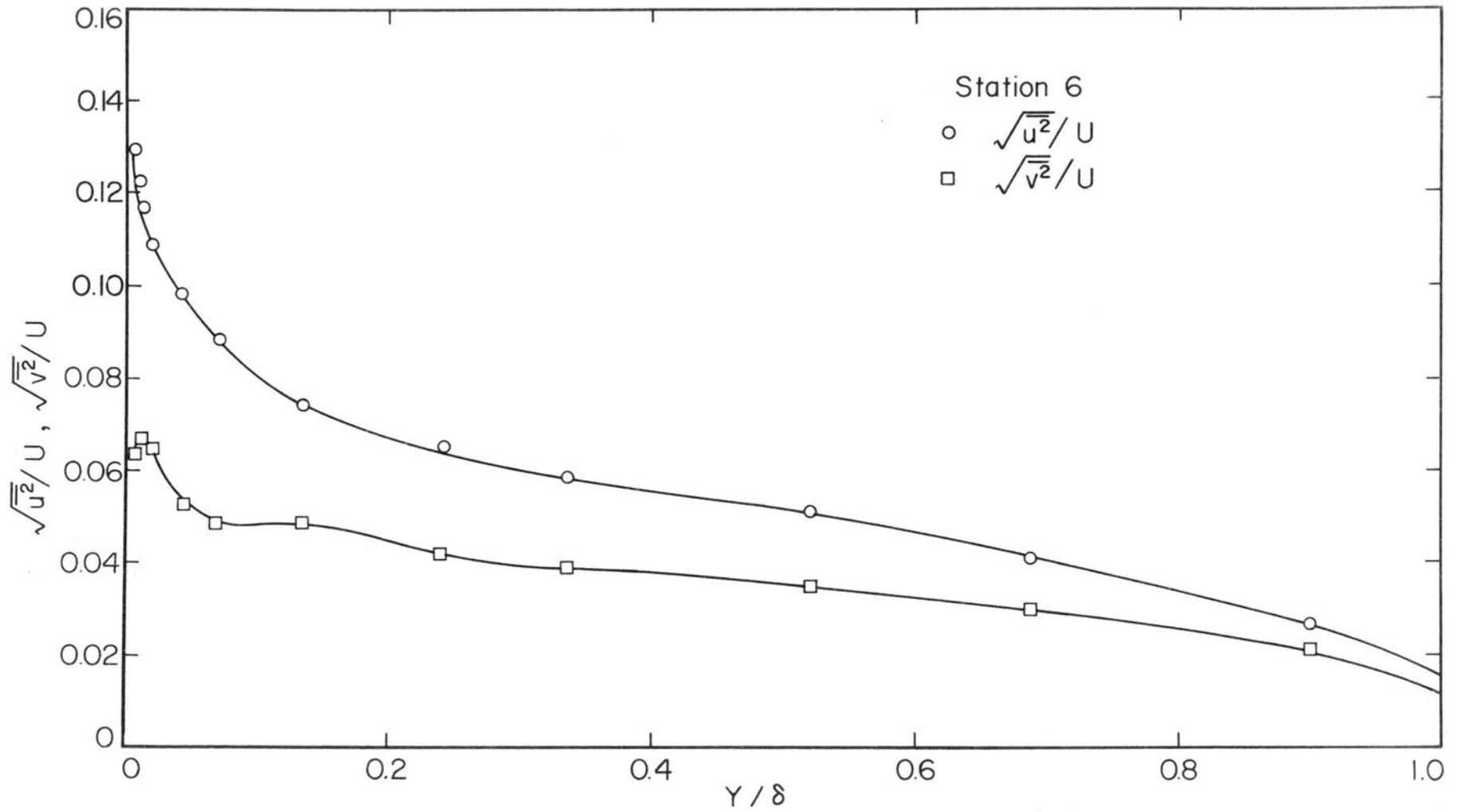


Fig. 57. Turbulence intensities, $U_\infty \approx 60$ ft/sec, $x = 60$ ft.

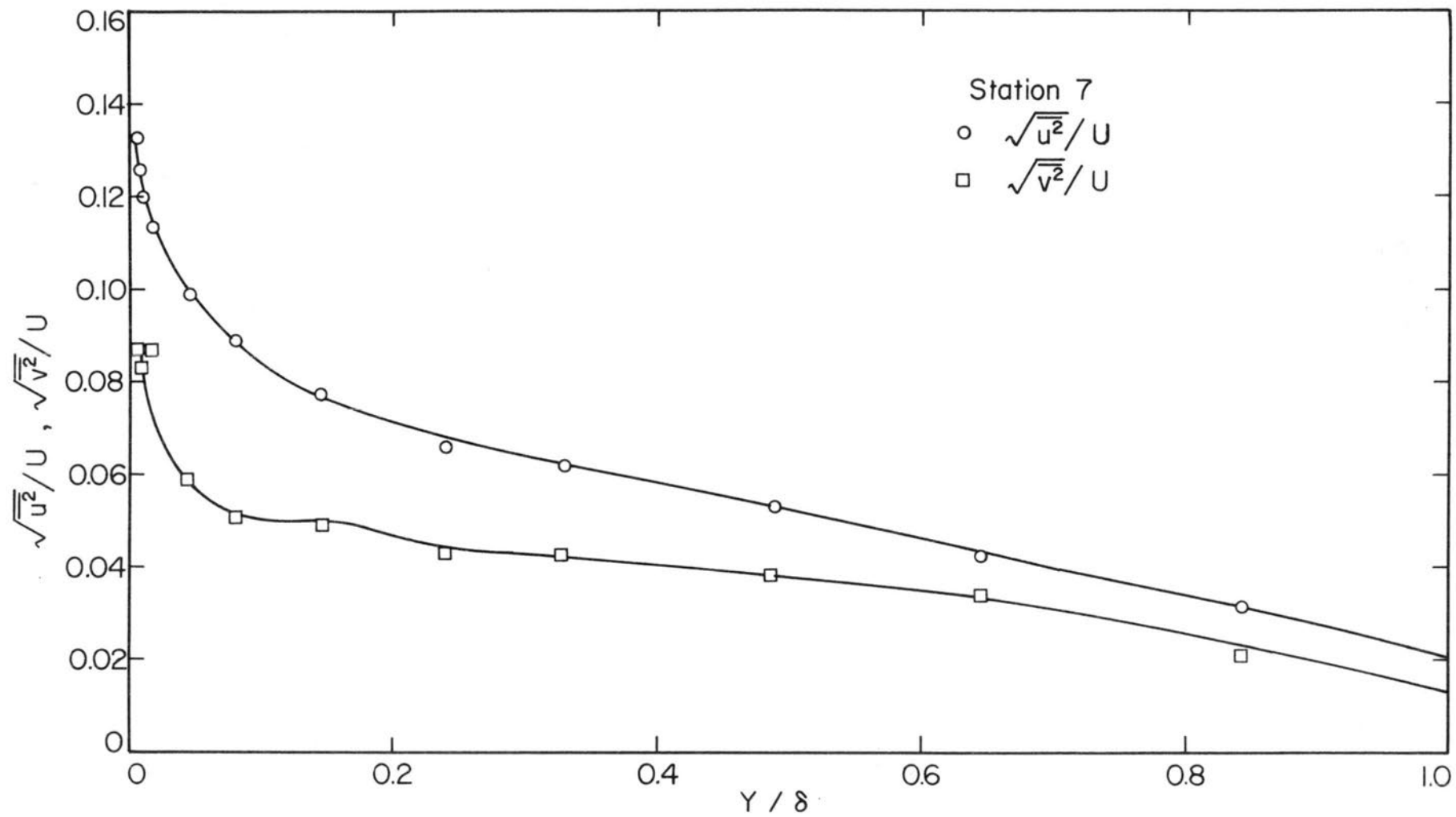


Fig. 58. Turbulence intensities, $U_\infty \approx 60$ ft/sec, $x = 70$ ft.

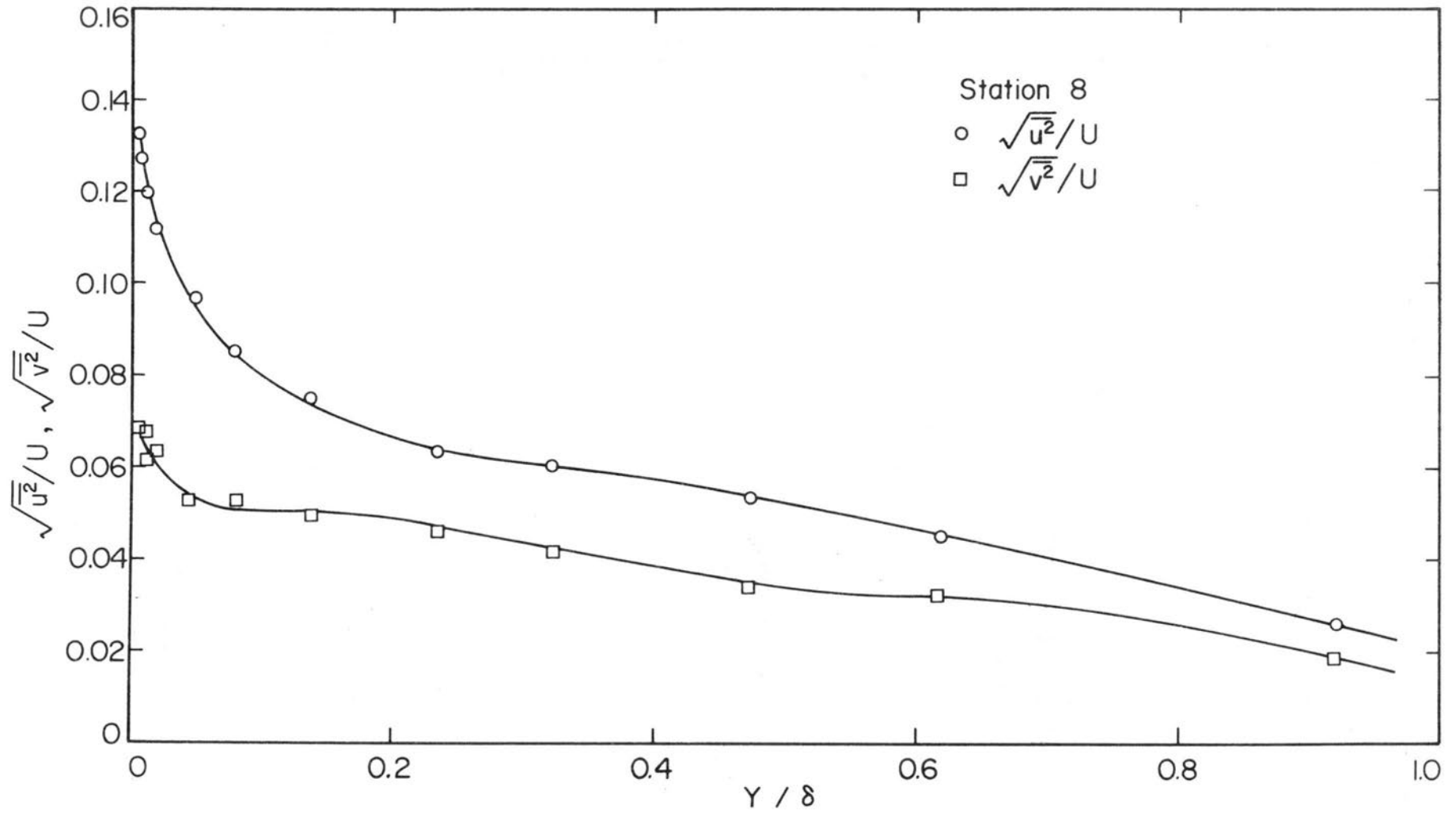


Fig. 59. Turbulence intensities, $U_\infty \approx 60$ ft/sec, $x = 80$ ft.

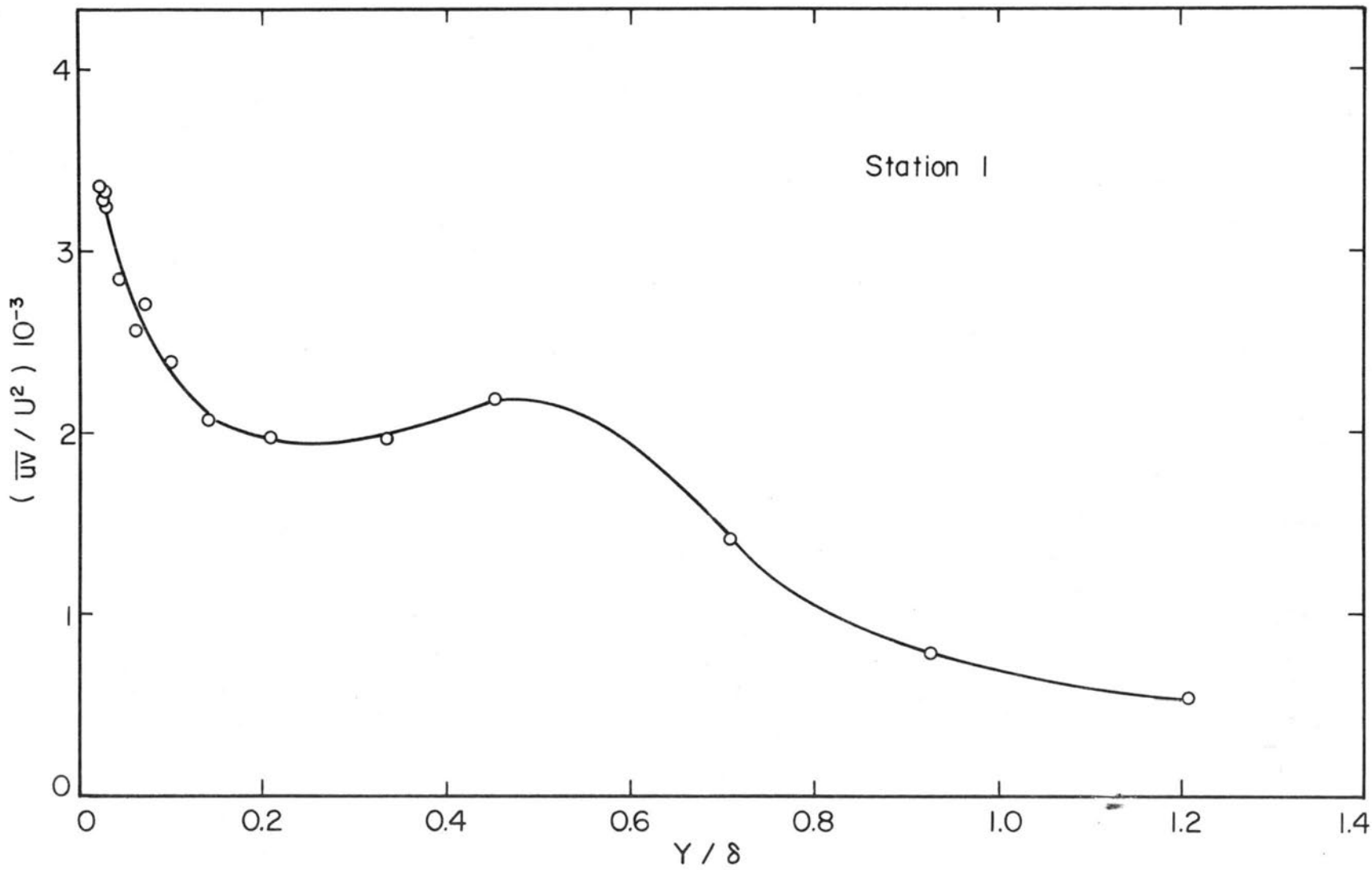


Fig. 60. \overline{uv}/U^2 distribution. $U_\infty \approx 60$ ft/sec, $x = 10$ ft.

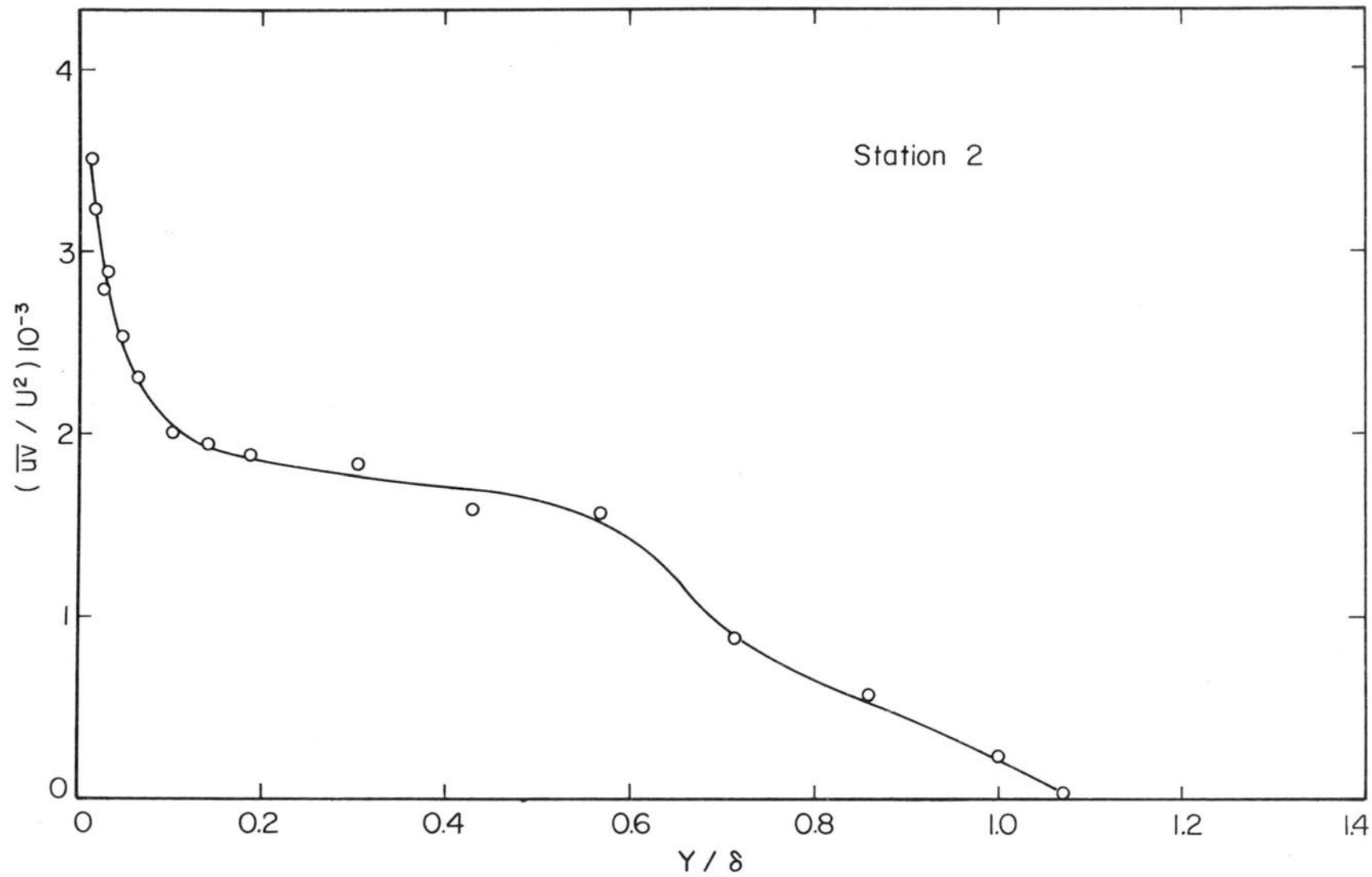


Fig. 61. \overline{uv}/U^2 distribution. $U_\infty \approx 60$ ft/sec, $x = 20$ ft.

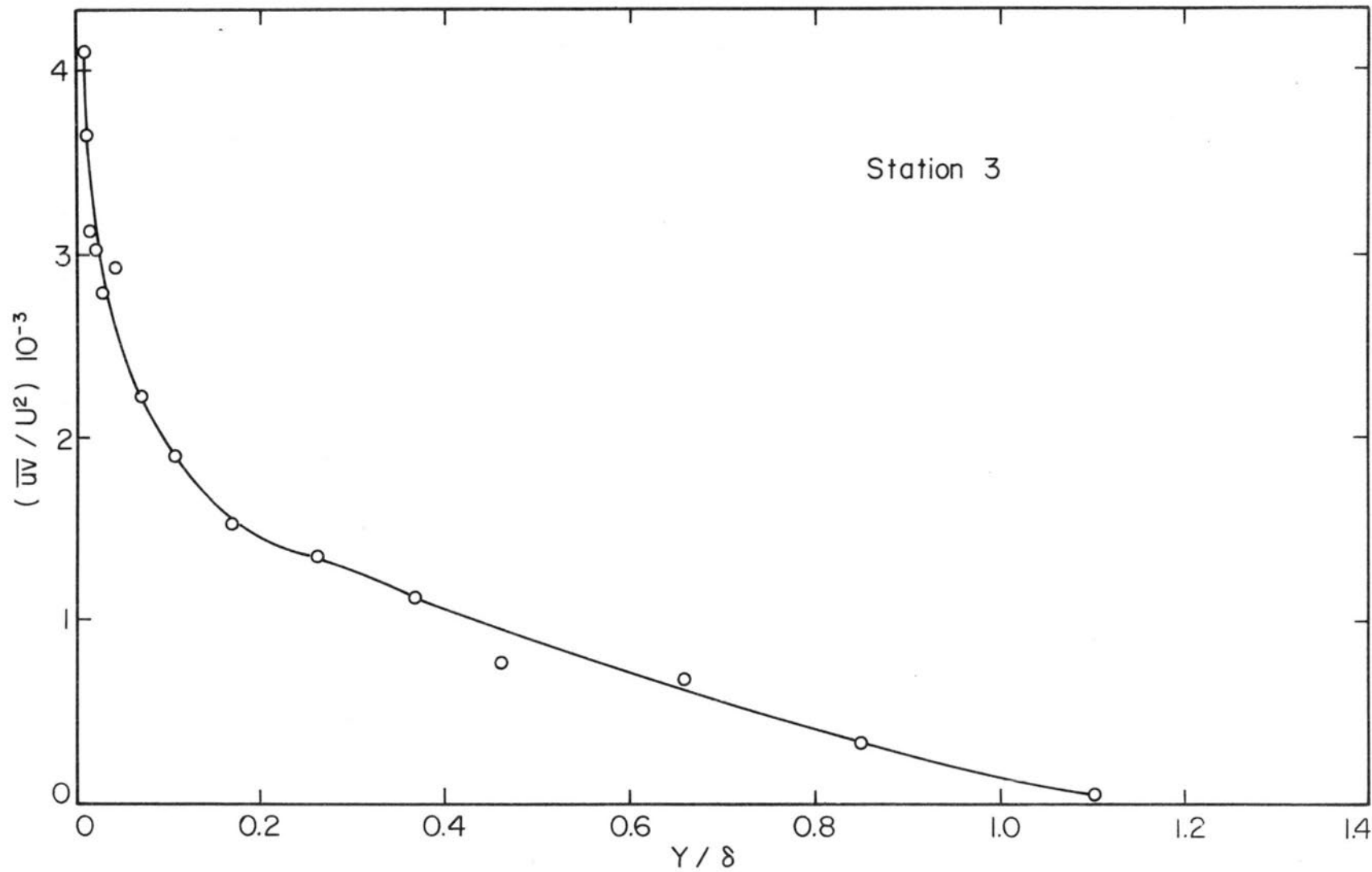


Fig. 62. \overline{uv}/U^2 distribution. $U_\infty \approx 60$ ft/sec, $x = 30$ ft.

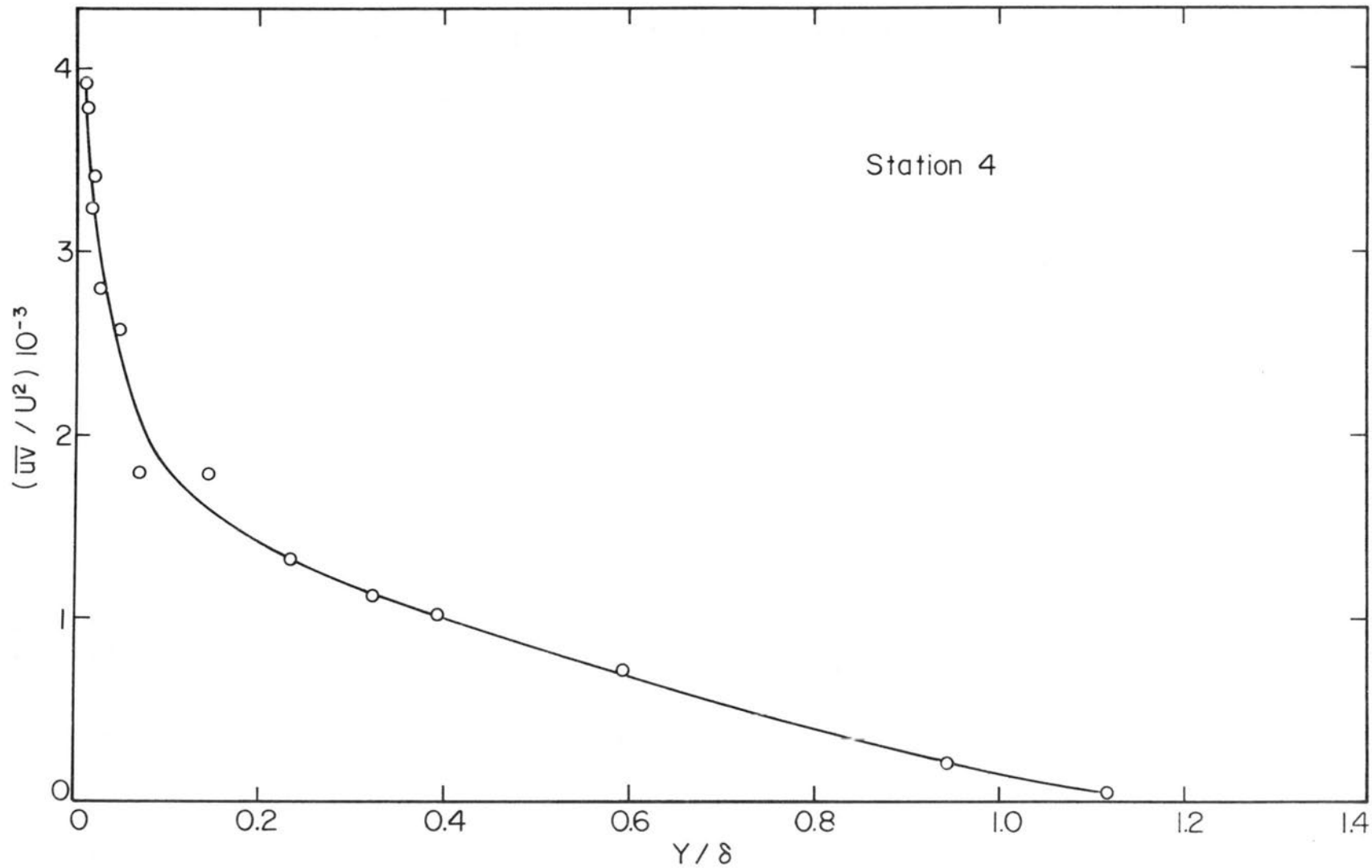


Fig. 63. \overline{uv}/U^2 distribution. $U_\infty \approx 60$ ft/sec, $x = 40$ ft.

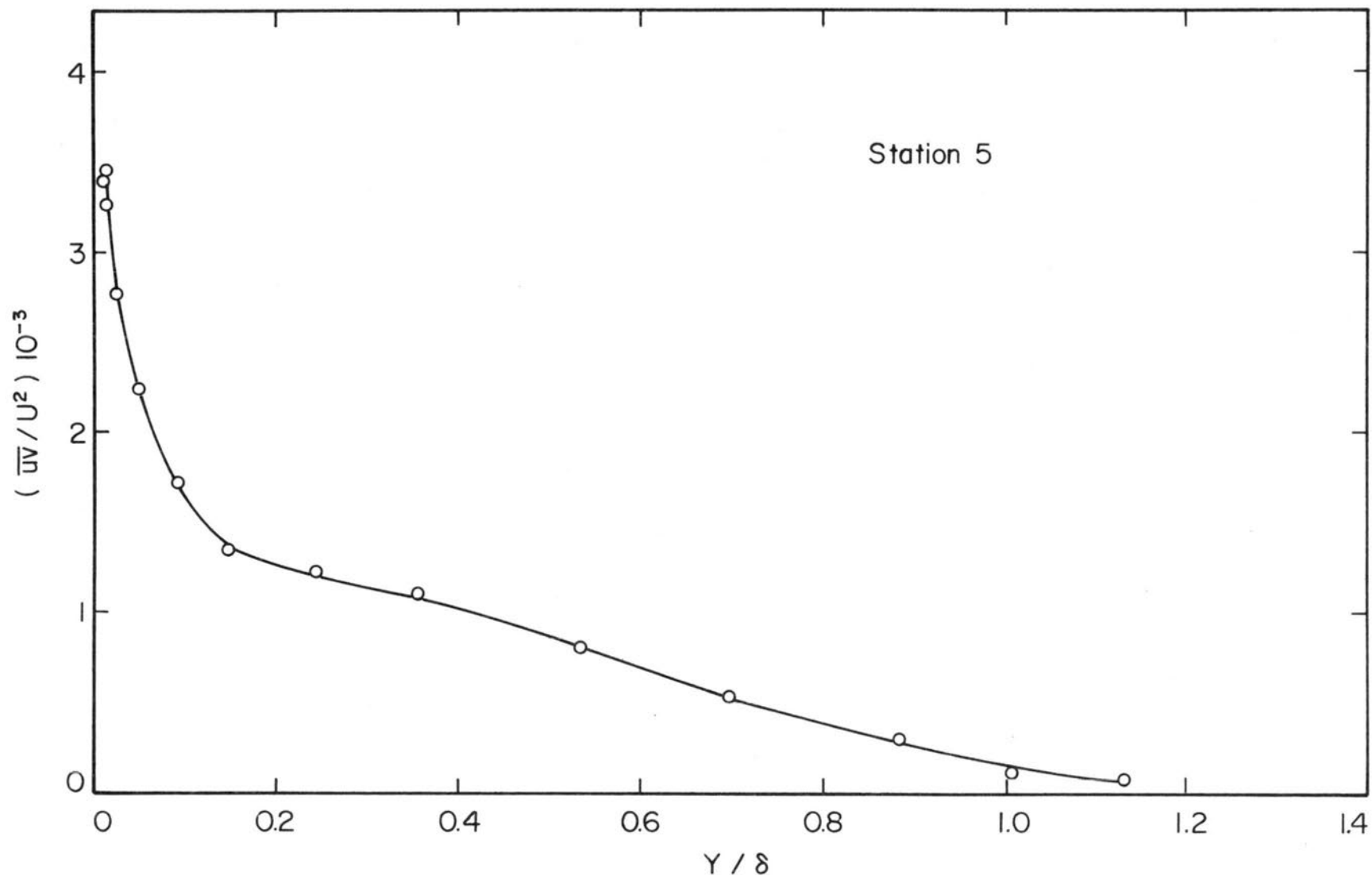


Fig. 64. \overline{uv}/U^2 distribution. $U_\infty \approx 60$ ft/sec, $x = 50$ ft.

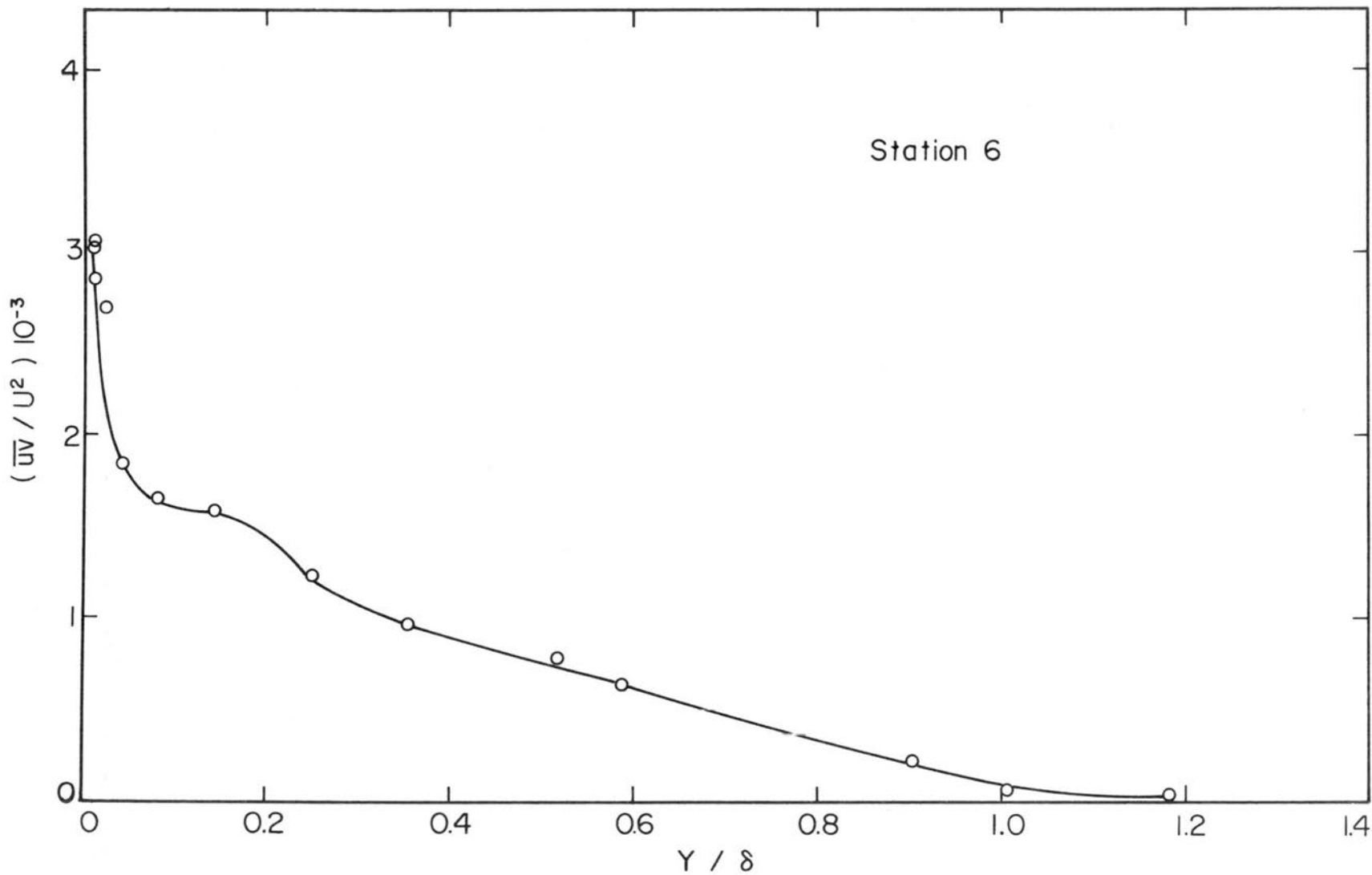


Fig. 65. \overline{uv}/U^2 distribution. $U_\infty \approx 60$ ft/sec, $x = 60$ ft.

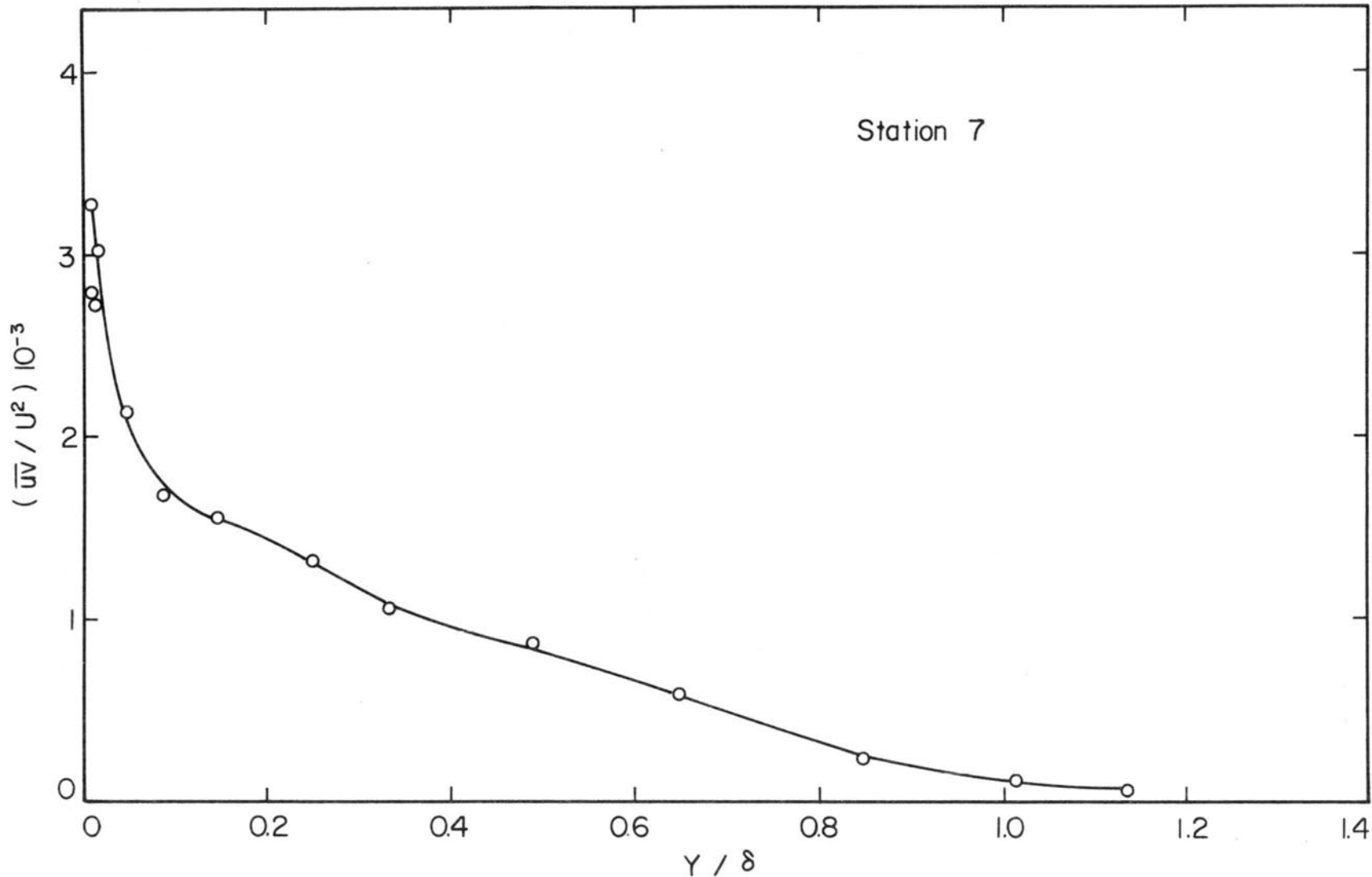


Fig. 66. \overline{uv}/U^2 distribution. $U_\infty \approx 60$ ft/sec, $x = 70$ ft.

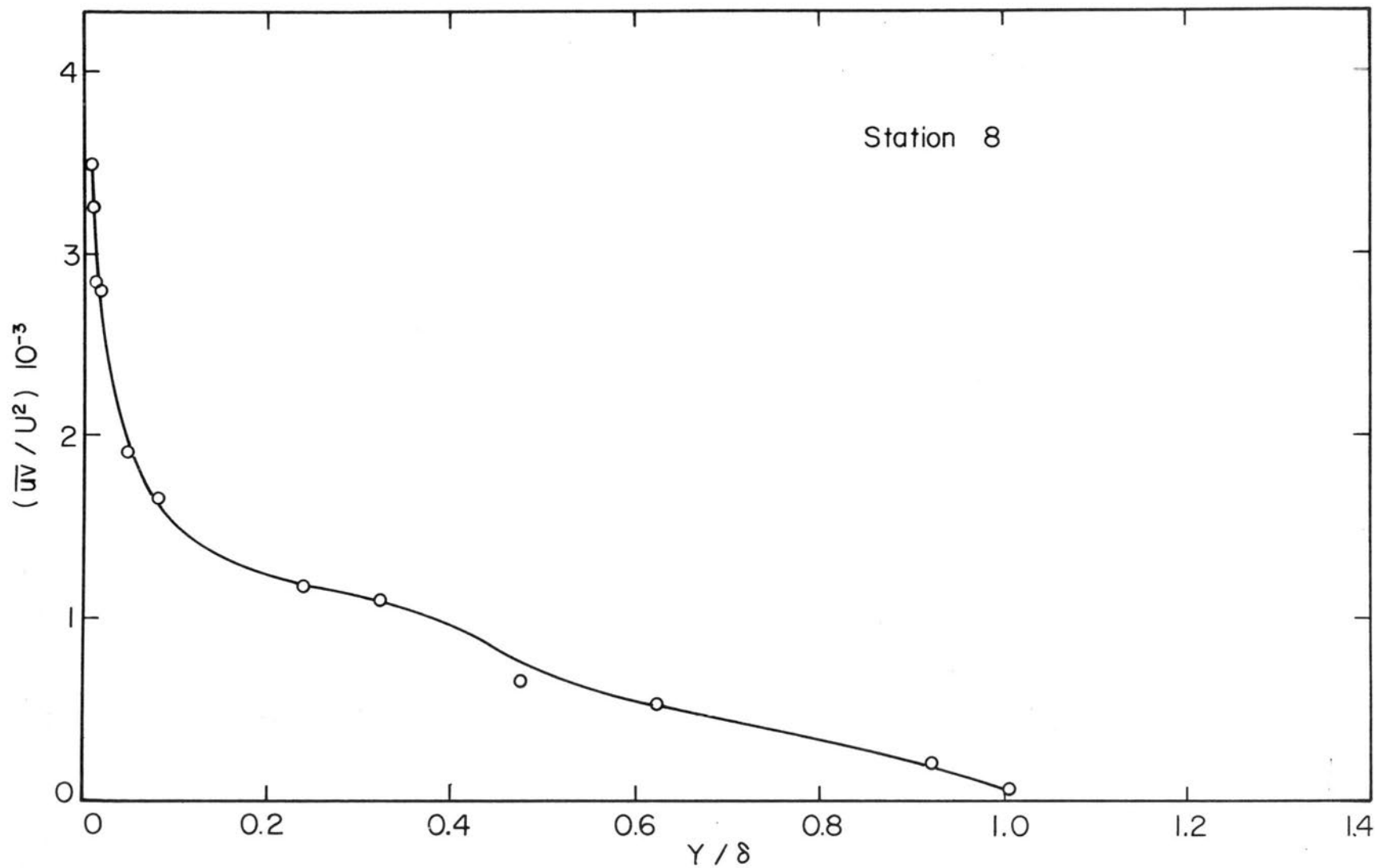


Fig. 67. \overline{uv}/U^2 distribution. $U_\infty \approx 60$ ft/sec, $x = 80$ ft.

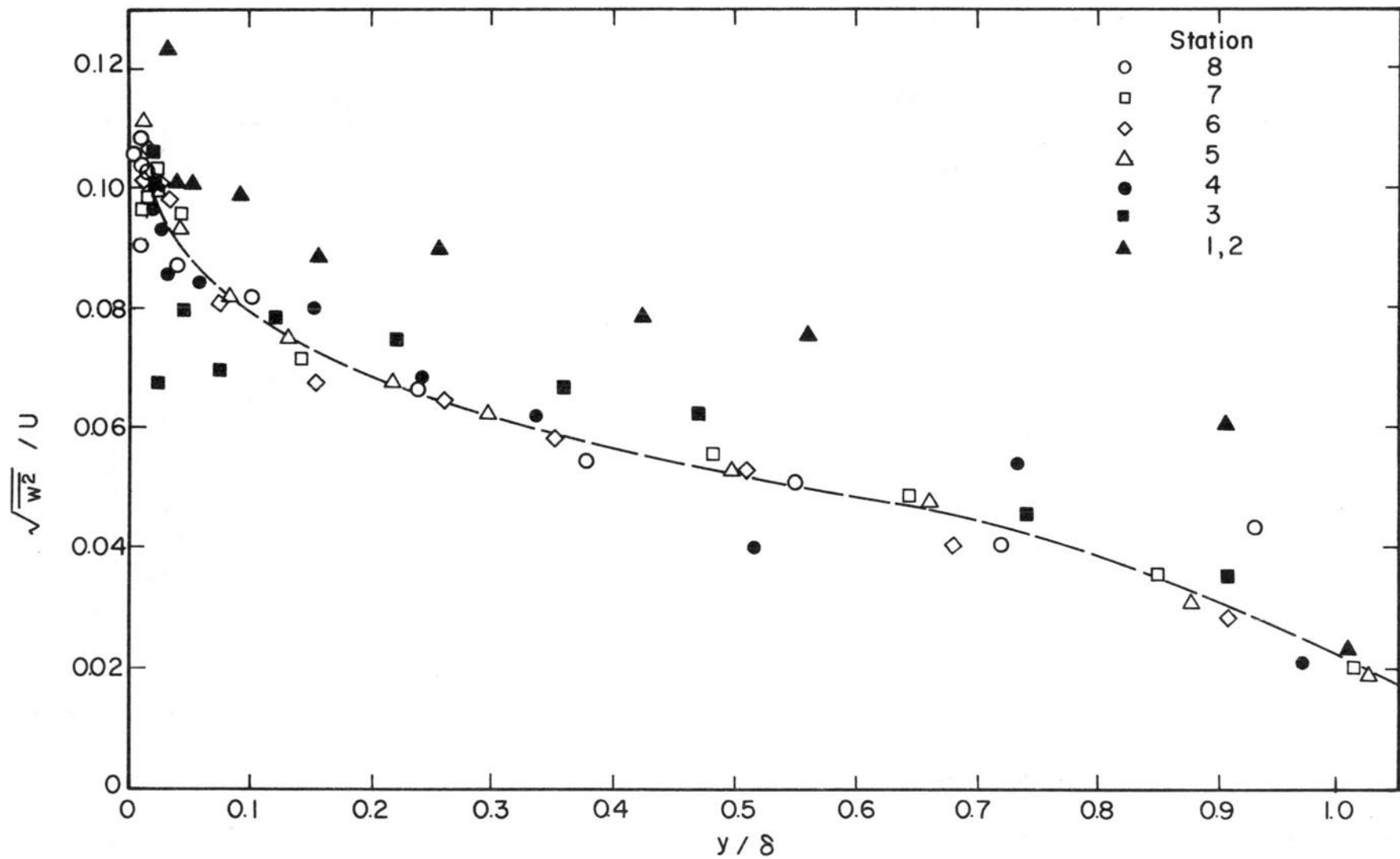


Fig. 68. Comparison of w-component of turbulence distributions along the boundary layer length.

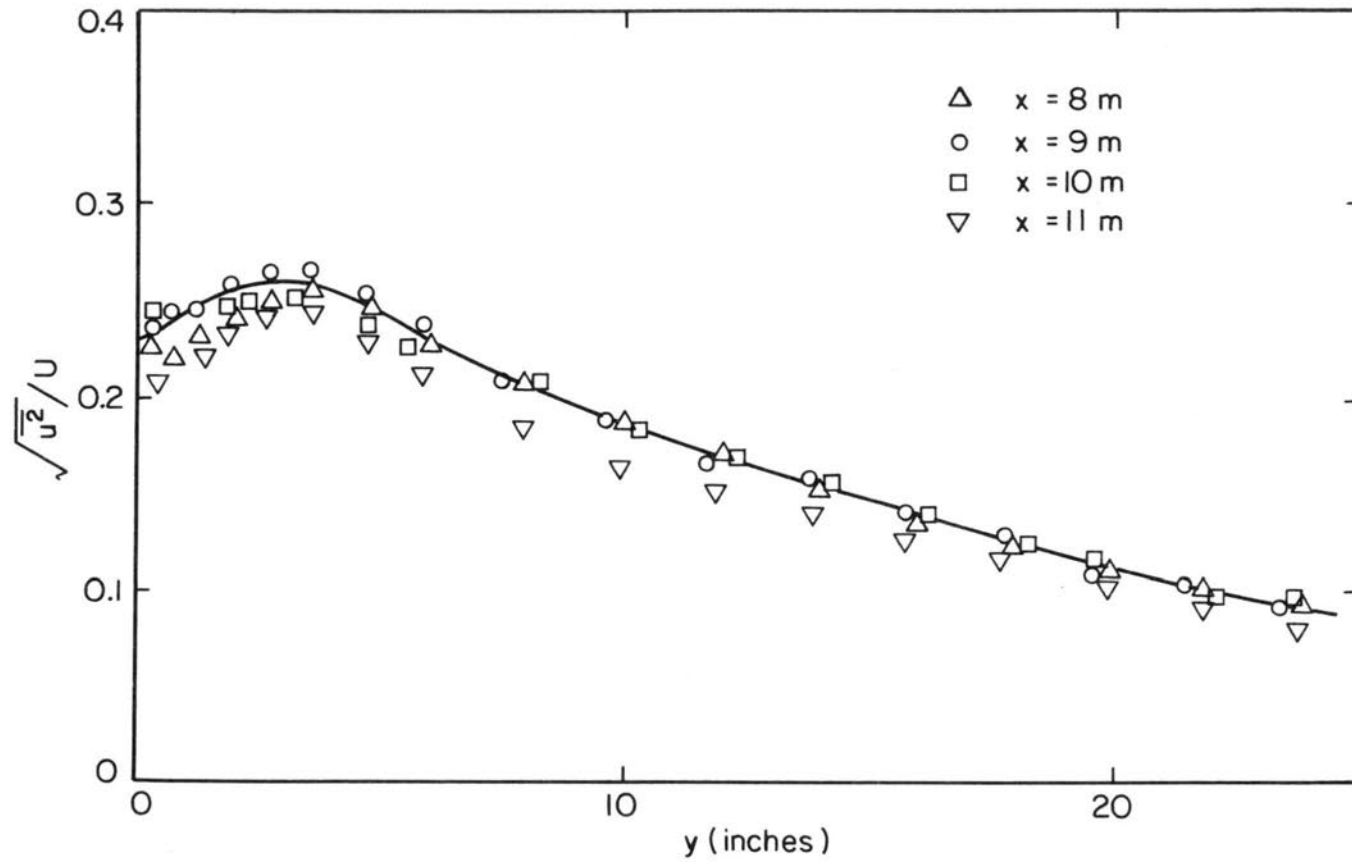


Fig. 69. Turbulence intensity distributions in the canopy flow field.

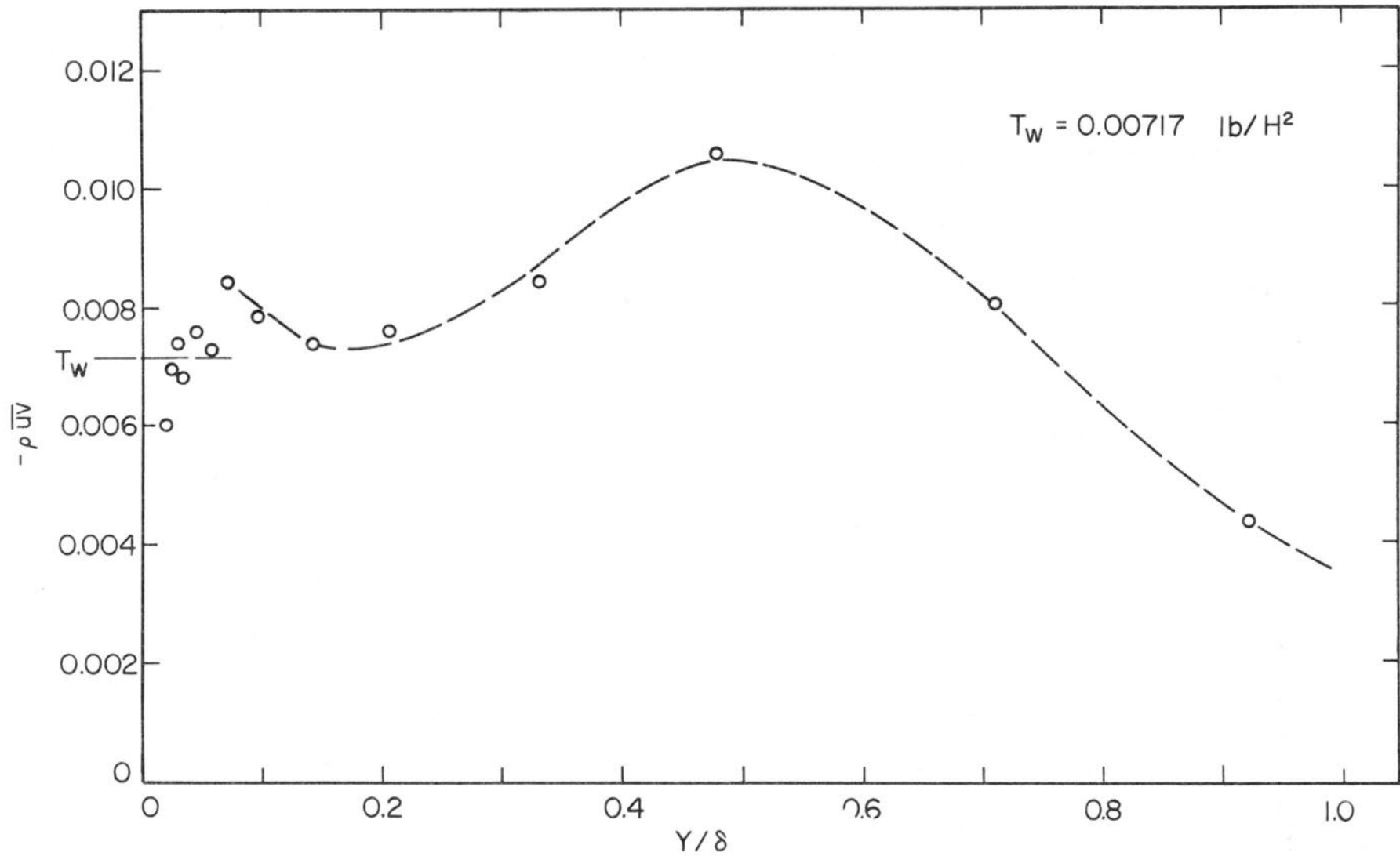


Fig. 70. Turbulent shear stress distribution. $U_\infty \approx 60 \text{ ft/sec}$, $x = 10 \text{ ft}$.

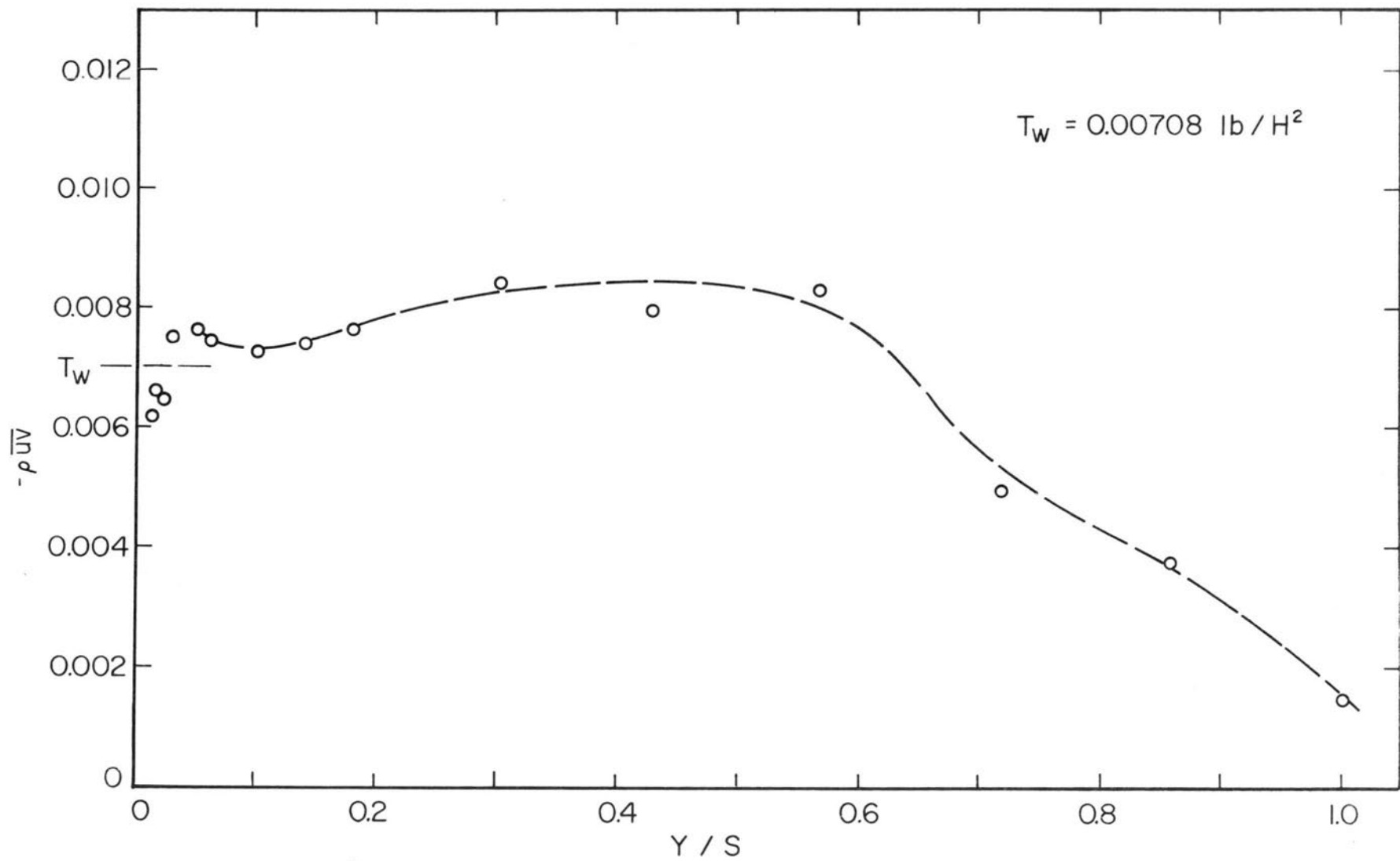


Fig. 71. Turbulent shear stress distribution. $U_\infty \approx 60 \text{ ft/sec}$, $x = 20 \text{ ft}$.

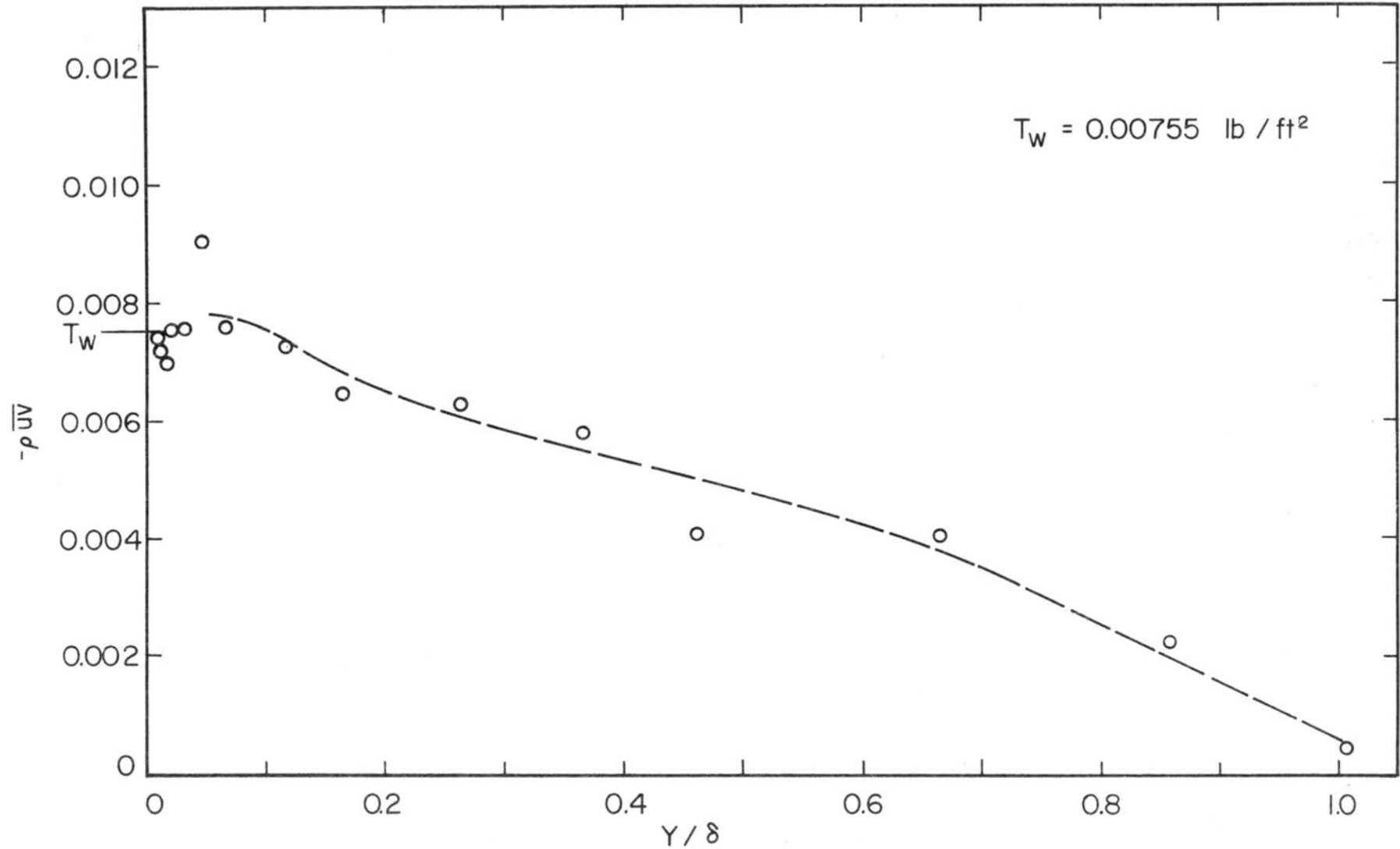


Fig. 72. Turbulent shear stress distribution. $U_\infty \approx 60 \text{ ft/sec}$, $x = 30 \text{ ft}$.

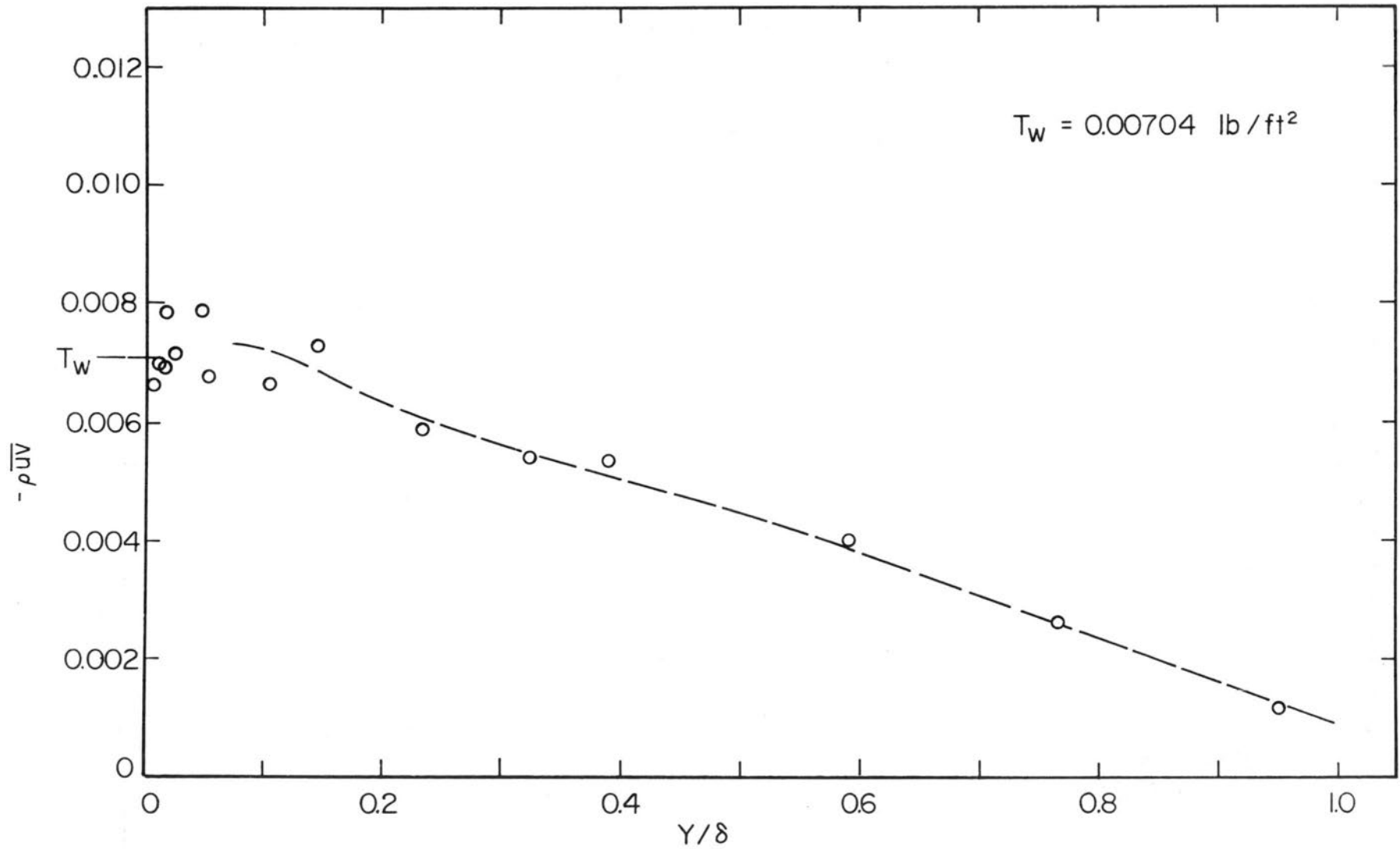


Fig. 73. Turbulent shear stress distribution. $U_\infty \approx 60 \text{ ft/sec}$, $x = 40 \text{ ft}$.

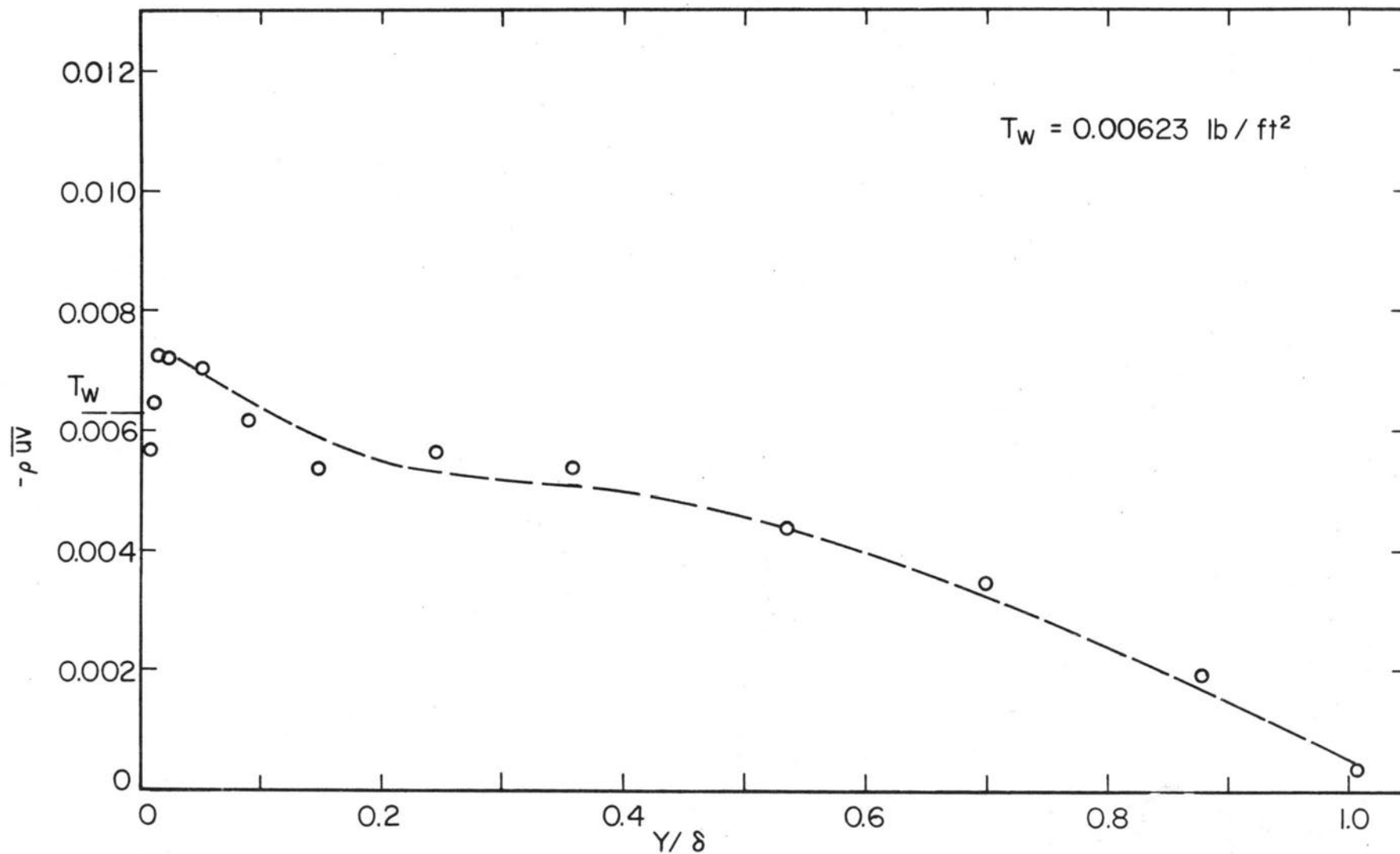


Fig. 74. Turbulent shear stress distribution. $U_\infty \approx 60 \text{ ft/sec}$, $x = 50 \text{ ft}$.

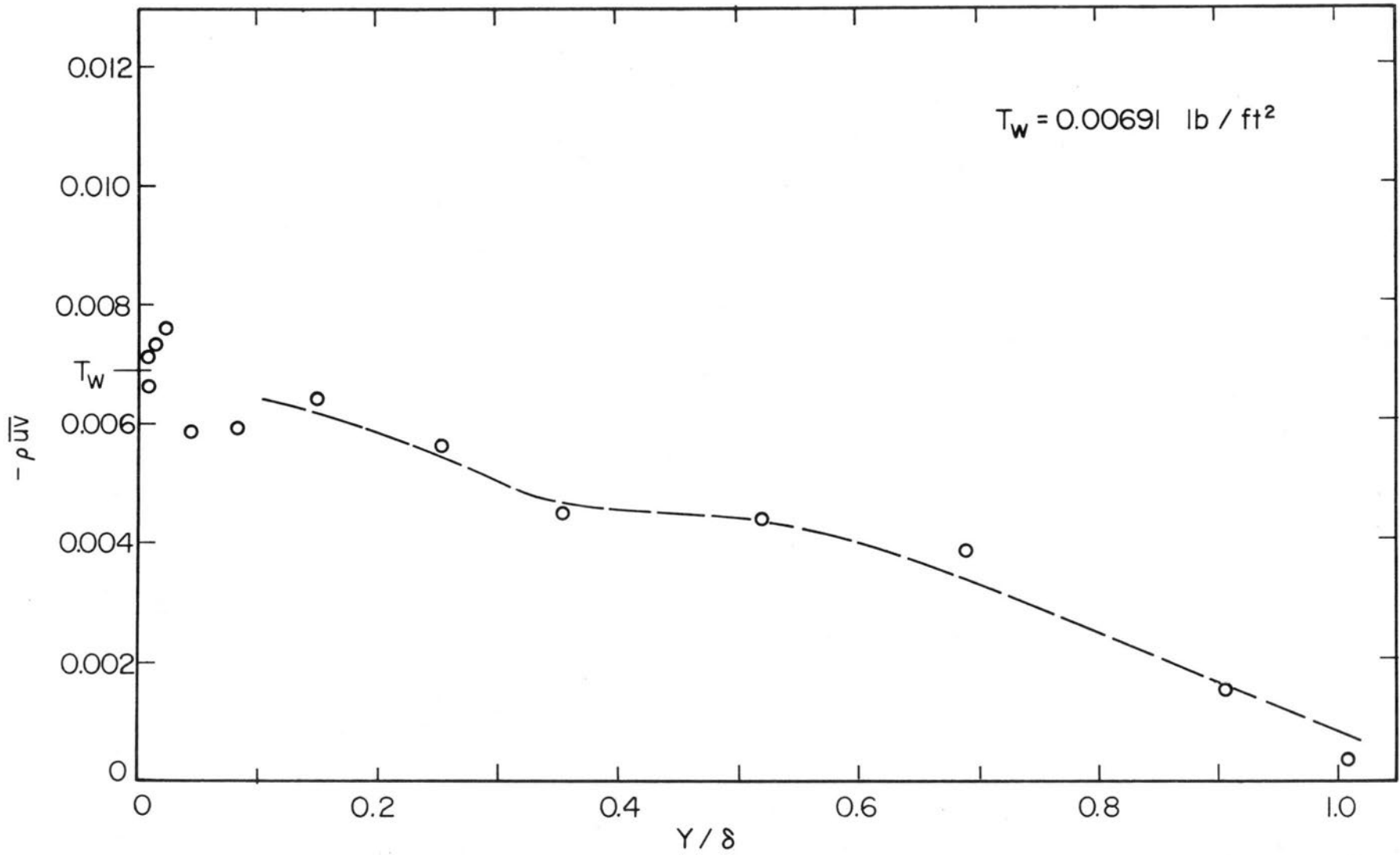


Fig. 75. Turbulent shear stress distribution. $U_\infty \approx 60 \text{ ft/sec}$, $x = 60 \text{ ft}$.

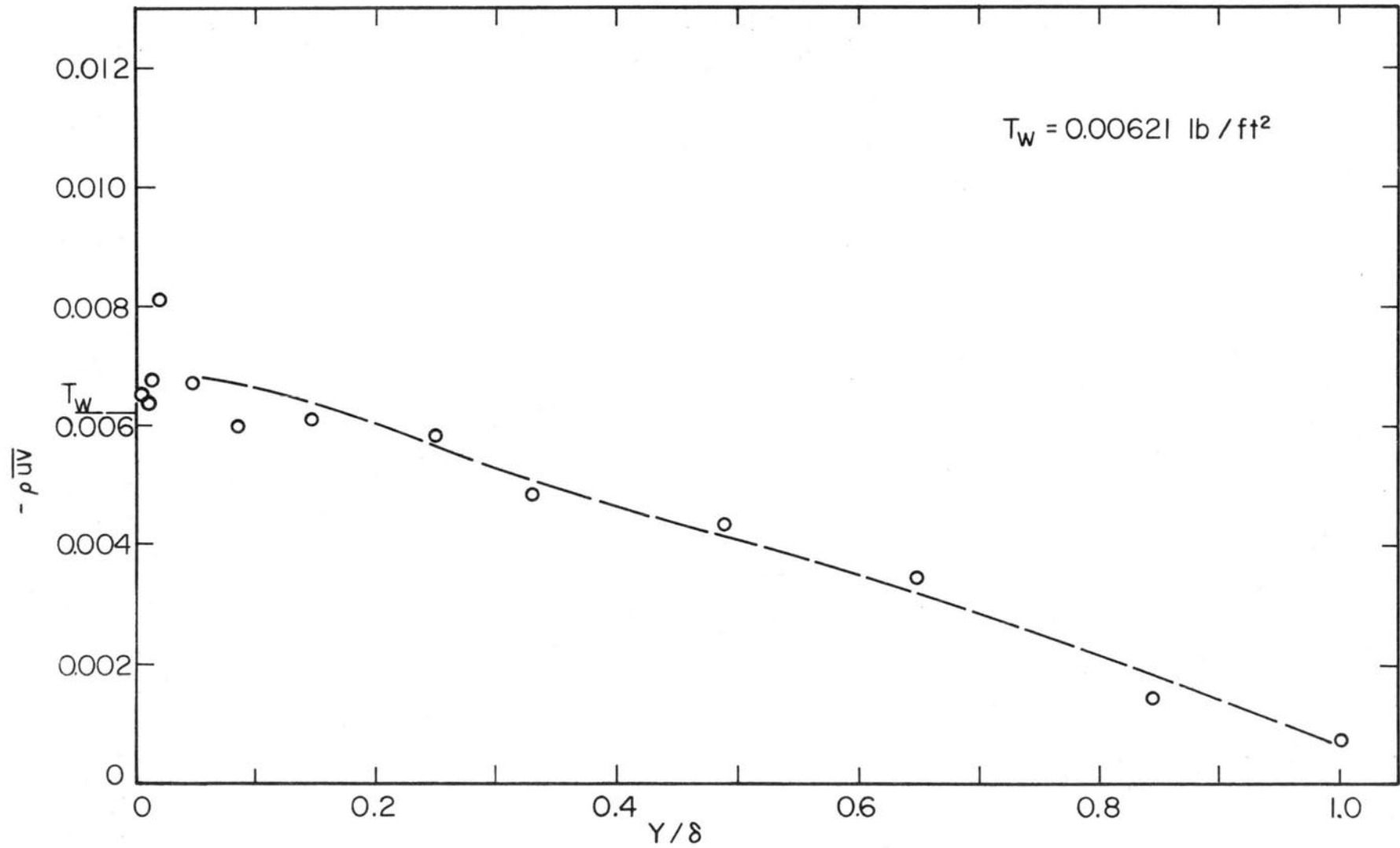


Fig. 76. Turbulent shear stress distribution. $U_\infty \approx 60 \text{ ft/sec}$, $x = 70 \text{ ft}$.

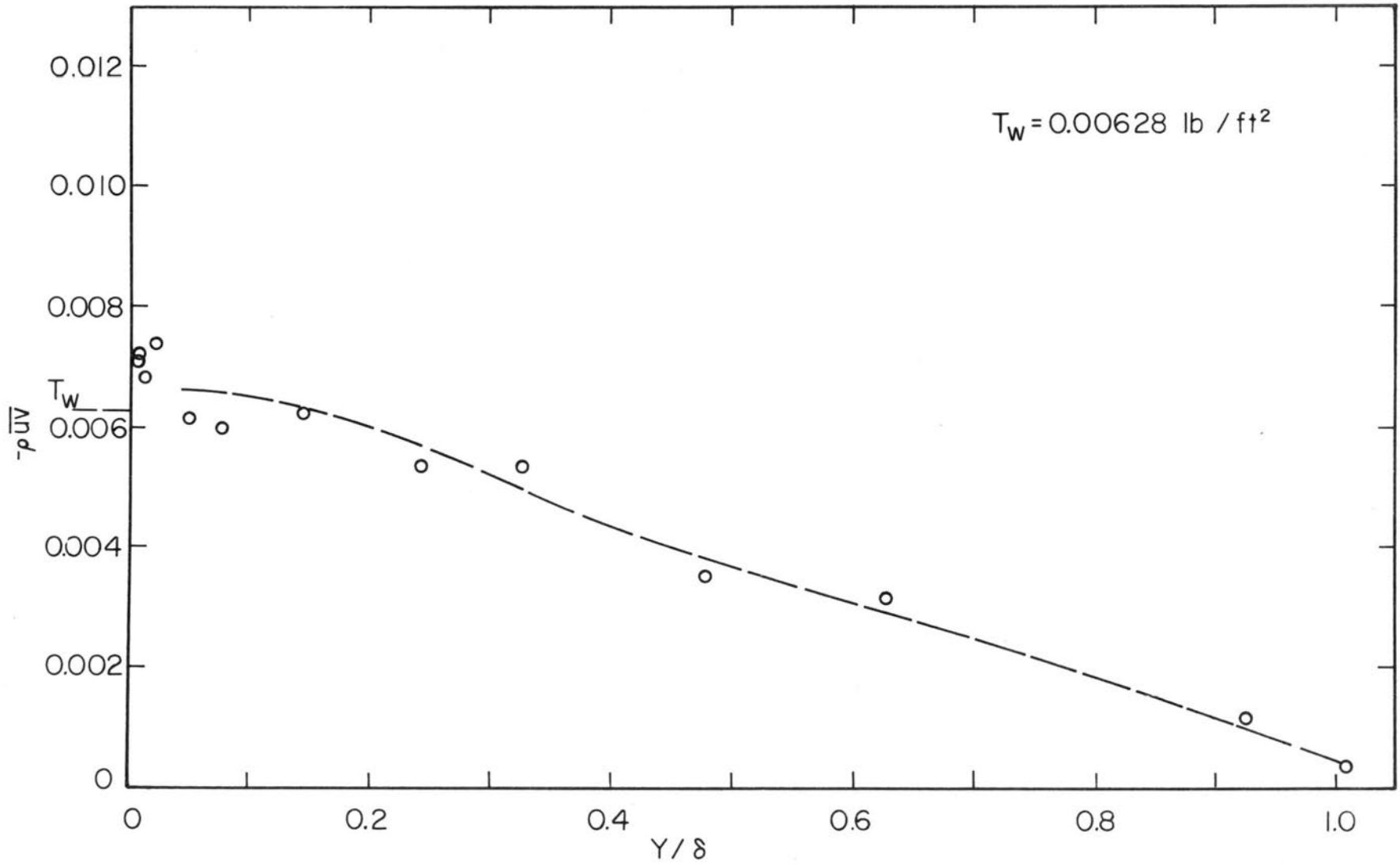


Fig. 77. Turbulent shear stress distribution. $U_\infty \approx 60 \text{ ft/sec}$, $x = 80 \text{ ft}$.

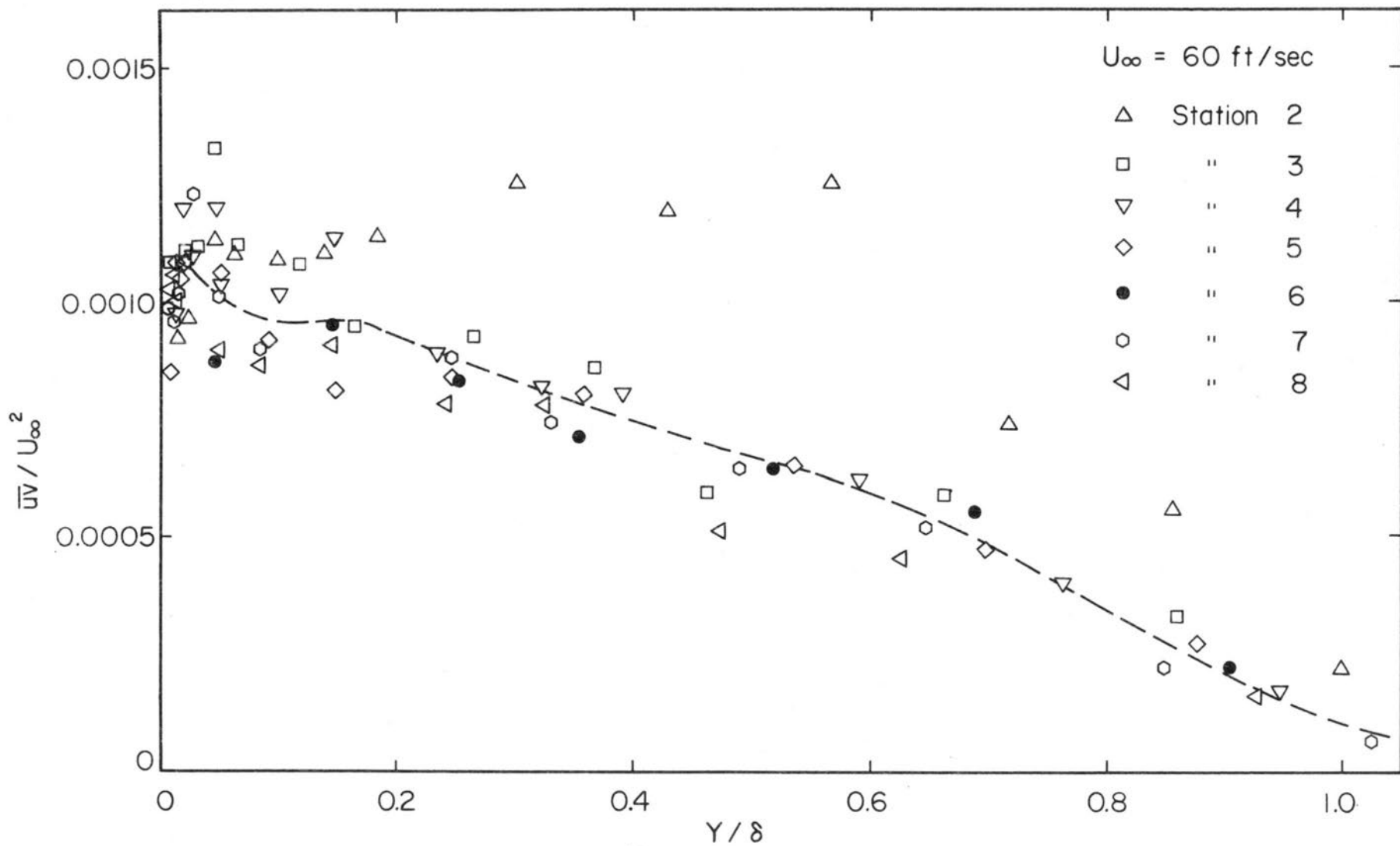


Fig. 78. Behavior of \overline{uv}/U_∞^2 along the boundary layer length.

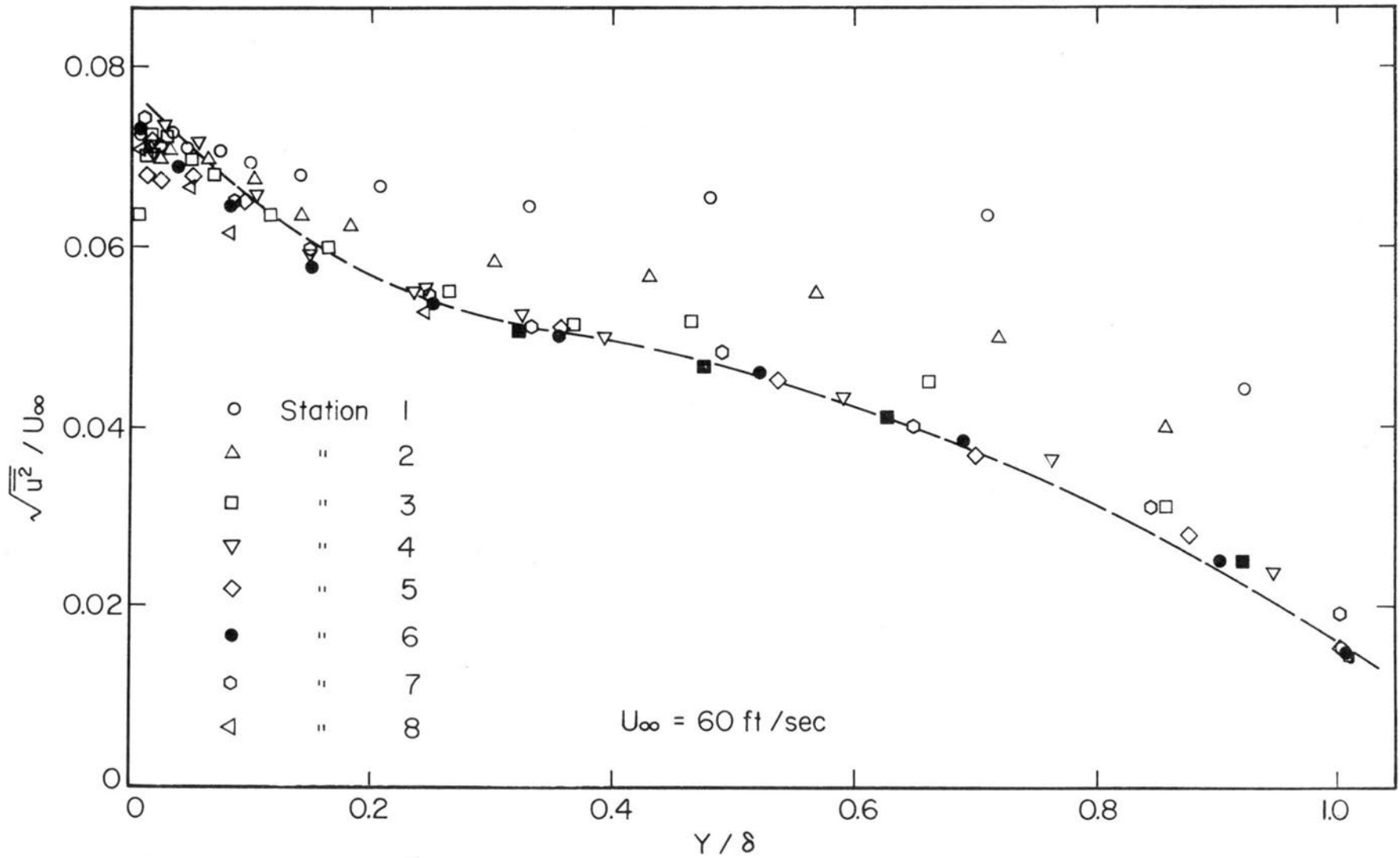


Fig. 79. Behavior of $\sqrt{\overline{u^2}} / U_\infty$ along the boundary layer length.

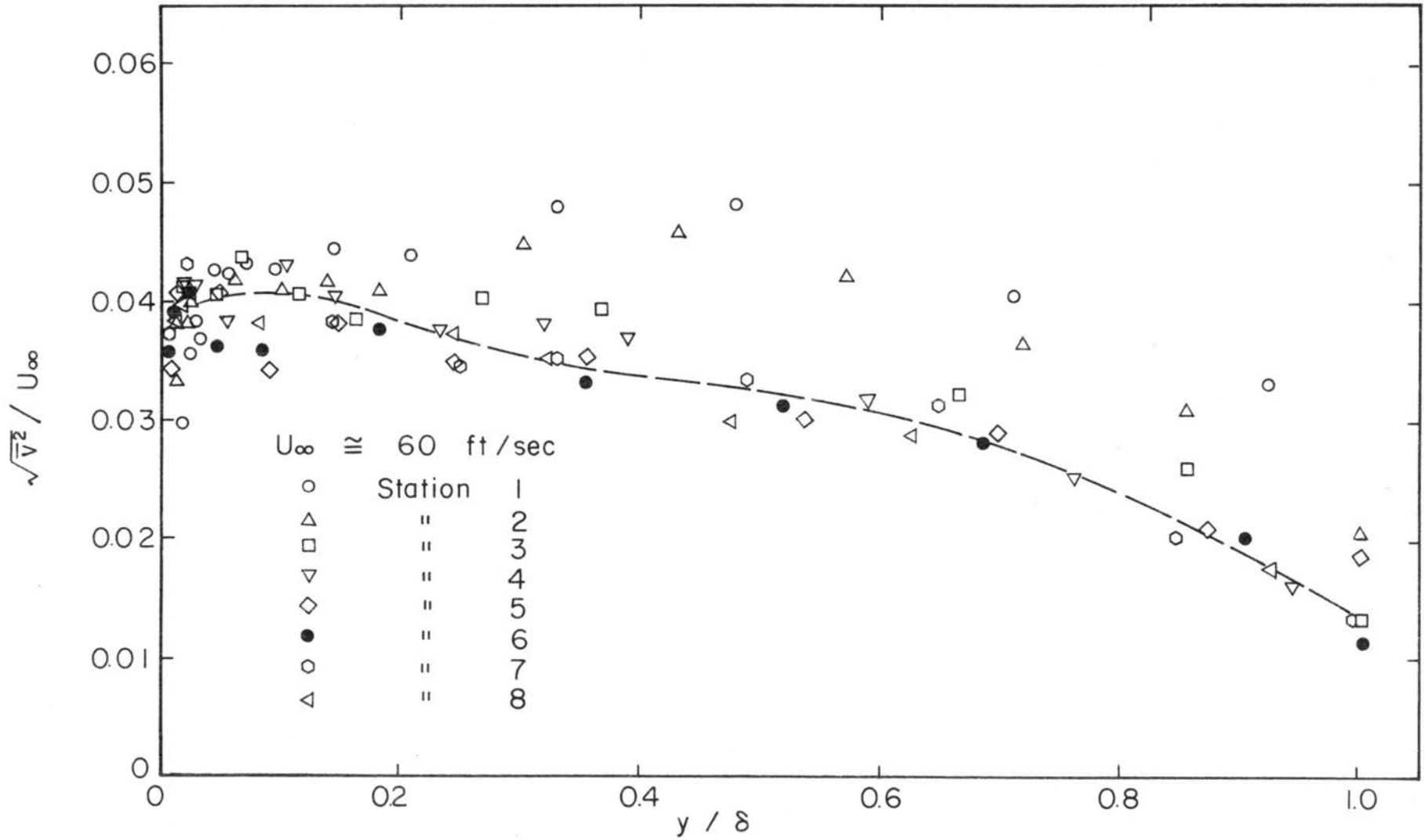


Fig. 80. Behavior of $\sqrt{v^2}/U_\infty$ along the boundary layer length.

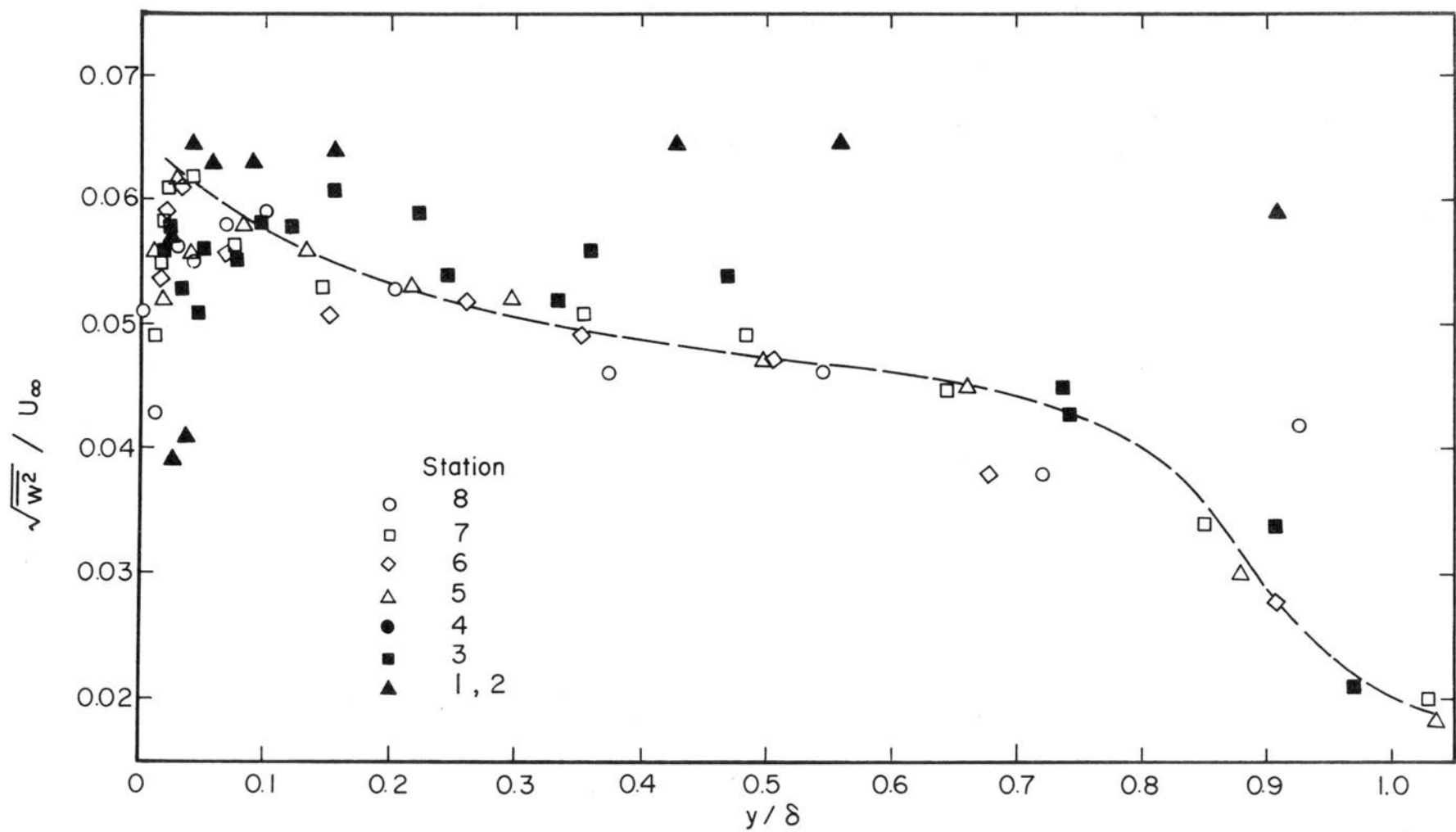


Fig. 81. Behavior of $\sqrt{w^2}/U_\infty$ along the boundary layer length.

DOCUMENT CONTROL DATA - R&D

(Security classification of title, body of abstract and indexing annotation must be entered when the overall report is classified)

1. ORIGINATING ACTIVITY (Corporate author) Fluid Mechanics Program, College of Engineering Colorado State University Fort Collins, Colorado		2a. REPORT SECURITY CLASSIFICATION Unclassified	
		2b. GROUP	
3. REPORT TITLE APPROACH OF TURBULENT BOUNDARY LAYER TO SIMILARITY			
4. DESCRIPTIVE NOTES (Type of report and inclusive dates) Technical Report			
5. AUTHOR(S) (Last name, first name, initial) Zoric, Dusan L.			
6. REPORT DATE September, 1968	7a. TOTAL NO. OF PAGES 203	7b. NO. OF REFS 53	
8a. CONTRACT OR GRANT NO. DA-AMC-28-043-65-G20	9a. ORIGINATOR'S REPORT NUMBER(S) CER68-69DLZ9		
b. PROJECT NO. 2246	9b. OTHER REPORT NO(S) (Any other numbers that may be assigned this report)		
c.			
d.			
10. AVAILABILITY/LIMITATION NOTICES Distribution of this document is unlimited.			
11. SUPPLEMENTARY NOTES		12. SPONSORING MILITARY ACTIVITY U.S. Army Materiel Command	
13. ABSTRACT A large scale turbulent boundary layer with no pressure gradient, developed on a flat plate 95 feet long has been investigated. Theoretical considerations of the existence of local similarity yield the requirements which should be found in the turbulent boundary layers in order that similarity exists. Measurements of the mean motion, the turbulent velocity components and the turbulent shear stress have been made for the free stream velocity range 60 to 100 ft/sec. Reynolds numbers based on the boundary layer thickness were of the order of 10^6 . Turbulence quantities were evaluated from a single rotating hot-wire probe along the entire length of the boundary layer. For all quantities measured, the uncertainty intervals were calculated in order to provide a measure of the reliability of the results. The large scale turbulent boundary layers are shown to approach closely the theoretical requirements for similarity. Displacement and momentum thickness grow as a linear function of x-coordinate, the form factor is constant. The constant wall shear stress requirement is very closely approached. An asymptotic similarity form is considered and reported. For similarity function of the turbulent shear stress distribution across the boundary layer thickness, an approximate linear function is proposed. The best average universal velocity profile is tabulated.			

14. KEY WORDS	LINK A		LINK B		LINK C	
	ROLE	WT	ROLE	WT	ROLE	WT
Turbulent boundary layer similarity Wind tunnel experimentation Turbulence measurements Turbulent shear stress distribution Mean velocity profiles Hot wire anemometry Uncertainty intervals						

INSTRUCTIONS

1. **ORIGINATING ACTIVITY:** Enter the name and address of the contractor, subcontractor, grantee, Department of Defense activity or other organization (*corporate author*) issuing the report.

2a. **REPORT SECURITY CLASSIFICATION:** Enter the overall security classification of the report. Indicate whether "Restricted Data" is included. Marking is to be in accordance with appropriate security regulations.

2b. **GROUP:** Automatic downgrading is specified in DoD Directive 5200.10 and Armed Forces Industrial Manual. Enter the group number. Also, when applicable, show that optional markings have been used for Group 3 and Group 4 as authorized.

3. **REPORT TITLE:** Enter the complete report title in all capital letters. Titles in all cases should be unclassified. If a meaningful title cannot be selected without classification, show title classification in all capitals in parenthesis immediately following the title.

4. **DESCRIPTIVE NOTES:** If appropriate, enter the type of report, e.g., interim, progress, summary, annual, or final. Give the inclusive dates when a specific reporting period is covered.

5. **AUTHOR(S):** Enter the name(s) of author(s) as shown on or in the report. Enter last name, first name, middle initial. If military, show rank and branch of service. The name of the principal author is an absolute minimum requirement.

6. **REPORT DATE:** Enter the date of the report as day, month, year; or month, year. If more than one date appears on the report, use date of publication.

7a. **TOTAL NUMBER OF PAGES:** The total page count should follow normal pagination procedures, i.e., enter the number of pages containing information.

7b. **NUMBER OF REFERENCES:** Enter the total number of references cited in the report.

8a. **CONTRACT OR GRANT NUMBER:** If appropriate, enter the applicable number of the contract or grant under which the report was written.

8b, 8c, & 8d. **PROJECT NUMBER:** Enter the appropriate military department identification, such as project number, subproject number, system numbers, task number, etc.

9a. **ORIGINATOR'S REPORT NUMBER(S):** Enter the official report number by which the document will be identified and controlled by the originating activity. This number must be unique to this report.

9b. **OTHER REPORT NUMBER(S):** If the report has been assigned any other report numbers (*either by the originator or by the sponsor*), also enter this number(s).

10. **AVAILABILITY/LIMITATION NOTICES:** Enter any limitations on further dissemination of the report, other than those imposed by security classification, using standard statements such as:

- (1) "Qualified requesters may obtain copies of this report from DDC."
- (2) "Foreign announcement and dissemination of this report by DDC is not authorized."
- (3) "U. S. Government agencies may obtain copies of this report directly from DDC. Other qualified DDC users shall request through _____."
- (4) "U. S. military agencies may obtain copies of this report directly from DDC. Other qualified users shall request through _____."
- (5) "All distribution of this report is controlled. Qualified DDC users shall request through _____."

If the report has been furnished to the Office of Technical Services, Department of Commerce, for sale to the public, indicate this fact and enter the price, if known.

11. **SUPPLEMENTARY NOTES:** Use for additional explanatory notes.

12. **SPONSORING MILITARY ACTIVITY:** Enter the name of the departmental project office or laboratory sponsoring (*paying for*) the research and development. Include address.

13. **ABSTRACT:** Enter an abstract giving a brief and factual summary of the document indicative of the report, even though it may also appear elsewhere in the body of the technical report. If additional space is required, a continuation sheet shall be attached.

It is highly desirable that the abstract of classified reports be unclassified. Each paragraph of the abstract shall end with an indication of the military security classification of the information in the paragraph, represented as (TS), (S), (C), or (U).

There is no limitation on the length of the abstract. However, the suggested length is from 150 to 225 words.

14. **KEY WORDS:** Key words are technically meaningful terms or short phrases that characterize a report and may be used as index entries for cataloging the report. Key words must be selected so that no security classification is required. Identifiers, such as equipment model designation, trade name, military project code name, geographic location, may be used as key words but will be followed by an indication of technical context. The assignment of links, rules, and weights is optional.

MINIMUM BASIC DISTRIBUTION LIST FOR USAMC SCIENTIFIC AND
TECHNICAL REPORTS IN METEOROLOGY AND ATMOSPHERIC SCIENCES

Commanding General U. S. Army Materiel Command Attn: AMCRD-RV-A Washington, D. C. 20315	(1)	Chief of Research and Development Department of the Army Attn: CRD/M Washington, D. C. 20310	(1)	Commanding General U. S. Army Combat Development Command Attn: CDCMR-E Fort Belvoir, Virginia 22060	(1)
Commanding General U. S. Army Electronics Command Attn: AMSEL-EW Fort Monmouth, New Jersey 07703	(1)	Commanding General U. S. Army Missile Command Attn: AMSMI-RRR Redstone Arsenal, Alabama 35809	(1)	Commanding General U. S. Army Munitions Command Attn: AMSMU-RE-R Dover, New Jersey 07801	(1)
Commanding General U. S. Army Test and Evaluation Command Attn: NBC Directorate Aberdeen Proving Ground, Maryland 21005	(1)	Commanding General U. S. Army Natick Laboratories Attn: Earth Sciences Division Natick, Massachusetts 01762	(1)	Commanding Officer U. S. Army Ballistics Research Laboratories Attn: AMXBR-B Aberdeen Proving Ground, Maryland 21005	(1)
Commanding Officer U. S. Army Ballistics Research Laboratories Attn: AMXBR-IA Aberdeen Proving Ground, Maryland 21005	(1)	Director, U. S. Army Engineer Waterways Experiment Station Attn: WES-FV Vicksburg, Mississippi 39181	(1)	Director Atmospheric Sciences Laboratory U. S. Army Electronics Command Fort Monmouth, New Jersey 07703	(2)
Chief, Atmospheric Physics Division Atmospheric Sciences Laboratory U. S. Army Electronics Command Fort Monmouth, New Jersey 07703	(2)	Chief, Atmospheric Sciences Research Division Atmospheric Sciences Laboratory U. S. Army Electronics Command Fort Huachuca, Arizona 85613	(5)	Chief, Atmospheric Sciences Office Atmospheric Sciences Laboratory U. S. Army Electronics Command White Sands Missile Range, New Mexico 88002	(2)
U. S. Army Munitions Command Attn: Irving Solomon Operations Research Group Edgewood Arsenal, Maryland 21010	(1)	Commanding Officer U. S. Army Frankford Arsenal Attn: SMUFA-1140 Philadelphia, Pennsylvania 19137	(1)	Commanding Officer U. S. Army Picatinny Arsenal Attn: SMUPA-TV-3 Dover, New Jersey 07801	(1)
Commanding Officer U. S. Army Dugway Proving Ground Attn: Meteorology Division Dugway, Utah 84022	(1)	Commandant U. S. Army Artillery and Missile School Attn: Target Acquisition Department Fort Sill, Oklahoma 73504	(1)	Commanding Officer U. S. Army Communications - Electronics Combat Development Agency Fort Monmouth, New Jersey 07703	(1)
Commanding Officer U. S. Army CDC, CBR Agency Attn: Mr. N. W. Bush Fort McClellan, Alabama 36205	(1)	Commanding General U. S. Army Electronics Proving Ground Attn: Field Test Department Fort Huachuca, Arizona 85613	(1)	Commanding General Deseret Test Center Attn: Design and Analysis Division Fort Douglas, Utah 84113	(1)
Commanding General U. S. Army Test and Evaluation Command Attn: AMSTE-EL Aberdeen Proving Ground, Maryland 21005	(1)	Commanding General U. S. Army Test and Evaluation Command Attn: AMSTE-BAF Aberdeen Proving Ground, Maryland 21005	(1)	Commandant U. S. Army CBR School Micrometeorological Section Fort McClellan, Alabama 36205	(1)
Commandant U. S. Army Signal School Attn: Meteorological Department Fort Monmouth, New Jersey 07703	(1)	Office of Chief Communications - Electronics Department of the Army Attn: Electronics Systems Directorate Washington, D. C. 20315	(1)	Assistant Chief of Staff for Intelligence Department of the Army Attn: ACSI-DERSI Washington, D. C. 20310	(1)
Assistant Chief of Staff for Force Development CBR Nuclear Operations Directorate Department of the Army Washington, D. C. 20310	(1)	Chief of Naval Operations Department of the Navy Attn: Code 427 Washington, D. C. 20350	(1)	Officer in Charge U. S. Naval Weather Research Facility U. S. Naval Air Station, Building 4-28 Norfolk, Virginia 23500	(1)
Director Atmospheric Sciences Programs National Sciences Foundation Washington, D. C. 20550	(1)	Director Bureau of Research and Development Federal Aviation Agency Washington, D. C. 20553	(1)	Chief, Fallout Studies Branch Division of Biology and Medicine Atomic Energy Commission Washington, D. C. 20545	(1)
Assistant Secretary of Defense Research and Engineering Attn: Technical Library Washington, D. C. 20301	(1)	Director of Meteorological Systems Office of Applications (FM) National Aeronautics and Space Administration Washington, D. C. 20546	(1)	Director U. S. Weather Bureau Attn: Librarian Washington, D. C. 20235	(1)
R. A. Taft Sanitary Engineering Center Public Health Service 4676 Columbia Parkway Cincinnati, Ohio	(1)	Director Atmospheric Physics and Chemistry Laboratory Environmental Science Services Administration Boulder, Colorado	(1)	Dr. Albert Miller Department of Meteorology San Jose State College San Jose, California 95114	(1)
Dr. Hans A. Panofsky Department of Meteorology The Pennsylvania State University University Park, Pennsylvania	(1)	Andrew Morse Army Aeronautical Activity Ames Research Center Moffett Field, California 94035	(1)	Mrs. Francis L. Wheedon Army Research Office 3045 Columbia Pike Arlington, Virginia 22201	(1)
Commanding General U. S. Continental Army Command Attn: Reconnaissance Branch ODCS for Intelligence Fort Monroe, Virginia 23351	(1)	Commanding Officer U. S. Army Cold Regions Research and Engineering Laboratories Attn: Environmental Research Branch Hanover, New Hampshire 03755	(2)	Commander Air Force Cambridge Research Laboratories Attn: CRXL L. G. Hanscom Field Bedford, Massachusetts	(1)
Commander Air Force Cambridge Research Laboratories Attn: CRZW 1065 Main Street Waltham, Massachusetts	(1)	Mr. Ned L. Kragness U. S. Army Aviation Materiel Command SMOSM-E 12th and Spruce Streets Saint Louis, Missouri 63166	(1)	Harry Moses, Asso. Meteorologist Radiological Physics Division Argonne National Laboratory 9700 S. Cass Avenue Argonne, Illinois 60440	(1)
President U. S. Army Artillery Board Fort Sill, Oklahoma 73504	(1)	Commanding Officer, U. S. Army Artillery Combat Development Agency Fort Sill, Oklahoma 73504	(1)	Defense Documentation Center Cameron Station Alexandria, Virginia 22314	(20)
National Center for Atmospheric Research Attn: Library Boulder, Colorado	(1)	Commander, USAR Air Weather Service (MATS) Attn: AWSSS/TIPD Scott Air Force Base, Illinois	(1)	Office of U. S. Naval Weather Service U. S. Naval Air Station Washington, D. C. 20390	(1)
Dr. J. E. Cermak, Head Fluid Mechanics Program Colorado State University Fort Collins, Colorado 80521	(15)	Dr. John Bogusky 7310 Cedardale Drive Alexandria, Virginia 22308	(1)	Dr. Gerald Gill University of Michigan Ann Arbor, Michigan 48103	(1)
Author	(1)				